

**DEVELOPMENT OF AN
ELECTROCHEMICAL BIOSENSOR FOR THE RAPID
IDENTIFICATION AND QUANTITATION
OF MICROORGANISMS**

by

Peter Ertl

A thesis
presented to the University of Waterloo
in fulfillment of the
thesis requirement for the degree of
Doctor of Philosophy
in
Chemistry

Waterloo, Ontario, Canada, 2000

© Peter Ertl 2000



National Library
of Canada

Acquisitions and
Bibliographic Services

395 Wellington Street
Ottawa ON K1A 0N4
Canada

Bibliothèque nationale
du Canada

Acquisitions et
services bibliographiques

395, rue Wellington
Ottawa ON K1A 0N4
Canada

Your file Votre référence

Our file Notre référence

The author has granted a non-exclusive licence allowing the National Library of Canada to reproduce, loan, distribute or sell copies of this thesis in microform, paper or electronic formats.

The author retains ownership of the copyright in this thesis. Neither the thesis nor substantial extracts from it may be printed or otherwise reproduced without the author's permission.

L'auteur a accordé une licence non exclusive permettant à la Bibliothèque nationale du Canada de reproduire, prêter, distribuer ou vendre des copies de cette thèse sous la forme de microfiche/film, de reproduction sur papier ou sur format électronique.

L'auteur conserve la propriété du droit d'auteur qui protège cette thèse. Ni la thèse ni des extraits substantiels de celle-ci ne doivent être imprimés ou autrement reproduits sans son autorisation.

0-612-60535-3

Canada

The University of Waterloo requires the signatures of all persons using or photocopying this thesis. Please sign below and give address and date.

Abstract

The diagnostics field is undergoing rapid changes and biosensors are a key technology because of their speed and simplicity. Rapid identification of bacterial strains remains a well-known problem in applied medicine; thus, the rapid detection of viable pathogens is an important diagnostic goal. We have investigated a new type of biosensor that is based on respiratory cycle activity measurements, by interrupting the microorganism's native respiratory chain with non-native external oxidants.

The respiratory cycle activity of *E. coli* JM105 is studied electrochemically by flow injection analysis (FIA) and chronoamperometry (CA) using ferricyanide and other electron-transfer mediators. Apparent Michaelis-Menten kinetics are observed when 10 mM succinate is included in the assay buffer, with obtained K_m values of 10.1 ± 0.6 mM and 14 mM ferricyanide for exponential and stationary phase *E. coli* JM105, respectively. In addition, cyanide inhibition studies with exponential phase *E. coli* show that ferricyanide is reduced mainly by cytochrome *o* oxidase (86%).

The rapid assessment of the respiratory cycle activity allows rapid and reliable screening for antibiotic susceptibility in microorganisms. Chronoamperometry and chronocoulometry of aerobically cultivated *E. coli* yield signals for reoxidation of the reduction product ferrocyanide that are much smaller if *E. coli* has been briefly incubated with an effective antibiotic compound. A range of antibiotic compounds (13) were examined by chronocoulometry and compared to standard agar disk-diffusion testing. Chronocoulometric results, obtained following 20 min incubation with antibiotic and 2 min measurement (at + 0.5 V vs Ag/AgCl at a Pt working electrode) in assay buffer (300 μ L) containing 50 mM ferricyanide and 10 mM succinate, yield 100% efficiency,

specificity and sensitivity. Quantitative determination of IC₅₀ values for penicillin G and chloramphenicol yield values that are 100-fold higher than those obtained by standard turbidity methods (10 h). Further, the addition of 5 μ M 2,6-dichlorophenolindophenol, a hydrophobic electron-transfer mediator, to the assay mixture allows susceptibility testing of a Gram-positive obligate anaerobe, *Clostridium sporogenes*. The rapid, new low-volume assay will facilitate clinical susceptibility testing, allowing appropriate treatment as soon as a clinical isolate can be obtained.

In the development of biosensors, biochemically selective recognition agents must be associated intimately with a transducer. The application of membranes that feature different surfaces was examined as potential immobilization matrices for lectins, where immobilized lectins recognize and bind to cell-surface lipopolysaccharides in a sensor array. Optimizations performed using the model lectin Concanavalin A show that immobilization methods involving preactivated membranes significantly reduce the time required to create a functional lectin layer on the membrane surface. Completeness and homogeneity of the applied lectin layer were confirmed by atomic force microscopy.

The application of a variety of lectins as recognition agents was then used to assess their usefulness in a sensor array. Chronocoulometric measurements of cells captured on the lectin modified membranes were performed in an assay buffer (200 μ L) containing 50 mM ferricyanide, 0.1 mM menadione, 10 mM succinate and 10 mM formate. The implementation of factor analysis (pattern recognition) allowed the discrimination of six microbial strains (*B. cereus*, *S. aureus*, *P. vulgaris*, *E. coli*, *E. aerogenes* and *S. cerevisia*). A biosensor that rapidly identifies pathogens, along with the assessment of antibiotic susceptibilities, will yield a useful and complete tool for medical diagnostics.

Acknowledgments

It was a great privilege to have Dr. Susan R. Mikkelsen, an enthusiastic scientist and dedicated mentor, as my Ph.D. supervisor; I want to thank her for allowing me the great opportunity to partake in her research group. Dr. Mikkelsen not only helped me through the difficult transition between Austria and Canada, but she also fostered my analytical thinking. Her continuous guidance and patience are greatly appreciated.

Mein besonderer Dank gilt meinen Eltern, die es mir nicht nur erleichtert haben ein Universitätsstudium in Kanada zu beginnen, sondern auch dafür, dass Sie mich immer in meinen Entscheidungen unterstützt haben. Ihren Beitrag zu meinem Doktorat möchte ich besonders herausheben, denn ohne Ihr jahrelanges Vertrauen und ständigen Aufmunterungen wäre diese Arbeit nicht möglich gewesen. Ebenso möchte ich mich bei meinem Bruder Anton herzlichst bedanken, der mir immer mit gutem Rate in schwierigen Situationen beigestanden ist. Deine unzähligen Anrufe und aufmunternden Worte waren mir immer wichtig und werden mir noch lange in Erinnerung bleiben.

Quiero agradecer la familia de Lily por su apoyo y por haberme recibido con los brazos abiertos. Nunca olvidaré el interés demostrado en mi trabajo; fué una experiencia que me dejó lleno de alegría e inspiración.

I would like to also thank my Committee members Dr. J. F. Honek, Dr. P. D. Josephy and Dr. J. G. Guillemette for their support and their guidance. I want to further acknowledge Karen Pike from the Biology Department for providing the bacterial strains used in this thesis. A special note of appreciation goes to Prof. A.P.F. Turner and Kathy Aubrey (Cranfield University, UK) for providing me with information on biosensor

markets and for giving me new insights into this exciting and rapidly changing technology.

The Austrian Ministry of Science and the Government of Ontario are greatly acknowledged for their assistance in the form of postgraduate scholarships (OGSST). I also want to thank the University of Waterloo for their continuous support for the past three years through University of Waterloo Graduate Scholarships and International Graduate Scholarships.

With great affection and admiration
I dedicate this thesis
to

Lilia S. Jiménez

who came into my life unexpectedly
and kept me both airborne and grounded
in the last two years of this work

Lily's enduring patience,
her laughter and encouragement
have been essential in both my thesis and
in the quality of my life.

The completion of this work also marks
the beginning
of our married life together.
My adventure with Lily continues.

For the support, good humour, and stability
that Lily has brought into my life,
I am truly grateful

Table of Contents

Abstract	iv
Acknowledgement	vi
Dedication	viii
Table of Contents	ix
List of Tables	xiii
List of Figures	xvii
List of Abbreviations	xxii

Chapter 1: Biosensors: A Technology for the New Millennium?

1.1 Introduction	1
1.1.1 Objective	1
1.1.2 Introduction	2
1.1.3 History	4
1.1.4 Electrochemical Biosensors	7
1.1.5 Biosensors for Microbial Detection	10
1.1.5.1 Commercially Available Biosensors for Bacterial Detection	18
1.1.6 Microbial Respiration	22
1.1.7 Thesis Organization	28
1.2 References	29

Chapter 2: Mechanism and Kinetics of Ferricyanide Reduction by *Escherichia coli*

2.1 Introduction	35
2.1.1 Objective	35
2.1.2 Introduction	36
2.1.3 Preceding Work	43
2.2 Experimental Section	49
2.2.1 Materials and Instrumentation	49
2.2.2 Methods	50
2.2.2.1 Cultivation of <i>E. coli</i> JM105	50
2.2.2.2 Sample Collection	51
2.2.2.3 Determination of Optical Density	51

2.2.2.4 Determination of Bacterial Dry Matter (BDM)	51
2.2.2.5 Determination of Colony Forming Units (cfu)	51
2.2.2.6 Flow Injection Analysis (FIA)	52
2.2.2.7 Chronoamperometry (CA)	52
2.3 Results and Discussion	53
2.3.1 Flow Injection Analysis	56
2.3.2 Chronoamperometry with RDE	61
2.4 Conclusions	88
2.5 References	90

Chapter 3: Microbial Ferricyanide Reduction in the Presence of Antibiotic Compounds

3.1 Introduction	95
3.1.1 Objective	95
3.1.2 Introduction	96
3.2 Experimental Section	103
3.2.1 Material and Instrumentation	103
3.2.2 Methods	104
3.2.2.1 Cultivation of Microorganisms	104
3.2.2.2 Measurement of Optical Density	105
3.2.2.3 Cyclic Voltammetry	105
3.2.2.4 Chronoamperometry	105
3.2.2.5 Chronocoulometry	106
3.2.2.6 Measurement of IC ₅₀ Values by Growth	107
3.2.2.7 Disk Diffusion Susceptibility Test	107
3.2.2.8 Determination of Colony Forming Units (cfu)	107
3.3 Results and Discussion	108
3.3.1 Chronoamperometry	108
3.3.1.1 Antibiotic Susceptibility Test	124
3.3.1.2 Exposure Time Studies	129
3.3.2 Chronocoulometry	133

3.3.2.1 Miniaturization of the Chronocoulometric Assay	138
3.3.2.2 Antibiotic Susceptibility Assay	163
3.3.2.3 Chronocoulometry with <i>Clostridium sporogenes</i> ATCC8075	173
3.4 Conclusions	176
3.5 References	177
Chapter 4: Lectin Immobilization: Creating a Biosensor Layer	
4.1 Introduction	182
4.1.1 Objective	182
4.1.2 Introduction	183
4.2 Experimental Section	190
4.2.1 Materials and Instrumentation	190
4.2.1.1 Buffer Solution	191
4.2.1.2 Biotinylated Peroxidase Solution	191
4.2.1.3 ABTS Reagent Solution	191
4.2.2 Methods	191
4.2.2.1 Cultivation of <i>E. coli</i> JM105	191
4.2.2.2 Agglutination Tests	192
4.2.2.3 Coomassie Blue Staining	192
4.2.2.4 Crosslinking of Lectins	193
4.2.2.5 Chronocoulometry on Lectin-Modified Membranes	193
4.2.2.6 ABTS - Assay	194
4.2.2.7 Preactivated Membranes	194
4.3 Results and Discussion	195
4.3.1 Agglutination Tests	195
4.3.2 Lectin-Modified Membranes	196
4.3.3 Avidin-Biotin Immobilization	207
4.3.3.1 Detection Using ABTS Assay	207
4.3.3.2 Detection of <i>E. coli</i> by Chronocoulometry	214
4.3.4 Lectin Immobilization on Preactivated Membranes	222
4.4 Conclusions	229

4.5 References	231
Chapter 5: Microbial Identification <i>via</i> Pattern Recognition	
5.1 Introduction	234
5.1.1 Objective	234
5.1.2 Introduction	235
5.2 Experimental Section	249
5.2.1 Materials and Instrumentation	249
5.2.1.1 Buffer Solution	250
5.2.1.2 Reagent Solution	250
5.2.2 Methods	250
5.2.2.1 Detection Limit	250
5.2.2.2 Lectin Immobilization	250
5.2.2.3 Optimization	251
5.2.2.4 Lectin Binding Kinetics	251
5.2.2.5 Chronocoulometry with Modified Electrodes	251
5.2.2.6 Agglutination Tests	252
5.2.2.7 Atomic Force Microscopy (AFM)	252
5.2.2.8 Microbial Growth Conditions	253
5.2.2.9 Viability Assay	253
5.2.2.10 Chemometric Data Analysis	254
5.3 Results and Discussion	255
5.3.1 Optimization	255
5.3.2 Lectin Binding Kinetics	259
5.3.3 Atomic Force Microscopy (AFM)	266
5.3.4 Chronocoulometry with the Biosensor Array	269
5.3.5 Microbial Identification <i>via</i> Pattern Recognition	279
5.4 Conclusions	284
5.5 References	286
Chapter 6: Summary and Suggestions for Further Research	290

List of Tables

Table 1.1:	Relevant Historical Events of Biosensor Development	5
Table 1.2:	Criteria of a Biosensor	19
Table 1.3:	Components of the Respiratory Chain	23
Table 2.1:	Biological Dry Matter and Corresponding Optical Density Values	55
Table 2.2:	Ferricyanide Reduction Rates Obtained by CA in Combination with other Hydrophobic Mediators	75
Table 2.3:	CA Results in the Presence of 5 μ M DMBQ and JG	77
Table 2.4:	Ferricyanide Reduction Rates in the Presence of Succinate	83
Table 3.1:	Mechanistic Information of Antibiotic Compounds	101
Table 3.2:	Disk Diffusion Susceptibility Results using <i>E. coli</i> (High Concentration)	109
Table 3.3:	Disk Diffusion Susceptibility Results using <i>E. coli</i> (Low Concentration)	111
Table 3.4:	Disk Diffusion Susceptibility Results using a Test Kit	112
Table 3.5:	Specific Activities Over Time of <i>E. coli</i> Stored on Ice	113
Table 3.6:	Calibration Slopes for Varying Antibiotics	121
Table 3.7:	Summary of all CA Results for 14 Antibiotics	124
Table 3.8:	Percent Activity for All Antibiotics	127
Table 3.9:	Specific Activity with Vancomycin and Trimethoprim using Stationary Phase <i>E. coli</i>	129
Table 3.10:	Specific Activity with Nalidixic Acid and Amphotericin using Stationary Phase <i>E. coli</i>	129
Table 3.11:	Specific Activity with Vancomycin and Trimethoprim using Exponential Phase <i>E. coli</i>	130

Table 3.12:	Specific Activity with Nalidixic Acid and Erythromycin using Exponential Phase <i>E. coli</i>	130
Table 3.13:	Specific Activity with Tetracycline and Chloramphenicol using Exponential Phase <i>E. coli</i>	130
Table 3.14:	Specific Activity with Bacitracin and Streptomycin using Exponential Phase <i>E. coli</i>	131
Table 3.15:	Chronocoulometry ($V = 41$ mL) in the Presence of Chloramphenicol	136
Table 3.16:	Chronocoulometry ($V = 300$ μ L) with a Two Step Assay	142
Table 3.17:	Chronocoulometry for Different Incubation Periods	145
Table 3.18:	Chronocoulometry with the Single Step Assay	147
Table 3.19:	Antibiotic Assay in the Presence of Succinate and Formate	150
Table 3.20:	Chronocoulometry obtained with Lysozyme	153
Table 3.21:	Chronocoulometric Traces in the Presence of EDTA	155
Table 3.22:	Detection Limit of the Chronocoulometric Assay	159
Table 3.23:	Linear Regression Analysis from Table 3.22	160
Table 3.24:	Chronocoulometry in the Presence of Succinate and Formate	162
Table 3.25:	Chronocoulometry in the Presence of Varying Antibiotics	164
Table 3.26:	Summary of the Chronocoulometric Antibiotic Assay	166
Table 3.27:	Categorization of the Chronocoulometric Assay	167
Table 3.28:	Optical Density Measurements obtained from Varying Concentrations of Chloramphenicol and Penicillin G	169
Table 3.29:	Chronocoulometric Measurements obtained from Varying Concentrations of Chloramphenicol and Penicillin	170
Table 3.30:	Chronocoulometry for <i>C. sporogenes</i>	173
Table 3.31:	Chronocoulometry with <i>C. sporogenes</i> and Lysozyme and Chloramphenicol	174

Table 4.1:	Results of Agglutination Studies	196
Table 4.2:	Coomassie Blue Staining of Lectins	197
Table 4.3:	Chronocoulometry on Lectin-modified Nitrocellulose	198
Table 4.4:	Chronocoulometry with Con A modified (crosslinked) Membranes	204
Table 4.5:	Consumed Charges obtained for Varying Con A Concentration on BiodyneA [®]	206
Table 4.6:	Consumed Charges obtained for Varying Con A Concentrations on Nitrocellulose	206
Table 4.7:	ABTS Conversion for the Avidin-biotinylated Peroxidase System	210
Table 4.8:	ABTS Conversion for Glutaraldehyde Crosslinked Avidin-Biotinylated Peroxidase System	211
Table 4.9:	ABTS Conversion by Peroxidase for Streptavidin	212
Table 4.10:	ABTS Assay for Varying Avidin Concentrations	213
Table 4.11:	Chronocoulometry for <i>E. coli</i> cells Trapped at the Electrode Surface	217
Table 4.12:	Chronocoulometry for Avidin-biotinylated Con A modified Membrane	219
Table 4.13:	Consumed Charges obtained for <i>E. coli</i> Captured Cells after a ten-minute Incubation Period in Reagent Solution	221
Table 4.14:	Chronocoulometry with ImmunodyneABC [®]	223
Table 4.15:	Chronocoulometry with Captured Cells onto Avidin or Streptavidin-biotinylated Con A ImmunodyneABC [®]	224
Table 4.16:	Chronocoulometry with Con A or BSA modified ImmunodyneABC [®]	225
Table 4.17:	Chronocoulometry with Con A or BSA Modified UltraBind [®]	226
Table 4.18:	Consumed Charges Obtained for Cells Captured onto Avidin or Streptavidin-biotinylated Con A modified UltraBind [®]	227

Table 4.19:	Comparison of UltraBind® to ImmunodyneABC®	228
Table 5.1:	Summary of Pathogenic Bacteria and Diseases	236
Table 5.2:	Cell Capture on Con A-modified ImmunodyneABC®	257
Table 5.3:	Signals obtained for Varying Lectins	258
Table 5.4:	Varying Capture Times for <i>A. hypogaea</i> and <i>C. fragile</i>	260
Table 5.5:	Varying Capture Times for <i>A. integrifolia</i> , <i>S. tuberosum</i> and <i>L. culinaris</i>	260
Table 5.6:	Varying Capture Times for <i>T. vulgaris</i> , <i>H. pomatia</i> and <i>G. nivalis</i>	261
Table 5.7:	Varying Capture Times for <i>P. americana</i> and BSA	261
Table 5.8:	Comparison of Lectin- <i>E. coli</i> Binding with Agglutination Tests and Chronocoulometry	265
Table 5.9:	Sensor Array using <i>E. coli</i> JM105	271
Table 5.10:	Sensor Array using <i>E. aerogenes</i> ATCC13048e	273
Table 5.11:	Sensor Array using <i>P. vulgaris</i> ATCC6380	275
Table 5.12:	Sensor Array using <i>B. cereus</i>	276
Table 5.13:	Sensor Array using <i>S. aureus</i> ATCC6538P	277
Table 5.14:	Sensor Array using <i>S. cerevisiae</i> ATCC9896	278
Table 5.15:	Reduced Eigenvalues found in the Data Matrix	280

List of Figures

Figure 1.1:	Schematic Representation of an Impedance Cell Circuit	15
Figure 1.2:	Summary of the Reactions of the Electron Transport Chain	24
Figure 2.1:	Schematic Presentation of Some Electron Donors and Acceptors of the Respiratory Chain	40
Figure 2.2:	Schematic Presentation of a Gram-negative Bacterial Cell Wall	42
Figure 2.3:	Growth Curve and Ferricyanide Reduction Rates of <i>E. coli</i> HB101	44
Figure 2.4:	FIA of <i>E. coli</i> HB101 in the Presence of Succinate and Formate	45
Figure 2.5a:	FIA Obtained for <i>E. coli</i> HMS174	48
Figure 2.5b:	SOD Content and Bacterial Dry Matter Obtained for <i>E. coli</i> HMS174	48
Figure 2.6:	Growth Curves of <i>E. coli</i> JM105	35
Figure 2.7:	Plot of Optical Densities vs Biological Dry Matter	55
Figure 2.8:	Schematic of the FIA System	57
Figure 2.9:	FIA Responses for Increasing Ferricyanide Concentrations	57
Figure 2.10:	FIA Raw Data for <i>E. coli</i>	58
Figure 2.11:	FIA Assay Data for Two-minute Injection Intervals	59
Figure 2.12:	Growth Curve and Ferricyanide Reduction of <i>E. coli</i> by FIA	60
Figure 2.13:	Schematic Presentation of CA	62
Figure 2.14:	Calibration Plot for Ferrocyanide	63
Figure 2.15:	Raw Data from CA	64
Figure 2.16:	Growth Curve and Ferricyanide Reduction of <i>E. coli</i> by CA	65
Figure 2.17:	CA Data for Increasing Ferricyanide Concentration	67

Figure 2.18:	Respiration Rates of Frozen Cells	69
Figure 2.19a:	CA for Varying Ferricyanide Concentrations of Exponential Phase <i>E. coli</i>	71
Figure 2.19b:	Eadie-Hofstee Plot (exponential phase)	71
Figure 2.20a:	CA for Varying Ferricyanide Concentrations of Stationary Phase <i>E. coli</i>	72
Figure 2.20b:	Eadie-Hofstee Plot (stationary phase)	72
Figure 2.21:	CA Raw Data	75
Figure 2.22:	Growth Curve and Sampling	77
Figure 2.23:	Ferricyanide Reduction in the Presence of DMBQ	78
Figure 2.24a:	Calibration Curve of Ferrocyanide/Benzoquinone	79
Figure 2.24b:	Reduction Rates in the Presence of Ferricyanide/Benzoquinone	79
Figure 2.25:	Cyclic Voltammetry on Glassy Carbon, Platinum and Gold Electrodes	81
Figure 2.26:	Ferricyanide Reduction at 22°C and 37°C	81
Figure 2.27:	Raw CA Traces Obtained for Varying Cultivation Times	81
Figure 2.28:	CA in the Presence of 50 μ M KCN	85
Figure 2.29:	CA in the Presence of 6 mM KCN	85
Figure 2.30:	Ferricyanide Reduction in the Presence of 50 μ M KCN	86
Figure 2.31:	CA Traces for Nitrogen purged Ferricyanide Solution	87
Figure 3.1:	Picture of the Agar Disk Susceptibility Test	110
Figure 3.2:	Storage Stability of <i>E. coli</i>	114
Figure 3.3:	CA Traces Obtained for Chloramphenicol and Trimethoprim	116
Figure 3.4:	CA Traces Obtained for Penicillin G and Tetracycline	116
Figure 3.5:	Cyclic Voltammetry of Tetracycline on Glassy Carbon, Platinum and Gold Electrode	118

Figure 3.6:	CA Traces Obtained at 37°C at a Pt RDE Electrode	119
Figure 3.7:	CA in the Presence of Penicillin G and Chloramphenicol	123
Figure 3.8:	CA in the Presence of D-Cycloserine and Penicillin G	123
Figure 3.9:	Exposure Time Curves for Stationary and Exponential Phase <i>E. coli</i>	132
Figure 3.10:	Chronocoulometric Traces in the Presence of Chloramphenicol	136
Figure 3.11:	Area Determination	138
Figure 3.12:	Precision Studies of the Chronocoulometric Assay	140
Figure 3.13:	Storage Stability of <i>E. coli</i> on Ice	143
Figure 3.14:	Ferricyanide Reduction after a five-minute Incubation Period	144
Figure 3.15:	Ferricyanide Reduction after a ten-minute Incubation Period	146
Figure 3.16:	Chronocoulometric Assay in the Presence of Chloramphenicol	148
Figure 3.17:	Chronocoulometry in the Presence of Formate	151
Figure 3.18:	Chronocoulometry in the Presence of NaHCO ₃	152
Figure 3.19:	Chronocoulometry in the Presence of Lysozyme	154
Figure 3.20:	Chronocoulometry in the Presence of EDTA	155
Figure 3.21:	Schematic Representation of Menadione	156
Figure 3.22:	Chronocoulometry for Varying Menadione Concentrations	157
Figure 3.23:	Chronocoulometry in the Presence of Menadione	158
Figure 3.24:	Chronocoulometry of Bacterial Dilutions	160
Figure 3.25:	Detection Limit	161
Figure 3.26:	Schematic Representation of the Antibiotic Susceptibility Assay	163
Figure 3.27:	Chronocoulometry in the Presence of Chloramphenicol, Penicillin G, Tetracycline and Bacitracin	165

Figure 3.28:	MIC Determination of Chloramphenicol and Penicillin G	172
Figure 3.29:	Chronocoulometry of <i>Clostridium sporogenes</i>	175
Figure 4.1:	Reaction Mechanism of DMA	200
Figure 4.2:	Reaction Mechanism of BS ³	200
Figure 4.3:	Reaction Mechanism of MBS	201
Figure 4.4:	Reaction Mechanism of EDC	202
Figure 4.5:	Schematic Representation of the ABTS Conversion	208
Figure 4.6:	Chronocoulometry with Trapped Cells	215
Figure 4.7:	Chronocoulometry with Increasing Incubation Periods	216
Figure 4.8:	<i>E. coli</i> Storage Stability on Ice	218
Figure 4.9:	Chronocoulometry using Biotinylated Con A modified Membrane	220
Figure 4.10:	Chronocoulometry using UltraBind [®] Membranes	226
Figure 5.1:	AFM Schematic Diagram	239
Figure 5.2:	Graphical Display of the Biosensor Array	245
Figure 5.3:	Consumed Charges Plotted against Colony Forming Units	256
Figure 5.4:	Chronocoulometry for Varying Cell Captured Times	263
Figure 5.5:	AFM Image of ImmunodyneABC [®] (5 x 5 μm)	267
Figure 5.6:	AFM Image of ImmunodyneABC [®] (1 x 1 μm)	267
Figure 5.7:	AFM Phase Image of ImmunodyneABC [®]	268
Figure 5.8:	AFM Phase Image of Con A modified ImmunodyneABC [®]	268
Figure 5.9:	Activity in the Presence of Succinate, Formate and Menadione	270
Figure 5.10:	Ferricyanide Reduction and Growth Curve of <i>E. aerogenes</i>	272
Figure 5.11:	Ferricyanide Reduction and Growth Curve of <i>P. vulgaris</i>	274

Figure 5.12:	Pattern Recognition Plot	282
Figure 5.13:	Pattern Recognition Plot of Mean Centered Data	282
Figure 5.14:	Three-dimensional Pattern Recognition Plot	283

List of Abbreviations

ABTS	2',2'-azino-bis(3-ethylbenzthiozoline-6 sulfuric acid)
AFM	atomic force microscopy
AQ	anthraquinone-1-sulfonate
ATP	adenosine triphosphate
BDM	bacterial dry matter
BSA	bovine serum albumin
BWF	biological warfare agents
CA	chronoamperometry
CC	chronocoulometry
cfu	colony forming units
CO	carbon monoxide
CTC	cyanoditolyt tetrazolium chloride
CV	cyclic voltammetry
CW	cell wall
cyt	cytochrome
DCIP	2,6 – dichlorophenolindophenol
DHAP	dihydroxyacetone phosphate
dia.	diameter
DL	detection limit
DMA	dimethyl adipimidate-2 HCl
DMBQ	2,3-dimethoxy-5-methylbenzoquinone
EDC	1-ethyl-3-(3-dimethylaminopropyl)carbodiimide HCL
EDTA	disodium ethylenediaminetetraacetate
EW	evanescent wave
FAD	flavin adenine dinucleotide
Fe(bpy) ₃ ³⁺	tris(2,2'-bipyridine)-iron(III)-hexafluorophosphate
FET	field-effect transistor
FIA	flow injection analysis
gaNAc	N-acetyl-galactosamine

glc	glucose
glcNAc	N-acetyl-glucoseamine
GOx	glucose oxidase
IC ₅₀	inhibitory concentration with 50% remaining activity
IPTG	isopropyl-β-D-thiogalactopyranoside
LAPS	light addressable potentiometric sensor
LP	lipoprotein
LPS	lipopolysaccharide layer
MALDI	matrix assisted laser desorption ionisation source
man	mannose
MBS	m-maleimidobenzyl-N-hydroxysuccinimide ester
MIC	minimum inhibitory concentration
MWCO	molecular weight cut off size
NAD ⁺	oxidized nicotinamide adenine dinucleotide
NADPH	reduced nicotinamide adenine dinucleotide phosphate
NAG	N-acetylglucosamine
NAM	N-acetylmuramic acid
NC	nitrocellulose
NeuNAc	sialic acid
OD ₆₀₀	optical density at 600 nm
P	protein
PC 1	principle component one
PCA	principle component analysis
PCR	polymerase chain reaction
PDH	primary dehydrogenase
PG	peptidoglycan
pI	isoelectric point
QCM	quartz crystal microbalance
R	rough lipopolysaccharide layer
RDE	rotating disk electrode
RSD	relative standard deviation

S	smooth lipopolysaccharide layer
sNC	supported nitrocellulose
SOD	(recombinant human Cu/Zn) superoxide dismutase
SPR	surface plasmon resonance
TL	thermolabile toxin
TS	thermostable toxin
UQ/UQH ₂	ubiquinone, oxidised/reduced form
μ	growth rate, h ⁻¹

Chapter 1

Biosensors: A Technology for the New Millennium?

1.1 INTRODUCTION

1.1.1 Objective

In this chapter various aspects of biosensors are discussed, with a focus on biosensors that detect microorganisms. The concept of biosensors as well as their applications in modern medicine, environmental protection and the food industry is introduced. The origins of biosensors, their history and development as well as future directions are also discussed. Following this, commercially available devices are reviewed with consideration of the challenges manufacturers face when attempting to commercialize biosensors. Furthermore, biosensors for microbial detection are then discussed with a focus on electrochemical sensors. Near the end of this chapter the mechanism behind the bacterial electron transport chain is introduced and its application to viability testing is discussed. This chapter provides the background information upon which the proposed biosensor is based, including electrochemical transduction of mediated redox-reactions. The proposed biosensor consists of an array of amperometric electrodes modified with lectins for selective recognition and binding of microorganisms. Pattern recognition, performed by means of multivariate factor analysis, is used to identify individual bacterial strains.

1.1.2 Introduction

The study of biosensors is motivated by practical application. Much interest has come from medical fields because they require rapid analysis of clinical samples, and if possible, *in vivo* monitoring of drugs, metabolites and proteins. The best-known clinical application is the glucose sensor for diabetics, which has become a classic subject for study in the field of biosensors. Nevertheless, the food industry is increasingly concerned about food quality control and has recognized the value of rapid methods to estimate shelf life, deterioration and contamination. Furthermore, the rise of biotechnology has stimulated the investigation of biosensor applicability to fermentation monitoring as a means to provide fast, real-time information about microbial populations. Also, increasing concerns about the industrial and natural environments has led researchers to further focus on sensors to detect pollutants such as carbon monoxide and herbicides.¹

Many definitions of the concept of biosensors have been used in the literature, but the most dominant and widely accepted is the following: “The biosensor is an analytical tool in which the sensing element is an enzyme, antibody, DNA, or microorganism and the transducer is an electrochemical (measures change in voltage or current), acoustic (measures change in frequency as a result of a change in mass bound to the surface of the device), or optical device (measures change in fluorescence, absorbance, or reflectance)”.²

The possible useful applications of biosensors have not only captured the imagination of the world’s commercial communities, but they have also captured a combination of multidisciplinary scientists from fields such as biology, physics and chemistry. Furthermore, these scientists have worked along with engineers to provide

innovative solutions to instrument design. Consequently, biosensors are applicable to clinical diagnostics, food analysis, cell culture monitoring, environmental control and various military situations. Ever-increasing demands for faster and more convenient analytical devices that can detect a wide variety of analytes has led to intense interest in biosensor technology, which is a fusion of biology, chemistry and electronics.³

Biosensors are also described as analytical instruments containing a sensing element of biological origin, which is either integrated within or in intimate contact with a physicochemical transducer. The aim is to produce a continuous electronic signal that is directly proportional to the concentration of a chemical, or set of chemicals, present in a sample. Sensing elements can be biocatalytic (enzymes, organisms, tissues) or affinity systems (antibodies, lectins, nucleic acids and cell receptors) or combinations of these. Biological recognition events are converted into processible signals by means of optical, electrochemical, calorimetric or piezoelectric transducers.¹

In summary, biosensors are particularly valuable when they provide continuous or near-continuous information about unpredictable fluctuations in the concentrations of analytes. Furthermore, biosensors are competitively advantageous because they are less expensive, more rapid and may be easier to use than conventional methods. Regardless of type, biosensors are amenable to miniaturisation and integration into multisensor arrays to further facilitate analysis *via* chemometric methods.

1.1.3 History

In 1956 Professor Leland C. Clark Jr. published his paper on the oxygen electrode and in 1962 at a New York Academy of Sciences symposium, he described how “to make electrochemical sensors more intelligent” by adding “enzyme transducers as membrane enclosed sandwiches”.⁴ The concept was illustrated by an experiment in which glucose oxidase was entrapped on the surface of a Clark oxygen electrode using a dialysis membrane. The decrease in measured oxygen concentration was proportional to glucose concentration.⁵ The conversion of glucose and molecular oxygen to gluconolactone and hydrogen peroxide was found to be better monitored electrochemically by reoxidizing hydrogen peroxide to molecular oxygen at the surface of the platinum electrode. In this device, the substrate (oxygen) was not consumed during measurement.⁶ Clark’s ideas became a commercial reality in 1975 with the launch of the Yellow Springs Instrument Company (Ohio) glucose analyser based on membrane-bound glucose oxidase and on the amperometric detection of hydrogen peroxide.⁷ This was the first of many biosensor-based laboratory analysers to be built by companies around the world. Soon after, potentiometric enzyme electrodes, thermal transducers for biosensors and fiber-optic sensors for the detection of ammonium, pH, pCO₂, pO₂ and alcohol were described.^{8,9,10,11} In 1975 bacteria were introduced as biological elements for the measurement of alcohol.¹² The late seventies also showed major advances in the *in vivo* application of glucose biosensors for subcutaneous implantation.¹³ Companies are still pursuing this possibility, but no device for general use is yet available.⁷ In 1983 Liedberg described the use of surface plasmon resonance in combination with immobilized antibodies to monitor affinity reactions in real time,¹⁴ while BIAcore (Pharmacia, Sweden) launched this

technology in 1990. Additional relevant historical events regarding fundamental inventions and commercialisation are listed in Table 1.1.

Table 1.1: Relevant events in the history of biosensor development.⁷

Date	Historical Event
1962	First description of a biosensor (amperometric enzyme electrode)
1969	First potentiometric biosensor
1970	Invention of ion-selective field-effect transistor (ISFET)
1972	First commercial biosensor: YSI glucose biosensor
1975	First microbe-based biosensor
1976	First bedside artificial pancreas
1980	First fibre optic pH sensor for <i>in vivo</i> blood gases
1982	First fibre optic-based biosensor for glucose
1983	First surface plasmon resonance (SPR) immunosensor
1984	First mediated amperometric biosensor (ferrocene)
1987	Launch of the MediSense ExacTech blood glucose analyser
1990	Launch of the Pharmacia BIACore SPR-based biosensor system
1992	i-STAT launches hand-held blood analyser
1996	Glucocard launched
1998	Launch of LifeScan FastTake blood glucose biosensor

The main market for biosensors became therapeutic diagnostics, which is still a very large and expanding market due to increasing concerns about preventive medicine. In 1996, the estimated biosensor market was worth US\$ 508 million, and approximately 95% of the market involved glucose sensing devices. MediSense, Boehringer Mannheim, and Bayer dominated 85% of the world biosensor market. However, in the year 2000, the projected world market for biosensors is US\$ 1,485 million, thus showing a three-fold increase within only 4 years. Although blood glucose biosensors still dominate the

market, their share declined from 95% to 86% of the total market. The remaining market is divided between medical (4%), pharmaceutical (4%) and environmental/food science (2%) applications. The majority of these sensors consist of an electrochemical transducer with an electron transfer mediated enzymatic reaction. The main suppliers of blood glucose sensors are Abbott (MediSense), Roche Diagnostics (Boehringer), Bayer and LifeScan (Inverness Medical). However, the overall top ten biosensor producing companies today (given in order of production scale) are Abbott (MediSense) with sales of US\$ 800 million, Bayer Diagnostics / Kyoto Daiichi / Menarini with US\$ 220 million, Roche Diagnostics (Boehringer) with US\$ 120 million, LifeScan (Inverness Medical) with US\$ 132 million, Molecular Devices with US\$ 59 million, i-STAT with US\$ 45 million, BIACore (Pharmacia) with US\$ 40 million, Yellow Spring Instruments (YSI) with US\$ 18.5 million, Eppendorf with US\$ 8 million and Omron Toyobo with US\$ 8 million in sales.⁷

Future market opportunities for biosensors have been predicted of US\$ 500 million per year for therapeutic products. Prior to reaching the market, the average research and development phase for a biosensor is expected to last 10 years and estimated to cost an average of US\$ 50 million dollars per year.⁷ Despite high development costs, it is evident that biosensor technology is still a young, dynamic and fast growing field, capable of attracting new companies for investment.

The second generation of biosensors has already reached either the research or developmental stages. Sensors are now being manufactured using screen-printing and inkjet-printing (picoliter) technology, while companies such as Affymetrix, have also started to develop ever-smaller gene chips.⁷ Sensor arrays capable of computing fast amounts of data (multi-factorial analysis) are now being used for the electronic nose and

will soon be available in the market.⁷ Further research and improvements will lead to biological recognition agents that not only offer sensitivity and specificity, but that are also inherently stable, inexpensive and easy to manufacture. Consequently, chemical approaches such as molecularly imprinted recognition elements that mimic biological systems are of current interest because they may allow repeated use of the sensor, even after autoclaving.¹⁵

1.1.4 Electrochemical Biosensors

Biosensors are classified and evaluated on the basis of design and functional characteristics such as sensitivity, cost, selectivity, versatility, range, availability, future adaptability and simplicity. On these bases, electrochemical biosensors are favoured over optical sensors mainly because of cost and availability, while piezoelectric and thermal sensors are fairly poorly rated on all characteristics.¹⁶ Amperometric biosensors form the majority of commercial biosensor devices available today; these biosensors operate at a fixed potential with respect to a reference electrode, while the measured signal is the working electrode current generated by the oxidation or reduction of species at its surface.

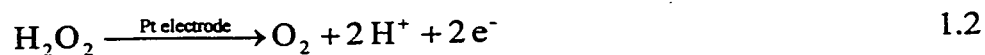
Four decades ago, the development of biosensors was based on enzymes as the biological elements. Today, the term element has been expanded to include antibodies, nucleic acids, whole cells or their fragments, plant and animal tissue and neuro-receptors. Commercially, however, the emphasis has still involved mostly enzymes, antibodies or whole cells. As previously mentioned, the transducer can take many forms, such as photometric detectors, potentiometric or amperometric electrodes and thermistors.

However, in this section the focus will be largely on the use of electrochemical devices to measure the change of potential or current over time.

Examples of enzyme-based electrochemical biosensors include the nitrite sensor, which is based on a highly sensitive nitrite reductase mediator-coupled amperometric detector;¹⁷ the phenol sensor, which is based on the enzyme polyphenol oxidase;¹⁸ the aldehyde biosensor, which determines the presence of NADH generated by the enzymatic activity of immobilised aldehyde dehydrogenase;¹⁹ and a cyanide sensor, which makes use of cytochrome oxidase.²⁰

Potentiometric and amperometric biosensors have also been used for the determination of organo-phosphorus pesticides in environmental samples,²¹ while amperometric biosensors have been used for the determination of cyanide, chlorphenols, atrazine, dithiocarbamates, and carbamate pesticides.²² Catalytic materials, membranes, and fabrication technologies for the construction of electrochemical biosensors have been reviewed.²³

Enzymes are widely applied to biosensor technology because of their specificity and catalytic (amplification) properties. A variety of enzymes belonging to classes of oxidoreductases and hydrolases have been involved in many biosensor applications.¹⁶ Oxidoreductases such as the glucose oxidase (GOx) transfer electrons from a donor (e.g. glucose) to an acceptor (e.g. oxygen) as outlined in Equation 1.1.⁶

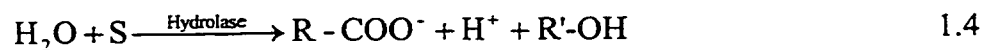


The liberation of hydrogen peroxide in the upper enzymatic reaction can then be monitored amperometrically at a platinum electrode.

Creatinine is an important clinical analyte that can be determined *via* hydrolase catalysed reactions.²⁴



In general, the transfer of functional groups to water (Eq. 1.3. and 1.4) results in a change of pH that can be monitored with pH-sensitive electrodes or field effective transistors.



Immobilised antibodies can also be used as highly selective reagents in biosensors. Unlike the enzyme-based biosensors where either the co-substrate or the product of an enzyme reaction is monitored, antibody-based biosensors detect antigen or antibody concentration either by direct changes in the transducer output resulting from the binding event, or by means of indirect competitive and displacement reactions using optical, piezoelectric, or electrochemical techniques.^{25,26} Nevertheless, the majority of the reported antibody-based biosensors (immunosensors) make use of irreversible binding chemistry and are therefore not reusable and thus expensive.

Biosensors have also been constructed using whole microbial cells that have been immobilized onto an electrochemical device. The concentration of the species of interest determines its rate of uptake and metabolism by the microorganism, and the respiratory activity of the microorganism. These whole-cell devices possess advantages over simple enzyme electrodes because whole cells are less sensitive to inhibition by solutes and tolerate higher pH changes and a wider range of temperatures. The cells are generally cultured in a medium containing a high concentration of metabolizable analyte, to induce production of a high level of the enzyme of interest inside the cells. These devices are

more stable than simple enzyme electrodes due to the natural environment of active enzymes within the microbial cell, and may also exhibit a longer lifetime and are usually less expensive because the active enzymes do not need to be isolated.²⁷ The disadvantages of whole-cell devices include slow response times, followed by a slow return time to the base line after use. Other problems may occur with cells that contain many enzymes capable of utilising a great variety of analytes (loss of selectivity). However, microbial sensors are considered to be suitable for on-line control of biochemical processes.²⁷

1.1.5 Biosensors for Microbial Detection

The quantification of microorganisms plays a vital role in fermentation technology, medical practice and environmental monitoring. Biomass concentration is a key variable used to indicate rates of growth, product synthesis, yield-coefficients and is also used for the calculation of specific rates and mass balance in any bioprocess. Therefore, real-time and rapid estimation of biomass is an important area of research. The term 'rapid method' is widely used to describe any method that significantly shortens the analysis time in comparison with conventional methods. These methods include the measurement of cell dry weight, viability count and turbidimetric methods. More specifically, the term 'rapid method' is applied to methods that require less than 24 h to obtain a result. Methods taking less than 1 h are often referred to as ultra or very rapid methods.²⁸

Conventional bacterial identification methods usually include a morphological evaluation of the microorganism as well as a test for the organism's ability to grow in various media under a variety of conditions. Although these techniques allow the detection of a single pathogen, they are also inherently time consuming and can take up to

72 h. Generally, a complex series of tests are required to confirm results obtained by means of biochemical screening, serological tests or DNA probes.²⁹

Instrumental methods involving biosensors are believed to detect and confirm the presence of pathogens in significantly less time than conventional methods. Optical, mass sensitive and electrochemical transducers have been used in combination with selective recognition agents. Optical transducers capable of detecting small changes in the refractive index, which occur when cells bind to immobilized receptors or antibodies, are particularly attractive for the application of direct bacterial detection. A thin layer (~ 100 nm) of a high refractive index material covers a thicker layer (~ 1 mm) of low refractive index material. At certain angles of incidence, light in the high refractive index layer undergoes total internal reflection allowing only a minute element of light or evanescent wave, to penetrate the sample overlayer. The interaction between the evanescent wave and the immobilized layer can be monitored in several ways. Intensity variations in absorbance or fluorescence are most commonly used for detection of analytes. In addition, on reflection light undergoes a phase change that can be measured by monitoring the angle at which this occurs.¹⁶ Several biosensors based on this evanescent principle have been used to detect bacterial pathogens. Transducers have included monomode dielectric waveguides, surface plasmon resonance and the resonant mirror.^{30,31,32}

Direct fluorescence techniques have also been used for bacterial identification, where naturally fluorescent components of the bacterium are examined. Generally, a mixture of fluorescent metabolic products can be detected when the organisms are exposed to ultraviolet light. This method has been used for identification of *Bacterioides* species that emit fluorescence of characteristic wavelengths when held under UV light.³³

However, since only fluorescent light-emitting bacteria can be examined by this method, fluorescence detection of bacteria is now conducted by attaching fluorophore-coupled antibodies onto proteins or polysaccharides present at the bacterial cell surface.²⁹ Antibodies provide the recognition capability used for bacterial identification, while the bound fluorophores allow detection by fluorescence microscopy. Fluorescein isothiocyanate and rhodamine isothiocyanate are the most common fluorophores used to tag antibodies. Numerous pathogens have been detected after selective cell-capture with fluorophore-labelled antibodies located on the surface of a fibre optic biosensor.^{34, 35}

Other researchers have used optical methods to detect bacterial metabolic activity by measuring the colour change induced by captured bacterial cells after incubation with a redox-active dye such as cyanoditoyl tetrazolium chloride (CTC). After incubating with CTC, the accumulation of the coloured reduced form of the dye in the bacterial cells has made it possible to detect *E. coli* O157:H7 in the range of 10^5 to 10^9 cfu/mL with an assay time of 4 h.³⁶

Luciferase-gene-carrying phages have shown potential for bioluminescence detection of bacteria. A bacterial virus is used to introduce the luciferase gene into the genome of the bacterium. After expression of the enzyme, the bacterium emits photons as a by-product of the luciferase reaction. This method has been used to detect a wide range of bacteria,³⁷ and represents a new, highly specific approach to detecting and recognising viable cells, but it lacks sensitivity in the presence of low bacterial numbers.

Another type of transducer that has gained wide recognition for biosensor applications involves mass-sensitive piezoelectric crystals. Piezoelectric biosensors are very attractive for bacterial identification because they offer real-time output, simplicity and cost effectiveness. In the last decade, many reports have been published using

piezoelectric sensors for a wide range of applications in the food industry, environmental monitoring, clinical diagnostics and biotechnology.^{25,38}

Piezoelectric crystals can be modified with antibodies to selectively capture bacteria. Upon capture, the mass increases at the surface, while the resonance frequency of oscillation decreases proportionally.¹⁶ Piezoelectric crystal immunosensors have been developed for *Vibrio cholerae*,³⁹ *Candida albicans*,⁴⁰ and *Salmonella typhimurium*.⁴¹ Antigen monolayers assembled onto gold surfaces associated with a quartz crystal microbalance (QCM) have also been used to detect *Chlamydia trachomatis* in urine samples.⁴² The disadvantages of piezoelectric sensors are the relatively long bacterial incubation period required, the difficulty involved in removing bacterial cells from the crystal surface, and their lack of sensitivity.

Electrochemical transducers have found their way into microbial biosensor technology because of their many advantages. Electrochemical transducers are capable of operating in turbid media and their high sensitivity has also made these sensors very likely candidates for miniaturisation. Furthermore, the continuous response of an electrode allows for on-line control, and the equipment necessary for electrochemical analysis is simple and inexpensive compared to most other analytical techniques.²⁹

There are three types of electrochemical measurement methods. Potentiometry includes methods in which a controlled (zero or nonzero) current is applied to the working electrode and the resulting shifts in potential are measured. Amperometric methodology considers all techniques in which current is measured in response to applied potential; while impedimetry measures impedance, conductance or capacitance in the absence of faradaic currents.¹⁶

Under ideal conditions an indicator electrode in contact with a solution containing a redox-active species will have a potential described by the Nernst equation (Eq. 1.5)

$$E_{cell} = E - E_{ref} = E^{\circ} + \frac{2.3 R T}{n F} \log \frac{C_O(0, t)}{C_R(0, t)} - E_{ref} \quad 1.5$$

where E_{cell} is the measured cell potential, E is the indicator electrode potential, E_{ref} is the potential of the reference electrode, E° is the standard potential for the redox reaction, R is the universal gas constant ($8.314 \text{ J K}^{-1} \text{ mol}^{-1}$), T is the Kelvin temperature, n is the number of electrons transferred in the reaction and F is the Faraday constant (96,487 coulombs). The obtained potential (E) of the indicator electrode can be used to find the concentration of the electroactive species (C_O and C_R).⁶

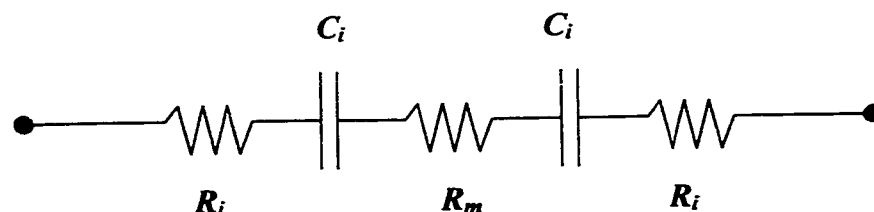
The most established amperometric methods for bioanalysis involve constant-potential amperometry, in which mass-transport controlled oxidation or reduction is used to quantitate the product (or substrate) of an enzymatic reaction. Rapid and reversible electrochemical reactions are described by the Cottrell equation (Eq.1.6).

$$i(t) = \frac{n F A D_O C_O}{\sqrt{\pi D_O t}} \quad 1.6$$

where i is the limiting current, measured at a potential where all analyte is oxidized or reduced, n and F have their usual meanings, D_O is the diffusion coefficient of the electroactive species, C_O is its bulk solution concentration and $(\pi D_O t)^{1/2}$ describes the thickness of the Nernst diffusion layer.⁴³

The impedance cell can be thought of as a simple electrical circuit, composed of two capacitors, that represent the two electrode-solution interfaces, separated by a series of three resistors that symbolize the polarization resistance at each electrode surface, with the electrolyte resistance in the centre, as shown in Figure 1.1.

Figure 1.1: Equivalent circuit of a typical impedance cell, where R_i and C_i represent the interfacial resistances and capacitances, respectively, while R_m is the resistance of the surrounding solution



The overall impedance of the cell, Z , consists of an overall capacitance C and a total resistance R , and depends on the angular frequency ω of the applied potential waveform, as shown in Equation 1.7.⁴³

$$Z^2 = R^2 + \frac{1}{(C \omega)^2} \quad 1.7$$

The recently developed light addressable potentiometric sensor (LAPS) is based on a field effect transistor (FET) and represents a major advance in bacterial immunoassay. In this device a pH-sensitive silicon nitride insulator functions as a phototransistor gate. Changes in pH at the gate solution interface cause a shift in the gate potential. This principle has been used in an immunoassay to detect *E. coli* O157:H7, since these bacteria acidify their surrounding media.⁴⁴

Almost any microorganism can be sensed amperometrically *via* their enzyme-catalysed electrooxidation/-reduction to quantitate the product / substrate of the enzymatic

reaction. This principle has been described in an early patent where the presence of a bacterial population was determined after reducing of a redox-active dye in the presence of glucose.⁴⁵ Amperometric biosensors have the advantage of being highly sensitive, rapid and inexpensive.⁴⁶ Instruments commonly measure current at defined times or integrate currents for a defined period (in the case of coulometry). In both cases the magnitude of the resulting signal is directly proportional to the concentration of the redox-active species. Furthermore, amperometric systems have linear concentration dependence, while potentiometric systems exhibit a logarithmic relationship as outlined in Equations 1.5 and 1.6.

The detection of *Salmonella* sp. is of importance in food processing and amperometric enzyme-linked assays have been applied.^{47,48} Amperometric enzyme-linked immunosensors for the detection of *S. aureus*, with detection limits of 10^4 to 10^5 cfu/mL have also been reported.⁴⁹ Moreover, an amperometric filtration-capture assay has been used to detect enterohaemorrhagic *E. coli* O157:H7, while immunomagnetic flow injection immunoassays have been developed to use antibody-coated super-paramagnetic beads to separate captured cells.^{50,51} A novel approach includes the use of partially immersed immunoelectrodes to rapidly detect *E. coli* O157:H7.⁵² This method is believed to facilitate the determination of 150 – 7000 cells/mL through enhanced hydrodynamic conditions.

Microbial metabolism usually results in an increase in both conductance and capacitance of the surrounding environment, thus causing a decrease in impedance. Impedance, conductance, capacitance and resistance are inter-related.⁵³ Impedimetric measurements record non-faradaic responses observed between two electrodes when a high frequency alternating potential is applied. Impedimetric methods are not analyte-

selective, but instead measure the bulk properties of the solution. These techniques have been widely used for the detection of bacteria, to monitor and detect specific food pathogens, and also for industrial microbial process control and for sanitation microbiology.⁵³⁻⁵⁶ Impedimetry has also been used for estimating microbial biomass and for detecting microbial metabolism.^{57,58}

Biosensors indeed include a large area of research, but as diverse as these areas are, they have at least one thing in common: the target analytes are always present in a complex biological matrix. This commonality places special demands on existing methods because each method has to be able to discriminate between analytes and interfering species. For this reason, all sensors aim for highest selectivity through surface modification or through the selective chemical and biochemical reactions in the assay mixture.

All of the previously described transducers can also be implemented into a newly emerging branch of highly selective biosensors. Gene probes will play an increasing role in health care, agriculture, and environmental monitoring^{59,60} and clinical applications of gene probes are an area of intensive development.⁶¹ The term gene probe describes a segment of nucleic acid which specifically recognises and binds to the complement nucleic acid target. The recognition is dependent on the formation of stable hydrogen bonds between the two complementary nucleic acid strands.^{59,61} Gene probes are already finding applications in detection of disease-causing microorganisms in water supplies, food, animal or human tissues.²⁹ The detection of specific DNA sequences provides the basis for tracking a wide variety of bacterial pathogens such as *Cryptosporidium parvum* and *E. coli*.^{62,63} The limitation of gene sensors is associated with cultivating bacteria to a detectable level because DNA hybridisation requires the presence of at least 10^6 bacteria.

Consequently, only methods involving polymerase chain reaction (PCR) have been employed to detect food borne pathogens (low detection limit), because this method allows the rapid multiplication of a single gene sequence. The PCR method is extremely sensitive and specific because bacteria can be detected directly, without cultivation, by extraction and isolation of nucleic acids from real samples. This is followed by hybridization, after which the presence of bacterial DNA can be determined using optical, mass sensitive and electrochemical transducers.²⁹ Although these DNA-based detection methods are able to determine the presence of a given microorganism in a sample, they are unable to determine whether those microorganisms are viable.

1.1.5.1 Commercially-Available Biosensors for Bacterial Detection

Although great effort has been directed towards the development of biosensors in the last few years, only a few biosensors for bacterial detection are now commercially available. Reasons may be market related or may also include technology-related challenges in the creation of a biosensor that has the necessary properties for reliable and effective use in routine applications. The challenges in developing such a biosensor involve the high specificity needed to distinguish the target bacterium in a multi-organism matrix; on the sensitivity needed to detect bacteria directly, without pre-enrichment; and on the need to rapidly provide real-time results. At the same time, the biosensor should also be simple in design and inexpensive to mass-produce.^{18,29} Table 1.2 presents the ideal properties of a bacterial sensor.

Table 1.2: Criteria and requirements of a perfect biosensor for microbial detection.^{16,29}

Low detection limit	Ability to detect a single bacterial cell in 1 – 100 mL
Species selectivity	Distinguish one bacterial species in the presence of others
Strain selectivity	Distinguish one bacterial strain from the same species
Assay time	5 – 10 min
Precision	1%
Assay protocol	No reagent addition is necessary
Measurement	Direct and without pre-enrichment step
Format	Highly automated
Operator	No skill needed
Viability	Ability to discriminate between live and dead cells
Size	Compact, portable, hand-held and designed for field use

Currently, there are five companies that produce special impedance-measuring instruments for clinical biology and for food hygiene application. Bactomatic (Princeton, NJ, USA) manufactures the Bactometer, which monitors conductance, capacitance or impedance in order to determine microbial growth in blood, cerebrospinal fluid and urine. Reported detection limits are 10^5 cells/mL with an analysis time of 3-8 h. Malthus Instruments (UK) produces the System 2000, which monitors only conductance and has a detection limit of 10^5 cells/mL and a total analysis time of 8-24 h. Furthermore, Don Whitley Scientific manufactures the “Rapid Automated Bacterial Impedance Technique” (RABIT) instrument, while Sy-lab offers the BacTrac and TEM (Centronic Sales, UK) produces the Bactobrige. All of these instruments monitor relative or absolute changes in impedance or conductance at regular intervals, but are cost-intensive and require lengthy periods of analysis (24 – 40 h).

Other electrochemical biosensors include the amperometric Midas Pro sensor (Biosensori, SpA., Milan, Italy) and the light addressable potentiometric sensor (Molecular Devices, USA), both of which have detection limits of 10^2 to 10^3 cells/mL. The Midas Pro sensor is based on the measurement of bacterial metabolic activity present *via* amperometry using a suitable mediator. Initially, the sample is pumped over a filter to retain bacteria, which is then inserted in the electrochemical cell. After the first amperometric response the bacteria present on the filter are killed with a strong biocide. A second measurement determines the interfering substances, which are subtracted from the first response.⁶⁴ The light-addressable potentiometric sensor (LAPS) represents a major advance in commercially available potentiometric bioanalysis. In this device, a pH-sensitive silicon nitride insulator functions as a phototransistor gate. Cellular metabolism causes acidification of the surrounding medium and has been used to detect pathogenic bacteria. In this device, antibodies are used to selectively capture *E. coli* O157:H7 on a membrane, where as detection occurs *via* urease label that causes acidification of the solution during reaction with urea.^{44, 65}

Two commercial devices are currently available for mass sensing with piezoelectric immunosensors. The PZ 106 Immunobiosensor System (Universal Sensors, New Orleans, LA), which contains a liquid flow cell to allow repetitive measurements of biospecific interactions, has a detection limit of 10^6 cells/mL and an analysis time of 40 min. The second model is the Quartz Crystal Analyser QCA 917 (EG&G, Princeton Applied Research, Princeton, USA), which is designed for simultaneous electrochemical and mass measurements.²⁹

The majority of the operating principles of microbial biosensors are based on optical detection such as fluorescence and bioluminescence, while resonant mirror and

evanescent wave measurements have been used more extensively. The Lumac Biocounter (Netherlands) and the Unilite (Biotrace, UK) sensors non-specifically detect bacteria at 10^3 cells through ATP-specific reactions (bioluminescence) and have an analysis time of 20 to 30 min. BIACore (Pharmacia, Sweden) offers a surface plasmon resonance sensor with a detection limit of 10^5 cells/mL and a minimum analysis time of 3 h. BioMerieux Vitek (MO) produces the Vitek AutoMicrobic System for bacterial detection with a detection limit of 10^4 cells/mL and a minimum analysis time of 4 h.²⁹

Gene probes have also been applied to the detection of disease-causing microorganism with detection limits as low as a single cell. Integrated Genetics (MA, USA) offers a DNA probe for *Salmonella* with a detection limit of 1 cell/g and an analysis time of 2 days. Similar analysis periods are found for Enzo Biochem (NY, USA) that produces a DNA probe for *Chlamydia*.²⁹

Other biosensors include the Thermal Activity Monitor (Thermometric, UK) that detects 10^5 cells/ml and takes 3 h for analysis. Here, the overall metabolic capacity of a sample is dependent on the number of cells present and can be measured using microcalorimeters.⁶⁶ The Coulter counter manufactured by Coulter Electronics (Canada) has been widely used and is known to have a detection limit of 10^4 cells/mL with a 30 min analysis time. A suspension of cells is passed through a small opening and the resistance measured between two electrodes gives information about the number of cells flowing through the opening.⁶⁷

All companies face the same challenge in transferring their technology from research to development and commercialisation. One of the difficulties the scientific community faces during the production of a biosensor can be appreciated in cases where the direct detection of viable bacteria is concerned. The infectious dose of pathogens such

as *Salmonella* or *E. coli* O157:H7 is 10 cells per 100 ml. In accordance to international standards, a biosensor must be able to provide a detection limit as low as a single organism in 100 mL potable water (in the case of *E. coli*), while at the same time, providing results using rapid and low cost analysis.

1.1.6 Microbial Respiration

Respiring microorganisms reduce components of their surrounding medium, and this can be quantitated using electrochemical methods with appropriate electron transfer mediators.⁶⁸ To date, many bioassays have been based upon measurement of microbial metabolism by redox-sensitive dyes, where detection occurs after a period of microbial growth, and thus do not provide real-time analysis.⁵¹ Nevertheless, a rapid assessment (10 – 15 min) of respiratory activity has the potential to overcome these problems.

In our study, the proposed biosensor is based on a rapid assessment of respiratory activity. To fully understand the basis for this rapid method, a closer look at the biochemical processes involved in bacterial respiration is necessary. The following summary considers only the electron-transport chains that terminate with the reduction of oxygen in aerobically-grown *Escherichia coli*.

In its natural environment, this facultative bacterium generates energy from both aerobic and anaerobic electron transfer pathways. The terminal components of the respiratory system found in *E. coli* are bound or associated with the cytoplasmic membrane and consists of a sequence of redox proteins that cycle between oxidized and reduced forms. Ultimately, energy generated by respiration is used to produce ATP by phosphorylation of ADP. Additionally, the respiratory complexes are organised in the

cytoplasmic membrane in such a way that they catalyse proton translocation, that is, electrons and protons are both translocated from the cytoplasm to the periplasm of the organism.^{69,70} It is important to realise that the expression levels of the individual respiratory chain components are subject to change by variation of the concentration of the terminal acceptor, or by changes in the medium. In other words, the respiratory chain is modular, consisting of a number of dehydrogenases and oxidases that are highly adapted to their surrounding environment. The respiratory chains of *E. coli* consist of at least 15 primary dehydrogenases and ten terminal reductases. Only those dehydrogenases and reductases known to be present during aerobic growth are listed in Table 1.3.

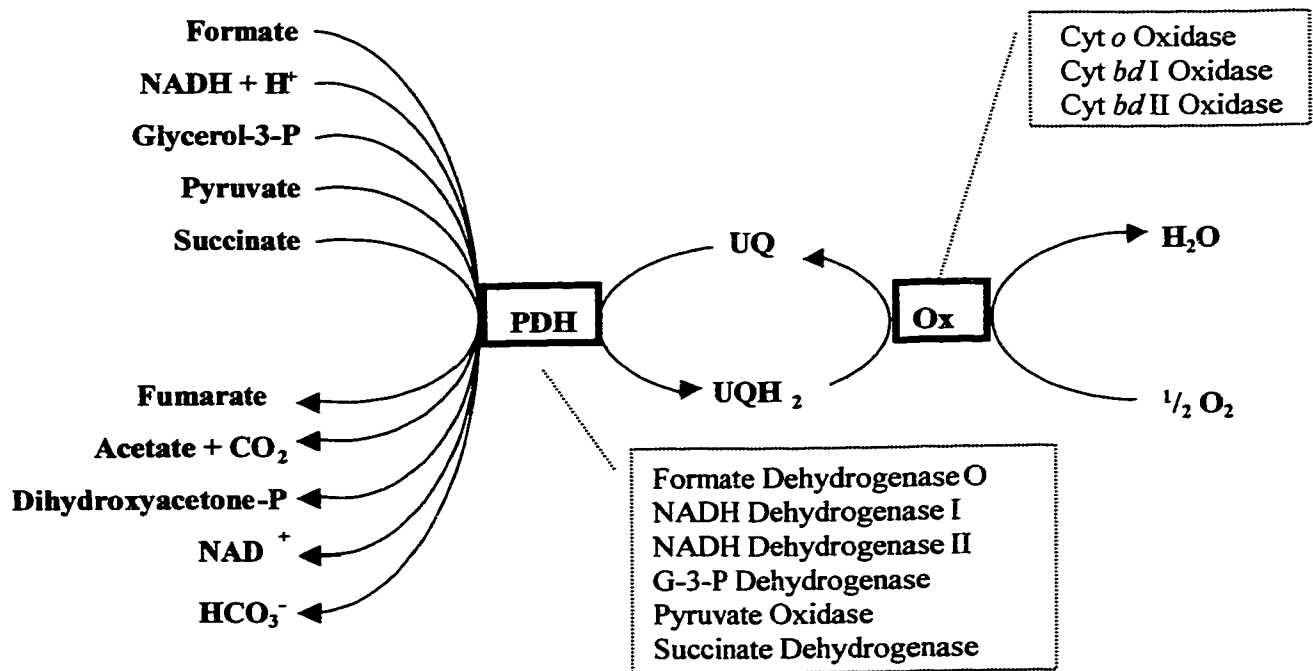
Table 1.3: Components of the respiratory chain of aerobically grown *E. coli*, their substrates and reported redox potentials.

Enzyme	Redox couple	E ^{o'} (V)*
<i>Primary dehydrogenases</i>		
Formate dehydrogenase	HCO ₃ ⁻ /HCO ₂ ⁻	- 0.43
Hydrogenase I, II	H ⁺ /H ₂	- 0.42
NADH dehydrogenase I, II	NAD ⁺ /NADH	- 0.32
Glycerol-3-P dehydrogenase	DHAP/Gly-3-P	- 0.19
Pyruvate oxidase	Acetate + CO ₂ /Pyruvate	
D-Lactate dehydrogenases	Pyruvate/D-lactate	- 0.19
L-Lactate dehydrogenases	Pyruvate/L-lactate	- 0.19
D-Amino acid dehydrogenase	2-oxoacid + NH ₄ ⁺ /amino acid	
Glucose dehydrogenase	Glucose/gluconate	- 0.14
Succinate dehydrogenase	Fumarate/succinate	+ 0.03
<i>Terminal reductases</i>		
Cytochrome oxidase <i>o</i>	O ₂ /H ₂ O	+ 0.82
Cytochrome oxidase <i>bd</i>	O ₂ /H ₂ O	+ 0.82

* Formal reduction potential of the redox couple

The terminal respiratory chains of *E. coli* consist of primary dehydrogenases and terminal reductases or oxidases, which are linked by quinones as outlined in Figure 1.2. Primary dehydrogenases do not rely on nicotinamide cofactors (NADH and NADPH) as do their soluble counterparts in the cytoplasm. Instead, primary dehydrogenases transfer electrons to membrane-soluble quinones, mainly ubiquinone-8, which in turn transport reducing-equivalents to membrane-bound *b*-type cytochromes, which then react with a cytochrome oxidase complex that ultimately reduces molecular oxygen to water. There exists a large variability in the composition of the respiratory chains because of the multitude of primary dehydrogenases, quinones and terminal reductases.⁷⁰⁻⁷²

Figure 1.2: Summary of the reactions of the electron-transport chain of aerobically-grown *E. coli*.



Under aerobic conditions, *E. coli* produces a range of primary dehydrogenases. Membranes isolated from aerobically grown bacteria contain the following respiratory enzymes: succinate dehydrogenase, NADH dehydrogenase, hydrogenase, glycerol-3-phosphate dehydrogenase, formate dehydrogenase, lactate dehydrogenase and D-amino acid dehydrogenase. All of these dehydrogenases contain redox-active prosthetic groups such as flavins, iron-sulfur centers and hemes.⁷¹

Although important, NADH dehydrogenase has a less significant role in bacterial respiration than does its counterpart in mammalian mitochondria. This phenomenon is related to the different predominant catabolic pathways present in *E. coli*. NADH dehydrogenase from *E. coli* has been extensively characterised: it has MW of ~ 47 kD, contains flavin as a prosthetic group, and can rapidly catalyse the reduction of quinones by NADH while translocating protons.⁷⁰

Formate dehydrogenase is induced in *E. coli* under a variety of growth conditions. Although one formate dehydrogenase is present in aerobically grown cells, most of the research has been conducted on the two forms of the enzyme that are present in cultures. Enzymes purified under these conditions consist of three sub-units: α (MW 110 kD), β (MW 32 kD) and γ (MW 20 kD), and also contain cytochrome *b*, iron sulfur centres, a molybdenum cofactor and covalently bound selenium (in the active site). There is also strong evidence that formate dehydrogenase pumps protons across the cytoplasmic membrane.^{70,71}

Hydrogenases catalyse the reversible oxidation of dihydrogen to protons and thus utilise H₂ as a respiratory substrate. *E. coli* has been reported to be able to produce a multiplicity of hydrogenases (two distinct hydrogenases in *E. coli* grown fermentatively

on glucose). Aerobically grown cells contain a membrane-bound hydrogenase with a MW of ~ 56 kD, with an iron-sulfur group and nickel.^{70,71}

Succinate dehydrogenase and fumarate reductase are very similar enzymes that catalyse the interconversion of succinate and fumarate. *E. coli* has two distinct membrane-bound flavin and iron-sulfur containing enzymes. The oxidizing enzyme, succinate dehydrogenase, is a primary dehydrogenase and is part of the tricarboxylic acid cycle. Succinate dehydrogenase activity is present at relatively high levels in membranes derived from cells grown aerobically on mannitol, fumarate, glycerol, succinate, acetate and lactate, but is usually not found at high levels in cells grown in glucose. Succinate dehydrogenase is composed of a flavin and iron-sulfur containing subunit, as well as two hydrophobic subunits. The reducing enzyme, fumarate reductase, functions as the terminal enzyme of certain anaerobic respiratory pathways. Under non-physiological conditions both the succinate dehydrogenase and the fumarate reductase has been shown to catalyse both reactions. However, in aerobically grown *E. coli* only succinate dehydrogenase is normally expressed.^{70,71}

E. coli produces four lactate dehydrogenases and two of them are NADH-linked soluble dehydrogenases. D-Lactate dehydrogenase has a MW of ~ 75 kD with noncovalently bound FAD as a prosthetic group. D-Lactate dehydrogenase also participates in the regeneration of NAD⁺ by reconvertng lactate to pyruvate, thus providing a cyclic system for reoxidation of NADH, independent of the NADH dehydrogenase. L-Lactate dehydrogenase, a primary dehydrogenase, is only induced in cells grown on DL-lactate and is located in the cytoplasmic membrane.^{70,71}

The D-amino acid dehydrogenase expressed in *E. coli* is also a primary dehydrogenase because the enzyme is membrane-bound and does not require the cofactor

NAD⁺. The enzyme consists of two subunits that contain a noncovalently bound FAD, nonheme iron and an iron-sulfur centre. The D-amino acid dehydrogenase is not part of the proton-translocating system, but releases reducing equivalents directly into the quinone pool.⁷⁰

E. coli can produce three distinct glycerol-3-phosphate dehydrogenases, where two are primary respiratory dehydrogenases. These are induced during aerobic growth or growth with nitrate on glycerol or glycerol-3-phosphate. The enzyme has two subunits of MW ~ 35 kD and contains a non-covalently bound FAD as cofactor.^{70,71}

Moreover, *E. coli* and other related enteric bacteria can synthesise three different quinones, ubiquinone as well as the two naphthoquinones, menaquinone and desmethylmenaquinone. In aerobic growth, the major quinone is ubiquinone, which is replaced by menaquinone in the aerobic stationary phase and during anaerobic growth. The lipid soluble quinones function as mobile carrier of hydrogen and of reducing equivalents (electrons) between dehydrogenases and b-type cytochromes.⁷¹ Cytochrome *b* is a membrane-bound component developed under aerobic conditions. Cytochrome *b*₅₅₆ is a hydrophobic cytochrome and an oligomer composed of identical polypeptides, each with a MW of ~ 17 kD. It contains equimolar amounts of heme and polypeptide, but does not bind CO through the axial ligation of histidin to the iron center.^{70,71}

The final electron transfer protein in the bacterial respiratory chain is the cytochrome oxidase complex. These oxidases catalyse the reduction of molecular oxygen by sequentially transferring one, two or four electrons *via* hemes to the enzyme-bound oxygen molecule, thus producing either superoxide (O₂⁻), peroxide (O₂²⁻) or water. Cytochrome *o* is the most widespread cytochrome oxidase in bacteria. Cytochrome *o* is tightly bound to the membrane with reported apparent K_m values for O₂ in the range of

1.4 to 2.4 μM . Cytochrome *o* consists of four subunits with ~ 50 kD and binds strongly to cyanide and CO. Cytochrome *o* also takes part in the proton translocation system. The cytochrome *bd* oxidase is the alternative major oxidase of *E. coli* and is synthesised under low oxygen tension or during *E. coli*'s stationary growth phase. Reported K_m values for oxygen are 0.27, 0.23 and 0.38 μM of the cytochrome *bd* oxidase.⁷⁰ A second cytochrome *bd* has been recently discovered as a bacterial response to nutrient limitations in the surrounding medium.⁷²

In summary, the electron-transport chain of aerobic *E. coli* is composed of many different dehydrogenases and terminal reductases (or oxidases), that are linked by quinones. Regulation of pathways and expression levels for individual enzymes are always in favour of high ATP levels or growth yields. Consequently, the electron-transport chain is a function of its adaptation to environmental and bioenergetic demands.

1.1.7 Thesis Organization

This thesis presents the results of research ultimately aimed at the detection of viable bacteria using electrochemical biosensors. Chapter 2 presents an investigation and optimization of mediated respiration measurements in order to gain a better understanding of physiologically-induced changes in bacterial cells. Chapter 3 shows the dramatic effect of antibiotic compounds on measured ferricyanide reduction rates. Various electrochemical techniques are presented to rapidly assess metabolic changes within the bacterial cell. Chapter 4 is concerned with the optimization of immobilization procedures of the recognition agent (lectins). The final chapter presents the proposed biosensor of this study, consisting of a sensor array that is composed of many electrochemical

transducers. The application of inexpensive and readily available membranes that are modified with lectins will allow the fabrication of disposable transducers at low monetary cost. The rapid assessment of respiratory cycle activity will yield real-time measurements and only detect viable pathogens. Although the sensor array will rely on clinical isolates, it will allow the application of chemometric data analysis methods to facilitate the identification of individual strains within a single bacterial species.

1.2 REFERENCES

1. Turner, A. P. F.; Karube, I.; Wilson, G. S. *Biosensors: Fundamentals and Applications*, Oxford University Press, New York, 1987.
2. Lopez-Avila, V. *Anal. Chem.* 1997, 69, 289R-305R
3. Turner, A. P. F. *Advances in Biosensors*, JAI Press Ltd, London, England, 1991.
4. Clark, L. C. *Ann. NY Acad. Sci.* 1962, 102, 29.
5. Updike, S. J.; Hicks, J. P. *Nature* 1967, 214, 986.
6. Wang, J. *Analytical Electrochemistry*, 2nd Ed., Wiley & Sons, Inc., 2000.
7. Newman, J. D.; Warner, J. P.; Tigwell, L. J.; Turner, A. P. F. *Biosensors - Boldly going into the new millennium*, technical report, Cranfield Biotechnology Centre, Cranfield University, UK, July 2000.
8. Guilbault, G. G.; Montalvo, J. *JACS* 1969, 91, 2164.
9. Cooney, C. L.; Weaver, J. C.; Tannenbaum, S. R.; Faller, S. R.; Shields, D. V.; Janke, M. *Enzyme Engineering*, Eds. E. K. Pye and L. B. Wingard, Plenum, New York, 1974.

10. Mosbach, K.; Danielsson, B. *Biochim. Biophys. Acta* 1974, 364, 140.
11. Voelkl, K. P.; Opitz, N.; Lubbers, D. W. *Fres. Z. Anal. Chem.* 1980, 301, 162.
12. Divis, C. *Ann. Microbiol.* 1975, 126A, 175.
13. Shichiri, M.; Kawamori, R.; Yamaski, R.; Hakai, Y.; Abe, H. *Lancet* 1982, 1129.
14. Liedberg, B.; Nylander, C.; Lundstrm, I. *Sensors and Actuators* 1983, 4, 299.
15. Vidyasankar, S.; Arnold, F. H. *Curr. Opin. Biotech.* 1995, 6, 218.
16. Cunningham, A. J. *Introduction to Bioanalytical Sensors*, John Wiley & Sons, Inc., New York, 1998.
17. Strehlitz, B.; Grundig, B.; Schumacher, W.; Kroneck, P. M. H.; Vorlop, K.-D.; Kotte, H. *Anal. Chem.* 1995, 1996, 68, 807.
18. Dennison, J. J.; Hall, J. M.; Turner, A. P. F. *Anal. Chem.* 1995, 67, 3922-3927.
19. Pariente, F.; Lorenzo, E.; Tobalina, F.; Abruna, H. D. *Anal. Chem.* 1995, 67, 3939.
20. Amine, A.; Alafandy, M.; Kaufmann, J.-M.; Pekli, M. N. *Anal. Chem.* 1995, 67, 2822.
21. Trojanowicz, M.; Hitchman, M. L. *Trends Anal. Chem.* 1996, 15, 38.
22. Besombes, J.-L.; Cosnier, S.; Labbe, P.; Reverdy, G. *Anal. Chim. Acta* 1995, 311, 255.
23. Newman, J. D.; White, S. F.; Tothill, I. E.; Turner, A. P. F. *Anal. Chem.* 1995, 67, 4594.
24. Cass, A. E. G. *Biosensors: A Practical Approach*, Oxford University Press, 1990.
25. Luong, J. H. T.; Guilbault, G. G.; Blum, J.; Coulet P. R. *Analytical applications of piezoelectric crystal biosensors*, in *Biosensor Principles and Applications*, Eds., Marcel Dekker, New York, 1991, pp. 107.

26. Mattiasson, B.; Hakanson, H. *Adv. Biochem. Eng.* 1992, 46, 81.
27. Kaurbe, I.; Nakanishi, K. *IEEE Engineering in Medicine and Biology* 1994, 365.
28. Hobsen, N. S.; Tothill, I. E.; Turner, A. P. F. *Biosens. Bioelectron.* 1996, 11, 455.
29. Ivintski, D.; Abdel-Hamid, I.; Atansasov, P.; Wilkins, E. *Biosens. Bioelectron.* 1999, 14, 599.
30. Lukosz, W.; Clerc, D.; Nellen, P. M.; Weiss, P. *Biosens. Bioelectron.* 1991, 6, 227.
31. Frat Amico, P. M.; Strobaugh, T. P.; Medina, M. B.; Gehring, A. G. *Biotechnol. Technol.* 1998, 12,571.
32. Cush, R.; Cronin, J. M.; Stewaet, W.J.; Maule, C. H.; Molloy, J.; Goodard, N. J. *Biosens. Bioelectron.* 1993, 8, 347.
33. Slots, J.; Reynolds, H. S. *J. Clin. Microbiol.* 1982, 16,1148.
34. Cao, K. L.; Anderson, G. P.; Ligler, F. S.; Ezzel, J. *J. Clin. Microbiol.* 1995, 33, 336.
35. Zhou, C.; Pivarnik, P.; Rand, A. G.; Letcher, S. V. *Biosens. Bioelectron.* 1998, 13, 495.
36. Pyle, B. H.; Broadway, S. C.; McFeters, G. A. *Appl. Environ. Microbiol.* 1995, 61, 2614.
37. Ramanathan, S.; Shi, W. P.; Rosen, B. P.; Daunert, S. *Anal. Chim. Acta* 1998, 369, 189.
38. Suleiman, A. A.; Guilbault, G. G. *Analyst* 1994,119, 2279.
39. Carter, R. M.; Mekalanos, J. J.; Jacobs, M. B.; Lubrano, G. J.; Guilbault, G. G. *J. Immunol. Meth.* 1995, 187, 121.

40. Muramatsu, H.; Kajiwara, K. Tamiya, E.; Karube, I. *Anal. Chim. Acta* 1986, 188, 257.
41. Prusarek-Sochaczewski, E.; Luong, J. H. T.; Guilbault, G. G. *Enzyme Microbiol. Technol.* 1990, 12,173.
42. Ben-Dov, I.; Willner, I.; Zisman, E. *Anal. Chem.* 1997, 69, 3506.
43. Kissinger, P. T.; Heineman, W. R. *Laboratory Techniques in Electroanalytical Chemistry*, 2nd Ed., Marcel Dekker, Inc., New York, 1996.
44. Gehring, A. G.; Patterson, D. I.; Si, T. *Anal. Biochem.* 1998, 258, 293.
45. Silverman, H. P.; Brake, J. M. U.S. Patent 3,506,544 (1970).
46. Ghindilis, A. L.; Atanasov, P.; Wilkins, M.; Wilkins, E. *Biosens. Bioelectron.* 1998, 13, 113.
47. Brooks, J. L.; Mirhabibollahi, B.; Kroll, R. G. *J. Appl. Bacteriol.* 1992, 73, 189.
48. Gehring, A. G.; Crawford, C. G.; Mazenko, R.S.; Van Houten, L. J.; Brewster, J. D. *J. Immunol. Meth.* 1996, 195,15.
49. Mirhabibollahi, B.; Brooks, J. L.; Kroll, R. G. *J. Appl. Bacteriol.* 1990, 68, 577.
50. Mazenko, R. S.; Rieders, F.; Brewster, J. D. *J. Microb. Meth.* 1999, 36, 157.
51. Perez, F. G.; Mascini, M.; Tothill, I. E.; Turner, A. P. F. *Anal. Chem.* 1998, 70, 2380.
52. Abdel-Hamid, I.; Ivnitski, D.; Atanasov, P.; Wilinks, E. *Electroanalysis* 1998, 10, 758.
53. Silley, P.; Forsythe, S. *J. Appl. Bacteriol.* 1996, 80, 233.
54. Swaminathan, B; Feng, P. *Annu. Rev. Microbiol.* 1994, 48, 401.
55. Warwerla, M.; Stolle, A.; Scholch, B.; Eisengruber, H. *J. Food Prot.* 1999, 62, 1488.

56. Colquham, K. O.; Timmis, S.; Fricker, C. R. *J. Appl. Bacteriol* 1995, 79, 635.
57. Dezensclos, T.; Asconcabrera, M.; Ascon, D.; Lebeault, J. M.; Paus, A. *Appl. Microbiol. Biotechnol.* 1994, 42, 232.
58. Palmquist, E.; Berggren, K. C.; Khayyami, M.; Danielsson, B.; Larsson, P.-O.; Mosbach, K.; Kriz, D. *Biosens. Bioelectron.* 1994, 9, 551.
59. Mikkelsen, S. R. *Electroanalysis* 1996, 8, 15.
60. Wang, J.; Rivas, G.; Cai, X.; Palecek, E.; Nielsen, P.; Shiraishi, H.; Dontha, N.; Luo, D.; Parrado, C.; Chicharro, M.; Farias, P.; Valera, F. S. *Anal. Chim. Acta* 1997, 347, 1.
61. Zhai, J. H.; Cui, H.; Yang, R.F. *Biotechnol. Adv.* 1997, 15, 43.
62. Wang, J.; Rivas, G.; Parrado, C.; Xiaohua, C. Flair, M. *Talanta* 1997, 44, 2003.
63. Wang, J.; Rivas, G.; Cai, X. H. *Electroanalysis* 1997, 9, 395.
64. Pasero, E.; Rossetti, C; Aiolfi, F. U.S. Patent 5,348,862 (1994).
65. McConnell, H. M.; Owicki, J. C.; Parce, J. W.; Miller, D. L.; Baxter, G. T.; Wada, H. G.; Pitchford, S. *Science* 1992, 257, 1906.
66. Boe, I.; Loverien, R. *J. Biotechnol. Bioeng.* 1990, 35, 1.
67. Seydel, J. K.; Wempe, E. *Drug Res.* 1980, 30, 298.
68. Takayama, K.; Kurosaki, T.; Ikeda, T. *J. Electroanal. Chem.* 1993, 356, 295.
69. Atlas, R.M. *Principles of Microbiology*, 2nd Edt., Wm. C. Braun Publishers, 1997.
70. Niedhardt, F. C.; Ingraham, J. L.; Low, K. B., Magasanik, B.; Schaechter, M.; Umberger, H. E. *Escherichia coli and Salmonella typhimurium: Cellular and Molecular Biology*, Eds., American Society for Microbiology, Washington, D. C., 1987.

71. Niedhart, F. C.; Uden, G.; Bongaerts, J. *Biochim. Biophys. Acta* 1997, 1320, 217.
72. Loewen, P. C.; Hu, B.; Strutinsky, J.; Sparling, R. *Can. J. Microbiol.* 1998, 44, 707.

Chapter 2

Mechanism and Kinetics of Ferricyanide Reduction by *Escherichia coli*

2.1 INTRODUCTION

2.1.1 Objective

In this Chapter, electrochemical measurements of ferricyanide reduction by *E. coli* is shown to be representative of its respiratory cycle activity. This respiration-based assay can be used to determine cell viability at various stages of growth. The mechanism of ferricyanide reduction and resulting enzyme kinetics were studied during *E. coli* exponential and stationary growth phases. Electrochemical measurements of ferricyanide reduction rates were made on host and recombinant strains of *E. coli*, and these can be used to indicate entry into the stationary growth phase. Two different electrochemical methods, electrochemical flow injection analysis (FIA) and chronoamperometry (CA), were compared for different *E. coli* growth rates and under different assay conditions. Furthermore, the mechanism and kinetics of ferricyanide reduction in the presence of respiratory enzyme co-substrates were investigated during various growth phases of *E. coli*. The effects of varying redox-mediators and their concentrations, as well as cyanide inhibition, oxygen depletion and temperature on ferricyanide reduction rates were studied and results were used to optimize the cell assay.

The results contribute to a better understanding of physiological or stress-induced changes in bacterial cells. Bacterial respiratory cycle activity measurements have been assessed as a rapid tool to indicate bacterial adaptation to a variety of limiting factors, such as carbon source, oxygen, and phosphates.

2.1.2 Introduction

The estimation of cell viability is a very active and diverse area of research and is of importance to basic and applied science. Traditionally, viability has been measured by counting the number of colony forming units (cfu) when diluted cell culture samples are allowed to reproduce on nutrient agar plates, and comparing this number to the total cell count.^{1,2} However, numbers obtained using this method often underestimate viability, due to the presence of viable but nonculturable cells.^{3,4} As a result, a variety of other principles has been shown to estimate cell viability. These include staining methods that allow the detection of membrane integrity⁴⁻⁸ or the activities of certain enzymes^{9,10} and a method based on the measurement of average cell size before and after exposure to a cell division inhibitor such as nalidixic acid.¹¹

These methods are undeniably time-consuming because long incubation periods are necessary prior to measuring the extent of microbial reproduction. Respiration measurements are inherently faster and can also form the basis for a variety of methods for determining cell viability and metabolic rates.¹²⁻¹⁸

In research and industrial settings, microbial growth is monitored and controlled to maximize the yield of native or recombinant proteins. Here, cell viability is of particular concern because potent recombinant expression systems can exhaust the metabolic capacity of the host cell, which consequently leads to cells death through over-expression of the recombinant protein.⁷⁴ Stress induced cell death ultimately limits recombinant protein or antibiotic production in industrial fermentation processes.

Chemostats contain *in situ* sensors that allow the control of pH and dissolved oxygen levels during cell cultivation. Additional off-line measurements of biomass and

medium composition commonly form the basis for time dependent induction of recombinant protein expression.^{19,20} In aerobic fermentation, bacterial growth rate is proportional to its specific respiration rate, which is the rate of oxygen consumption divided by cell density or biomass.¹⁹⁻²¹ Strong evidence suggests terminal oxygen reduction is the rate-limiting step in the overall growth of batch cultures.^{22,23} Respiration during aerobic fermentation can be controlled by varying agitation or airflow rates, in order to maintain a constant dissolved oxygen level, regardless of cell density.^{19,21}

Aerobic respiration in *E. coli* results from a number of parallel paths, as described in Chapter 1 section 1.6. These paths eventually converge in the cytoplasmic membrane at the terminal oxidase shortly after electron transfer reactions that are catalysed by membrane-bound primary dehydrogenases.²⁴⁻²⁸ A great deal has been learned within the past decade about the components of the *E. coli* respiratory chain²⁴⁻²⁶ and its regulation.^{27,28} It is now known that the transition from the exponential to stationary growth phase triggers significant changes in protein expression within cells.

During batch culture growth, *E. coli* eventually depletes its surrounding medium of at least one essential nutrient. The limiting nutrient may be the source of carbon (such as glucose or glycerol), nitrogen or phosphate. However, oxygen depletion of cultures can occur with rapidly growing exponential phase cultures in shake-flasks, where levels of dissolved oxygen are not controlled.

Depletion of any one of these nutrients triggers the production of a different sigma subunit (σ^S) for the enzyme RNA polymerase. This subunit is believed to change the enzyme binding selectivity for promoter sequences in the *E. coli* genome, thus altering the relative expression levels of promoted genes.²⁹ The transition from the

normal σ^D subunit, present during exponential growth, to about 30% σ^S has been found in stationary phase cultures.²⁹ The increase of σ^S has been shown to cause increased production of certain respiratory enzymes, including pyruvate oxidase, glycerol-3-phosphate dehydrogenase and the recently discovered cytochrome *bd* II oxidase, as well as various outer membrane and periplasmic proteins. The latter response allows cells to survive nutrient limitation and to change their physiology to provide maximal protection against diverse stress conditions.^{27,28}

E. coli, as well as other Gram-negative microorganism, can directly reduce non-native, hydrophilic oxidants such as ferricyanide.³⁰⁻³² The terminal components of the Gram-negative respiratory chain are associated with the inner (cytoplasmic) membrane,²⁴ but are accessible to small, hydrophilic oxidants like ferricyanide, because the outer membrane contains channel proteins (porins) that allow free diffusion of low-molecular weight species (MW \leq about 1 kD) into the periplasmic space.³³

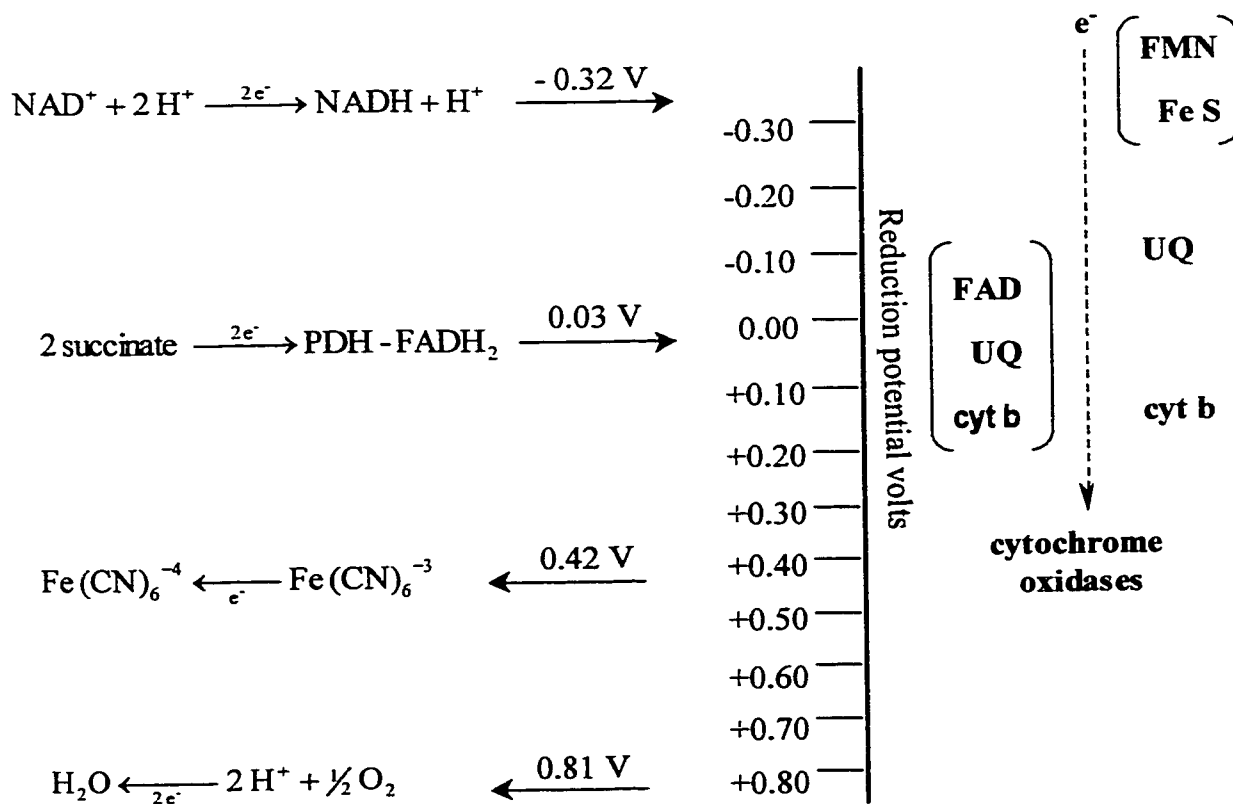
Respiration has been quantitated in aerobic, anaerobic, prokaryotic and eukaryotic cells as well as in specialised tissues, using a variety of non-native oxidants such as ferricyanide,^{30-32,34-38} ferric chelates,³⁹ 2,6-dichlorophenolindophenol (DCIP),^{37,38,40,41} phenazine and phenoxazine derivatives,^{36,42,43} benzoquinone^{36,37,44} and quinone derivatives,^{32,17} and methyl viologen.⁴⁵ These compounds possess appropriate reduction potentials and are readily quantitated in their reduced forms.

Mediated respiration measurements, such as colorimetric assays, have been used to determine cell viability by measuring the extent of dye reduction as indicated by the appearance or disappearance of an absorbance signal.⁴⁶ An example of this principle involves colourless tetrazolium salts which can be reduced to coloured formazan dyes

through respiration. Nevertheless, drawbacks include the toxicity and insolubility of formazan dyes and their low colour intensities.¹²

Combinations of oxidants are sometimes used where a hydrophobic membrane permeable mediator at a low concentration is combined with a hydrophilic terminal acceptor present at a higher concentration. The hydrophobic mediator accumulates in the bacterial membrane and is used to shuttle electrons from the site of the respiratory chain through the cell membrane. One example of such a combination is DCIP and ferricyanide, a combination that has been used with *E. coli* O157³⁸ and beer yeasts.⁴⁷ Electrochemical measurements of direct ferricyanide reduction by suspensions of *E. coli* have also been reported.^{30-32,38,48} The reduction potential of the ferri-/ferrocyanide redox couple (+ 0.418 V vs. NHE⁴⁹) is positive in relation to all components of the respiratory chain oxidase (Figure 2.1), suggesting that any of the preceding primary dehydrogenase reactions may contribute to observed ferricyanide reduction. *E. coli* studies have shown that additions of glucose, succinate, lactate and formate can increase observed ferricyanide reduction rates; similar effects have been observed with other microorganisms.⁴⁸ Electrochemical respiration measurements have been used in cell-based biosensors developed to quantitate metabolizable substrates^{36,41,44,48,50} and also in living fuel cells, where respiration generates a spontaneous current.^{39,40,51} Cells grown on a certain substrate are immobilised on an electrode surface to construct mediated enzyme-based biosensors that respond to that substrate. Substrate exposure induces high concentrations of the substrate-metabolising enzyme which is selective to the substrate.⁵² The stabilising, natural environment of enzymes (cytoplasm of cells) found in these electrodes was of great interest to scientists.

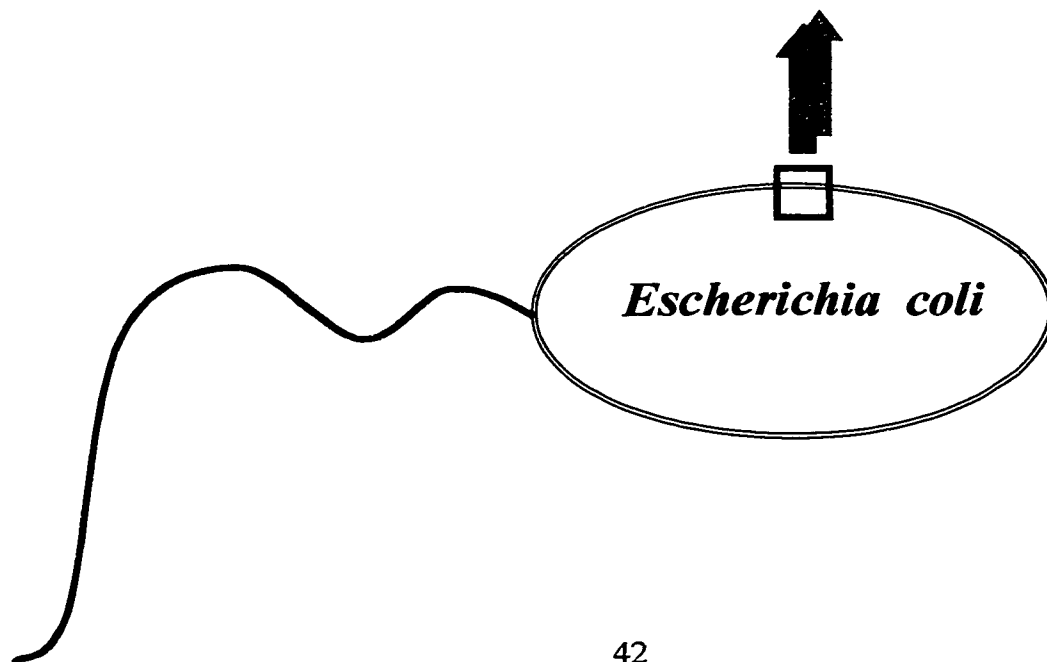
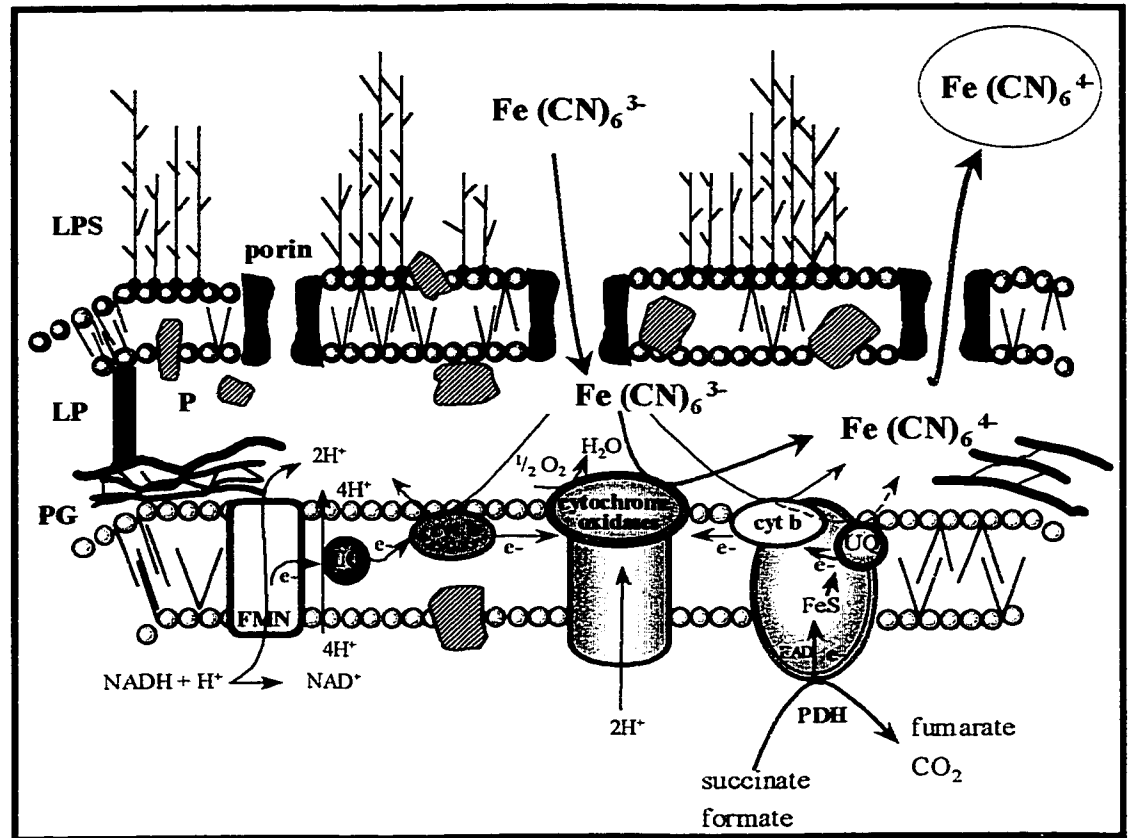
Figure 2.1: Schematic presentation of some electron donors and acceptors of the respiratory chain of aerobically grown *E. coli* with their reduction potentials.



Their presence in the natural environment were thought to contribute to the enhanced operational and storage ability of the sensors in comparison with simple immobilised enzyme biosensors.⁵³ Ferrocyanide concentrations are readily measured by amperometry or potentiometry^{30,37,38,54,55} and its concentration increase over time is directly related to microbial respiratory cycle. As outlined in Figure 2.2 ferricyanide can diffuse into the periplasmic space through porin proteins and thus interact with inner membrane-bound redox enzymes and cytochromes. Consequently, the iron (III) form of ferricyanide is reduced to its iron (II) form (ferrocyanide), which diffuses out of the cell towards areas of lower ferrocyanide concentration.

When recombinant protein expression is induced in *E. coli*, the effect is similar to entrance into the stationary growth phase, since the cellular metabolic machinery shifts from its normal reproductive pathways towards the synthesis of a metabolically irrelevant product.^{29,51,56,57} As a result of this metabolic shift, cells effectively experience starvation, in particular if a strong promoter is attached to the inserted gene.⁵⁶ A recent study has shown that recombinant protein overexpression causes an accumulation of two proteins normally produced during heat shock response.⁵⁷ Furthermore, a separate study showed that *E. coli* subjected to heat shock (40°C) produced the same sigma subunit for RNA polymerase (σ^S) as is normally produced upon entry into the stationary growth phase.²⁹ The ultimate effect of this transition on a recombinant organism is cell death due to ribosome destruction,⁵⁷ although its effect on the quality and quantity of recombinant protein has not yet been investigated.

Figure 2.2: Schematic presentation of a Gram-negative bacterial cell wall featuring the electron transport chain. Proposed mechanism of ferricyanide reduction can be seen in the enlarged box.



2.1.3 Preceding Work

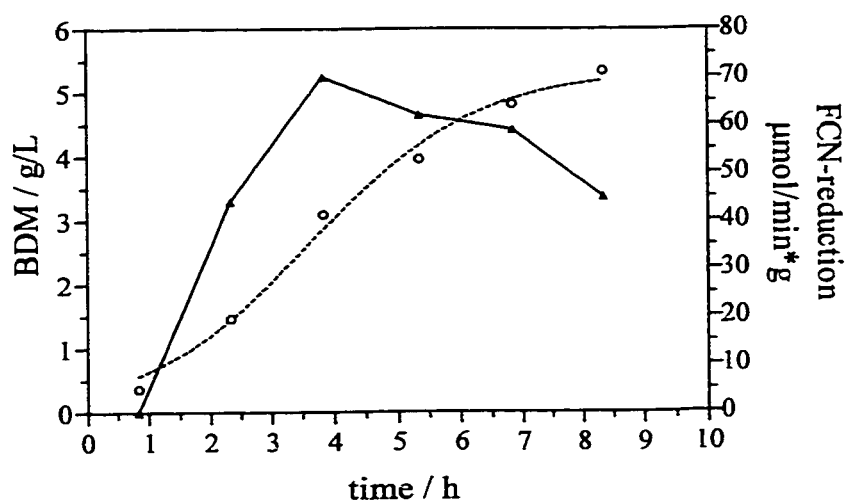
An investigation of ferricyanide reduction on a recombinant strain of *E. coli*, engineered to express human Cu/Zn superoxide dismutase, was conducted by Dr. S. R. Mikkelsen at the Institute of Applied Microbiology, State University of Agricultural Sciences, Vienna Austria. Since this viability assay is based on Dr. Mikkelsen's investigation, it is necessary to present an overview of her results.⁵⁸

Electrochemical measurements were initially performed with flow injection analysis and ferricyanide reduction rates were obtained from *E. coli* HB101 samples taken from three replicate aerobic batch fermentations conducted in shake flasks. Maximal ferricyanide reduction activity occurred during exponential growth phase (cells respire maximally) and a slow decline was observed as the cultures entered the stationary phase. These results were typical of all obtained from shake-flask experiments, which lack control of pH and dissolved oxygen concentration. The FIA method showed maximal specific reduction rates with late exponential phase grown *E. coli* of 36 ± 4 $\mu\text{mol}/\text{min}\cdot\text{g}$ ($n = 3$).

The same strain of *E. coli* was also grown in a batch culture using a chemostat to control pH and dissolved oxygen. The shape of the ferricyanide reduction curves was found to be identical to those observed for shake-flask cultures with a mid-exponential phase maximum. This was followed by a decline in the specific respiration rate as soon as the cell entered the stationary phase (see Figure 2.3). However, the magnitude of the maximal specific respiration rate is much higher under controlled conditions, reaching a value of $70 \mu\text{mol}/\text{min}\cdot\text{g}$, compared to the value of $36 \mu\text{mol}/\text{min}\cdot\text{g}$ obtained under shake-flask culture conditions. Controlling pH and dissolved oxygen concentrations revealed a

two-fold increase in ferricyanide reduction rates with this organism. The two-fold increase demonstrates that control of pH and dissolved oxygen concentration significantly increases ferricyanide reduction rates. Under these conditions, the higher availability of dissolved oxygen in the growth media results in maximum expression levels of the cytochrome *o* oxidase during exponential growth phase of *E. coli*.

Figure 2.3: Growth curve of bacterial dry matter (dashed lines) and specific ferricyanide reduction rates (solid line) obtained for a batch chemostat cultivation of *E. coli* HB101 using flow injection analysis.

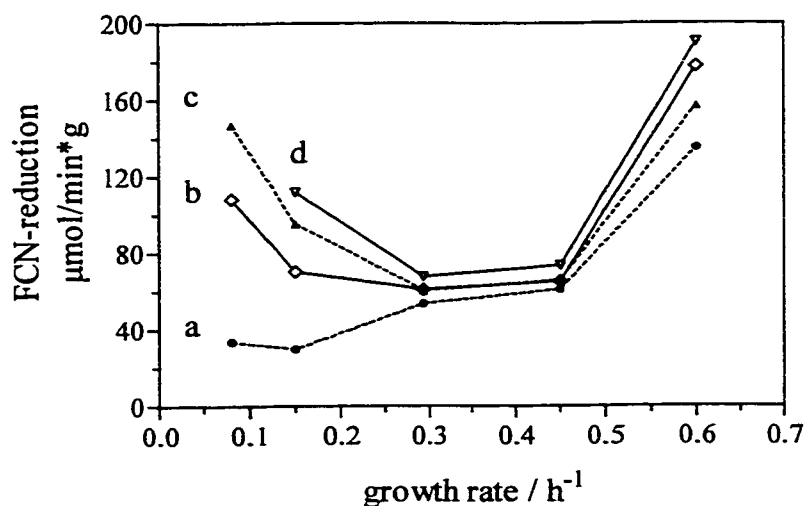


Continuous cultures of *E. coli* HB101 were also examined to allow control of bacterial growth rate, in order to compare conditions between exponential (high growth) and stationary (slow growth) rates. Various respiratory substrates were tested in preliminary experiments using 5-minute incubation periods with 10 mM substrate prior to ferricyanide addition. The tested substrates included glucose, pyruvate, succinate, formate, glycerol-3-phosphate, proline, lactate, acetate and malate, using cultures with

growth rates of 0.5 h^{-1} and above. Glucose, proline, and glycerol-3-phosphate yielded small increases above the control value, which was obtained in the absence of substrate (the largest was glucose with an 8% increase). Meanwhile, succinate and formate increased the control rate by 40% and 51%, respectively. Notably, NADH was not investigated due to anticipated interference with electrochemical measurements.

Figure 2.4 shows a plot of specific ferricyanide reduction rate compared to growth rate for *E. coli* HB101, where measurements were made using FIA in the absence and presence of succinate and formate. As expected, the presence of the above substrates caused increasing ferricyanide reduction.²²

Figure 2.4: Specific ferricyanide reduction rate by FIA as a function of continuous culture growth rate for *E. coli* HB101, following 5 min incubation in the absence (a) and presence of (b) 10 mM succinate, (c) 10 mM formate, and (d) 10 mM succinate plus 10 mM formate.



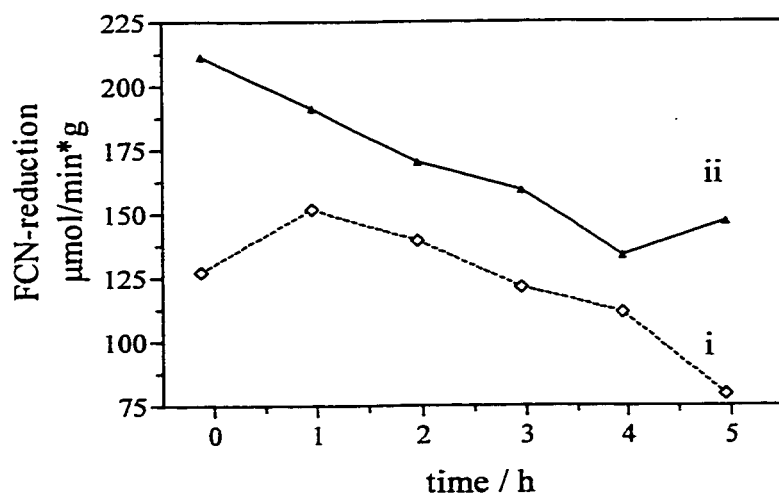
Incubation with the respiratory substrates succinate and formate, displayed small differences in their signals at higher growth rates when compared to controls lacking additives. On the other hand, differences were readily apparent at lower growth rates, where reduction rates increased significantly following incubation in succinate and formate. These results suggest that significant changes in protein expression occur when growth rates for this organism drop below 0.3 h^{-1} .

A second continuous culture of *E. coli* HB101, with a growth rate (μ) of 0.3 h^{-1} , was used to examine the concentration dependence of the ferricyanide reduction rates obtained in the presence of formate and succinate. The results indicate that specific ferricyanide reduction rates are concentration-dependent because small increases in succinate and formate concentrations yield a substantial respiratory signal increase (10 to 100-fold). It should be noted that intracellular concentrations of the above compounds after a 5-minute incubation period are not known.

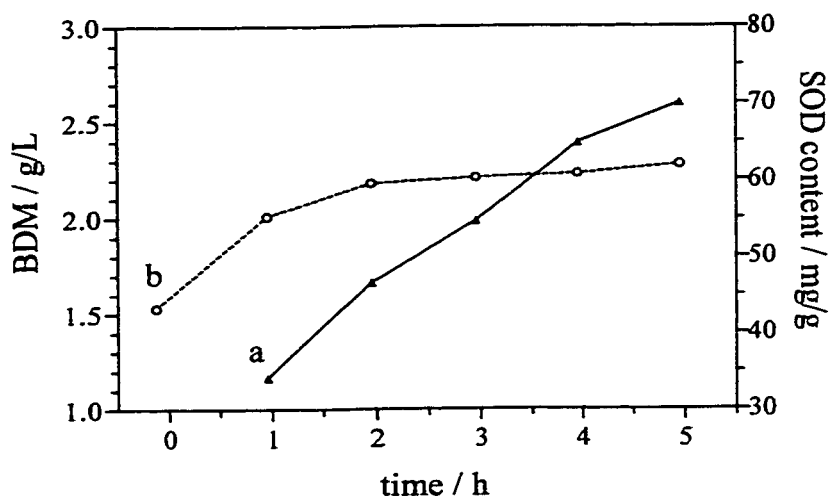
To further investigate the difference between exponential and stationary phase behavior, a separate experiment was undertaken in which *E. coli* HB101 was cultured in a fermentor under pH and oxygen-controlled conditions. Subsequently, a continuous culture with a slow growth rate of 0.08 h^{-1} was established. Samples taken from this culture (3 x 15 mL) were diluted 1:1 in shake-flasks using a fresh medium containing no glucose. Following a 3h incubation period at 37°C and 200 rpm, samples were once again collected and chilled. Results obtained *via* FIA yielded a specific ferricyanide rate of $10 \pm 3 \mu\text{mol}/\text{min-g}$ in the absence of respiratory substrates. Incubation in the presence of 10 mM succinate conveyed a specific reduction rate of $90 \pm 7 \mu\text{mol}/\text{min-g}$.

Observed differences in ferricyanide reduction in the presence of succinate and formate during the transition from the exponential to stationary phase in *E. coli* encouraged the investigation of metabolic shifts in recombinant batch fermentation. In this experiment, recombinant human Cu/Zn superoxide dismutase (SOD) was produced by *E. coli* strain HMS174 (DE3)(pET3ahSOD). This organism was grown to late exponential phase prior to induction of SOD expression by the addition of IPTG to the fermentor. Figure 2.5 shows the results of the FIA assay performed in the absence and presence of a succinate/formate mixture along with SOD activity and bacterial dry matter determinations. It is evident that the amount of biomass becomes constant at a value of about 2.2 g/L two hours after induction, while a steady increase in SOD activity was simultaneously observed. After an incubation period of 5 h, values of 70 mg SOD/g protein were observed. However, specific ferricyanide reduction rates showed steady decreases in values within 1 – 4 h following induction. After 5 h, stationary-phase like behavior is observed, and can be seen in the difference in respiratory cycle activities measured in the absence and presence of succinate and formate. These results indicate that cells have initiated the heat-shock/stationary phase entry response that ultimately causes ribosome destruction and cell death.^{29,51,56,57,74} The high specific SOD activity present at this point suggests that under these culture conditions, optimal harvesting of SOD would take place 4 h after induction.

Figure 2.5: Recombinant production of human Cu/Zn superoxide dismutase by *E. coli* HMS174(DE3)(pET3ahSOD) as a function of time following induction:
 (a) Specific ferricyanide reduction rate (FIA) obtained in the (i) absence and (ii) presence of 10 mM succinate and 10 mM formate.



(b) SOD content per gram total protein (a), from ELISA and bacterial dry matter values (b) obtained for samples taken during this cultivation.



2.2 EXPERIMENTAL SECTION

2.2.1 Materials and Instrumentation

Potassium hexacyanoferrate (II), potassium hexacyanoferrate (III), cobalt (II) chloride hexahydrate, D-(+)-glucose monohydrate and sodium L-lactate were obtained from Fluka. Anthraquinone-1-sulfonate, 1,4 benzoquinone, Janus Green B and 2,3-dimethoxy-5-methyl-1,4-benzoquinone were obtained from Aldrich. Potassium cyanide and glycerol were purchased from BDH. Succinic acid, sodium formate, dipotassium hydrogen phosphate trihydrate, potassium dihydrogen phosphate, trisodium citrate dihydrate, magnesium sulfate heptahydrate, calcium chloride dihydrate, ammonium chloride, ammonium sulfate, extract of yeast powder, (No. 3753), sodium hydroxide, potassium hydroxide, iron(II) sulfate heptahydrate, manganese(II) sulfate monohydrate, aluminum chloride hexahydrate, zinc(II) sulfate heptahydrate, disodium molybdate dihydrate, copper(II) chloride dihydrate, sodium chloride and boric acid were supplied by Merck. Difco provided bacto-tryptone powder. Solutions and media were prepared using distilled, deionized water.

Escherichia coli JM105 was obtained from the strain collection of the Department of Biology, University of Waterloo.

Fermentations conducted in shake flasks were maintained at 37°C and 200 rpm in a water bath shaker supplied by New Brunswick Scientific. Optical density measurements were made at 600 nm using a Cary 1 double-beam uv-visible spectrophotometer.

The flow injection system used with *E. coli* JM105 samples consisted of a Waters Model 510 HPLC pump with a Rheodyne 7125 Injector (20 µL sample loop) and a thin-layer amperometric detector (E. G. & G. Princeton Applied Research Model 400 with

glassy carbon working, Ag/AgCl reference and stainless steel auxiliary electrodes). The mobile phase flow rate was set to 0.3 mL/min.

Electrochemical measurements were performed using a PAR Model 263 Potentiostat with a glassy carbon rotating disk electrode at 600 rpm (PAR Model 616) at + 0.8 V vs an Ag/AgCl reference electrode (Bioanalytical Systems), using a stainless steel auxiliary electrode.

2.2.2 Methods

2.2.2.1 Cultivation of *E. coli* JM105

A stock solution of trace elements for growth media was prepared in 5 N HCl (Merck) and contained the following compounds: FeSO₄·7H₂O (40 g/L), MnSO₄·H₂O (10 g/L), AlCl₃·6H₂O (10 g/L), CoCl₂·6H₂O (4 g/L), ZnSO₄·7H₂O (2 g/L), Na₂MoO₄·2H₂O (10 g/L), CuCl₂·2H₂O (1 g/L) and H₃BO₃ (0.5 g/L).

The growth medium contained the following components: KH₂PO₄ (2.88 g/L), K₂HPO₄·3H₂O (5.76 g/L), tryptone (2.4 g/L), yeast extract (1.2 g/L), trisodium citrate dihydrate (1.2 g/L), MgSO₄·7H₂O (0.48 g/L), CaCl₂·2H₂O (0.048 g/L), (NH₄)₂SO₄ (1.63 g/L), NH₄Cl (1.34 g/L), glucose (13.2 g/L) and 240 µL of the trace element stock solution per liter of medium. Glucose was prepared as a concentrated aqueous solution, sterilized separately and added to the growth medium prior to inoculation. Cultivations were performed by adding of 1 mL of 1:1 glycerol:cell culture mixture that had been stored at -80°C to 50 mL of growth medium in a shake flask. Growth proceeded for a maximum of 10 h in an incubator shaker at 37°C and 200 rpm.

2.2.2.2 Sample Collection

Cultivations in shake-flasks were sampled periodically by transferring 1-2 mL to Eppendorf tubes and chilling the samples to 0°C for a minimum of 10 min.

2.2.2.3 Determination of Optical Density

A measured aliquot (1 mL) of the cell suspension was centrifuged at 14,000 rpm for 10 min (Microfuge E, Beckman). The supernatant was removed and the pellet was reconstituted by the addition of 1 mL distilled water. Sample dilution factors ensured the measured optical density (600 nm) was between 0.1 and 0.8, using distilled water as a reference.

2.2.2.4 Determination of Bacterial Dry Matter (BDM)

Once culture samples (10 mL) were centrifuged (5,000 rpm, 10 min; Beckman Model J2-21) the supernatant was decanted and the pellets were twice resuspended in 10 mL water and recentrifuged. At this point, washed cells samples were quantitatively transferred to a preweighed beaker, dried at 105°C, cooled in a dessicator and weighed again.

2.2.2.5 Determination of Colony Forming Units (cfu)

Bacterial cells were harvested in the exponential phase and 100 µL aliquots of 1 mL samples were diluted in buffer (medium lacking proteins, glucose and trace elements). Aliquots (100 µL) of each dilution step were transferred and spread equally on to agar plates and incubated for 24 h at 37°C. Cell counts on agar plates showing 0-5, 5-50, 50-100 and 100-500 cells were used to calculate the cfu/mL in the original cell suspension.

2.2.2.6 Flow Injection Analysis (FIA)

The FIA mobile phase was identical to the *E. coli* growth medium, except that no glucose, trace elements, tryptone or yeast extract were present. Using an ice bath, cell

culture samples were cooled down to 0°C for a minimum of 10 min prior to sample preparation. Unless otherwise indicated, 200 µl of cell suspension were centrifuged at 14,000 rpm for 1 min. The supernatant was discarded, the walls of the tube were carefully dried and the cells were resuspended in 700 µL of mobile phase by vortexing for 30 s and incubating at ambient temperature (25°C) for 270 s (total incubation of 5 min). A potassium ferricyanide solution (700µL, 10.0 mM K₃Fe(CN)₆ dissolved in mobile phase) was then added to the sample and vortexed. With the working electrode poised at + 0.8 V vs Ag/AgCl, three injections of this mixture were made at 180 s intervals. Injections of standard 5 µM ferrocyanide solutions were made before and after each experiment. Linearity up to a concentration of 500 µM standard ferrocyanide was periodically checked.

2.2.2.7 Chronoamperometry (CA)

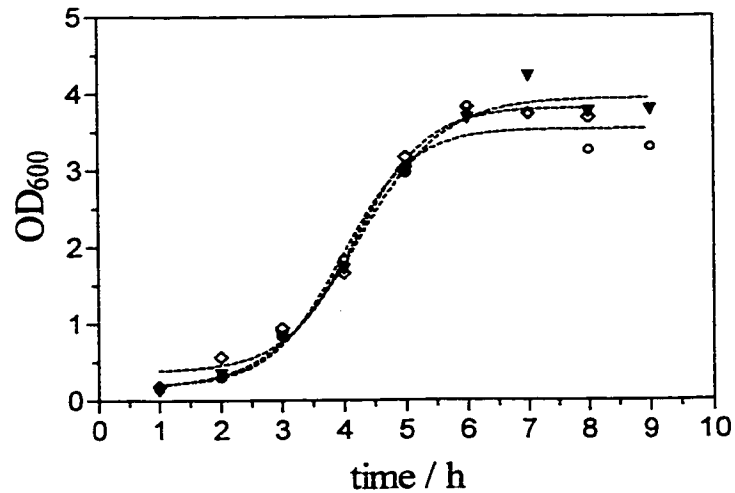
Background current was allowed to stabilise in each chronoamperometric experiment for up to 5 min prior to bacterial sample injection into 100.0 mL of buffer containing 5mM ferricyanide (the buffer is identical to the flow injection mobile phase). Prior to injection, bacterial samples were cooled down to 0°C (>10 min), centrifuged and resuspended in buffer. The signal was recorded continuously for about 15 min following addition of the *E. coli* sample. Calibrations were performed using potassium ferrocyanide over the 0 – 100 µM concentration range.

2.3 RESULTS AND DISCUSSION

Optical density (OD₆₀₀) values of bacterial samples harvested in the exponential phase were correlated to the biological dry matter (BDM in g/L) and colony forming units (cfu).

Figure 2.6 shows three typical sigmoid shaped *E. coli* JM105 growth curves exhibiting the lag phase (within first 3 h), followed by the exponential phase (from 3rd to 6th h) and the stationary phase (between the 6th and 9th h) of cultivation.

Figure 2.6: Growth curves of optical density measured at 600 nm from aerobically grown *E. coli* JM105 in shake-flasks obtained on consecutive days. Each point is the average value of four replicate measurements.



BDM values can be calculated from OD₆₀₀ values using the following equation (Eq. 2.1) obtained from the calibration plot in Figure 2.7.

$$OD_{600} = 0.02 \pm 0.04 + 1.56 \pm 0.03 \times BDM (g/L) \quad 2.1$$

The calibration curve was obtained by comparing optical densities at 600 nm to dry matter (g/L) values derived from a series of cell sample dilutions. Linear regression for the values in Table 2.1 shows a linear fit (r^2) of 0.993 with a calibration slope of 1.56 ± 0.03 ($n = 17$). For example, a bacterial cell culture harvested after 5 h with an OD_{600} of 2.0 ± 0.1 ($n = 4$), is converted into a BDM of 1.27 ± 0.07 g/L, thus yielding a RSD 6 %.

In addition, colony-forming units (cfu) were obtained after a series of cell dilutions were allowed to grow on agar plates (triplicate) overnight at 37°C. Agar plate cell counts yielded $5.4 \pm 0.4 \times 10^8$ cfu / mL ($n = 5$) for an OD_{600} of 3.3 ± 0.2 ($n = 6$). Hence the conversion of OD_{600} values to colony forming units is done with the Equation 2.2.

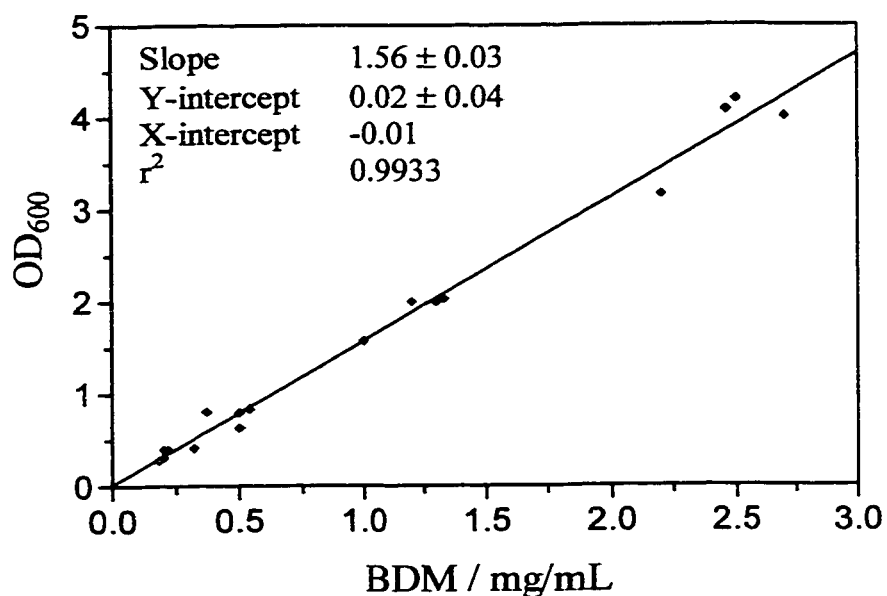
$$\text{cfu / mL} = \frac{OD_{600}}{3.3 \pm 0.2} \times 0.54 \pm 0.04 \times 10^9 \quad 2.2$$

For example, a bacterial cell culture harvested after 5 h with an OD_{600} of 2.0 ± 0.1 ($n = 4$) is converted into 0.33×10^9 cfu/mL, thus yielding a RSD of 10%.

Table 2.1: Biological dry matter and corresponding optical density values for the plot shown in Figure 2.7.

OD ₆₀₀	0.28	0.40	0.317	0.40	0.42	0.81	0.80	0.63
BDM g/L	0.18	0.20	0.20	0.22	0.32	0.37	0.50	0.50
OD ₆₀₀	0.84	1.58	2.00	2.00	2.04	3.27	4.00	4.10
BDM g/L	0.54	1.00	1.20	1.30	1.33	2.20	2.46	2.50

Figure 2.7: Plot of optical densities and biological dry matter, BDM (g/L), values found for each OD₆₀₀ value.



2.3.1 Flow Injection Analysis

Figure 2.8 shows the instrumental set-up where aliquots of the assay mixture are injected into the FIA system for the determination of ferricyanide reduction rates during growth of *E. coli* JM105. This experimental approach disregards the separation of bacterial cells from the reagent solution prior to injection and thus simplifies the preparation procedure. A volume of 20 μL in the injection loop is preferred over the other tested loops of 50 μL and 100 μL to achieve reproducible and repeatable results within the detector range. Under these assay conditions, maximum signals from the assay mixture corresponded to ferrocyanide concentrations below 10 μM . Figure 2.9 shows that excellent linearity ($r^2 = 0.999$; $n = 22$) is obtained with a ferrocyanide concentration range of 0.2 to 50 μM . Each measurement includes five injections, as shown in Figure 2.10, representing two standard ferrocyanide injections bracketing the three timed injections of the *E. coli* assay mixture. Figure 2.10 also shows a typical FIA measurement obtained for a 6 h cell culture ($\text{OD}_{600} = 2.97$). The increase in current with time was used to calculate the rate of increase in ferrocyanide concentration. Specific reduction rates normalised for bacterial dry matter are calculated with the following equation:

$$\text{spec. activity } (\mu \text{ mol/min} \cdot \text{g}) = \frac{\text{raw rate} \times V_{\text{total}} \times d}{\text{BDM} \times V_{\text{bac}}} \quad 2.3$$

where:

raw rate	increase of ferrocyanide over time, $\mu\text{mol/L}\cdot\text{min}$
V_{total}	total volume of the assay mixture, L
V_{bac}	volume of the cell suspension, L
BDM	bacterial dry matter, g/L
d	dilution factor

Figure 2.8: Schematic of electrochemical set-up of the flow injection analysis system having a stainless steel counter (CE) and a carbon working electrode (WE) that is poised at + 0.8 V vs. Ag/AgCl reference electrode.

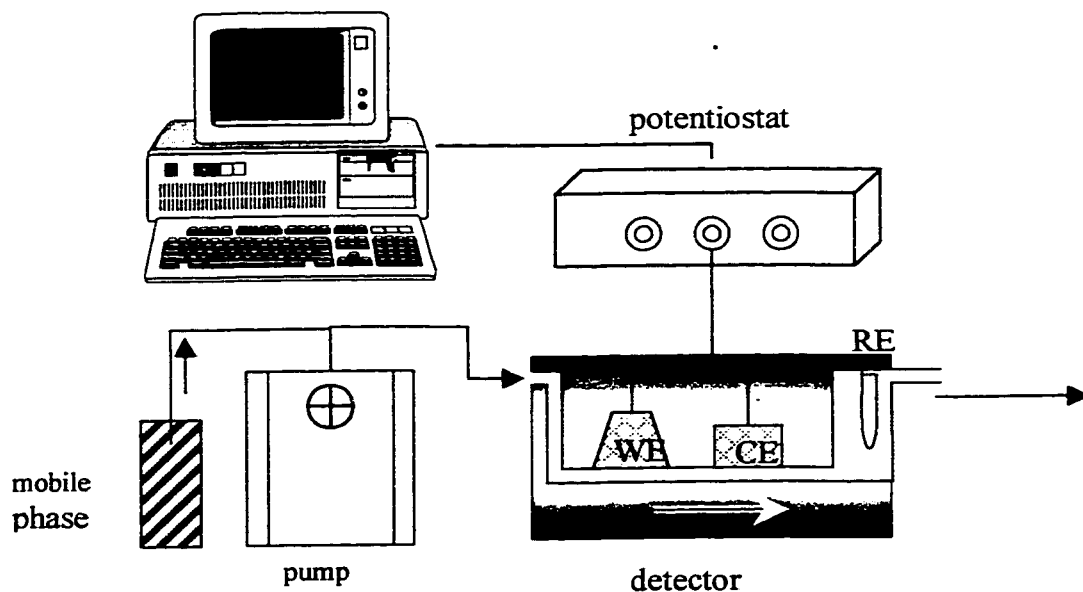


Figure 2.9: Flow injection analysis responses obtained for increasing ferrocyanide concentration.

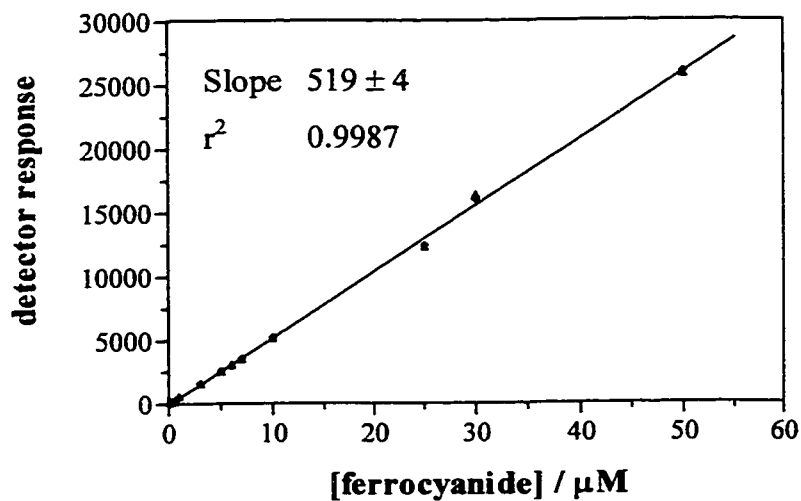
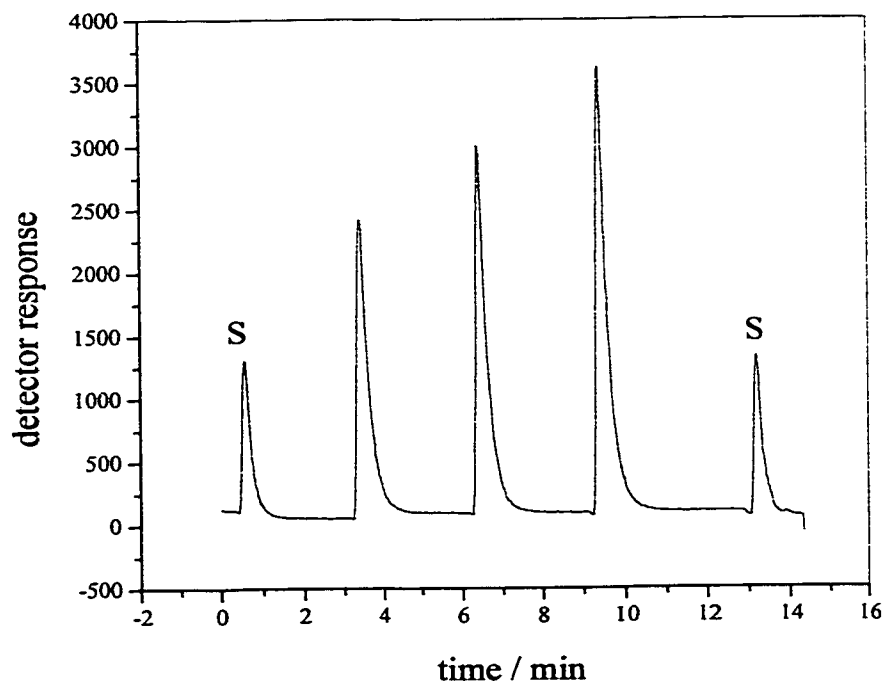


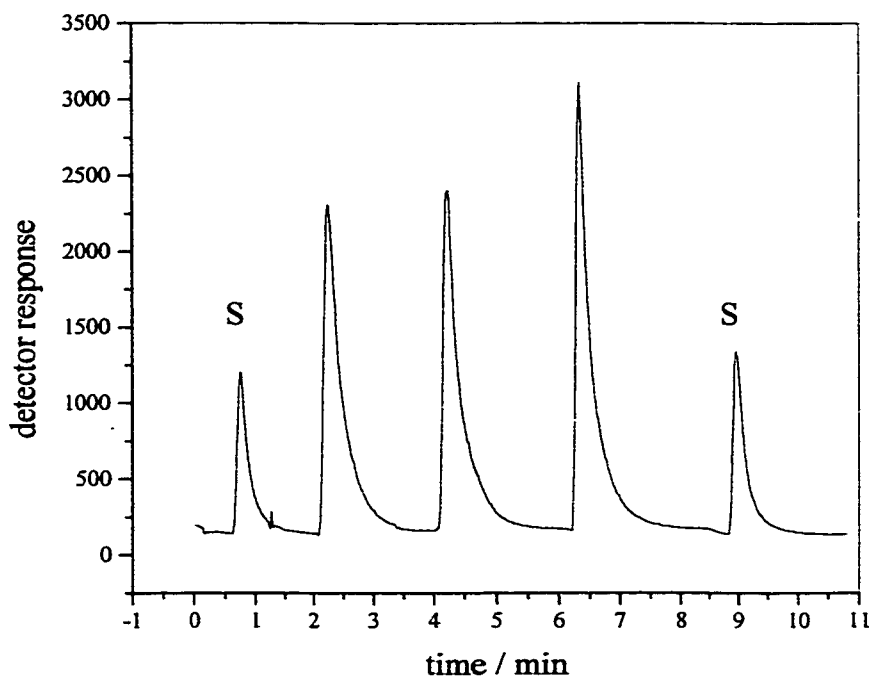
Figure 2.10: Flow injection raw data obtained for exponential phase *E. coli* JM105 ($OD_{600} = 2.97$). Concentrations of ferrocyanide standards (S) are $5.32 \mu\text{M}$ and cell samples are injected at three-minute intervals.



Ferrocyanide standard peaks at the beginning and end of each measurement were used to check for changes in sensitivity due to possible electrode fouling, and to correlate detector signals to ferrocyanide concentration. Cell samples with a measured OD_{600} higher than 2.0 (cells at the mid-exponential phase) had to be diluted prior to injection into the FIA system in order to keep response signals within the detector range ($0.2 - 50 \mu\text{M}$ ferrocyanide). This feature clearly illustrates the low detection limit of this method, which allows measurements at very low OD_{600} or cfu numbers.

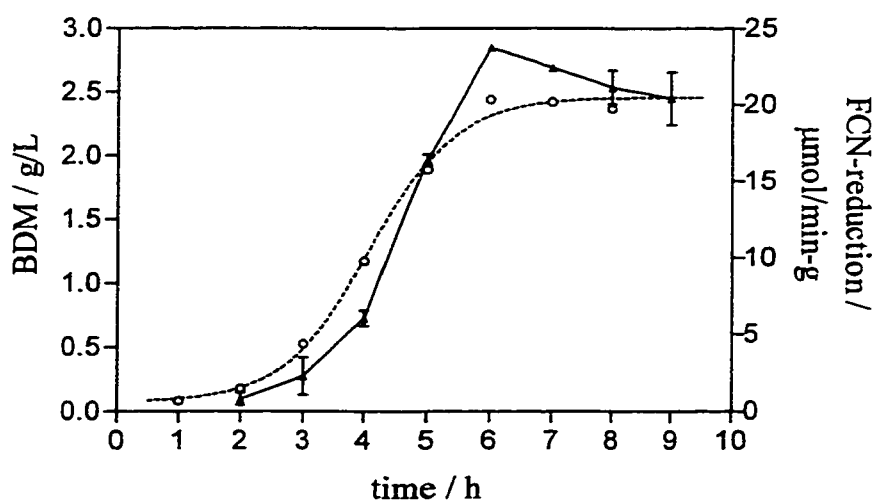
Cell samples were injected during 2 min intervals in an attempt to decrease analysis time. On several occasions, we found identical reduction peak heights for the two initial cell samples injected as illustrated in Figure 2.11. This led to the conclusion that not all reduction sites of the multi-enzyme complex in the bacterial cell wall are fully saturated with ferricyanide within this short period of time. Consequently, samples of the cell assay mixture were injected after 3, 6 and 9 min exposure to ferricyanide.

Figure 2.11: FIA assay data of cell samples ($OD_{600} = 1.66$) injected at two-minute intervals. Concentrations of ferrocyanide standards (S) are $5.02 \mu\text{M}$.



The catalytic behaviour of *E. coli* throughout an entire growth curve is shown in Figure 2.12. As long as the cells remained in the lag-phase (first 3 h) adapting to the new medium and environmental conditions, the specific ferricyanide reduction rate was low. As soon the cells entered the exponential phase (3rd – 6th h), where cells grow with maximum speed due to unlimited nutrients present in the medium, the ferricyanide reduction rate increased to a maximum at the end of the exponential phase; values then decreased over time in the stationary phase. The maximal reduction rate in this FIA experiment was 24 $\mu\text{mol}/\text{min-g}$ and was found at $\text{OD}_{600} = 3.8$ or BDM 2.44 g/L (late exponential-phase). This type of curve, with a late exponential-phase maximum, has also been observed for oxygen uptake rates.²²

Figure 2.12: Growth curves of biological dry matter (dashed line) and specific ferricyanide reduction rate obtained by flow injection analysis (solid line) for a shake-flask culture of *E. coli* JM105.



2.3.2 Chronoamperometry with RDE

Chronoamperometry is a potential-step technique where the excitation signal is a step change in applied voltage. The initial potential, at which no faradaic reactions occur, is changed to a potential at which the surface concentration of the electroactive species is effectively zero. In chronoamperometry, the current is monitored over time.⁵⁹

Chronoamperometric measurements were performed with a glassy carbon rotating disk working electrode, Ag/AgCl reference and stainless steel auxiliary electrodes, as presented in Figure 2.13. Thus, the hydrodynamics are controlled by the rotating disk electrode. The hydrodynamic flow pattern resulting from rapid rotation of the disk moves liquid horizontally out and away from the centre of the disk with a consequent axial flow to replenish liquid at the surface as shown by the arrows in Figure 2.13. The equation for the limiting current obtained in this experiment is given by the Levich equation.⁵⁹

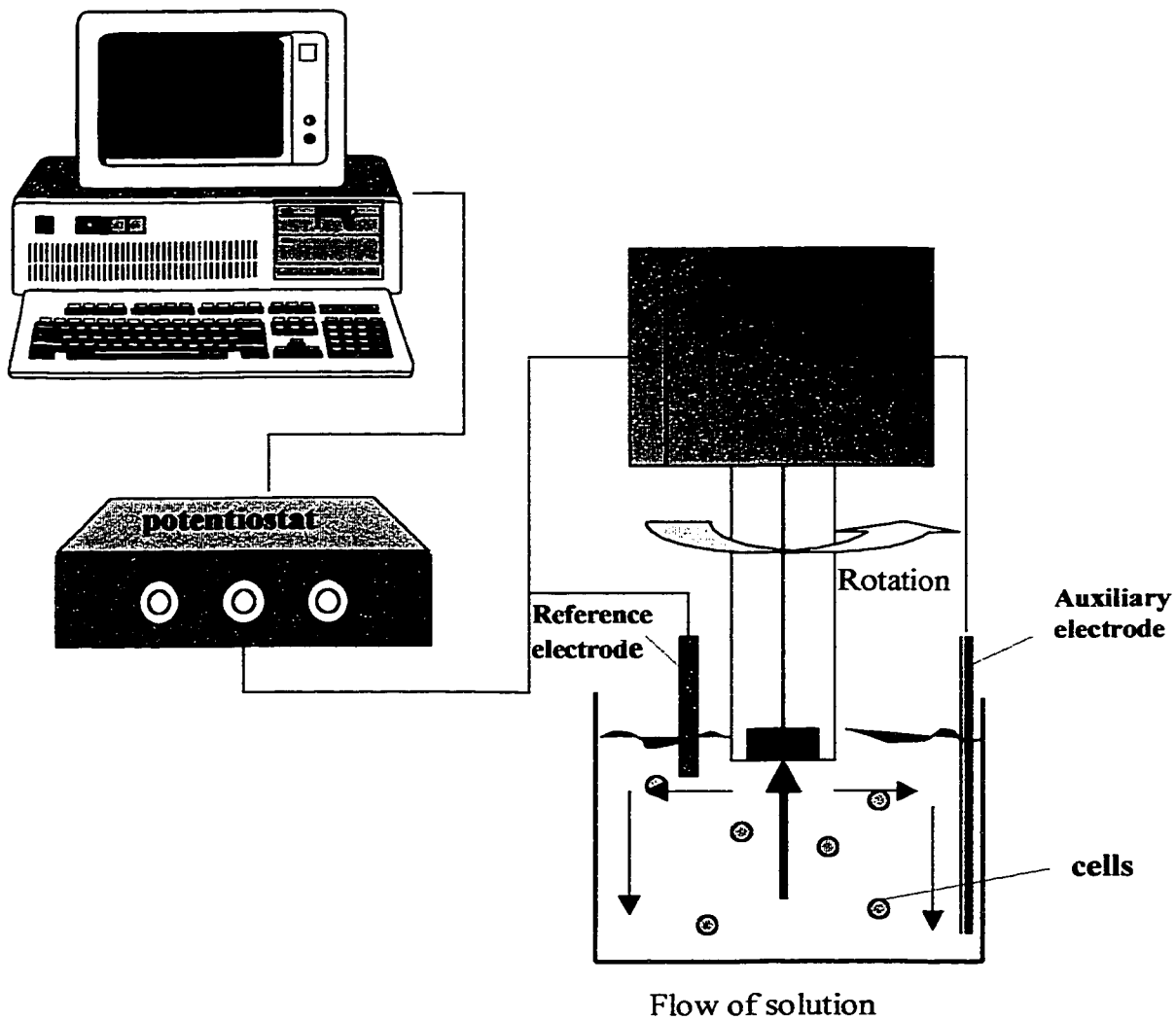
$$i_l = 0.620 n F A C^o D^{2/3} \nu^{1/6} \omega^{1/2} \quad 2.4$$

where:

i_l	limiting current, A
n	number of electrons, eq/mol
F	Faraday's constant, 96,485 C/eq
A	electrode area, cm ²
D	diffusion coefficient, cm ² /s
C^o	solution concentration, mol/cm ³
ν	kinematic viscosity of the fluid, cm ² /sec
ω	angular velocity of the disk ($\omega = 2\pi N$, N = rps)

Hydrodynamic flow enhances mass transfer from the bulk of the reagent solution to the electrode surface. The limiting current is thus a function of the angular velocity of the disk.⁵⁹ In addition, the hydrodynamic flow keeps the bacteria dispersed in the solution while the accumulation of ferrocyanide is constantly measured over time.

Figure 2.13: Schematic presentation of the chronoamperometric set-up.



Bacterial samples were injected into the electrochemical cell containing 100 mL of the buffered reagent solution (5 mM ferricyanide) and the ferricyanide reduction rate was measured over a period of 20 min at room temperature.

The specific activity ($\mu\text{mol}/\text{min}\cdot\text{g}$) is calculated using the raw rate, the calibration slope for ferrocyanide, the total volume and the BDM given the following equation.

$$\text{spec. activity} = \frac{\text{raw rate } \left(\frac{\text{nA}}{\text{s}}\right)}{\text{cal. slope } \left(\frac{\text{nA}}{\mu\text{M}}\right)} * 60 \left(\frac{\text{sec}}{\text{min}}\right) * \frac{V \text{ (L)}}{\text{BDM (g)}} \quad 2.5$$

where:

raw rate	reduction slope, nA/s
cal. slope	slope of the calibration curve, nA/ μM
V	total volume, L
BDM	bacterial dry matter normalised for volume, g

In Figure 2.14, a typical calibration curve obtained with known concentrations of ferrocyanide in the absence of bacterial cells is shown. The calibration slope of $-32.2 \pm 0.4 \text{ nA}/\mu\text{M}$ was used in equation 2.5 (above) to determine specific ferricyanide reduction rate values.

Figure 2.14: Plot of current against ferrocyanide concentration obtained by chronoamperometry (CA) with the rotating disk electrode set at 600 rpm. This calibration curve shows a linear fit ($r^2 = 0.993$) with a slope of $-32.2 \pm 0.4 \text{ nA}/\mu\text{M}$. Each point is the average of 3 measurements.

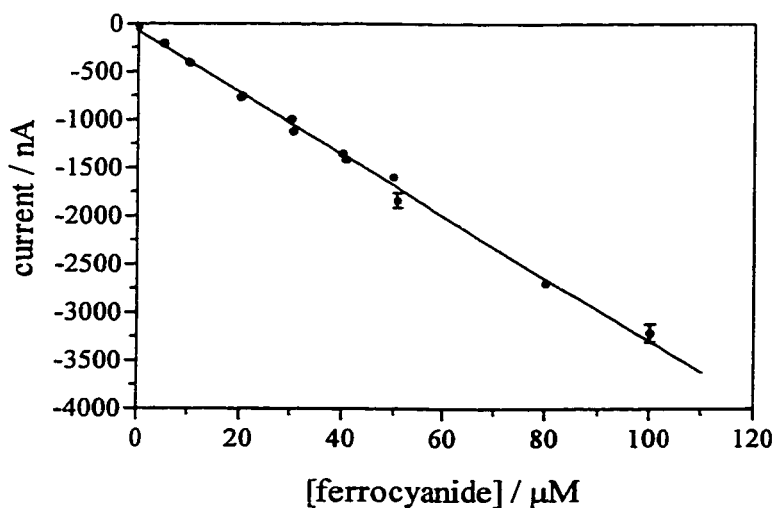
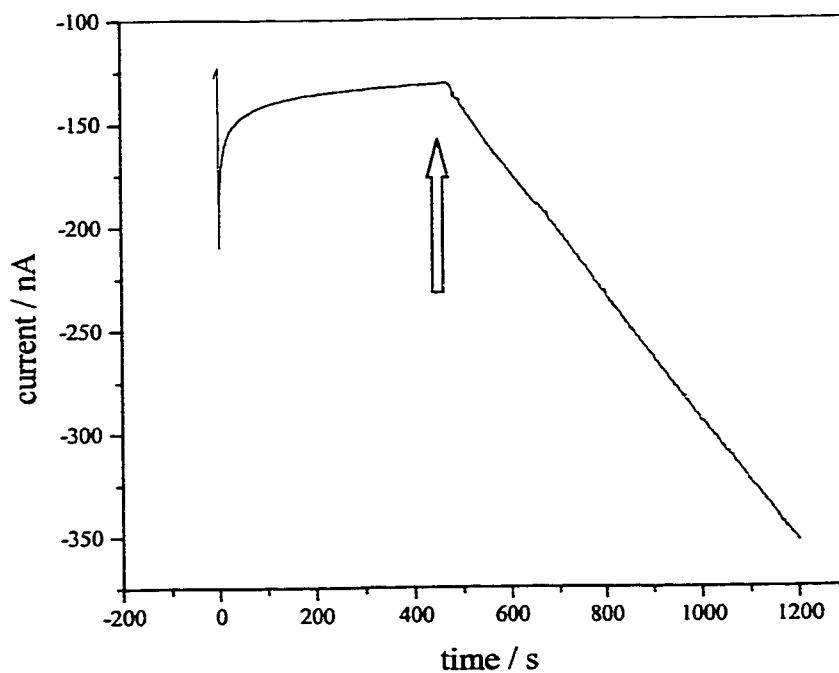


Figure 2.15 shows a typical raw data plot correlating current against time in the same electrochemical cell using the chronoamperometric method; this method was used to monitor ferrocyanide accumulation as a result of ferricyanide reduction by *E. coli* JM105. Centrifuged and resuspended cell samples were injected (see arrow) into the electrochemical cell as soon as the current levelled off after approximately 5 min. The increasing magnitude of the current indicates ferrocyanide concentration increase in the electrochemical cell. The CA experiments allows continuous data acquisition (3 points per second) of bacterial ferricyanide reduction over a period of 15 min.

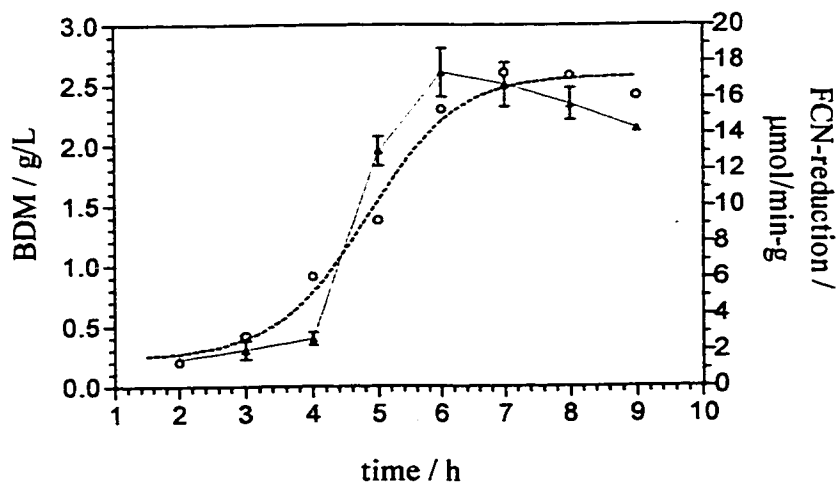
Figure 2.15: Raw data from a CA experiment with exponential-phase *E. coli* JM105 (shake flask culture) having an optical density of 1.82 or a BDM of 1.15 g/L.



The geometry of the rotating disk electrode (outer dia. 13 mm) used in our experiments required a minimum volume of 40 mL of the electrochemical cell in order to maintain stable hydrodynamic conditions with a rotation rate of 600 rpm. To operate with similar dilution factors to those that were used in the FIA experiments, amperometric measurements were performed using 1 mL of cell suspension a total volume of 101 mL.

Figure 2.16 shows specific ferricyanide reduction rates measured during the growth of *E. coli* JM105. CA results showed an increase in specific reduction rates to a maximum at the end of the exponential phase, followed by a decrease as the culture enters the stationary phase. The maximum value of the specific reduction rate obtained in the CA experiment was $17 \mu\text{mol}/\text{min-g}$, which is similar to the maximum rate obtained by FIA ($24 \mu\text{mol}/\text{min-g}$). Despite the large difference in volume ($20 \mu\text{L}$ for FIA and 101 mL in CA) excellent agreement was observed between the two methods (see Figures 2.12 and 2.16).

Figure 2.16: Ferricyanide reduction rates obtained using chronoamperometry (solid line, $n = 3$) and biological dry matter (dashed line) for a shake flask culture of *E. coli* JM105.



The FIA reduction rate was calculated from three individual measurements over time, whereas the CA value was measured constantly (3 points per second) over the same or longer period of time. Random fluctuations in the values were taken into account and effectively averaged out by the CA method. Consequently, the CA method is favoured over the FIA method because of its less labour-intensive experimental set-up, as well as its superior data collection capability.

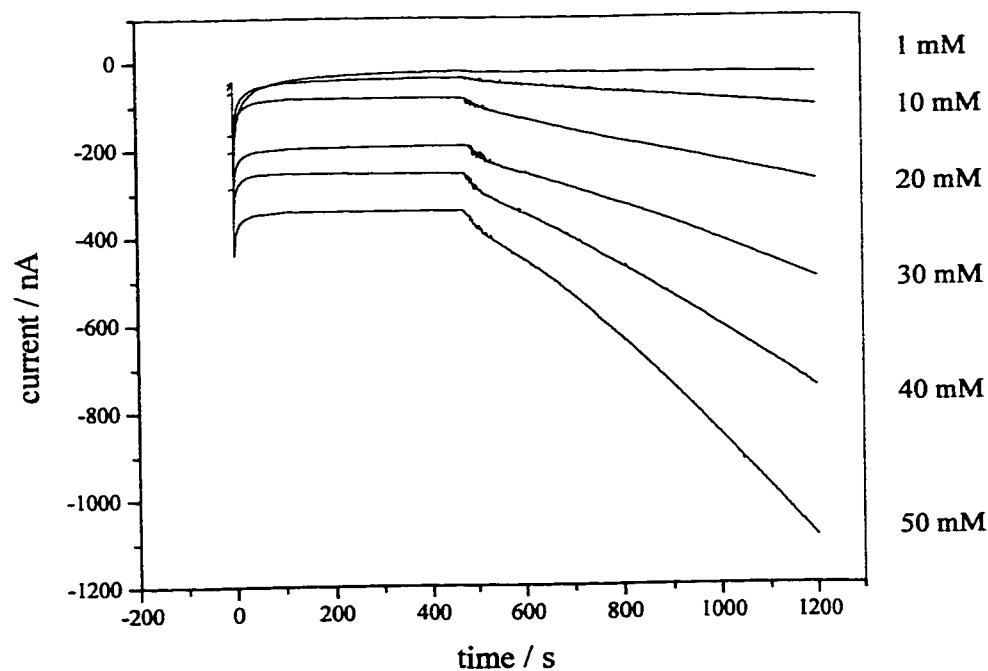
The shapes of the growth curves shown in Figures 2.12 and 2.16 are attributed to the change in protein expression levels that accompany stationary phase entry. Factors that influence the transition from exponential to stationary phase growth include declining sources of carbon, phosphorus and nitrogen. Initially, low concentrations of these nutrients trigger specific responses designed to allow efficient scavenging of the limiting ingredient or to facilitate the use of an alternative carbon source.²⁷ Ultimately, the exhaustion of an essential nutrient in the medium increases the intracellular concentration of σ^S , which is the sigma subunit for the stationary phase RNA polymerase.^{27,28} During this transition, the cell increases synthesis of certain enzymes, such as pyruvate oxidase, glycerol-3-phosphate dehydrogenase, and cytochrome *bd* II oxidase. The latter enzyme is homologous to existing *cyt bd* I oxidase, but its expression is triggered by δ^S rather than low-oxygen (micro-aerophilic) conditions.^{24,27,60}

An attempt at modelling uptake rates and enzyme kinetics has recently been undertaken for late-exponential phase *Gluconobacter industries* in the presence of glucose, and *Pseudomonas fluorescence* in the presence of nicotinic acid. Both types of microorganisms were trapped on the surface of a glassy carbon electrode and reduction rates were measured using oxidants such as DCIP, benzoquinone or molecular oxygen.

However, ferricyanide was only applied to *P. fluorescens*.³⁷ In this study, kinetic constants were defined in relation to cell concentrations instead of using concentrations of specific enzymes or transporters. This resulted in a method that allows comparison between organisms.

Figure 2.17 shows a plot of raw chronoamperometric data obtained for late exponential phase *E. coli* JM105 ($OD_{600} = 3.1$) with increasing ferricyanide concentrations. Differences in plateau levels before injecting *E. coli* (~500 s) into the electrochemical cell were signs of an increase in background signal due to a higher ferricyanide concentration, where a small percentage of electroactive impurities would lead to significant currents.

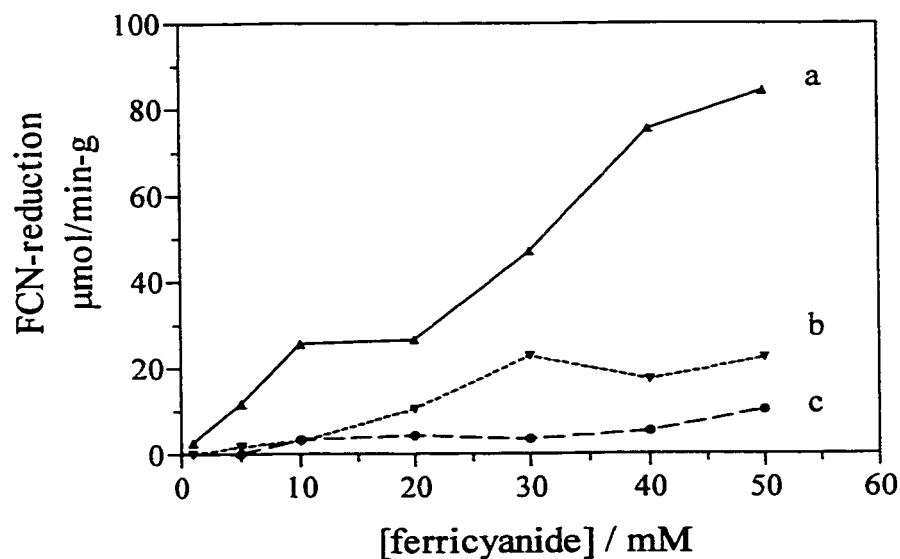
Figure 2.17: CA raw data for increasing ferricyanide concentration (1 – 50 mM) with exponential phase *E. coli* ($OD_{600} = 3.1$).



Measurements conducted with ferricyanide concentrations above 20 mM show an initial slow reduction rate within 2 min of *E. coli* injection. The initial slow rate might be attributed to the same pre-saturation phenomenon discussed in the FIA section and was not subjected to further investigation.

In Figure 2.18, reduction rates for varying concentrations of ferricyanide in the same culture (curve a) were compared to frozen (curve b) and multiply frozen (curve c) samples. Bacterial samples stored at -15°C for 24 h were referred to as frozen samples (curve b), while samples that were thawed and refrozen (-15°C) for a second consecutive 24 h period (curve c) were considered multiply frozen samples. This experiment illustrated the destructive effect of freezing (-15°C) on *E. coli* in the absence of a protective agent such as glycerol. When water is frozen at this temperature, large water crystals form due to the slow formation of the ice lattice structure. These ice crystals form inside and outside bacterial cells and are thus able to cut through cell membranes, which ultimately leads to cell death.³³ In a sample stored in the absence of glycerol for 24 hour at -15°C the reduction rate decreased to 30% of its original value in the presence of 50 mM ferricyanide. After freezing the same sample for a second consecutive 24 h interval, bacterial reduction activity declined to 12%, which means that 88 % of total viability had been lost. The significant decrease in respiratory activity obtained after 24 h clearly demonstrates that free enzymes, which might have been released from the cytosol of ruptured bacterial cells into the ferricyanide solution, do not contribute significantly to the overall respiratory signal of viable bacterial cells.

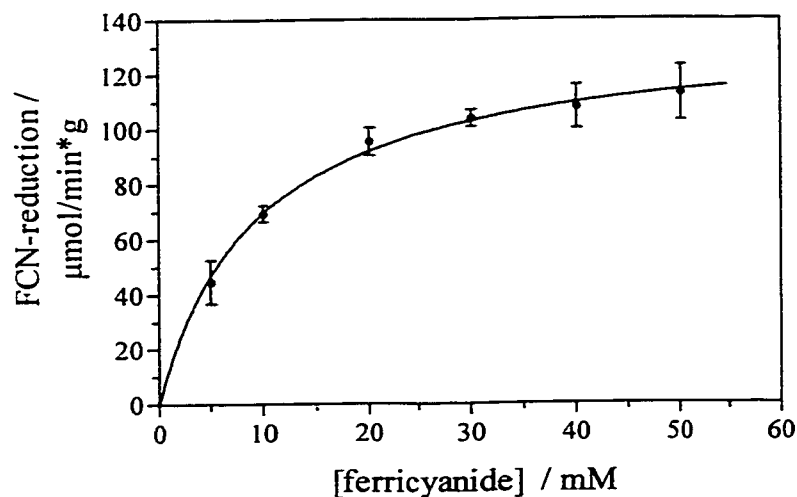
Figure 2.18: Comparison of respiration rates of freshly cultured (a), frozen (b) and multiply frozen cells (c) with increasing ferricyanide concentration. Exponential phase ($OD_{600} = 3.3$) *E. coli* JM105 cells were assayed by the CA method. Each value represents the mean of 2 replicate measurements.



The addition of 10 mM succinate to the CA assay solution was found to be essential in order to observe apparent Michaelis-Menten kinetics with exponential or stationary phase *E. coli* JM105 with respect to ferricyanide concentration. Although a variety of different enzymes are involved in the reduction of ferricyanide, kinetic studies can be performed by modelling the complex multi-enzyme reduction process using simple Michaelis-Menten kinetics.³⁷ At this point, by disregarding membrane permeability effects, bacterial cells behave like bags of enzymes with kinetics that appear to follow a Michaelis-Menten type equation (see Figure 2.19a and 2.20a). Figures 2.19b and 2.20b show Eadie-Hofstee plots for late-exponential phase ($OD_{600} = 3.1$) and stationary phase ($OD_{600} = 4.3$) samples taken from shake-flask cultivations, respectively.

Apparent K_m values of the multienzyme complex obtained for ferricyanide resulted in 10.1 ± 0.6 mM for the exponential phase and 14.4 ± 1.2 mM for stationary phase cells. The apparent V_{max} value for late exponential phase cells of 138 ± 3 $\mu\text{mol}/\text{min-g}$ is slightly higher than the value of 127 ± 5 $\mu\text{mol}/\text{min-g}$ obtained for stationary phase cells. The differences in the apparent K_m and V_{max} values of young and old cells indicate that these bacteria exchange their enzymes over time to adapt to environmental changes. The apparently higher affinity of exponential phase cells for ferricyanide is a possible result of different expression levels of porin proteins, succinate dehydrogenases and various terminal cytochrome oxidases. In comparison apparent K_m values obtained for the natural electron acceptor oxygen are much lower and have been reported to be 2.9 μM for exponential phase cells (cyt *o* oxidase) and 0.38 μM for stationary cells (cyt *bd* I oxidase).⁶⁰ However, ferricyanide is a highly charged, unnatural electron acceptor and thus affinities to cytochrome oxidases do not necessarily reflect those reported for oxygen. Nevertheless, these values were 7-8 fold lower than the value of 17 $\mu\text{M/s}$ (normalized to 1 mg/mL dry matter, which is 1020 $\mu\text{mol}/\text{min-g}$) reported for ferricyanide reduction by *P. fluorescens* in the presence of 10 mM nicotinic acid; this organism's apparent ferricyanide K_m was 7.2 ± 1.5 mM.³⁷

Figure 2.19: a) Specific ferricyanide reduction rate by CA as a function of ferricyanide concentration, for *E. coli* JM105 grown in shake flask cultures to exponential phase (OD₆₀₀ 3.1).



b) Eadie-Hofstee plot used to determine apparent Michaelis-Menten constants. Linear regression shows a slope ($-K_m$) -10.1 ± 0.6 mM, Y-intercept (V_{max}) 138.0 ± 3.0 μmol/min-g and a linear fit of (r^2) 0.984

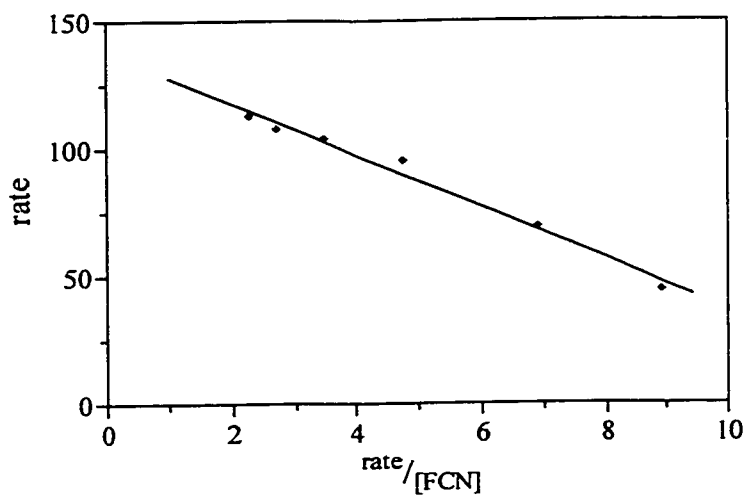
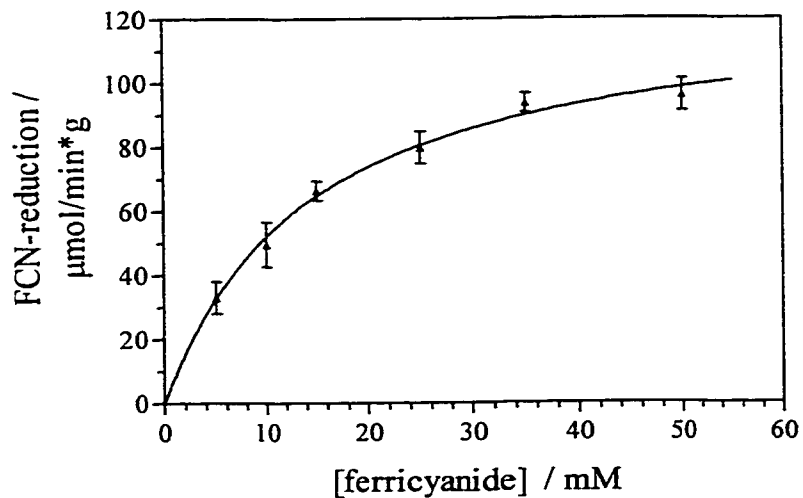
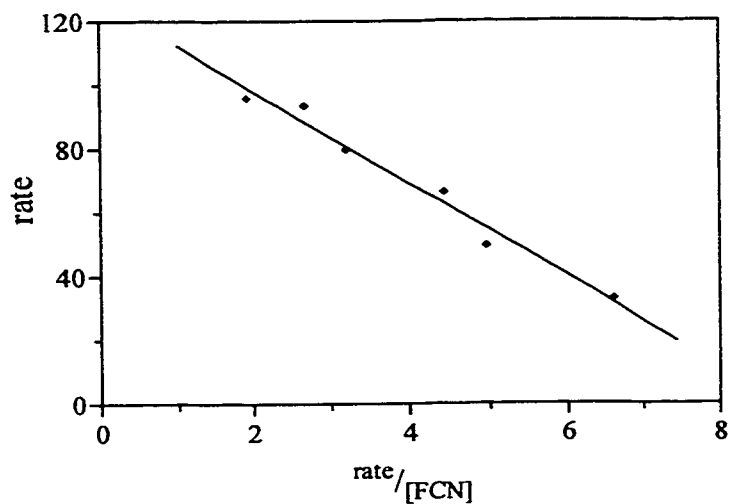


Figure 2.20: a) Specific ferricyanide reduction rate by CA as a function of ferricyanide concentration, for *E. coli* JM105 grown in shake flask cultures to stationary phase (OD₆₀₀ 4.1).



b) Eadie-Hofstee plot used to determine apparent Michaelis-Menten constants. Linear regression shows a slope ($-K_m$) -14.4 ± 1.2 mM, Y-intercept (V_{max}) 126.7 ± 5.1 μmol/min-g and a linear fit of (r^2) 0.973.



The measured ferricyanide reduction rates in the presence of succinate must depend on the rate of substrate uptake as well as on both concentration and intrinsic kinetic properties of the respiratory enzymes. It is important to note that in the presence of substrates such as succinate we are no longer measuring respiration, but instead we are measuring the transport and oxidation kinetics for these substrates. Furthermore, respiration measurements also depend on expression levels for the substrate transporters and dehydrogenases, which shift dramatically in *E. coli* as culture growth rates slow to stationary-phase subsistence levels.^{27,28} For example, the levels of pyruvate oxidase, glycerol-3-phosphate dehydrogenase and cytochrome *bd* II oxidase are known to increase while the level of succinate dehydrogenase decreases due to lower expression levels of the catalytic A subunit.⁶³ It is also clear that the composition of the membranes also change to allow cells to use any available nutrients and to protect them from diverse stress conditions. The expression of the aerobic C₄-dicarboxylic acid transporter (*dctA*) which is responsible for succinate uptake across the cytoplasmic (inner) membrane, was recently shown to increase 19-fold in the stationary phase.⁶⁴ A specific bi-directional transporter for formate, called *focA*, is also known to exist in the cytoplasmic membrane of aerobic *E. coli*,⁶⁵ although its expression levels have not yet been investigated as a function of growth rate. However, the anaerobic formate transporter (*focB*) is also known to be induced during periods of nitrogen limitation.⁶⁶ The main ion-selective porin in *E. coli*, called *phoE*,⁶⁷ is induced by phosphate limitation conditions.⁶⁸ Meanwhile, the main cation-selective porins (*ompF* and *ompC*), which are better understood, are strictly regulated by nutrient limitation (growth rate),⁶⁹ osmolarity⁷⁰ and temperature.⁷¹ Regulators for nutrient limitation and stationary phase gene expression include cyclic AMP, which increases as growth rates decrease,⁷² and the stationary phase sigma subunit

of RNA polymerase, which is induced at growth rates of 0.1 h^{-1} and below, for several strains of *E. coli*.⁷³

The chronoamperometric traces shown in Figure 2.21 displays three different ferricyanide reduction rates over the 35-minute monitoring period using a mid-exponential bacterial samples ($\text{OD}_{600} = 2.2$) and in the presence of 50 mM ferricyanide and 10 mM succinate. Slope 1 was indicative of an initially slow rate within the first 120 s to ferricyanide exposure, followed by a maximum reduction rate (slope 2) that steadily levelled off until the net current became zero (slope 3). The decrease in respiration rate observed after 20 min exposure to ferricyanide is thought to be due to either depletion of intracellular substrates or osmotic shock caused by the relatively high ferricyanide concentration (50 mM). No further investigation of the two slow reduction rates was done and all calculations for specific activities were performed using the slope of the highest reduction rate (slope 2).

Reduction rates obtained for 50 mM ferricyanide showed maximum values of $\sim 80 \mu\text{mol}/\text{min}\cdot\text{g}$ and after adding 10 mM succinate to the reagent solution, values increased to $\sim 130 \mu\text{mol}/\text{min}\cdot\text{g}$. In contrast, initial experiments using no succinate and $\sim 5 \text{ mM}$ ferricyanide showed signals that were 6-fold lower ($\sim 20 \mu\text{mol}/\text{min}\cdot\text{g}$) than those obtained in the presence of 50 mM ferricyanide and 10 mM succinate.

Using a fixed initial ferricyanide concentration of 50 mM, various hydrophobic mediators were tested at low concentration ($5 \mu\text{M}$) with exponential-phase *E. coli* JM105 by CA method in an attempt to further increase the specific reduction rates measured (see Table 2.2). These compounds may be present at much higher concentrations within the membranes due to partitioning and may facilitate ferricyanide reduction by bypassing slower, natural electron-transfer pathways.

Figure 2.21: Ferricyanide reduction rates in the presents of 50 mM ferricyanide and 10 mM succinate, over a time period of 35 min with bacterial samples harvested in the mid-exponential ($OD_{600} = 2.2$) show three reduction rates.

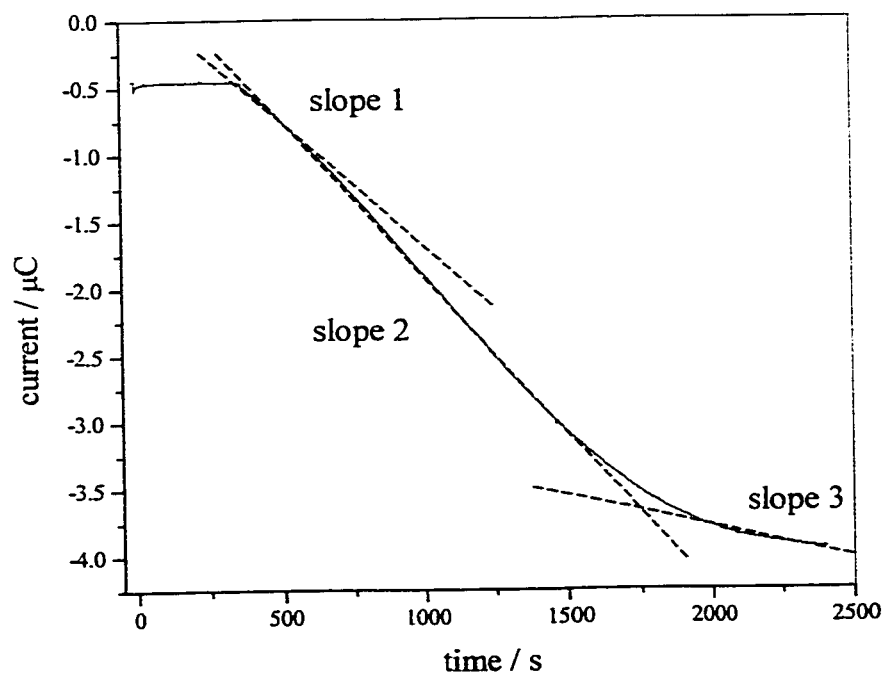


Table 2.2: Specific ferricyanide reduction rates obtained by CA using 50 mM ferricyanide in combination with various hydrophobic mediators at concentrations of 5 μ M with exponential-phase *E. coli* JM105.

Mediators	OD 3.1	Activity	OD 3.4	Activity
	μ mol/min-g	%	μ mol/min-g	%
None	28.0	100	44.7	100
Janus Green B	32.9	122	52.3	117
Dimethoxymethyl-benzoquinone	31.3	112	51.1	114
Dichlorophenolindophenol	21.3	46		
Benzoquinone	24.2	86		
Anthraquinone	7.8	27		

Results in Table 2.2 show no significant increase in specific ferricyanide reduction rate as when anthraquinone-1-sulfonate (AQ), DCIP and benzoquinone were added to the assay solution. Nevertheless, a small (10 - 22%) increase was observed with the addition of 2,3-dimethoxy-5-methylbenzoquinone (DMBQ) and Janus Green (E° (SHE) = + 0.013 and + 0.014 V, respectively, determined by cyclic voltammetry).

Ferricyanide reduction rates were investigated in the presence and absence of 5 μ M Janus Green and DMBQ, using *E. coli* samples at the exponential and stationary-phase of growth. Figure 2.22 shows the growth curve of a shake-flask culture of *E. coli* JM105 while the arrows indicate the time cultures were harvested; these results are given in Table 2.3. The addition of DMBQ to the reagent solution increased the reduction rate of mid-exponential grown cells ($OD_{600} = 2.25$) by 14% when stationary-phase cells ($OD_{600} = 3.9$) increased by 11%. A similar pattern was seen when using Janus Green, where reduction rates with late exponential phase cells ($OD_{600} = 2.3$) increased the signal by 21% while late stationary-phase cells ($OD_{600} = 3.9$) increased by 17%.

Ferricyanide reduction rates in the absence and presence of DMBQ during the growth of *E. coli* JM105 are shown in Figure 2.23. All of these curves have the same general shape, with values increasing to late-exponential phase maxima. However, addition of DMBQ to the growth medium increases reduction rates about 10–20 % throughout *E. coli* cultivation.

Figure 2.22: Growth curve of shake-flask culture of *E. coli* JM105, where arrows indicate the times when cell cultures were sampled to obtain the results in Table 2.3.

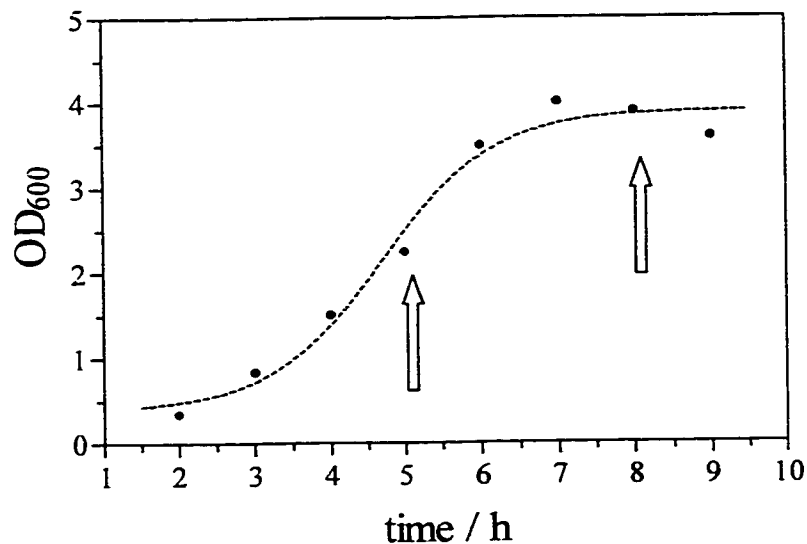
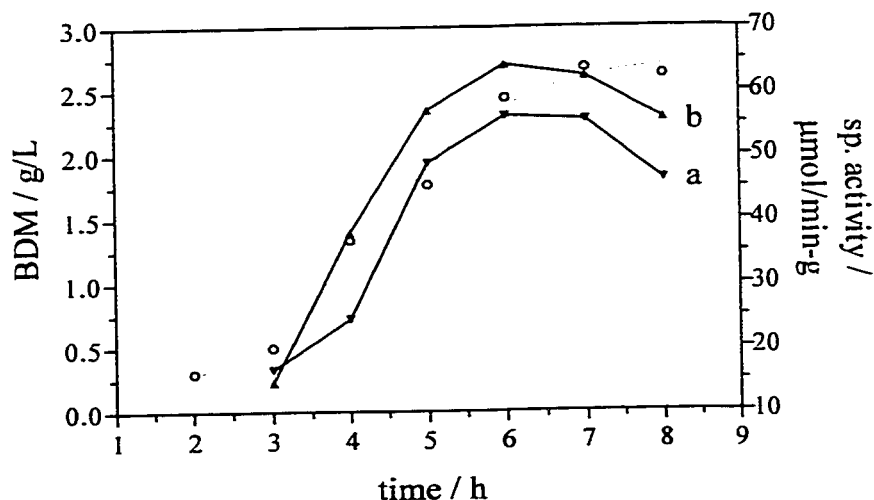


Table 2.3: CA results for ferricyanide reduction in the absence and presence of 5 μ M DMBQ and Janus Green (JG) for exponentially and stationary-phase grown *E. coli*.

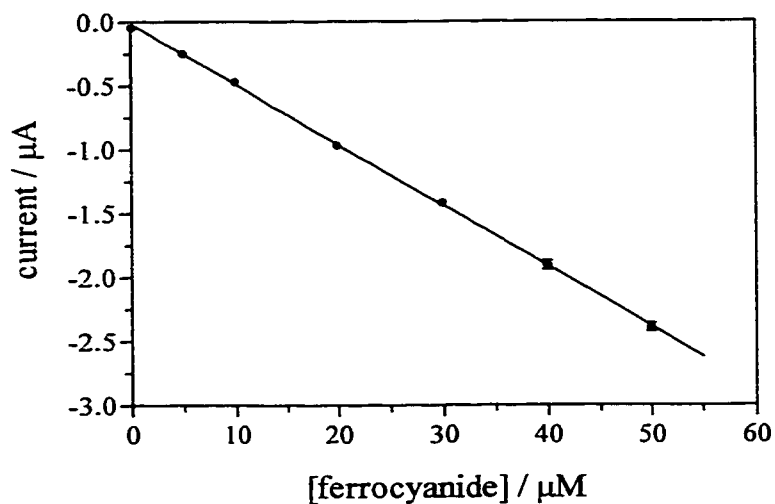
reagent	cultivation		rate		relative activity %
	time	OD ₆₀₀	μ mol/min-g	μ mol/min-g	
FCN	5h	2.25	59.0	49.4	100
FCN/DMBQ	5h	2.25	56.8	66.8	114
FCN/JG	5h	2.25	63.6	67.6	121
FCN	8h	3.9	37.2	28.2	100
FCN/DMBQ	8h	3.9	34.3	38.4	111
FCN/JG	8h	3.9	35.5	41.3	117

Figure 2.23: Ferricyanide (50 mM) reduction rates obtained for *E. coli* JM105 grown in the absence (a) and presence (b) of 5 μ M DMBQ.

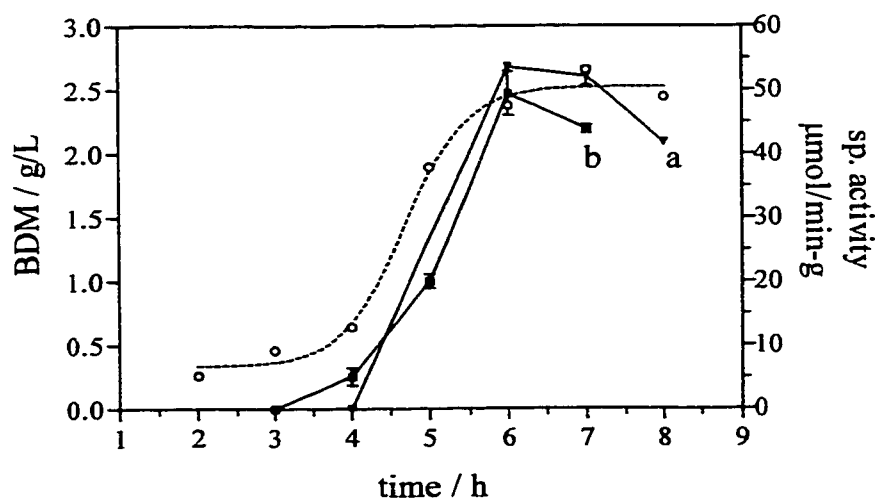


The effects of low ferricyanide concentrations (10 and 5 mM) in combination with a relatively high benzoquinone concentration (0.962 and 0.498 mM) on ferricyanide reduction rate was then investigated. Figure 2.24a shows the calibration curve obtained under these conditions with a linear fit of $r^2 = 0.998$ and a RSD from the slope of 0.1% ($n = 14$). Figure 2.24b shows that reduction rates measured under these conditions are similar. Interestingly, reduction rates obtained for 50 mM ferricyanide in the absence of benzoquinone ($54 \mu\text{mol}/\text{min}\cdot\text{g}$) are identical to those obtained with 10 mM ferricyanide and 1 mM benzoquinone ($53 \mu\text{mol}/\text{min}\cdot\text{g}$). However, reduction measurements in the presence of high concentrations of benzoquinone are imprecise, possibly due to polymerization (e.g. at BDM of 2.38 g/L the error of the calculated best fit slope of -1.9 nA/s is $\pm 0.8 \text{ nA/s}$).

Figure 2.24: a) Calibration curve of chronoamperometric current ($E = + 0.8 \text{ V vs Ag/AgCl}$, glassy carbon RDE at 600 rpm) against ferrocyanide / benzoquinone (ratio 10:1) concentration at room temperature. Values represent the mean of triplicate measurements.



b) Reduction rates for *E. coli* obtained in the presence of 10 mM ferricyanide with 0.9 mM benzoquinone (a) and 5 mM ferricyanide and 0.5 mM benzoquinone (b).



All subsequent experiments made use of ferricyanide only to determine reduction rates for *E. coli*. These results suggest that diffusion-controlled transfer of ferri/ferrocyanide ions proteins at an initial concentration of 50 mM through porin is efficient enough to shuttle electrons from the inner cell membrane to the working electrode.

In order to optimize the viability assay, assay temperature and working electrode material were varied. Figure 2.25 shows cyclic voltammograms obtained for 1 mM ferrocyanide in the presence of 10 mM succinate with glassy carbon, platinum and gold working electrodes. This figure shows that all three materials could be used to monitor ferrocyanide accumulation; however, these materials may interact with bacterial cells and growth medium differently and may be fouled to different extents. The results in Figure 2.25 show that the Pt electrode yields the greatest reversibility (smallest peak separation) and the largest peak currents for the ferri-/ferrocyanide couple.

Ferricyanide reduction by bacterial cells at 37°C instead of room temperature (22°C) is expected to yield higher reduction rates, since this represents the physiological temperature of *E. coli*. Figure 2.26 compares the ferricyanide reduction rates of exponential phase grown *E. coli* ($OD_{600} = 1.74$) kept at 37°C with those kept at 22°C using the three different types of working electrodes. This temperature increase resulted in a two-fold increase of respiratory cycle activity with small variations depending on the type of electrode used.

Figure 2.25: Cyclic voltammograms obtained for 1 mM ferrocyanide in the presence of 10 mM succinate conducted on glassy carbon (a), platinum (b) and gold (c) electrodes.

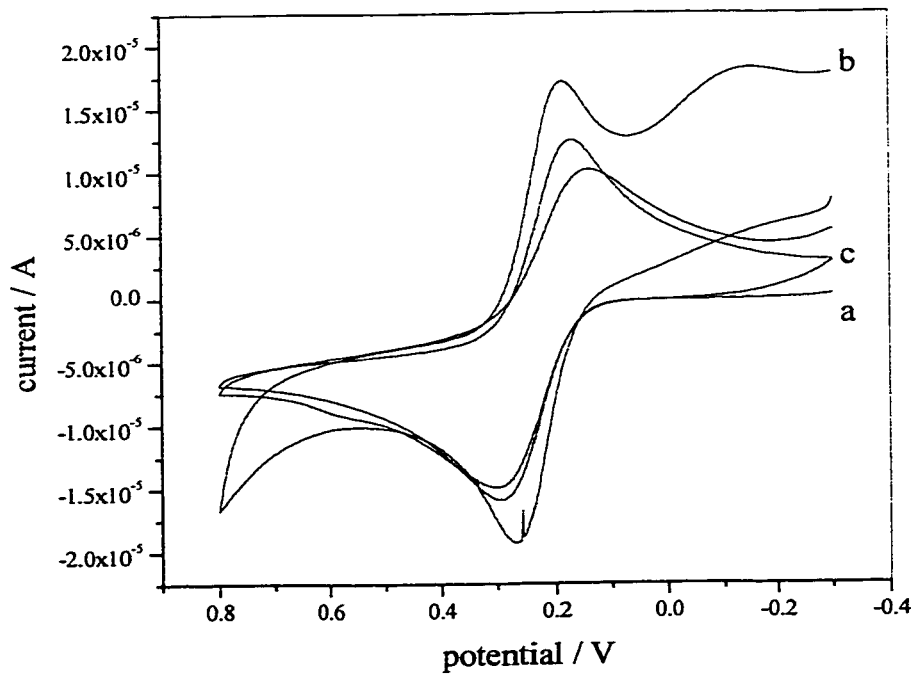
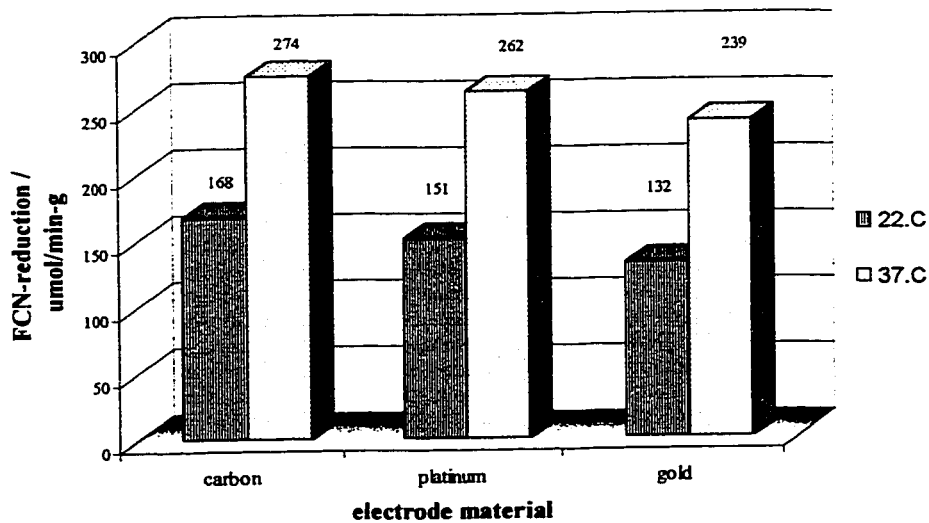
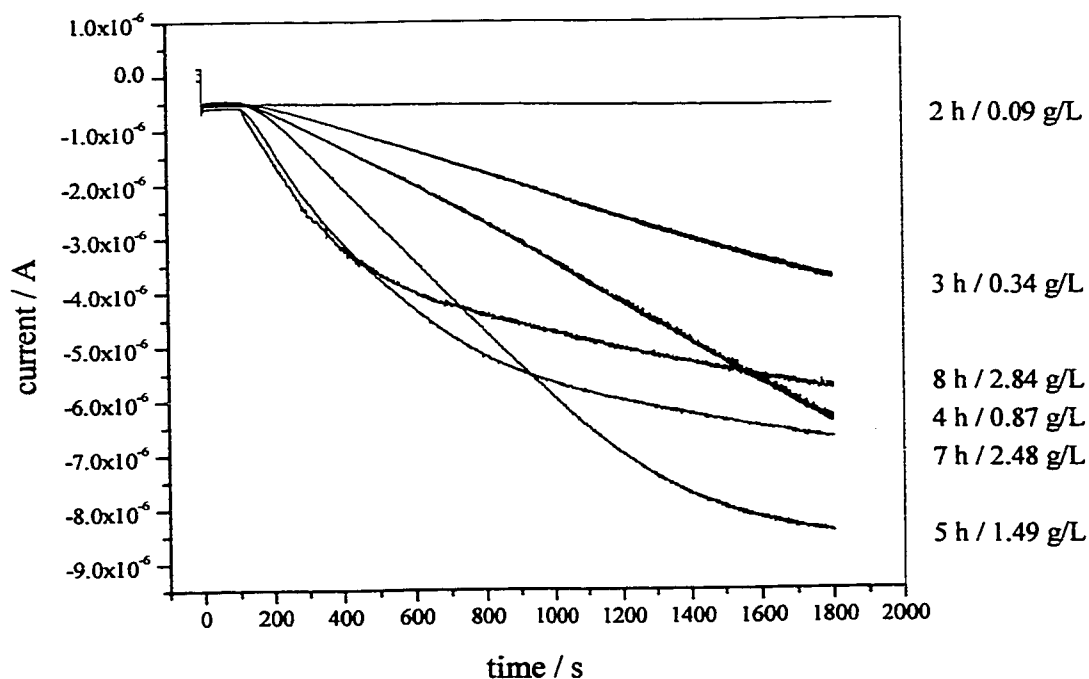


Figure 2.26: Ferricyanide reduction rates (50 mM ferricyanide and 10 mM succinate) of exponential phase grown *E. coli* ($OD_{600} = 1.74$) obtained for 37°C with these of 22°C, in the presence of different electrode materials.



Raw chronoamperometric traces obtained for samples collected during growth of *E. coli* JM105 at 37°C can be seen in Figure 2.27. The CA results show an increase in specific reduction rates with increasing cultivation time to a maximum at the exponential phase followed by a decrease as the culture entered the stationary phase. When specific rates are measured during the first 200 s of curves, the maxima of the CA experiments occur at a specific reduction rates of 222 $\mu\text{mol}/\text{min}\cdot\text{g}$ (see Table 2.3).

Figure 2.27: Raw CA-traces measured at 37°C with Pt working electrode (600 rpm, $E = +0.5 \text{ V vs Ag/AgCl}$) in the presence of 10 mM succinate during the growth of *E. coli* JM105. Insets indicate the time (h) and BDM (g/L) at which a cell sample was taken from the culture.



This experiment, conducted with a ferricyanide concentration of 50 mM and in the presence of 10 mM succinate at 37°C, shows a 13-fold increase in respiratory cycle activity (17 $\mu\text{mol}/\text{min-g}$) compared to initial reduction rates found for 5 mM ferricyanide at room temperature (22°C). CA results (Figure 2.27) also show that reduction rates, up to mid-exponential phase grown *E. coli*, are constant and linear (until an OD_{600} of ~ 2 or 4 h cultivation time) for a measurement period of 25 min. Cells grown after a BDM of 1.49 g/L (or mid exponential-phase) exhibited the highest reduction rates, but also showed signs of curvature indicating intracellular substrate depletion, which affected respiratory cycle well before the end of the activity after 20 min measurement time.

Table 2.4: Specific ferricyanide reduction rates for *E. coli* JM105 in the presence of 10 mM succinate. Measurements are performed at 37°C with platinum as the working electrode (+ 0.5 V vs. Ag/AgCl).

time	BDM	spec. rate	average
h	g/L	$\mu\text{mol}/\text{min-g}$	$\mu\text{mol}/\text{min-g}$
2	0.09	2, -	
3	0.34	151, 146	148
4	0.87	206, 205	206
5	1.49	221, 222	222
7	2.43	164, 159	161
8	2.82	168, 182	175

Late stationary phase cells (BDM of 2.43 and 2.82 g/L) showed not only decreased respiratory cycle activity but also displayed more dramatic signs of intracellular substrate depletion after a respective 10 and 5 min of measurement time. The nonlinear traces may

also serve as an indicator of changes in cellular composition associated with stationary phase entry for *E. coli*. For this reason, we defined the optimum runtime for ferricyanide reduction measurements at 37°C as 15 min.

Under these optimized conditions, the inhibition of ferricyanide reduction by cyanide ions was studied using CA and a Pt RDE, since this method allows continuous data acquisition over long periods of time. Cyanide is a known inhibitor of the terminal cytochrome oxidases, with reported K_i values of 50% inhibition of 10 μM for cyt *o* oxidase and 2 mM for cyt *bd* I oxidase.⁶⁰ Figure 27 shows CA traces obtained using mid exponential-phase cells in the absence (a) and presence (b) of 50 μM KCN, whereas Figure 2.29 shows the reduction rates in the absence (a) and presence (b) of 6 mM KCN. Traces obtained using 50 μM and 6 mM KCN exhibit an initial burst of ferricyanide reduction once cells are added to the assay mixture. However, after about 3 min exposure to cyanide, the ferricyanide reduction rate decreases significantly, as seen by the early curvature in the current-time trace in Figure 2.30. This is consistent with the known binding of cyanide to the fully oxidized and partially reduced forms of the oxidase.⁶⁰⁻⁶² Prior to adding the cell suspension into the CA assay mixture, all cytochrome oxidase complexes are present in their fully reduced form since the suspension is oxygen-depleted. Once respiratory turnover begins, cyanide begins to bind and inhibits the terminal enzymatic reaction. Chronoamperometric traces become linear after the first 2-3 min of exposure to cyanide and measurements made between 5 and 10 min yield 16 % ($n = 3$) and 14 % ($n = 4$) remaining ferricyanide reductase activity with 50 μM and 6 mM cyanide, respectively. Consequently, cyanide inhibition results suggest that 84-86% of electrons came from cytochrome *o* oxidase.

Figure 2.28: Chronoamperometric traces for exponential-phase *E. coli* JM105 ($OD_{600} = 1.82$) obtained in the absence (a) and presence (b) of $50 \mu\text{M}$ KCN.

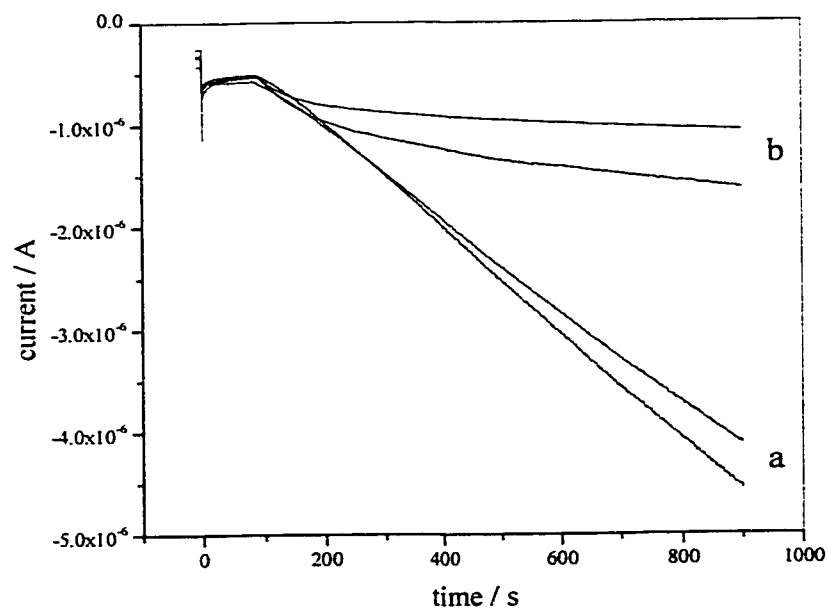


Figure 2.29: Chronoamperometric traces for exponential-phase *E. coli* JM105 ($OD_{600} = 2.21$) obtained in the absence (a) and presence (b) of 6 mM KCN.

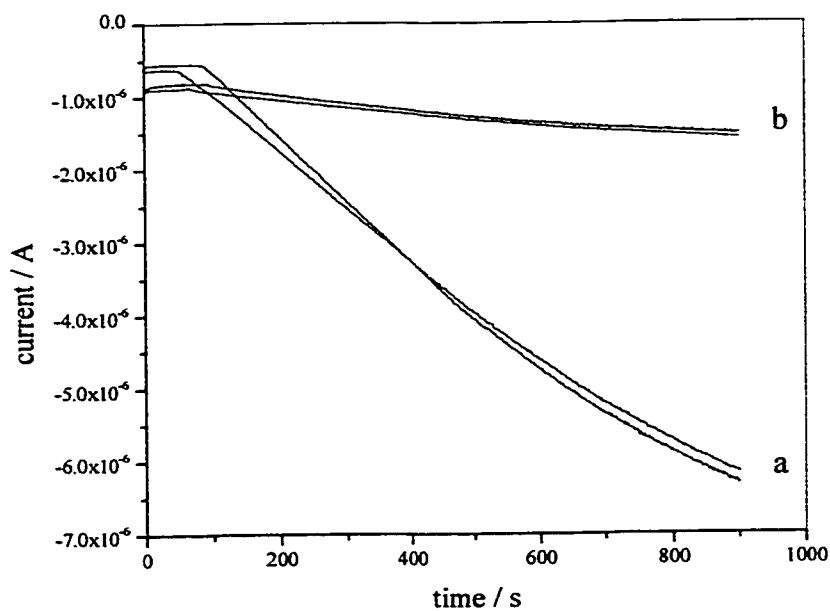
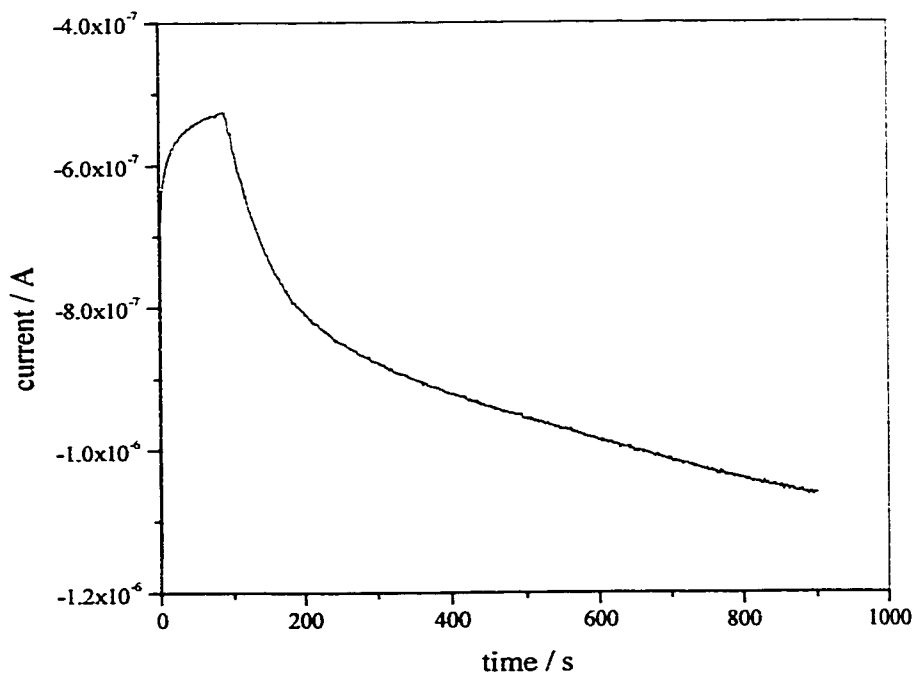


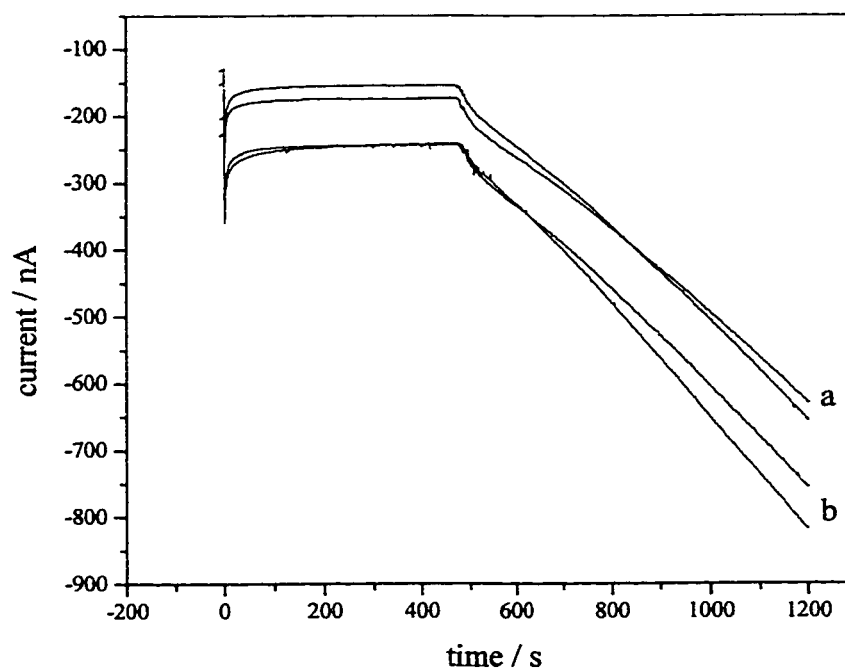
Figure 2.30: Ferricyanide reduction of exponentially-phase grown *E. coli* ($OD_{600} = 2.11$) in the presence of $50 \mu\text{M KCN}$.



This similarity in values at such different cyanide concentrations suggests the main terminal oxidase present in these exponential-phase cells is the more cyanide sensitive cytochrome *o* oxidase. These results are consistent with literature findings that show that the two cyt *bd* species are not detectable in exponential-phase cells.⁶¹ Therefore, ferricyanide accepts electrons mainly from cytochrome *o* oxidase in exponentially-growing cells. Meanwhile, the remaining 14 % ferricyanide reductase activity in the 6 mM cyanide must result from reactions with other components of the respiratory chain.

Since the K_m values of the terminal oxidases for O_2 are quite low, further investigation of the effect of deaeration on ferricyanide reduction rates were conducted. The oxygen K_m values are $2.9 \mu\text{M}$ for cyt *o* oxidase and $0.38 \mu\text{M}$ for cyt *bd* I oxidase.⁶⁰ However, with 50 mM ferricyanide present as an external oxidant, deaeration and blanketing of the CA assay solution with N_2 for 40 min had no measurable effect on the specific ferricyanide reduction rates of exponential-phase *E. coli* JM105 (see Figure 2.31).

Figure 2.31: Chronoamperometric traces of exponentially-phase grown *E. coli* (BDM 1.99 g/L) in the absence (a) and presence (b) of nitrogen. Nitrogen was used to deaerate the reagent solution.



2.4 CONCLUSIONS

Bacterial cultures were examined using electrochemical flow injection analysis (FIA) and chronoamperometry (CA) at varying growth rates and under different assay conditions. We found an excellent ferricyanide reduction rate agreement for *E. coli* for these methods. The experimental approach disregards the separation of bacterial cells from the reagent solution during the electrochemical measurement; these results represent respiratory cycle activity for viable *E. coli* cells. Since CA allows continuous data acquisition over long periods of time, it is considered the more precise method for assessing physiological changes of viable cells as opposed to FIA.

We have shown that samples of chilled and resuspended cells incubated in the presence of the respiratory substrate succinate prior to CA yield information complementary to that provided by standard oxygen-uptake measurements found in the literature.

Increasing the total ferricyanide concentration to 50 mM and adding succinate to the assay mixture as well as increasing temperature to resemble the physiological conditions of *E. coli* yielded a 13-fold increase in magnitude of CA signals. Furthermore, the addition of various hydrophobic mediators to the assay mixture, including Janus Green and 2,3-dimethoxy-5-methylbenzoquinone (DMBQ), only showed a small signal improvement.

Apparent Michaelis-Menten kinetics were observed with respect to ferricyanide concentration when 10 mM succinate was included in the assay buffer. Apparent K_m values of 10.1 ± 0.6 mM and 14.4 ± 1.2 mM ferricyanide were obtained for exponential and stationary phase *E. coli* JM105, respectively.

Cyanide inhibition measurements showed that ferricyanide accepts electrons mainly from cytochrome *o* oxidase (86%), while remaining ferricyanide reduction in the presence of 6 mM or 50 μ M cyanide must result from reactions with other components of the respiratory chain. In addition, oxygen deaeration studies showed no measurable effect on specific reduction rates of exponential-phase *E. coli* JM105.

In summary, ferricyanide reduction was studied by flow injection analysis (FIA) and chronoamperometry (CA) using the strain *Escherichia coli* JM105. We found that measured reduction rates are dependent on expression levels of cytochrome oxidases and substrate transporters. Enzyme expression levels in *E. coli* have been shown to shift dramatically during the growth of a bacterial culture. Overexpression of recombinant proteins in engineered organisms may also trigger the heat-shock/stationary response that ultimately leads to cell death. For this reason optimal time for harvesting is crucial and, therefore, a method is needed that rapidly identifies shifts in the metabolic rate. The newly developed method can thus be used to indicate metabolic shifts in a recombinant strain, and can also be used as a tool to establish the optimal time for harvesting recombinant proteins.

2.5 REFERENCES

1. Button, D. K.; Schut, F.; Quang, P.; Martin, R.; Robertson, B. R. *Appl. Environ. Microbiol.* 1993, 59, 881.
2. Lloyd, D.; Hayes, A. *J. FEMS Microbiol. Lett.* 1995, 133, 1.
3. Duncan, S.; Glover, L. A.; Killham, K.; Prosser, J. I. *Appl. Environ. Microbiol.* 60, 1994, 1340.
4. Jepras, R. I.; Carter, J.; Pearson, S. C.; Paul, F. E.; Wilkinson, M. J. *Appl. Environ. Microbiol.* 1995, 61, 2696.
5. Lopez-Amoros, R.; Comas, J.; Vives-Rigo, J. *Appl. Environ. Microbiol.* 1995, 61, 2521.
6. Bowen, I. D. in "Cell Aging and Cell Death", Davies, I. Sigeo, D. C., Eds., *Soc. Exp. Biol. Sem. Ser.* 25, Cambridge University Press, 1984.
7. Mason, D. J.; Lopez-Amoros, R.; Allman, R.; Stark, J.M.; Lloyd, D. *J. Appl. Bacteriol.* 1995, 78, 309.
8. Matsunaga, T.; Okochi, M.; Nakasono, S. *Anal. Chem.* 1995, 67, 4487.
9. Breeuwer, P.; Drocourt, J. L.; Rombouts, F. M.; Abee, T. *Appl. Environ. Microbiol.* 1994, 60, 1467.
10. Nyren, P; Edwin, V. *Anal. Biochem.* 1994, 220, 39.
11. Kogure, K.; Simidu, U.; Taga, N. *Can. J. Microbiol.* 1979, 25, 415.
12. Pyle, B. H.; Broadway, S. C.; McFeters, G. *Appl. Environ. Microbiol.* 1995, 61, 4304.
13. Kaprelyants, A. S.; Kell, D. B. *J. Microbiol. Meth.* 1993, 17, 115.

14. Lesuisse, E.; Casteras-Simon, M.; Labbe, P. *Anal. Biochem.* 1995, 226, 375.
15. Dailey, H. A.; Lasceles, J. *J. Bacteriol.* 1977, 129, 815.
16. Willams, H. D.; Poole, R. K. *Current Microbiol.* 1987, 15, 319.
17. McManus, D. C.; Josephy, P. D. *Arch. Biochem. Biophys.* 1993, 304, 367.
18. Ikeda, T.; Kato, K.; Tatsumi, H.; Kano, K. *J. Appl. Electroanal. Chem.* 1997, 440, 265.
19. Omstead, D. R. (Ed.) "*Computer Control of Fermentation Processes*" CRC Press, Boca Raton, 1990.
20. Georgiou, G. *AIChE Journal* 1988, 34, 1233.
21. Crueger, W.; Crueger, A. "Biotechnology: A Textbook of Industrial Microbiology," 2nd Ed., Sinauer (Science Tech Publishers), Madison, WI, 1990.
22. Anderson, K. B.; von Meyenburg, K. *J. Bacteriol.* 1980, 144, 114.
23. Sun, I. L.; Crane, F. L. *Biochim. Biophys. Acta* 1985, 811, 233.
24. Gennnis, R. B.; Stewart, V. in "*Escherichia coli and Salmonella typhimorium: Cellular and Molecular Biology*" F. C. Niedhardt, Editor-in-Chief, American Society for Microbiology, Washington, 1997.
25. Uden, G.; Bongaerts, J. *Biochim. Biophys. Acta* 1997, 1320, 217.
26. Strurr, M. G.; Krulwich, T. A.; Hicks, D. B. *J. Bacteriol.* 1996, 176, 1742.
27. Hengge-Aronis, R. in "*Escherichia coli and Salmonella typhimorium: Cellular and Molecular Biology*," F. C. Niedhardt, Editor-in-Chief, American Society for Microbiology, Washington, 1997. Volume 1.
28. Loewen, P. C.; Hu, B.; Strutinsky, J.; Sparling, R. *Can. J. Microbiology* 1998, 44, 707.
29. Jishage, M.; Ishihama, A. *J. Bacteriol.* 1995, 177, 6832.

30. Ramsay, G.; Turner, A. P. F. *Anal. Chim. Acta* 1988, 215, 61.
31. Ding, T.; Schmid, R. D. *Anal. Chim. Acta* 1990, 234, 247.
32. Gaisford, W. C.; Richardson, N. J.; Haggett, B. G. D.; Rawson, D. M. *Biochem. Soc. Trans.* 1991, 19, 15.
33. Atlas, R. M. "Principles of Microbiology," 2nd Ed., Wm. C. Brown, Dubuque (Iowa), 1997.
34. Hadjipetrou, L. P.; Gray-Young, T.; Lilly, M. D. *J. Gen. Microbiol.* 1966, 45, 479.
35. Crane, F. L.; Sun, I. L.; Clark, M. G.; Grebing, C.; Loew, H. *Biochim. Biophys. Acta* 1985, 811, 233.
36. Kulys, J.; Wang, L.; Razumas, V. *Electroanalysis* 1992, 4, 527.
37. Ikeda, T.; Kurosaki, T.; Takayama, K.; Kano, K.; Miki, K. *Anal. Chem.* 1996, 68, 192.
38. Perez, F. G.; Mascini, M.; Tothill, I. E.; Truner, A. P. F. *Anal. Chem.* 1998, 70, 2380.
39. Tanaka, K.; Vega, C. A.; Tamamushi, R. *Bioelectrochem. Bioenerg.* 1983, 11, 135.
40. Nishikawa, S.; Sakai, S.; Karube, I.; Matsunaga, T.; Suzuki, S. *Appl. Environ. Microbiol.* 1982, 43, 814.
41. Takayama, K.; Kurosaki, T.; Ikeda, T.; Nagasawa, T. *J. Electroanal. Chem.* 1995, 381, 47.
42. Turner, A. P. F.; Ramsay, G.; Higgins, I. *J. Biochem. Soc. Trans.* 1983, 11, 445.
43. Bennetto, H. P.; Striling, J. L.; Tanaka, K.; Vega, C. A. *Biotechnol. Bioeng.* 1983, 25, 559.
44. Takayama, K.; Kurosaki, T.; Ikeda, T. *J. Electroanal. Chem.* 1993, 356, 295.

45. Tatsumi, H.; Takagi, K.; Fujita, M.; Kano, K.; Ikeda, T. *Anal. Chem.* 1999, 71, 1753.
46. Winding, A.; Binnerup, S. J.; Sorensen, J. *Appl. Environ. Microbiol.* 60, 1994, 2869.
47. Chunxiang, X.; Gang, L.; Haobin, C.; Yue, X. *Sens. Actuators B* 1993, 12, 45.
48. Richardson, N. J.; Gardner, S.; Rawson, D. M. *J. Appl. Bacteriol.* 1991, 70, 422.
49. Szentrimay, R.; Yeh, P.; Kuwana, T. in “*Electrochemical Studies of Biological Systems*”, R. F. Gould, Ed., American Chemical Society, Washington, 1977, p. 143.
50. Miki, K.; Tsuchida, T.; Kawagoe, M.; Kinoshita, H.; Ikeda, T. *Denki Kagaku* 1994, 62, 1249.
51. Atlung, T.; Bronsted, L. *J. Bacteriol.* 1994, 176, 5414.
52. Katrlík, J.; Brandsteter, R.; Svorc, J.; Rosenberg, M.; Miertus, S. *Anal. Chim. Acta* 1997, 356, 217.
53. Hasebe, Y.; Yokobori, K.; Fukasawa, K.; Kogure, T.; Uchiyama, S. *Anal. Chim. Acta* 1997, 357, 51.
54. Rabinowitz, J. D.; Vacchino, J. F.; Beeson, C.; McConnell, H. M. *J. Am. Chem. Soc.* 1998, 120, 2464.
55. Jouenne, T.; Junter, G. A. *FEMS Microbiol. Lett.* 1990, 68, 313.
56. Kurland, C. G.; Dong, H. *Mol. Microbiol.* 1996, 21, 1.
57. Dong, H.; Nilsson, L.; Kurland, C. G. *J. Bacteriol.* 1995, 177, 1497.
58. Ertl, P.; Ladstaedter, B.; Bayer, K.; Mikkelsen, S. R. *Anal. Chem.* 2000, 72, 4949.
59. Kissinger, P. T.; Heineman, W. R. “*Laboratory Techniques in Electroanalytical Chemistry*”, 2nd Ed., Marcel Dekker, Inc. NY, 1996.
60. Kita, K.; Konishi, K.; Anraku, Y. *J. Biol. Chem.* 1984, 259, 3375.

61. Pudek, M. R.; Bragg, P. D. *Arch. Biochem. Biophys.* 1974, 164, 682.
62. Tsubaki, M.; Mogi, T.; Hori, H.; Sato-Watanabe, M.; Anraku, Y. *J. Biol. Chem.* 1996, 271, 4017.
63. Xu, J.; Johnson, R. C. *J. Bacteriol.* 1995, 177, 938.
64. Davies, S. J.; Golby, P.; Omrani, D.; Broad, S. A.; Harrington, V. L.; Guest, J. R.; Kelly, D. J.; Andrews, S. C. *J. Bacteriol.* 1999, 181, 5624.
65. Kaiser, M.; Sayers, G. *Microbiology*, 1997, 143, 775.
66. Andrews, S. C.; Berks, B. C.; McClay, J.; Ambler, A.; Quail, M. A.; Golby, P.; Guest, J. R. *Microbiology* 1997, 143, 3633.
67. Benz, R.; Darveau, R. P.; Hancock, R. E. *Eur. J. Biochem.* 1984, 140, 319.
68. Benz, R.; Schmid, A.; Hancock, R. E. *J. Bacteriol.* 1985, 162, 722.
69. Liu, X.; Ferenci, T. *J. Bacteriol.* 1998, 180, 3917.
70. Hall, M. N.; Silhavy, T. J. *J. Mol. Biol.* 1981, 146, 23.
71. Lugtenberg, B.; Peters, R.; Bernheimer, H.; Berendsen, W. *Mol. Gen. Genet.* 1979, 147, 251.
72. Notley-McRobb, L.; Death, A.; Ferenci, T. *Microbiology* 1997, 143, 1909.
73. Notley, L.; Ferenci, T. *J. Bacteriol.* 1996, 178, 1465.
74. Kramer, W.; Welmecker, G.; Weik, R.; Mattanovich, D.; Bayer, K. *Ann. N. Y. Acad. Sci.* 1996, 782, 323.

Chapter 3

Microbial Ferricyanide Reduction in the Presence of Antibiotic Compounds

3.1 INTRODUCTION

3.1.1 Objective

In Chapter 2 electrochemical measurements were shown to allow rapid and reliable determination of losses in the respiratory chain activity. In this chapter, the same kind of measurements are shown to rapidly detect changes in cell metabolism induced through the toxic effects of antibiotics. In this study *E. coli* was used as a model organism for gram-negative facultative anaerobes, while *C. sporogenes* was used as a model organism for gram-positive obligate anaerobes. A range of antibiotics was used in this study to determine whether the effects of antibiotics on bacterial respiratory cycle activity can be measured electrochemically, and whether these effects are mechanism-dependent. Results of the optimized electrochemical assay were compared to a standard method and were also evaluated by calculation of specificity, sensitivity and efficiency.

3.1.2 Introduction

In recent years, a large research effort has been directed towards the study of new antibiotics,^{1,2} and towards understanding the mechanisms of antibiotic resistance in microorganisms.³⁻⁵ Clinical studies have shown increased resistance of known pathogenic organisms towards commonly prescribed antibiotics, such as penicillin, vancomycin, tetracycline and chloramphenicol.^{6,7} While specific genes (VanA and VanB) are responsible for vancomycin resistance,⁸ studies have shown that several genes contribute to a more general resistance to hydrophobic antibiotics.⁹ These genes are responsible for multidrug and drug-specific efflux pumps that bind and transport drugs out of the cytoplasm. Four major categories of efflux pump are known to exist; these are called the ATP binding cassette family (ABC), the major facilitator superfamily (MFS), the small multidrug resistance family (SMR), and the resistance/nodulation/division family (RND).⁹ The above classifications are based on mechanism and occurrence, since for example the ABC superfamily is driven by ATP hydrolysis and occurs in bacteria, archaea and eukaryotes, while the SMR family catalyses drug:H⁺ antiport and is known to occur only in prokaryotes.⁹

In general, the susceptibility of an organism towards an antibiotic is defined by its minimum inhibitory concentration (MIC), which is the minimum antibiotic concentration that prevents growth of 99.9% of the target organism at an initial concentration of 10⁵ to 10⁶ cells/mL.¹⁰ MICs are routinely measured in clinical settings and in drug research by a variety of manual and automated methods. The oldest and simplest method in current use is the disk-diffusion test. Here, antibiotic-impregnated disks are placed on the surface of an inoculated agar plate and incubated overnight. After visible cell growth has occurred

on the agar plate the diameter of the no-growth area surrounding each disk is subsequently measured.¹¹ The E-test® is a more modern version of disk-diffusion in which a strip impregnated with a concentration gradient of antibiotic is placed on the agar surface. In this case, a well-defined transition occurs after incubation that separates a low-concentration growth area from a high-concentration growth inhibition area. Here, MIC values can be quantitatively determined, since the location of the transition is directly related to the MIC value.^{12,13} Automated systems, such as the Vitek® assay, allow inoculation of multiwell plates or cards that have an array of antibiotics or a range of individual antibiotics. After a long incubation period, metabolically active stains are used to optically follow cell growth through the accumulation of a coloured dye.¹⁴ An electrochemical method has also been used to determine antibiotic susceptibilities on Gram-negative bacteria. Here, impedance changes measured over time (4 to 6 h) indicate the extent of bacterial growth. Differences in impedance signals obtained in the absence and presence of an antibiotic compound determine antibiotic susceptibility.¹⁵ Nevertheless, MIC values obtained for one organism using different methods are often significantly different, and a standard susceptibility testing method has not been defined,¹⁶ although all methods currently in use monitor microorganism growth in the presence of antibiotics. As a result, lengthy incubation periods (4 h or more) are needed to allow accurate measurement of the extent of growth.

A recent study has examined the cost and health benefits of rapid antibiotic susceptibility testing.¹⁷ Same-day versus next-day reporting was compared for a 1-yr period at a major U.S. hospital, including 765 individual susceptibility tests, performed using the Vitek® method. This comparison showed that same-day testing provided

results, on average, 5.2 h faster than next-day reporting, resulting in 1.7% fewer mortalities and a cost saving of over US\$ 4 million (\$1750 per patient). Such dramatic benefits further emphasise the need for more rapid susceptibility testing methods.

Microbial resistance to antibiotic compounds, particularly penicillin G and vancomycin, which were considered the last line of defence, has increased exponentially in recent years. This development has become a serious concern for health practitioners throughout the world.^{54,55} The quantitative determination of microorganism susceptibility to antimicrobial compounds, in the form of minimum inhibitory concentration (MIC) or 50% inhibition concentration (IC₅₀) values, in a rapid-throughput, automated format, has not yet been achieved. Currently used methods, such as the Kirby-Bauer or Vitec® assays, require initial cell growth in order to monitor growth inhibition by antibiotics. Monitoring occurs after incubating cells for several hours in the presence or absence of indicator dyes.^{11,20,26,28,56-59} None of the available methods use metabolic measurements to determine the effects of antibiotics on microorganisms. Furthermore, no available methods can measure microorganism activity in the absence of significant cell growth.

Microorganism growth or the ability to reproduce under given culture conditions, is only one of several definitions of “viability”, the fraction of the total cell population that may be considered alive. Although growth-based methods are widely accepted, they have been shown to significantly underestimate viable cell counts, because a fraction of the cell population is often viable but nonculturable under the specific conditions used to estimate growth.¹⁸ In addition to viability estimates by growth-based methods such as counts of colony-forming units (cfu), which indicate those cells able to reproduce under given conditions,¹⁹ several other definitions of viability have formed the bases for viable

cell counts. These include the presence of intact membranes as indicated by membrane potential-sensitive dyes,²⁰ the presence of localised enzyme activities, such as esterases,²¹ inorganic phosphatase,²² and β -galactosidase,²³ as well as the ability of cells to elongate in the presence of a cell division inhibitor.²⁴ Further, the rate of extracellular acidification, reflecting the rate of production of acidic products of energy metabolism (such as lactic acid and CO₂) has been used to determine cell viability in combination with antibiotics. Here, differences in acidification rates in the absence and presence of ampicillin were used to indicate whether exposure to an antimicrobial agent has killed a significant portion of the microbial population, present in the sensor.²⁵

Viability has also been estimated through the measurement of respiration using redox-sensitive dyes. The presence of a functioning respiratory chain, in effect, indicates both membrane integrity and localised oxidoreductase activity. Several growth-based antibiotic susceptibility tests employ dyes that are reduced by components of the respiratory chains of the organisms, to monitor the extent of growth.²⁶⁻²⁸ In these tests, the extent of dye reduction (and the resulting colour change) is proportional to the concentration of viable cells in the culture.

Electrochemical measurement of ferricyanide reduction by a variety of organisms has been reported in the literature³¹⁻³⁸ and was the subject of a detailed investigation in Chapter 2. In some of the reported studies, cell suspensions were monitored amperometrically,³¹⁻³³ while in others, cells were trapped on electrode surfaces and used as biosensors for metabolizable substrate quantitation.³⁴⁻³⁷ In one application, an *E. coli* modified electrode was implemented to detect chlorinated phenol pollutants.³

Results presented in Chapter 2 show that specific rates for the reduction of ferricyanide by viable *E. coli* cells that have been cooled to arrest cell growth are particularly sensitive to growth conditions and metabolic rates. Brief incubations of cell suspensions with the respiratory substrates succinate and formate resulted in ferricyanide reduction rates that are significantly higher than rates observed in the absence of these substrates. It was also found that signals decreased significantly upon entry into the stationary phase or the initiation of the ribosome-destruction cascade that occurs at the end of recombinant fermentations.^{29,30}

In this chapter, electrochemical methods are shown to rapidly detect changes in cell metabolism induced by the toxic effects of antibiotic compounds. Specific ferricyanide reduction rates were measured after brief (10-20 min) incubations of *E. coli*, a Gram-negative facultative anaerobe, and *C. sporogenes*, a Gram-positive obligate anaerobe, with effective antibiotic drugs. Antibiotics from different classes, with different mechanisms of action were included in this study: some affect cell wall synthesis (penicillin G, D-cycloserine, vancomycin, bacitracin and cephalosporin C); others affect protein synthesis (tetracycline, erythromycin, chloramphenicol and streptomycin) and DNA synthesis (nalidixic acid, rifampicin and trimethoprim): nystatin and amphotericin are known to affect the cell membranes of certain fungi.^{10,39,40}

More details regarding the mechanisms of action of these antibiotics may be found in Table 3.1. Chronoamperometry and chronocoulometry were used to optimize the assay for sub-mL assay volumes, to find conditions of maximum difference between signals obtained in the absence and presence of antibiotic compounds. Results suggest that this assay can form the basis of a new, very rapid (20 min) method for testing antibiotic susceptibility in microorganisms.

Table 3.1: Properties and mechanistic information of the antibiotic compounds examined in this work.³⁹⁻⁴²

Penicillin G	Inhibits stage 3 of PG synthesis that occurs in the cell wall. Active against Gram-positive strains at low concentrations and Gram-negative strains at high concentrations. Normally tested using <i>S. aureus</i> by means of turbidimetry (5h) or plates (24h). Its effective range is 0.5-4 U/mL on plates against <i>S. aureus</i> . Bactericidal.
D-Cycloserine	Inhibits two enzymes that use D-alanine as substrate (racemase and synthetase) in stage 1 of PG synthesis. Inhibition occurs in cytoplasm during preparation of precursors. Its effective range is 50-200 µg/ml against <i>E. coli</i> . Active against Gram-positive and Gram-negative bacteria. Bactericidal.
Rifampicin	Binds to RNA polymerase and specifically inhibits DNA-dependent RNA polymerase by inhibiting the initiation process. Active against Gram-positive bacteria and Gram-negative at high concentrations.
Vancomycin	Inhibits stage 3 of PG synthesis, which is the polymerization of glycan. By binding to PG precursors, vancomycin inhibits the transglycosylation step that occurs in the cell wall. (High MW and not autoclavable) Its effective range is 20-200 U/mL against <i>S. aureus</i> and <i>B. subtilis</i> . Active against Gram-positive bacteria. Bactericidal.
Bacitracin	Lipid-soluble polypeptide. It inhibits stage 2 of PG synthesis in the membrane, where it binds to undecaprenyl-PP and inhibits its dephosphorylation. It is unable to penetrate the outer membrane of Gram-negative bacteria. Bacitracin needs divalent cations (Cd^{2+} , Mn^{2+} , and Zn^{2+} best, not Mg or Ca) for activity. Relatively non-polar due to side chains of amino acid residues. Completely inhibits <i>M. lysodeiliticus</i> at 0.1 µM. Its effective range is 0.5-4 U/mL against <i>S. subflava</i> or <i>Micrococcus flavus</i> . Bactericidal.

Tetracycline	Binds to the 30S ribosomal subunit and thus prevents aminoacyl-tRNAs binding to the ribosome. Does not affect DNA or RNA cell wall synthesis. Active against Gram-negative and Gram-positive bacteria (not autoclavable). Its effective range against <i>S. aureus</i> or <i>B. cereus</i> is 0.5-1.6 µg/mL. On plates, 5 min after adding 0.1-1 µg/mL to a <i>S. aureus</i> culture (exponential phase), 80-90% of protein synthesis was inhibited. Bacteristatic.
Chloramphenicol	Inhibits peptidyltransferase activity of the 50S ribosomal subunit by binding directly to ribosomal RNA. Concentration needed for inhibition is 10 µg/ml with Gram-positive and 0.2-5 µg/ml for Gram-negative bacteria. Tested against <i>B. subtilis</i> on plates; its effective range is 10-100 µg/mL. Bacteristatic.
Erythromycin	Binds to the 50S ribosomal subunit and stimulates the dissociation of peptidyl-tRNA from ribosomes during translocation. Active against Gram-positive bacteria. Tested on plates using <i>S. aureus</i> displaying an effective range of 0.5-2µg/mL. Bacteristatic.
Streptomycin	Inhibits initiation and causes misreads of mRNA by irreversibly binding to the 30S ribosomal subunit. Misreads occur if 30S is already bound to mRNA when streptomycin binds. Active against Gram-negative and Gram-positive bacteria. Its effective range against <i>S. aureus</i> is 3-40 µg/mL. R-factor resistance or many Gram-negative species has reduced effectiveness of the antibiotic. Eukaryotic cell-sensitive e.g. <i>S. cerevisiae</i> . Bactericidal.
Nalidixic acid	Inhibits bacterial DNA gyrase, which is involved in DNA replication by hydrolyzing a phosphodiester bond in one dsDNA strand. DNA gyrase is essential for replication of the bacterial chromosome. Nalidixic acid is not effective against eukaryotes, but is well tolerated by animals. With exponential phase <i>E. coli</i> , 10 µg/mL stops DNA synthesis in 10 min. RNA and protein synthesis as well as cell mass are unaffected. This antibiotic is active against both Gram-positive and Gram-negative strains.

Trimethoprim	Inhibits nucleoside biosynthesis of tetrahydrofolic acid, which is a one-carbon donor in purine/pyrimidine biosynthesis. Trimethoprim inhibits dihydrofolate reductase in bacterial cells only. Active against Gram-negative and Gram-positive bacteria.
Amphotericin	A polyenemacrolide (heptanene), which is a cell wall channel-former when, combined with cholesterol. Effective at 1 μ g/ml for fungi.
Nystatin	Inactive against bacteria, but it binds and disrupts fungal cell membranes. Disruption is limited to those having a steroid of proper configuration in its membrane (has steroidal binding site). Inhibits respiration due to leaks in cell membrane.
Cephalosporin C	Same as Penicillin G. Tested with <i>Salmonella gallinarum</i> . Its effective range is 10-100 μ g/mL.

3.2 EXPERIMENTAL SECTION

3.2.1 Materials and Instrumentation

All antibiotics were obtained from Sigma and were used as received. *E. coli* JM105 and *C. sporogenes* ATCC 8075 were obtained from the strain collection of the University of Waterloo, Department of Chemistry and Department of Biology, respectively. Sources of chemicals used in the growth medium and the electrochemical assays were the same as described in Chapter 2.

Optical density was measured at 600 nm using a Cary 1 double-beam uv-visible spectrophotometer. Chronoamperometry and chronocoulometry were performed using a

PAR Model 263 potentiostat with a PAR Model 616 platinum disk electrode ($A = 0.126 \text{ cm}^2$, chronoamperometry) or a platinum stationary voltammetry electrode ($A = 0.027 \text{ cm}^2$, Bioanalytical Systems). Prior to each run, electrodes were polished with slurries of 1.0 and $0.5 \mu\text{m}$ alumina (Buehler) and sonicated in distilled water. Incubation with antibiotics and electrochemical measurements were done at 37°C , if not indicated otherwise.

3.2.2 Methods

3.2.2.1 Cultivation of Microorganisms

E. coli JM105 was cultured aerobically in shake-flasks at 37°C and 250 rpm using a glucose-limited, chemically-defined growth medium. Growth conditions were the same as those described in Chapter 2. Anaerobic cultivation of *C. sporogenes* was performed at 37°C in a cultivation tube in 20 mL sterile medium containing KH_2PO_4 (2.88 g/L), $\text{K}_2\text{HPO}_4 \cdot 3\text{H}_2\text{O}$ (5.76 g/L), tryptone (2.4 g/L), yeast extract (1.2 g/L), trisodium citrate dihydrate (1.2 g/L), $\text{MgSO}_4 \cdot 7\text{H}_2\text{O}$ (0.48 g/L), $\text{CaCl}_2 \cdot 2\text{H}_2\text{O}$ (0.048 g/L), $(\text{NH}_4)_2\text{SO}_4$ (1.63 g/L), NH_4Cl (1.34 g/L), glucose (13.2 g/L) and 240 μL of the trace element stock solution per liter of medium ($\text{FeSO}_4 \cdot 7\text{H}_2\text{O}$ (40 g/L), $\text{MnSO}_4 \cdot \text{H}_2\text{O}$ (10 g/L), $\text{AlCl}_3 \cdot 6\text{H}_2\text{O}$ (10 g/L), $\text{CoCl}_2 \cdot 6\text{H}_2\text{O}$ (4 g/L), $\text{ZnSO}_4 \cdot 7\text{H}_2\text{O}$ (2 g/L), $\text{Na}_2\text{MoO}_4 \cdot 2\text{H}_2\text{O}$ (10 g/L), $\text{CuCl}_2 \cdot 2\text{H}_2\text{O}$ (1 g/L) and H_3BO_3 (0.5 g/L) in 5 M HCL). The growth medium was deaerated using nitrogen for 30 min prior to inoculation with *C. sporogenes* ATCC 8075. Cultivation tubes (20 mL) were incubated at 37°C for 48 h and all handling and sampling was performed under nitrogen flow.

3.2.2.2 Measurement of Optical Density

Aliquots of cell suspension were centrifuged (14000 rpm) for 5 min; the supernatant was discarded and the pellet was resuspended in 1 mL of distilled water. The optical density of the resuspended cells was measured spectrophotometrically at 600 nm using water as a reference. The obtained OD₆₀₀ values of *E. coli* JM105 were averaged and converted into bacterial dry matter values (BDM, g/L) through a calibration curve (OD₆₀₀ = 1.55*BDM + 0.02). The calibration curve was attained by comparing OD₆₀₀ values for a series of dilutions of cell suspensions with masses, obtained by drying aliquots of these dilutions overnight at 105°C as described in Section 2.2.2.4 (Chapter 2).

3.2.2.3 Cyclic Voltammetry

Three working electrode materials (glassy carbon, gold and platinum, A = 0.126 cm²) were examined using 1.0 mM solutions of potassium ferrocyanide in buffer (growth medium as above without glucose, tryptone, yeast extract and trace elements) prepared in the absence and presence of antibiotics. Scan rates of 5 and 50 mV/s were used with a potential range of – 40 to + 800 mV vs AgCl for each antibiotic and electrode material.

3.2.2.4 Chronoamperometry

Aliquots of the *E. coli* cell culture were harvested in mid-exponential phase or stationary phase and stored on ice. A test for stability showed that *E. coli* could be stored on ice for a period of 3.5 h before specific ferricyanide reduction rates began to significantly change (decrease) as shown in Figure 3.2. Unless otherwise noted, a 1.00 mL aliquot of the sample with known OD₆₀₀ was centrifuged for 5 min at 14,000 rpm. This pellet was subsequently resuspended in buffer (growth media as above without glucose, tryptone, yeast extract and trace elements), containing or lacking the antibiotic. An incubation

period of 15 min at 37°C was implemented (if not otherwise stated). Depending on its solubility, the antibiotic concentration ranged from 0.1 – 10 mM. After this preincubation step, the sample was added to the electrochemical cell containing 40 mL of the buffered reagent solution (50 mM ferricyanide and 10 mM succinate in the same buffer) and the ferricyanide reduction rate was measured over 500 s at 37°C. The electrochemical cell consisted of a platinum-rotating disk working electrode (600 rpm) at an applied potential of +0.5 V vs Ag/AgCl with a stainless steel wire as an auxiliary electrode. The specific activities ($\mu\text{mol}/\text{min}\cdot\text{g}$) were calculated using the reduction slope (nA/sec), the calibration slope for ferrocyanide (calibration was routinely performed at the end of a series of bacterial measurements and values near $-50 \text{ nA}/\mu\text{M}$ were routinely obtained) and the various calibration slopes for the antibiotics, as well as total volume (L) and BDM (g) as shown in Equation 2.5 (Chapter 2). The remaining reduction activity (percent activity) of *E. coli* after exposure to the antibiotic was obtained by comparing the specific activities of the blank with the antibiotic solutions.

3.2.2.5 Chronocoulometry

Aliquots of the bacterial cell cultivation were harvested and stored on ice for a minimum of 10 min. Throughout the optimization of the solution assay, a variety of conditions were used but only the final bioassay is described here in detail.

Twenty microlitres ($20 \mu\text{L}$) of untreated bacterial suspension were combined in an Eppendorf tube with $130 \mu\text{L}$ of buffer (growth medium as above without glucose, tryptone, yeast extract and trace elements) prepared in the presence or absence of antibiotic, and incubated for 10 min at 37°C. At this time, $150 \mu\text{L}$ 0.1 M potassium ferricyanide solution containing 20 mM succinate was added and the resulting solution

was incubated for 10 min at 37°C. The three electrodes, Pt working ($A = 0.027 \text{ cm}^2$), Ag/AgCl reference and stainless steel auxiliary electrode were then inserted. The working electrode potential was stepped to + 500 mV, and the resulting current integrated over a two minute measurement period to produce a plot of total charge against time.

3.2.2.6 Measurement of IC_{50} Values by Growth

IC_{50} values for antibiotic compounds were estimated using a broth dilution assay. *E. coli* JM105 was inoculated in growth medium containing various concentrations of antibiotics (chloramphenicol and penicillin G). After 10 h at 37°C, the OD_{600} value of each culture was measured. Blank cultures (no antibiotic) were included to ensure viability of the organism.

3.2.2.7 Disk Diffusion Susceptibility Test

Filter paper disks (1 cm diameter) were saturated with antibiotic solutions of the same concentration as were used for electrochemical measurements. The disks were evenly distributed on agar plates that had been inoculated with *E. coli* JM 105 and were incubated overnight at 37°C. Growth at the edge of the disk was indicative of *E. coli* resistance towards the antibiotic at that particular concentration, while zones of no growth surrounding the disks indicated sensitivity.

3.2.2.8 Determination of Colony Forming Units (cfu)

Bacterial cells were harvested during their exponential phase of growth and 100 μL aliquots of 1 mL samples were diluted in buffer (medium lacking proteins, glucose and trace elements). 100 μL of each dilution step were transferred and spread equally on to agar plates and incubated for 24 h at 37°C. Cell counts of agar plates showing 0 - 5, 5 - 50, 50 - 100 and 100 - 500 cells were used to calculate the cfu/mL cell suspension.

3.3 RESULTS AND DISCUSSION

3.3.1 Chronoamperometry

Initially, antibiotic susceptibilities of *E. coli* JM105 were determined using the traditional agar-disk diffusion method, because these testing resembled the reference or standard method to which the electrochemical method was compared to, and therefore were particular important. The results of the disk diffusion susceptibility tests are shown in Table 3.2. These compounds are known to be selective towards either Gram-negative or Gram-positive organisms (or fungi, in the case of nystatin and amphotericin), and are grouped according to their mechanism of action. It can be seen that *E. coli* JM105 is resistant to bacitracin, erythromycin, streptomycin and nystatin at concentrations at least 10-fold higher than the MIC values reported for these compounds using other microorganisms.^{10,38,39} Figure 3.1 displays a photographic enlargement of the filter disk susceptibility test, where bacterial growth around the edge of the filter was considered a sign of resistance. Results indicate bacterial cells were resistant to streptomycin and bacitracin, while trimethoprim and chloramphenicol were found to inhibit bacterial growth.

Table 3.2: Properties and disk diffusion susceptibility results with *E. coli* JM105 of the antibiotic stock solutions.

Compound	Target of action*	Disk diffusion susceptibility results	
		conc. (mM)	sensitivity
Penicillin G	Cell wall, Gram +/-	5.05	Sensitive
D-Cycloserine	Cell wall, Gram +/-	5.19	Sensitive
Vancomycin	Cell wall, Gram +	4.99	Sensitive
Bacitracin	Cell wall, Gram +	5.06	Resistant
Cephalosporin C	Cell wall, Gram -	1.03	Sensitive
Tetracycline	Protein synthesis, Gram +/-	5.14	Sensitive
Erythromycin	Protein synthesis, Gram +	4.96	Resistant
Chloramphenicol	Protein synthesis, Gram +/-	4.96	Sensitive
Streptomycin	Protein synthesis, Gram +/-	5.00	Resistant
Nalidixic acid	DNA, Gram +/-	1.05	Sensitive
Rifampicin	DNA, Gram +	0.49	Sensitive
Trimethoprim	DNA, Gram +/-	2.51	Sensitive
Amphotericin	Cell membrane, fungi	0.09	Resistant
Nystatin	Cell membrane, fungi	0.28	Resistant

*The known spectrum of activity is shown as Gram +, - or +/- for antibiotics that are generally effective against Gram-positive, Gram-negative or both types of microorganism (exceptions to the general classifications are also known for several microorganisms).¹⁰.

39,40

Figure 3.1: Picture of the agar disk susceptibility test, where filter disks were soaked in (a) 2.51 mM trimethoprim, (b) 4.96 mM chloramphenicol, (c) 5.06 mM bacitracin and (d) 5.00 mM streptomycin (filter disks 6-times their original size). This figure is included for illustrative reasons only; actual tests were performed using a different Petri dish for each antibiotic (with control) and with replication (n = 4)



The disk diffusion susceptibility tests (Table 3.3) were performed using antibiotic concentrations that resembled the final concentrations used in the electrochemical assay. At these concentrations, sensitivities were identical to those obtained at 41-fold higher concentrations (Table 3.2), except in the case of rifampicin. *E. coli* exhibits resistance at 12 μ M rifampicin, but is sensitive at 0.49 mM. It is believed that rifampicin, an agent generally toxic to Gram-positive bacteria, only exhibits activity against the Gram-negative *E. coli* at very high concentrations.

Table 3.3: Properties and disk diffusion susceptibility results with *E. coli* JM105 of antibiotic compounds at their final concentration in the electrochemical assay.

Compound	disk diffusion susceptibility results	
	conc. (μ M)	sensitivity
Penicillin G	122	Sensitive
D-Cycloserine	127	Sensitive
Vancomycin	122	Sensitive
Bacitracin	123	Resistant
Cephalosporin C	24	Sensitive
Tetracycline	125	Sensitive
Erythromycin	121	Resistant
Chloramphenicol	121	Sensitive
Streptomycin	122	Resistant
Nalidixic acid	26	Sensitive
Rifampicin	12	Resistant
Trimethoprim	61	Sensitive
Amphotericin	3	Resistant
Nystatin	7	Resistant

Table 3.4 shows the result of a commercially available disk diffusion test kit for antibiotic susceptibility (Mastering-S; Mast Laboratories Ltd. Merseyside UK).

Table 3.4: Disk diffusion susceptibility results with *E. coli* JM105 of antibiotic compounds present in test kit.

Compound	Total Amount	Disk diffusion susceptibility results
Chloramphenicol	25 μg	Sensitive
Erythromycin	5 μg	Resistant
Penicillin G	1 unit	Resistant
Streptomycin	10 μg	Resistant
Tetracycline	25 μg	Sensitive
Fusidic acid	10 μg	Resistant
Methicillin	10 μg	Resistant
Novobiocin	5 μg	Resistant

The results obtained from the commercial disk diffusion test kit confirmed that *E. coli* JM105 is susceptible to chloramphenicol and tetracycline, and resistant towards erythromycin and streptomycin under these conditions. With a total activity of 1 unit of penicillin G, *E. coli* JM105 exhibited resistance. This is characteristic of penicillin G with Gram-negative bacteria, as mentioned in the mechanistic information in Table 3.1. These results were not surprising since concentrations used were at least 10-fold higher than reported MIC values with these antibiotics for other microorganism.^{10,39,40}

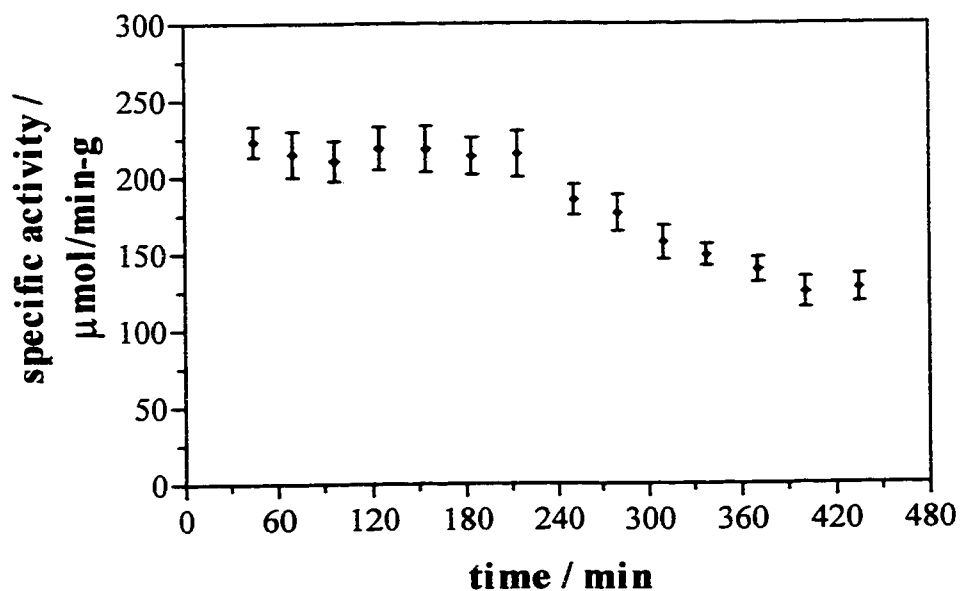
Prior to chronoamperometric experimentation, bacterial samples were stored on ice in order to arrest cell growth and thus maintain constant cell mass over long periods of time. To determine the effect of low temperature storage on bacterial respiratory activity, stability tests were performed. Figure 3.2 shows bacterial ferricyanide reduction activity ($\mu\text{mol}/\text{min-g}$) obtained for *E. coli* JM105 over time. After bacterial samples (1 ml aliquots) were stored on ice for known times, cell samples were centrifuged and resuspended in buffer prior to addition into the electrochemical cell (40 mL, 50 mM ferricyanide, 10 mM succinate), where the current was monitored for a total period of 15 min. Figure 3.2 shows stable and reproducible reduction activities over a time period of 3.5 to 4 h, after which a steady decline followed. These results indicate that viable bacterial cells slow their metabolic rates significantly after 3.5 to 4 h exposure to low temperature. Similar behaviour has been found in additional stability studies of exponential phase grown *E. coli* (see Table 3.5).

Table 3.5: Specific activities of exponential grown *E. coli* that were stored on ice over time.

Time on ice	Specific activities of exponential grown <i>E. coli</i> JM105* cultures		
		$\mu\text{mol}/\text{min-g}$	
min	OD ₆₀₀ 1.8	OD ₆₀₀ 2.1	OD ₆₀₀ 2.5
50	184.1	223.0	239.7
90	190.7	218.0	230.3
155	187.0	218.8	238.2
210	191.0	215.0	227.7
260	196.2	185.2	240.7
300	140.8	157.5	182.4

*Mean of duplicate measurements

Figure 3.2: Storage stability of exponential phase *E. coli* JM105 ($OD_{600} = 2.3$) on ice obtained by chronoamperometry. Each value represents the mean of duplicate measurements.



Preliminary chronoamperometric experiments were performed at room temperature using 102 mL (total volume). The electrochemical set-up consisted of a glassy carbon rotating disk electrode set at 600 rpm, and Ag/AgCl reference and stainless steel wire auxiliary electrodes. Bacterial cells were harvested in the exponential phase ($OD_{600} = 2.18$) and stored on ice. The centrifuged cells were resuspended in buffer (5 min) at room temperature. An aliquot of the bacterial sample (2.00 mL) was added to 100 mL of the reagent solution as indicated by the arrow in Figure 3.3, where currents for ferrocyanide oxidation were recorded over a period of 30 min. After 600 s, an aliquot of

the antibiotic stock solution was injected and microbial responses were monitored for the remaining 20 min. Figure 3.3 also shows chronoamperometric traces obtained in the absence and presence of chloramphenicol (0.197 mM) and trimethoprim (0.051 mM). Before injection of the antibiotic compound, all curves exhibit a similar linear change in current over time, corresponding to an increase in ferrocyanide concentration in the assay solution. After injection of the antibiotics to the assay solution, non-linearity in the latter stages of the assay in comparison to control experiments (lacking antibiotic) is observed. These results suggest that exposure to antibiotics may cause changes in respiratory cycle activity. However, a clear correlation could not be established because control experiments exhibited similar chronoamperometric curves.

Further experiments were conducted with antibiotics already present in the assay solution, in order to increase the exposure time of bacterial cells to the antibiotic compounds. For this reason, the runtime was extended to 40 min. Figure 3.4 shows chronoamperometric traces obtained for a control (lacking antibiotic) as well as tetracycline (0.097 mM) and penicillin G (0.10 mM). Within the first 7-8 min after of *E. coli* injection ($OD_{600} = 2.2$), all three curves show identical reduction rates but later show different plateau levels, with the control levelling off last, after about 30 min. These results encouraged a more thorough and systematic investigation of the effects of antibiotic compounds on bacterial ferricyanide reduction.

Figure 3.3: Chronoamperometric traces of ferricyanide reduction of *E. coli* after the injection ($t = 600$ s) of 1 mL (a) buffer, (b) 4.96 mM chloramphenicol and (c) 2.51 mM trimethoprim to 102 mL of the bioassay.

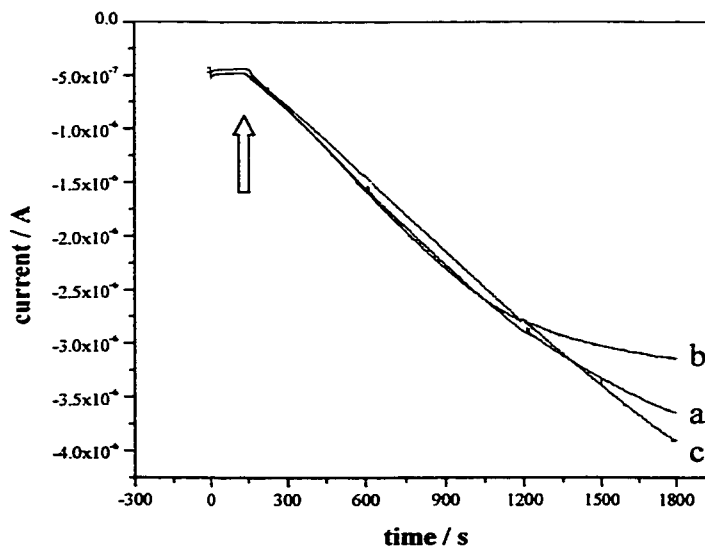
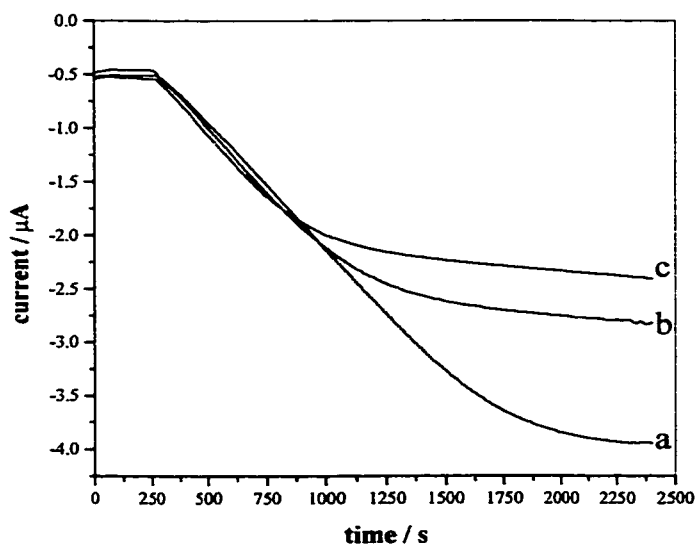


Figure 3.4: Chronoamperometric traces of ferricyanide reduction of *E. coli* (a) in the absence and presence of (b) 0.01 mM penicillin G and (c) 0.097 mM tetracycline.



The curvature exhibited in the chronoamperometric traces in Figures 3.3 and 3.4 may be attributed to either changes in ferricyanide reduction rates or to electrode fouling by the antibiotic compounds. Fouling by bacterial cell or medium components was shown not to occur in Chapter 2, where a glassy carbon electrode was also used. Cyclic voltammetry was then performed on buffered solutions of 1 mM ferrocyanide prepared in the absence and presence of the antibiotics listed in Table 3.1, to determine if adsorption of the antibiotics occurs and leads to electrode fouling. Figure 3.5 shows voltammograms recorded on (a) glassy carbon, (b) platinum, and (c) gold working electrodes in the absence or presence 2.25 mM tetracycline. The increase in peak separation that occurs on the glassy carbon and gold electrodes in the presence of tetracycline (Figure 3.5a and c) indicates slower ferri/ferrocyanide electron transfer kinetics and suggests adsorption of tetracycline onto the glassy carbon and gold surfaces. On the other hand, voltammograms recorded at a platinum working electrode (Figure 3.5b) are superimposable, thus showing that tetracycline has no noticeable effect on the kinetic behaviour of the ferri/ferrocyanide redox couple at Pt. The full range of antibiotics listed in Table 3.1 was also tested by means of cyclic voltammetry using glassy carbon, platinum and gold electrodes. Results obtained from this survey showed that only platinum had no noticeable difference in voltammograms obtained in the presence of antibiotics. Therefore, platinum was selected as the working electrode material for all subsequent experimentation.

Further chronoamperometry experiments investigating the effects of antibiotics on *E. coli* JM105 were performed, but this time a reduced volume of 41.0 mL was used, and a platinum rotating-disk electrode was also implemented. In order to increase bacterial metabolic rates, measurements were conducted at 37°C, which is the physiological temperature of *E. coli*. Antibiotics were present at low concentration in the assay buffer

which also contained 50 mM ferricyanide and 10 mM succinate. Subsequently, centrifuged and resuspended cells (1.00 mL) were added to this solution (40.0 mL) at $t = 2$ min, and current was recorded for a total of 30 min.

Figure 3.5: Cyclic voltammograms of 1.00 mM ferrocyanide in assay buffer, in the absence and presence of 2.25 mM tetracycline, at 50 mV/s and 20°C at (a) glassy carbon, (b) platinum and (c) gold working electrodes.

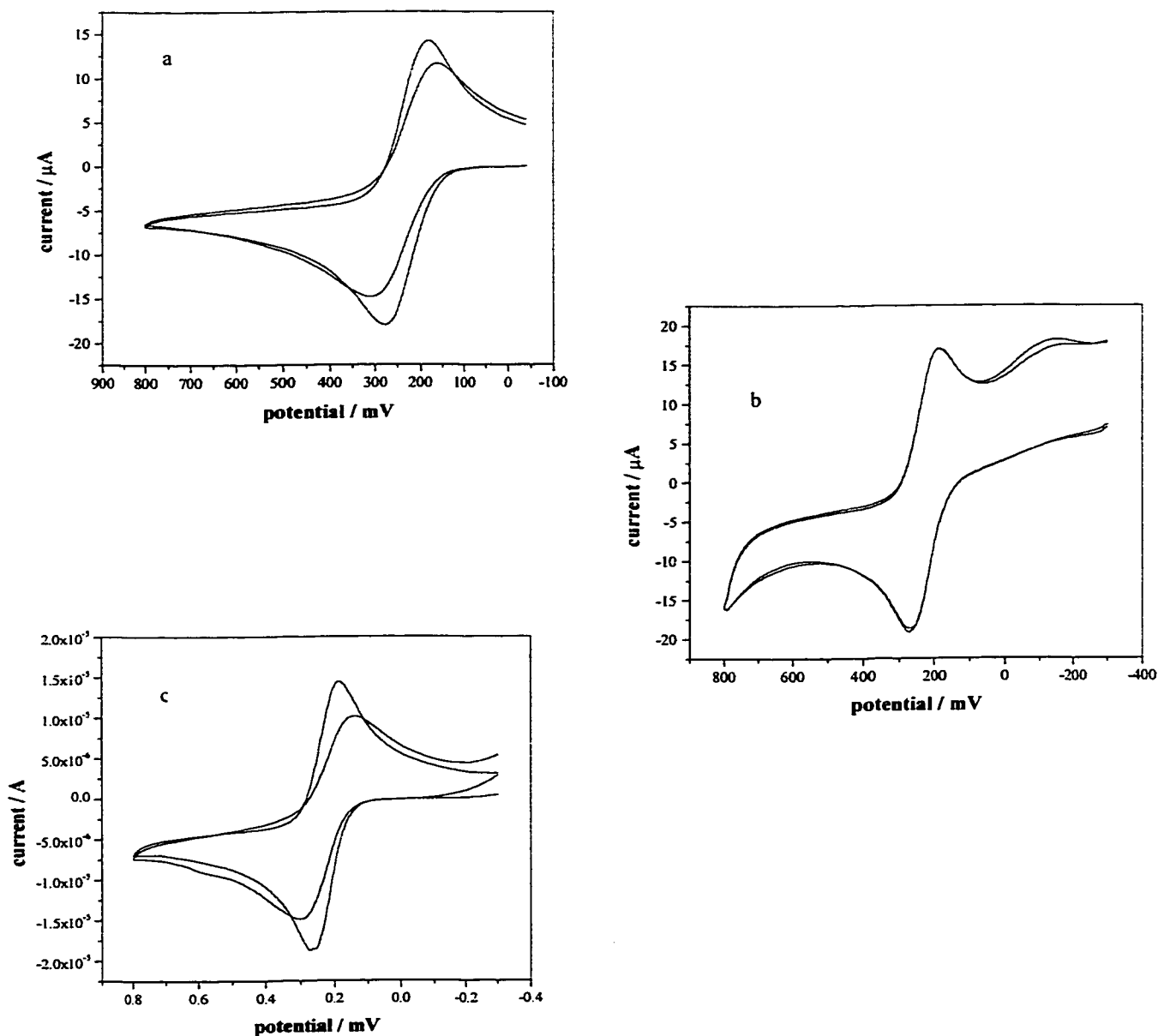
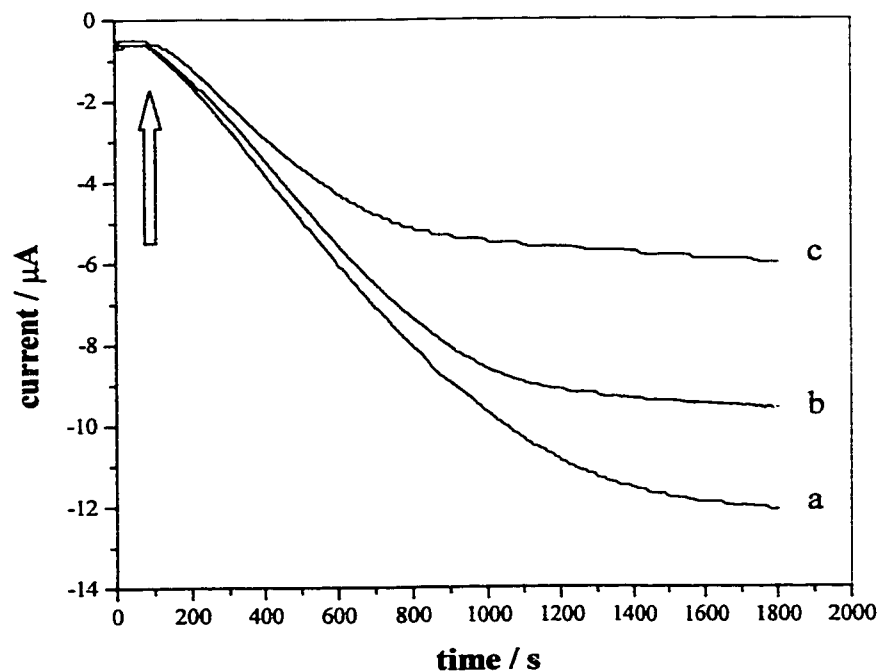


Figure 3.6 shows chronoamperometric traces obtained in this manner in the absence and presence of trimethoprim and chloramphenicol. All three curves exhibit an initially linear change in current with time. Significant deviations from linearity begin to occur after about 10 min. All three curves tend towards plateau levels for the remaining 20 min of the assay. This curvature was found when testing antibiotics as well as with the control (lacking antibiotic), although the control (Figure 3.6a) begins to plateau at a later time in the assay.

Figure 3.6: Chronoamperometric traces obtained at 37°C at a Pt RDE ($A = 0.126 \text{ cm}^2$, 600 rpm) at + 0.50 V vs Ag/AgCl in assay buffer containing 50 mM $\text{K}_3\text{Fe}(\text{CN})_6$ and (a) no antibiotic, (b) 127 μM trimethoprim and (c) 124 μM chloramphenicol. The addition of 1.00 mL resuspended *E. coli* JM105 cells to 40 mL assay buffer is indicated by the arrow.



E. coli adsorption onto the Pt electrode surface would be expected to cause observed plateaus due to fouling. To exclude this as a possibility, control experiments were performed involving replicate runs made without polishing the electrode surface between runs. Experimental results showed identical traces, indicating that *E. coli* does not adsorb onto the rotating disk electrode surface. The curvature observed with controls must be therefore attributed to either exhaustion of intracellular respiratory substrates or to osmotic shock due to cell exposure to the high ionic strength buffer (50 mM $K_3Fe(CN)_6$). The differences in time at which non-linearity begins when using chloramphenicol and trimethoprim might be a direct result of the antibiotic compound.

Figure 3.6 also shows a significant difference in the slopes obtained in the initial linear region of the chronoamperometric traces that takes place over the first 10 min of the assay. Ferricyanide reduction slopes obtained in the presence of trimethoprim and chloramphenicol are lower than that obtained in their absence. This suggests inhibition of respiratory activity due to the brief exposure of *E. coli* JM105 to the antibiotic compound. This phenomenon was not observed in experiments conducted at room temperature (see Figure 3.4) where all initial slopes were identical. Instead, an increase from room temperature (22°C) to 37°C not only increased the bacterial reduction activity (as shown in Chapter 2), but also enhanced the kinetics of antibiotic uptake into cell. Incubation of *E. coli* JM105 on agar plates in the absence and presence of filter disks saturated with either trimethoprim or chloramphenicol show that the organism is sensitive to both of these antibiotics. Antibiotic concentrations in this assay were the same as those used for the disk-diffusion test in Table 3.2. Calibrations were routinely performed at the end of each series of bacterial measurements, and values near $-50 \text{ nA}/\mu\text{M}$ were obtained in acceptable experiments. Calibrations were performed using a series of ferrocyanide

concentrations in the presence of antibiotics. The slopes of these calibration curves were then used to calculate metabolic rates in the presence of antibiotic compounds. The specific activities ($\mu\text{mol}/\text{min}\cdot\text{g}$) of bacterial ferricyanide reduction rates in the presence of antibiotics were calculated using the calibration slopes listed below.

Table 3.6: Calibration slopes obtained from the linear regression of a series of ferricyanide concentrations in the presence of antibiotic compounds.

Antibiotic compound	Concentration μM	Calibration slope* $\text{nA}/\mu\text{M}$	Linear fit r^2
Cephalosporin C	24	-46.2 ± 1.7	0.987
Rifampicin	12	-54.5 ± 5.7	0.901
Amphotericin	3	-54.4 ± 4.7	0.903
Penicillin G	123	-52.9 ± 1.0	0.996
Vancomycin	24	-51.1 ± 1.8	0.988
D-Cycloserine	126	-55.4 ± 0.4	0.999
Bacitracin	122	-50.8 ± 0.7	0.998
Tetracycline	125	-48.6 ± 1.2	0.993
Streptomycin	122	-56.3 ± 1.0	0.997
Trimethoprim	62	-49.6 ± 3.8	0.945
Nystatin	7	-47.5 ± 0.6	0.999
Nalidixic acid	25	-56.7 ± 1.0	0.997
Chloramphenicol	121	-51.6 ± 1.5	0.992
Erythromycin	123	-56.8 ± 0.5	0.999

*Triplicate measurements with a total number of $n = 12$ for each antibiotic.

Constant specific ferricyanide reduction rates could only be obtained within a limited time of 3.5 h for bacterial storage on ice (see Figure 3.2). Therefore surveying all available antibiotics required several bacterial cultivations, which led to differences in control rates. For this reason, results obtained using antibiotics are expressed as a percentage of the control rate, obtained in the absence of antibiotics. Following a 15 min incubation period, cell suspensions (1 mL) were added to the 40 mL assay buffer containing 50 mM ferricyanide and 10 mM succinate; the ferricyanide reduction current was monitored over a period of 500 s.

Figure 3.7 shows typical chronoamperometric traces obtained using exponential-phase *E. coli* JM105 in the absence and presence of penicillin G and chloramphenicol. These antibiotics caused significantly slower accumulation of ferrocyanide. This is evident from the small changes in current signals over time in comparison to control traces. Disk diffusion susceptibility tests, involving overnight incubation of agar plates, showed this strain of *E. coli* is sensitive to both of the above antibiotics. Both antibiotic concentrations as present in the initial incubation and dilution steps of the electrochemical assay displayed sensitivity when the agar plate method was employed (see Tables 3.2 and 3.3).

The chronoamperometric traces shown in Figure 3.8 suggest that *E. coli* antibiotic susceptibility can be measured within a period of 23 min for cells harvested in the stationary phase. As previously described, an aliquot (1 mL) of an overnight culture of *E. coli* were centrifuged and resuspended in the buffered 5.13 mM D-cycloserine or 5.04 mM penicillin G solution (15 min) and injected into the electrochemical cell.

Figure 3.7: Chronoamperometric traces obtained at 37°C using a Pt rotating disk electrode of exponential phase *E. coli* JM 105 following 15 min incubation in the absence (a) and presence of (b) 5.05 mM penicillin G and (c) 4.96 mM chloramphenicol.

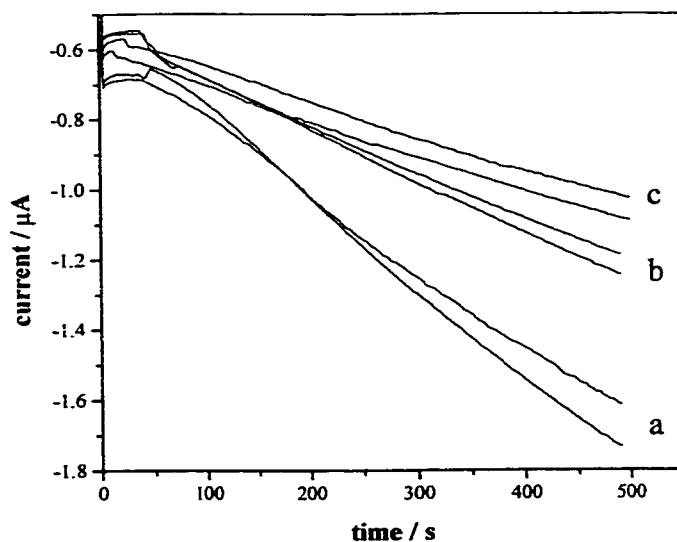


Figure 3.8: Chronoamperometric traces obtained for stationary phase grown *E. coli* JM105 in the absence (a) and presence of (b) 5.13 mM D-cycloserine and (c) 5.04 mM penicillin G prior to injection.

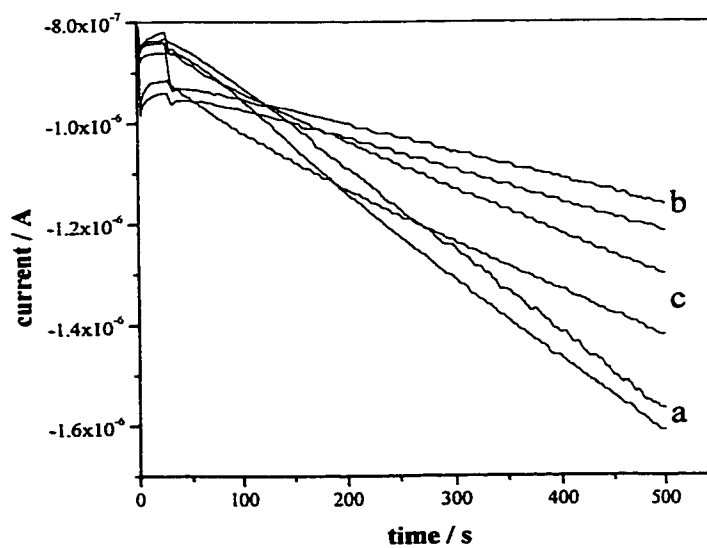


Figure 3.8 shows typical chronoamperometric traces obtained for stationary phase *E. coli* in the absence (a) and presence of 5.13 mM D-cycloserine (b) or 5.04 mM of penicillin G (c). Once again, these antibiotics significantly decreased the measured ferricyanide reduction rates, as was also observed with exponential grown *E. coli*.

3.3.1.1 Antibiotic Susceptibility Test

A full listing of raw data obtained from measurements on all 14 antibiotics using both exponential and stationary-phase *E. coli* JM105 is given in Table 3.7. Table 3.8 shows these results after conversion to percent activities.

Table 3.7: Summary of all CA results obtained during the survey of 14 antibiotics

Antibiotic (conc., mM)	Growth Phase*	OD ₆₀₀	Specific rate ($\mu\text{mol}/\text{min}\cdot\text{g}$) for	
			Control	Antibiotic
Chloramphenicol (4.96)	E	2.56	58.4 \pm 7.5 (n = 4)	27.7 \pm 0.3 (n = 2)
	S	3.12	129.1 \pm 14.6 (n = 5)	49.8 \pm 7.1 (n = 3)
Erythromycin (4.96)	E	2.56	58.4 \pm 7.5 (n = 4)	64.2 \pm 2.3 (n = 2)
	S	3.12	129.1 \pm 14.6 (n = 5)	122.2 \pm 12.3 (n = 3)
Cephalosporin C (1.03)	E	2.22	42.7 \pm 3.5 (n = 5)	29.0 \pm 1.1 (n = 2)
	S	3.03	72.2 \pm 10.8 (n = 4)	28.5 \pm 4.9 (n = 3)
Rifampicin (0.49)	E	2.22	42.7 \pm 3.5 (n = 5)	44.0 \pm 2.3 (n = 2)
	S	3.03	72.2 \pm 10.8 (n = 4)	78.5 \pm 11.3 (n = 3)
Nalidixic Acid (1.05)	E	2.41	123.0 \pm 10.7 (n = 2)	163.7 \pm 8.1 (n = 3)
	S	4.33	30.7 \pm 13.2 (n = 5)	64.3 \pm 1.9 (n = 2)
Amphotericin (0.09)	E	2.41	123.0 \pm 10.7 (n = 2)	154.8 \pm 15.7 (n = 3)
	S	4.33	30.7 \pm 13.2 (n = 5)	58.9 \pm 8.0 (n = 3)

Table 3.7: continue

Antibiotic (conc., mM)	Growth Phase*	OD ₆₀₀	Specific rate ($\mu\text{mol}/\text{min-g}$) for	
			Control	Antibiotic
Penicillin G (5.05)	E	2.76	61.1 \pm 8.4 (n = 5)	32.1 \pm 4.6 (n = 3)
	S	3.37	32.6 \pm 2.3 (n = 4)	20.1 \pm 0.9 (n = 2)
Vancomycin (4.99)	E	2.76	61.1 \pm 8.4 (n = 5)	33.1 \pm 3.9 (n = 2)
	S	3.37	32.6 \pm 2.3 (n = 4)	12.0 \pm 2.7 (n = 3)
Bacitracin (5.06)	E	1.85	122.6 \pm 21.3 (n = 5)	206.3 \pm 42.5 (n = 3)
	S	1.99	30.1 \pm 11.4 (n = 4)	54.0 \pm 6.7 (n = 2)
D-Cycloserine (5.19)	E	1.85	122.6 \pm 21.3 (n = 5)	68.1 \pm 7.1 (n = 2)
	S	1.99	30.1 \pm 11.4 (n = 4)	21.2 \pm 2.1 (n = 3)
Tetracycline (5.14)	E	2.28	120.3 \pm 5.6 (n = 4)	31.0 \pm 0.4 (n = 2)
	S	2.11	58.6 \pm 5.6 (n = 4)	29.1 \pm 2.3 (n = 2)
Streptomycin (5.00)	E	2.28	120.3 \pm 5.6 (n = 4)	109.2 \pm 15.0 (n = 3)
	S	2.11	58.6 \pm 5.6 (n = 4)	58.2 \pm 3.8 (n = 2)
Trimethoprim (2.51)	E	3.03	183.4 \pm 11.2 (n = 3)	165.3 \pm 18.0 (n = 2)
	S	3.14	77.3 \pm 2.8 (n = 4)	111.0 \pm 8.4 (n = 3)
Nystatin (0.28)	E	3.03	183.4 \pm 11.2 (n = 3)	175.3 \pm 5.0 (n = 2)
	S	3.14	77.3 \pm 2.8 (n = 4)	78.4 \pm 4.4 (n = 2)

* E = exponential phase (6 h) and S = stationary phase (10 h) *E. coli*

Table 3.8 shows the summarised results obtained from exponential phase *E. coli* compared with stationary phase cells. Remaining activities were calculated as a percentage where control measurements (lacking antibiotic) were defined as 100% activity. Each percentage (remaining activity) was obtained by averaging the values gathered from two or three replicate measurements. Replicate measurements made on

control samples from both exponential and stationary grown *E. coli* always yielded RSD values below 13%. Generally, where the chronoamperometric assay displayed significant decreases (< 85% activity) in ferricyanide reduction rates, no growth was observed on agar plates when using the disk diffusion susceptibility test (Table 3.2). Examples of antibiotics that displayed decreased respiratory activity and inhibition of growth on agar plates include penicillin G, D-cycloserine, vancomycin, cephalosporin C, tetracycline and chloramphenicol. Furthermore, four antibiotics (erythromycin, streptomycin and nystatin) that yielded resistance to *E. coli* JM105 in the overnight agar-plate susceptibility test showed no significant change in ferricyanide reduction rates in the chronoamperometric assay. From these results it is clear that lower ferricyanide reduction rates are generally indicative of antibiotic effectiveness against this organism.

Nevertheless, exceptions to this general conclusion are also evident when chronoamperometric results are compared to those obtained by disk-diffusion testing (Table 3.2). The three antibiotic compounds nalidixic acid, rifampicin and trimethoprim showed susceptibility with the agar disk-diffusion test, but did not yield a decrease in respiratory cycle activity (Table 3.7 and 3.8). Furthermore, significant increases (> 120% activity) in ferricyanide reduction rates were observed. Those antibiotics that produced higher reduction rates when using cells harvested during both phases of growth include: bacitracin, a polypeptide active against Gram-positive bacteria; nalidixic acid, a cell division inhibitor; and amphotericin, an antifungal. Trimethoprim and rifampicin (both inhibit DNA synthesis) caused increased reduction rates only with stationary phase *E. coli* JM105 cells.

Table 3.8: Chronoamperometric assay of ferricyanide reduction rates following 15 min incubation of *E. coli* JM105 with antibiotics.

Antibiotic	Concentration*	Percent activity for <i>E. coli</i> grown to	
	mM	Exponential Phase	Stationary Phase
Penicillin G	5.05	52%	61%
D-Cycloserine	5.19	56%	70%
Vancomycin	4.99	54%	37%
Bacitracin	5.06	170%	179%
Cephalosporin C	1.03	68%	40%
Tetracycline	5.14	26%	50%
Erythromycin	4.96	110%	97%
Chloramphenicol	4.96	47%	39%
Streptomycin	5.00	91%	100%
Nalidixic Acid	1.05	133%	210%
Rifampicin	0.49	100%	110%
Trimethoprim	2.51	92%	144%
Nystatin	0.28	96%	100%
Amphotericin	0.09	126%	192%

* Antibiotic concentration during 15 min incubation with cell suspension; 1.00 mL of this suspension was added to 40 mL of assay buffer containing 50 mM ferricyanide during chronoamperometric measurement.

It is known that ineffective antibiotics may cause an increase in cellular activity in resistant bacteria.⁴⁰ One similar example of such behaviour was found in the literature, where the peptide antibiotic nisin was found to stimulate oxygen consumption by *E. coli*, but was shown to have no effect on the growth of the same organism.⁴³ Bacitracin is also a peptide antibiotic, and is thought to be incapable of penetrating the outer membrane of Gram-negative bacteria.⁴⁴ For this reason, it is believed that both bacitracin and

amphotericin activate the defence system of Gram-negative *E. coli*, thus resulting in higher metabolic rates as measured by the chronoamperometric assay. Nalidixic acid, a bactericidal, inhibits the bacterial DNA gyrase involved in DNA replication.⁴⁵ Experiments using exponential phase *E. coli* have shown that 10 $\mu\text{g/mL}$ nalidixic acid (39 μM) stops DNA synthesis within 10 min, but does not affect RNA and protein synthesis.⁴⁶ Trimethoprim is a potent competitive inhibitor of bacterial dihydrofolate reductase, an enzyme involved in nucleoside synthesis, while rifampicin binds specifically to the DNA-dependent RNA polymerase.^{40,47} Neither of these compounds form covalent bonds with their targets, and it is possible that the 40-fold dilution of the cell-plus-antibiotic mixture into the ferricyanide assay buffer causes reversal of binding. The increase of active efflux of the drugs from the cytoplasm into the assay buffer may account for increased metabolic rates, measured *via* ferricyanide reduction.

Table 3.8 also shows differences in 'percent activity' values between exponential and stationary phase grown *E. coli*. Further experiments were performed to identify the best growth stage to employ when dealing with specific antibiotic groups. Nevertheless, no information could be obtained on whether antibiotic susceptibility is more pronounced in exponential or stationary phase grown cells. Consequently, it was impossible to determine if cell wall, protein synthesis or DNA synthesis inhibitors are more active during the exponential or stationary phases of cell growth (as seen when using penicillin G and cephalosporin C).

Stationary phase cells exhibited increased respiratory activity in the presence of nalidixic acid, rifampicin and trimethoprim (DNA-synthesis inhibitors) although no growth was observed on agar plates. This might indicate that a 15 min incubation in the antibiotic stock solution is not sufficient to cause a measurable change in cellular activity.

3.3.1.2 Exposure Time Studies

The effects of varying antibiotic exposure times on specific ferricyanide reduction rate were further investigated using stationary phase and exponential phase grown *E. coli*. Centrifuged cells were resuspended in buffered antibiotic solutions and specific activities were determined for each incubation time. Data obtained in this manner are listed in Table 3.9 - 3.14.

Table 3.9: Specific activity* ($\mu\text{mol}/\text{min}\cdot\text{g}$) for each incubation step of stationary phase *E. coli* ($\text{OD}_{600} = 2.13$; $t = 9$ h) by chronoamperometry.

Exposure time min	Blank*	Vancomycin*	Trimethoprim*
	-	4.99 mM	2.51 mM
5	138	160	142
10	134	134	153
15	129	68	201
20	36	-	-

Table 3.10: Specific activity* ($\mu\text{mol}/\text{min}\cdot\text{g}$) for each incubation step of stationary phase *E. coli* ($\text{OD}_{600} = 1.68$; $t = 8.5$ h) by chronoamperometry.

Exposure time min	Blank*	Nalidixic Acid*	Amphotericin*
	-	1.05 mM	0.09 mM
5	106	-	255
10	150	306	322
15	158	298	258
20	54	201	192
25	34	165	241

Table 3.11: Specific activity* ($\mu\text{mol}/\text{min}\cdot\text{g}$) for each incubation step of exponential phase *E. coli* ($\text{OD}_{600} = 2.12$; $t = 5.5$ h) by chronoamperometry.

Exposure time min	Blank*	Vancomycin*	Trimethoprim*
	-	4.99 mM	2.51 mM
5	179	252	314
10	166	120	154
15	170	58	140

Table 3.12: Specific activity* ($\mu\text{mol}/\text{min}\cdot\text{g}$) for each incubation step of exponential phase *E. coli* ($\text{OD}_{600} = 2.37$; $t = 5.5$ h) by chronoamperometry.

Exposure time min	Blank*	Nalidixic Acid*	Erythromycin*
	-	1.05 mM	5.00 mM
5	255	341	255
10	223	289	234
15	239	205	245
20	241	201	234
30	160	195	-

Table 3.13: Specific activity* ($\mu\text{mol}/\text{min}\cdot\text{g}$) for each incubation step of exponential phase *E. coli* ($\text{OD}_{600} = 1.63$; $t = 5.0$ h) by chronoamperometry.

Exposure time min	Blank*	Tetracycline*	Chloramphenicol*
	-	5.14 mM	4.96 mM
5	163	51	58
10	140	38	42
15	125	36	53
20	153	24	34
30	49	23	28

Table 3.14: Specific activity* ($\mu\text{mol}/\text{min}\cdot\text{g}$) for each incubation step of exponential phase *E. coli* ($\text{OD}_{600} = 2.05$; $t = 5.5$ h) by chronoamperometry.

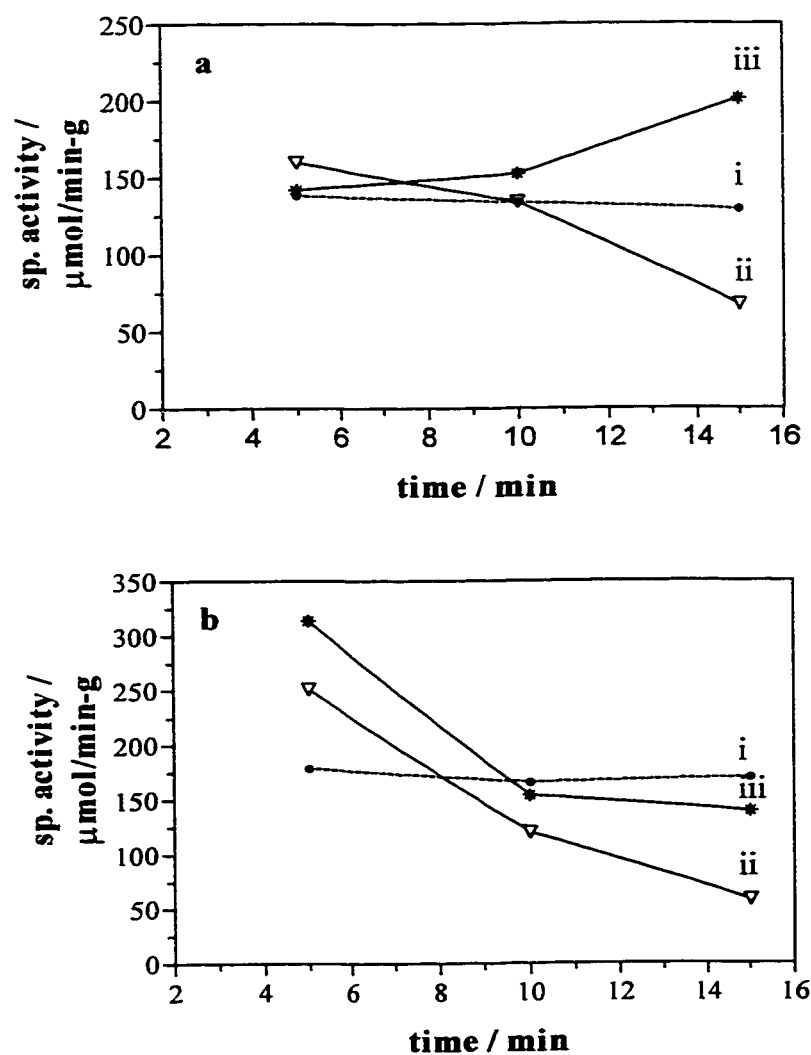
Exposure time min	Blank*	Bacitracin*	Streptomycin*
	-	5.06 mM	5.00 mM
5	238	275	212
10	192	342	201
15	187	354	180
20	169	337	210
30	123	318	198

The effects of differential antibiotic exposure periods on bacterial metabolic rates were investigated. *E. coli* cells harvested in the exponential phase and incubated using trimethoprim (DNA-inhibitor), for 15 min exhibited a decrease in respiratory activity, while stationary grown cells incubated using the same antibiotic and for the same period of time exhibited an increase in ferricyanide reduction. These results are characteristic of short exposure time experiments. However, control measurements made in the absence of antibiotics consistently showed a significant decrease in ferricyanide reduction rates after incubation times exceeded 15 min for stationary phase cells and 20 min for cells harvested during their exponential phase. A decrease in cellular activity was seen in all experiments indicating that cells may have been depleted of intracellular respiratory substrates after a certain amount of time. As a direct result, further experiments using antimicrobial compounds were limited to incubation times of 15 and 20 min, depending on cellular growth phase.

Figure 3.9 shows results obtained using (a) stationary- and (b) exponential-phase *E. coli* JM105 in the presence of vancomycin and trimethoprim. Over 15 min cell

exposure time to 4.99 mM of vancomycin caused a distinct drop in respiratory activity in both growth phases of *E. coli*. However, the presence of 2.51 mM of trimethoprim yielded an increased ferricyanide reduction rate for stationary-phase *E. coli*, whereas exponential-phase bacterial cells showed decreased rates within the same time period.

Figure 3.9: Exposure time curves of (a) stationary-phase and (b) exponential-phase *E. coli* JM105 obtained in the absence (i) and presence of 4.96 mM vancomycin (ii) and 2.51 mM trimethoprim (iii).



In summary, chronoamperometric results obtained in this study remain inconclusive, since increasing ferricyanide reduction rates over time can be seen in both control and antibiotic experiments. Further investigations on the effects of incubation time should be performed, but in the presence of respiratory substrates, such as succinate or formate, to ensure stable control reduction rates over longer periods. Unpublished results performed by Gil Francisco and Peter Ertl suggests that time related antibiotic effects on bacterial respiration can be studied by adding succinate to the antibiotic solution.

3.3.2 Chronocoulometry

To extend this work to a practical, rapid and more sensitive antimicrobial susceptibility test, a constant antibiotic concentration (with minimal dilution) throughout the incubation and measurement periods was desired, as well as a decrease in the assay volume and measurement time. Chronocoulometry allows not only measurements on small sample volumes, but also exhibits superior sensitivity and speed. The applied waveform of chronocoulometry is the same as in chronoamperometry, but in chronocoulometry the current is integrated so that the monitored response is the charge (Q). By integrating the current and presenting the charge as a function of time, some of the information obtained in the current response becomes more easily extractable. The measured charge represents the sum of three components:⁴⁸

1. Electrolysis of electroactive species in the solution, at a rate that is controlled by diffusion to the electrode ($Q_{\text{diffusion}}$).
2. Electrolysis of electroactive species adsorbed onto the electrode surface ($Q_{\text{adsorption}}$).
3. Charging of the electrode-electrolyte double-layer capacitance to the new potential ($Q_{\text{dl charging}}$).

or

$$Q_{\text{total}} = Q_{\text{diffusion}} + Q_{\text{adsorption}} + Q_{\text{dl charging}} \quad 3.1$$

$$Q_{\text{total}} = \int_0^t i \, dt = \frac{2nFA C_0^o D_0^{1/2} t^{1/2}}{\pi^{1/2}} + nFA\Gamma_0 + Q_{\text{dl}} \quad 3.2$$

where:

Γ_0	amount of adsorbed reactant in mol/cm ²
i	current, A
n	number of electrons
F	Faraday's constant, 96,485 C/eq
A	electrode area, cm ²
D_0	diffusion coefficient of analyte, cm ² /s
C_0	concentration of analyte, mol/cm ³

Double-layer charging and oxidation of the adsorbed electroactive species occur almost instantaneously at the beginning of the run, whereas the charge required for oxidation of analyte (ferrocyanide) in the solution exhibits a diffusion-controlled time dependency. By subtracting the background, which is measured in a separate experiment on the supporting electrolyte (buffer containing 50 mM ferricyanide and 10 mM succinate; reagent solution) in the absence of bacteria, the remaining information is exclusively related to the analyte.⁴⁸

Initial chronocoulometric experiments were performed using a set-up similar to that used when performing chronoamperometry measurements. Centrifuged and resuspended cell samples (2 min in buffer) were injected (1 mL) into the electrochemical cell (volume of 40 mL) containing 50 mM ferricyanide and 10 mM succinate and incubated over a period of 15 min at 37°C. At this point, the Pt working electrode ($A = 0.126 \text{ cm}^2$) was poised at + 0.5 V vs Ag/AgCl for a total runtime of 60 s.

Figure 3.10 shows chronocoulometric traces obtained in the absence (a) and presence (b) of 1.02 mM chloramphenicol. These traces show unexpected linearity over the 60 s measurement period, and significant decreases can be seen between control traces and those obtained in the presence of chloramphenicol. The linearity of these traces may be attributed to the continually increasing concentration of ferrocyanide in the assay solution. Results reveal that a assay runtime of 60 s, following a 15 min preincubation period, can readily distinguish between control and chloramphenicol samples. Electrochemical runtime has thus been reduced from 800 s to 60 s.

Chronocoulometric results listed in Table 3.15 were calculated as the difference in integrated current between 30 and 60 s. Values obtained from the control measurements ($n = 4$) yielded a relative standard deviation (RSD) of 3.6 %. The shorter runtime and the improved relative standard deviation (4% instead of 13%) demonstrate the benefits of chronocoulometry over chronoamperometry.

Figure 3.10: Chronocoulometric traces obtained at 37°C at a Pt electrode ($A = 0.126 \text{ cm}^2$) for exponential phase *E. coli* JM105 ($OD_{600} = 3.27$) following 15 min incubation in 40mL reagent solution (50 mM ferricyanide and 10 mM succinate) in the absence (a) and presence (b) of 1.02 mM chloramphenicol. (In this case (c) is background)

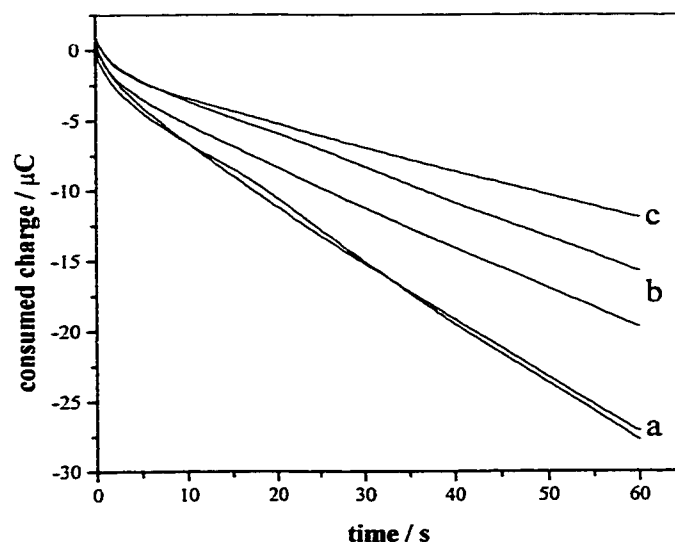


Table 3.15: Ferricyanide reduction by late exponential phase *E. coli* JM105 ($OD_{600} = 3.27$) obtained with chronocoulometry ($V_t = 41 \text{ mL}$) in the absence and presence of 1.02 mM chloramphenicol.

Name	Consumed charge, μC (between $t_1 = 30 \text{ s}$ and $t_2 = 60 \text{ s}$)
1 Background*	5.0
2 Control	12.0
3 Control	11.9
4 Chloramphenicol	7.5
5 Chloramphenicol	8.5
6 Control	12.7
7 Control	11.7

*Chronocoulometry performed in the absence of bacterial cell suspension

3.3.2.1 Miniaturization of the Chronocoulometric Assay

This section is mainly concerned with the down-scaling and optimization of the chronocoulometric assay. The objective was to find assay conditions under which microtiter-scale susceptibility tests would exhibit minimum relative standard deviations while showing maximum signal differences between control and antibiotic tests. For that reason, various volumes, incubation and runtimes were tested in the absence and presence of antibiotics.

To perform chronocoulometric measurements in small volumes, miniature reference and working electrodes were used. As indicated in Equation 3.2 current (and therefore charge) is a function of the working electrode surface area. Therefore, the exact electrochemical surface area was determined prior to experimentation. The platinum electrode was polished using alumina for 3 min, followed by sonication in methanol for 5 min prior to each run. Chronoamperometric measurements were performed in 0.1 M KCl containing 4.0 mM $K_4Fe(CN)_6$ (ferrocyanide), at a pH of 6.4. The electrochemical surface area was determined by plotting $i^{1/2}$ vs time and using the Cottrell equation 3.3 for planar electrodes to calculate the surface area.^{48,49}

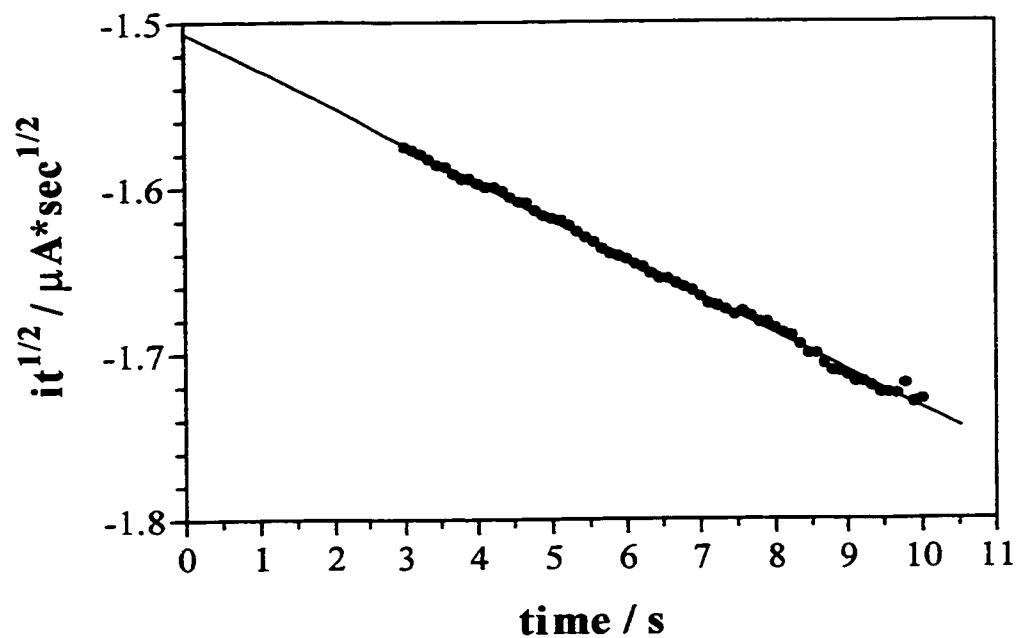
$$i^{1/2} = \frac{n F A C_0 D^{1/2}}{\pi^{1/2}} \quad 3.3$$

where:

$i^{1/2}$	current at $t = 0$, $-1.5 \mu A \cdot s^{1/2}$
n	number of electrons, 1
F	Faraday's constant, 96,485 C/eq
A	electrode area, cm^2
D_0	diffusion coefficient of $K_4Fe(CN)_6$, $6.5 \times 10^{-6} cm^2/s$ ⁴⁹
C_0	concentration of $K_4Fe(CN)_6$, $4 \times 10^{-6} mol/cm^3$

The value $it^{1/2}$ ($-1.5 \mu\text{A}\cdot\text{s}^{1/2}$) was obtained by extrapolating the linear regression (see Figure 3.11) to $t = 0$ and inserting this value into Equation 3.3. The new platinum working electrode was found to have an electrochemical surface area of 0.027 cm^2 . Its geometric area, for comparison is 0.025 cm^2 ($r = 0.09 \text{ cm}$).

Figure 3.11: Chronocoulometric traces obtained for 0.1 M KCl containing $4 \text{ mM K}_4\text{Fe}(\text{CN})_6$.



The chronocoulometric 2-step assay consists of combining an aliquot of the chilled bacterial cell suspension (centrifuged, resuspended in buffer and stored on ice) with an aliquot of buffer solution (\pm antibiotic), incubating for period of time (10 to 15 min) at 37°C, adding the reagent solution containing 50 mM ferricyanide and 10 mM succinate and performing the chronocoulometric run (as shown in Example 1 and 2).

Example 1:

Assay volume: 1200 μ L

chQ runtime 120s; total assay time 27 min;

Step 1 [200 μ L *E. coli* + 200 μ L buffer (\pm anti.); 15 min at 37°C]

Step 2 [add 800 μ L reagent (50 mM FCN/10 mM succinate); 10 min at 37°C]

OD ₆₀₀ 2.53	Control (n = 7)	61.4 \pm 16.7 μ C/min (RSD 27%)	100%
1.02 mM	Chloramphenicol (n = 3)	50.9 \pm 9.2 μ C/min	83%
1.00 mM	Tetracycline (n = 2)	54.6 \pm 4.7 μ C/min	89%

Example 2:

Assay volume: 300 μ L

chQ runtime 120s; total assay time of 17 min

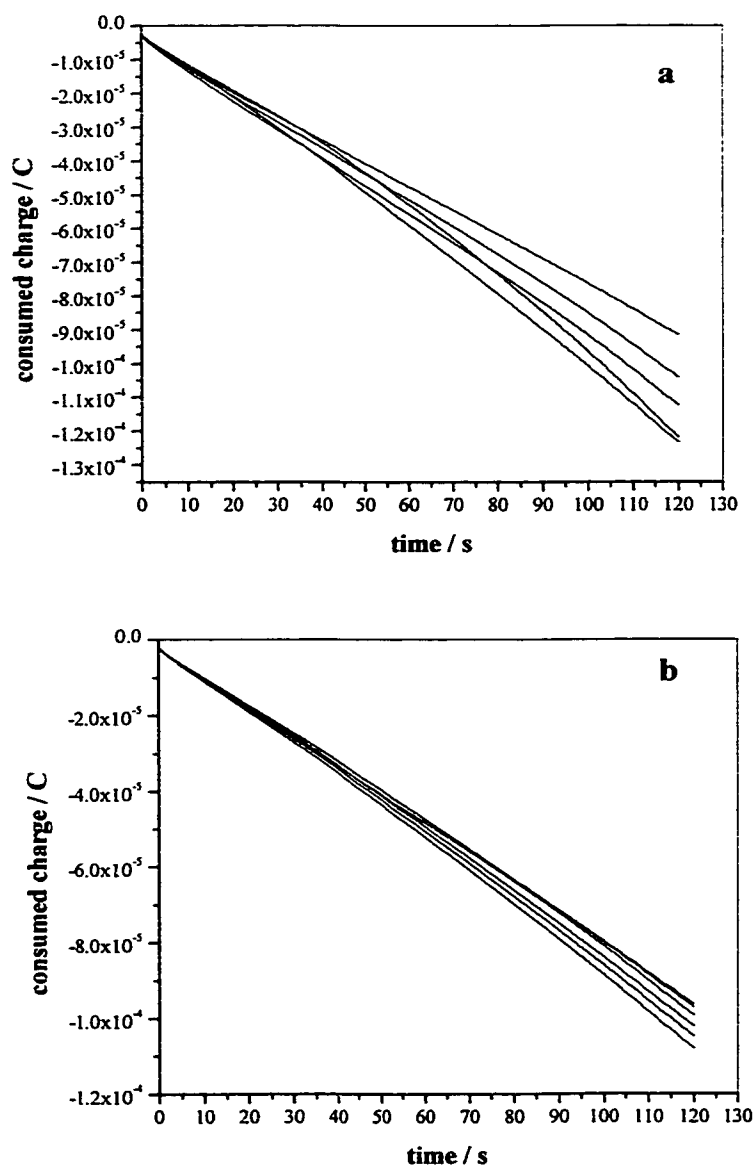
Step 1 [50 μ L *E. coli* + 50 μ L buffer (\pm anti.); 10 min at 37°C]

Step 2 [add 200 μ L reagent (75 mM FCN/10 mM succinate); 5 min at 37°C]

OD ₆₀₀ 2.83	Control (n = 7)	45.7 \pm 2.5 μ C/min (RSD 8%)	100%
5.02 mM	Chloramphenicol (n = 4)	25.6 \pm 3.9 μ C/min	56%
OD ₆₀₀ 2.79	Control (n = 4)	53.2 \pm 1.1 μ C/min (RSD 2%)	100%
1.25 mM	Chloramphenicol (n = 8)	40.3 \pm 9.9 μ C/min	75%

Figure 3.12 shows precision results for control measurements performed in the volume of (a) 1200 μL , (b) 300 μL . Data displays a RSD of 27% ($n = 7$) and 8% ($n = 7$), respectively.

Figure 3.12: Chronocoulometric traces obtained at 37°C at a Pt electrode ($A = 0.027 \text{ cm}^2$) with exponential-phase *E. coli* JM105 and at assay volume of (a) 1200 μL and 300 μL .



Initial volume reduction from 41.0 mL to 1.200 mL induced combining 200 μL *E. coli* ($\text{OD}_{600} = 2.53$) with 200 μL buffer (\pm antibiotic), incubating 15 min (37°C), then adding 800 μL reagent containing 50 mM ferricyanide and 10 mM succinate for a second incubation step (10 min, 37°C). Chronocoulometry was then performed for 120 s, and the difference in total charge between 60 and 120 s was determined. The controls showed an average value of $61 \pm 17 \mu\text{C}/\text{min}$ ($n = 7$), while incubation with 1.02 mM chloramphenicol yielded 83% of this signal ($51 \pm 9 \mu\text{C}/\text{min}$, $n = 3$) and incubation with 1.00 tetracycline yielded 89% of the control signals ($55 \pm 5 \mu\text{C}/\text{min}$, $n = 2$). A separate precision study conducted with control samples under these conditions yielded an RSD value of 21% ($n = 6$).

The volume and assay time were further reduced to 300 μL and 17 min, respectively, as follows. *E. coli* (50 μL) and buffer (\pm antibiotic, 50 μL) were incubated 10 min (37°C), 200 μL reagent (50 mM ferricyanide, 10 mM succinate) were then added for 5 min at 37°C , and chronocoulometry was then performed for 120 s. In one test ($\text{OD}_{600} = 2.83$) control values of $46 \pm 3 \mu\text{C}/\text{min}$ ($n = 7$) were reduced to $26 \pm 4 \mu\text{C}/\text{min}$ ($n = 4$) in the presence of 5.02 mM chloramphenicol (56% remaining activity), while in a second test at lower chloramphenicol concentration (1.25 mM, $\text{OD}_{600} = 2.79$), control values of $53 \pm 1 \mu\text{C}/\text{min}$ ($n = 4$) were reduced to $40 \pm 10 \mu\text{C}/\text{min}$ ($n = 8$), or 75% of the control value. These volumes and the 120 s chronocoulometry runtime were used in all subsequent experiments.

For practical reasons, we also examined the omission of the centrifugation step prior to incubation in the buffer (\pm antibiotic) solution. Now, 50 μL of the untreated *E. coli* suspension was combined with 50 μL of buffer and incubated for 5 min. At that

point, 200 μL of the reagent solution was injected and incubated for an additional 5 min. Table 3.16 shows results obtained using the two-step assay for exponential-phase *E. coli* JM105. Background measurements of the cell-free reagent solution (50 μL sterile growth-medium + 50 μL buffer + 200 μL reagent) showed no significant contributions from the medium components. It is evident that omitting the centrifugation step resulted in a signal increase by a factor of 5.

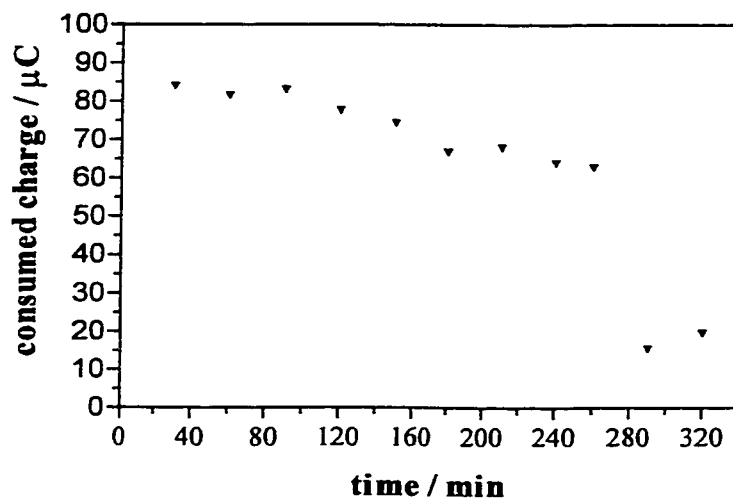
Table 3.16: Chronocoulometric reduction signals obtained for *E. coli* (OD_{600} 2.97) with a two step assay.

	Consumed charge, $\mu\text{C}/\text{min}^*$ (no centrifugation)	Consumed charge, $\mu\text{C}/\text{min}^*$ (with centrifugation)
1	83.4	18.9
2	77.4	16.5
3	71.2	10.4
4	74.1	13.7
5	65.0	12.9
6	62.7	10.3
7	61.2	-
8	61.9	-
Mean	69.6 ± 8.2	13.8 ± 3.4
RSD	12%	25%

* Values are background subtracted

Figure 3.13 shows results obtained by this procedure on control samples, where the stability of ferrocyanide oxidation signals was examined over time. Respiratory cycle activity declines slowly over time, whereas a distinct loss of activity could be observed after 4.5 h (270 min) storage on ice.

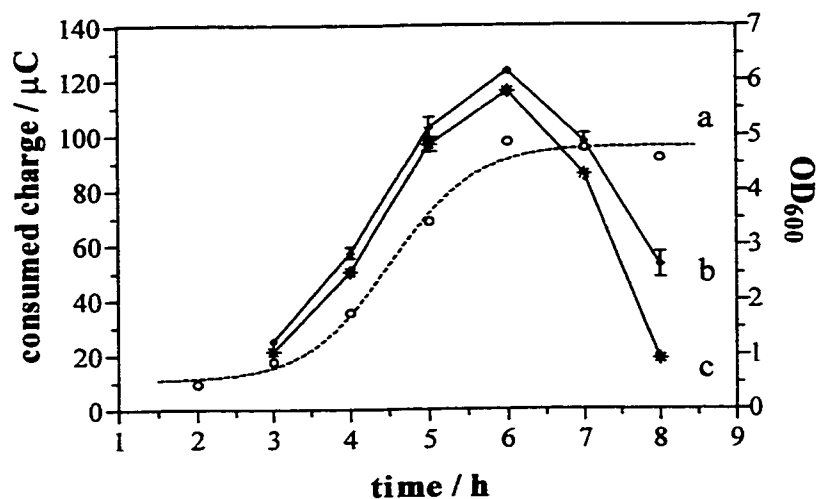
Figure 3.13: Consumed charges of ferricyanide reduction by *E. coli* (OD₆₀₀ 3.03) plotted vs storage time on ice. Chronocoulometric assay (runtime 120 s) where first 50 μL *E. coli* (stored on ice) were incubated with 50 μL buffer (5 min; 37°C) and then combined with 200 μL reagent solution (5 min; 37°C).



The influence of bacterial growth stage on antibiotic susceptibility was studied using this improved two-step assay. An aliquot of the chilled, untreated cell suspension (50 μL) is combined with 50 μL of buffer in the absence (a) and presence (b) of 5.06 mM chloramphenicol and incubated for 10 min at 37°C. At this point, 200 μL of a buffered reagent solution containing 75 mM of ferricyanide and 15 mM of succinate was added and incubated for another 5 min. Following incubation, measurements were taken with the potential stepped to +0.5 V; the resulting current was integrated over a period of 120 s. The black dotted curve (a) in Figure 3.14 shows the typical sigmoidal shaped bacterial growth curve, which exhibits a lag-phase (initial 3 h), followed by the exponential-phase (3rd to 6th h) and stationary-phase (after the 6th h). Ferricyanide reduction signals obtained in the (b) absence and (c) present of the antibiotic chloramphenicol indicated a small but noticeable difference in curvature. Remarkably, the shapes of both reduction curves are

identical and resemble those curves previously obtained in respiration vs growth studies (e.g. see Figure 2.16, Chapter 2). The shapes of the curves were identical even though signals obtained using chronocoulometry were not normalised for bacterial dry matter (μC), while those found using chronoamperometry were expressed as specific activities ($\mu\text{mol}/\text{min}\cdot\text{g}$). The number of cells does not significantly affect the shape of the respiratory cycle signals.

Figure 3.14: Growth curve for *E. coli* JM105 obtained by (a) optical density at 600 nm, and chronocoulometric assay after 10 min incubation in buffer prepared in the absence (b) and presence (c) of 5.06 mM chloramphenicol, followed by a 5 min incubation in 75 mM ferricyanide solution. Values represent the average of two replicate measurements.



Chronocoulometric signals were significantly enhanced by these optimization steps, but observed differences between the absence and presence of antibiotics decreased dramatically. Incubation time was then varied to increase this difference. Table 3.17 shows results obtained for control and for chloramphenicol samples incubated at varying

times in the reagent solution. In order to increase the amount of antibiotic during the first incubation step, 90 μL instead of 50 μL of the buffer containing or lacking 1.03 mM chloramphenicol was combined with 10 μL of cell culture solution and incubated for 15 min at 37°C. At this point, 200 μL of the reagent solution was added and incubated for either 5 or 10 min prior to taking the chronocoulometric measurement. This extension in incubation time (5 to 10 min) increased control signals (without antibiotic) by a factor of 1.4, while also keeping reduction signals in the presence of chloramphenicol constant. The results in Table 3.17 show that an incubation time of 10 min allows observation of the distinct toxic effects of antibiotic compounds.

Table 3.17: Chronocoulometric traces obtained for different incubation times in reagent solution after exposing the bacterial cell suspension to 1.03 mM chloramphenicol.

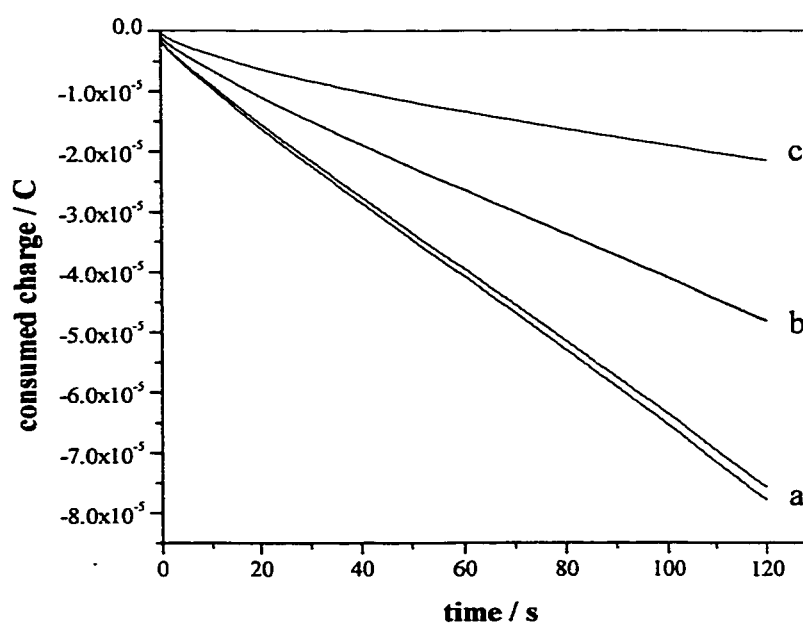
OD ₆₀₀ 3.47	Chronocoulometric traces* vs incubation time in reagent	
	5 min	10 min
Control (n = 3)	17.4 ± 0.6 $\mu\text{C}/\text{min}$	24.8 ± 1.7 $\mu\text{C}/\text{min}$
Chloramphenicol (n = 2)	14.5 ± 0.9 $\mu\text{C}/\text{min}$	15.1 ± 0.8 $\mu\text{C}/\text{min}$
Percent remaining activity	83%	61 %

* Values are background subtracted (no bacteria present)

To finalise the bioassay, both incubation periods were combined into a single step. This simplification is advantageous because the concentration of the antibiotic compound is then kept constant throughout the assay. In addition, we increased the amount of bacterial cell suspension, in order to produce higher reduction values. Therefore, 20 μL of the untreated bacterial cell suspension was combined with 280 μL of reagent solution (50 mM ferricyanide and 10 mM succinate), prepared in the absence or presence of

antimicrobial compounds. Following incubation for 10 min at 37°C, the potential was stepped to + 0.5 V vs Ag/AgCl and the measured current was integrated over 120 s. Figure 3.15 shows chronocoulometric traces obtained in this manner for late exponential-phase *E. coli* (OD₆₀₀ 3.46) in the absence (a) and presence (b) of 5.04 mM chloramphenicol as well as for (c) the cell-free reagent solution.

Figure 3.15: Chronocoulometric traces obtained for *E. coli* JM105 (OD₆₀₀ 3.46) after 10 min incubation in ferricyanide solution in the absence (a), presence (b) of 5.04 mM chloramphenicol and reagent (background) only (c).



Even with this short assay time of 12 min, the effects of chloramphenicol on bacterial ferricyanide reduction are readily visible. We further conducted stability measurements to confirm these results with bacteria stored on ice over an extended period of time. Data from this survey obtained with the new single-step assay are shown in Table 3.18. Results show a small, steady decrease in metabolic rates over the measured period of 3.5 h, which is consistent with previous obtained stability tests. Over the entire time frame of ~ 3.5 h, changes in the bacterial metabolism (reduction rate) due to the effect of chloramphenicol can be seen and the average remaining activity was 40% after exposure to chloramphenicol.

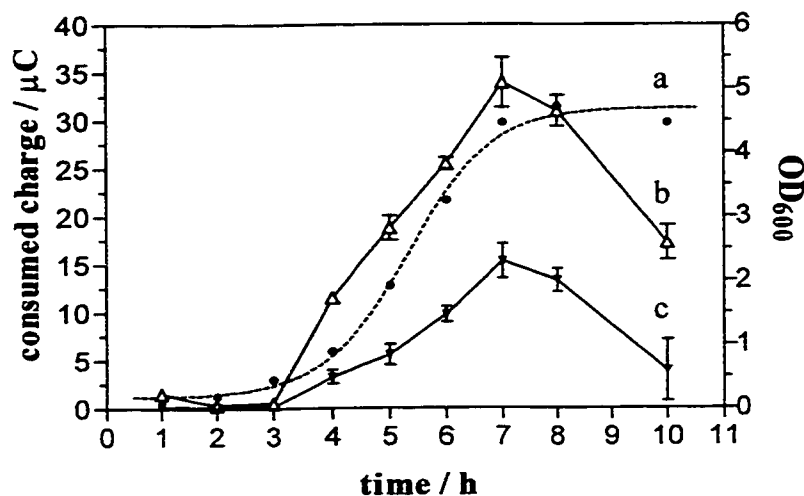
Table 3.18: Chronocoulometric traces obtained for exponential-phase *E. coli* JM105 (OD₆₀₀ 3.46) with the single-step assay in the absence and presence of 5.04 mM chloramphenicol.

Time on ice min	Consumed charges,* $\mu\text{C}/\text{min}$	
	Control	Chloramphenicol
30	33.5	
45	29.1	
60		13.7
75		13.6
90	30.2	
105	29.5	
120		10.5
135		11.1
150	26.9	
165	28.2	
180		12.3
195		10.4

* Values are background (no bacterial cells present) subtracted

This chronocoulometric assay was used to examine the growth curve of *E. coli* JM105 with measurements made in the absence and presence of chloramphenicol, to determine whether the microorganism is more susceptible at earlier or later phases of growth. Figure 3.16 shows the results of this experiment, where culture samples were also examined for turbidity (OD_{600}) to yield a traditional growth curve where the lag, exponential and stationary phases of growth are readily apparent.

Figure 3.16: Growth curve for *E. coli* JM105 obtained by (a) optical density at 600 nm, and chronocoulometric assay (single-step) after 10 min incubation in 50 mM ferricyanide prepared in the absence (b) or presence (c) of 4.78 mM chloramphenicol.



Interestingly, in all samples for which significant chronocoulometric signals were obtained (between 4 and 10 h), the chronocoulometric signals observed in the presence of chloramphenicol remained constant between 40-50% of the control value. These findings suggest that reliable diagnostic decisions are possible at both early and later stages of microbial growth. Remarkably, the percent remaining activity obtained for both the

chronoamperometric and the chronocoulometric assay are identical for 5 mM chloramphenicol and range between 40 to 50% (see Table 3.8) in both cases.

Further experiments showed that antibiotics exhibiting a fast impact on the respiratory behaviour of *E. coli*, such as chloramphenicol, cephalosporin C and penicillin G, were not readily oxidized by ferricyanide, and thus allowed results within 15 min. However, the ferricyanide in the reagent solution reacted with tetracycline, resulting in exceptionally high background currents. It is possible that tetracycline was oxidized by ferricyanide, which in turn produced a false positive signal (increased respiratory cycle activity). In the case of trimethoprim, longer antibiotic exposure periods were required to measure metabolic differences. Consequently, broad-range antibiotic susceptibility screening would involve two separate incubation steps. The first step involves cell incubation using antibiotic compounds, while the second step requires the addition of the reagent solution.

In order to expand the range of the chronocoulometric assay, five non-antibiotic compounds (formate, lysozyme, EDTA, NaHCO₃ and menadione) were examined for their effects on measured bacterial reduction rates. Formate was studied along with succinate and other respiratory substrates in earlier studies (see Chapter 2, Section 2.2.3), and it was found to cause significant increases in ferricyanide reduction rates. In order to evaluate their applicability to the antibiotic-susceptibility assay, five antibiotic compounds (chloramphenicol, erythromycin, penicillin G, cephalosporin C and D-cycloserine) were tested using the single-step chronocoulometric assay. An aliquot of the bacterial suspension (20 μ L) was combined with 280 μ L of buffer containing 50 mM of ferricyanide, 10 mM succinate and 10 mM formate. This mixture was incubated for 15 min, both in the absence and presence of antibiotics. Initial experiments showed that the

addition of 10 mM of formate to the antimicrobial susceptibility assay buffer decreased differences observed, between the absence ($56.8 \pm 0.8 \mu\text{C}$) and presence of 5.11 mM of chloramphenicol ($51.3 \pm 0.3 \mu\text{C}$) to 90% remaining activity. To increase differences between observed signals we extended the incubation time of the reagent solution to 15 min. Data obtained is listed in Table 3.19.

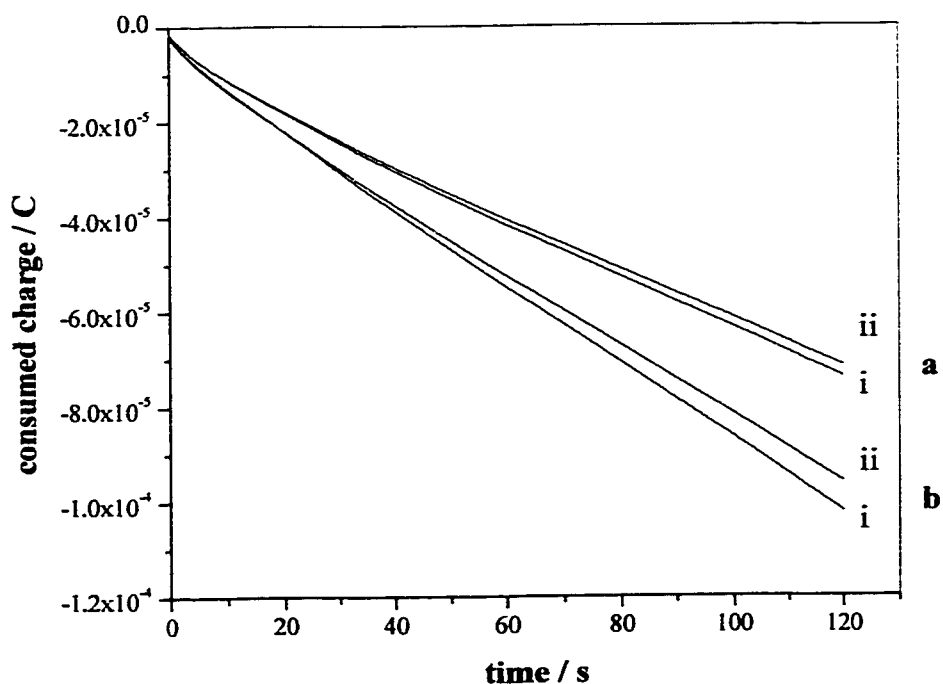
Table 3.19: Chronocoulometric signals obtained for *E. coli* JM105 (OD₆₀₀ 3.8) after 15 min incubation in reagent solution (50 mM FCN, 10 mM succinate and 10 mM formate) in the presence various antibiotics.

	Name	Consumed charges*	
		$\mu\text{C}/\text{min}$	Remaining activity
-	Control	71.8 ± 2.1	100%
5.11 mM	Chloramphenicol	59.1 ± 1.7	82%
2.07 mM	Erythromycin	78.7 ± 1.4	109%
4.83 mM	Penicillin G	66.4 ± 5	92%
7.62 mM	Cephalosporin C	65.8 ± 0.3	92%
6.37 mM	D-Cycloserine	66.0 ± 7	92%

* Average of two replicate measurements; background subtracted

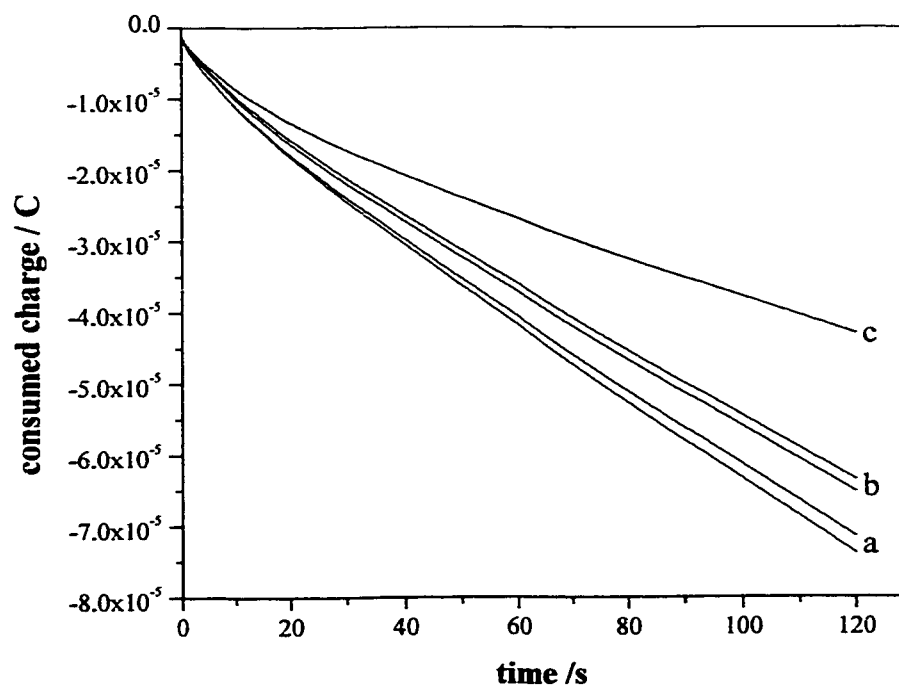
All antibiotics that were known to be effective against *E. coli* JM105 (via disk-diffusion susceptibility test) were now showing apparent decreases in ferricyanide reduction rates, although precision was poor. The extended exposure time to 15 min increased differences for signals observed in the absence and presence of chloramphenicol from 10 to 18% (see Figure 3.17), but this increase was not significant enough to investigate this application any further.

Figure 3.17: Chronocoulometric traces obtained for *E. coli* JM105 (OD₆₀₀ 3.8) in the absence (i) and presence (ii) 5.11 mM chloramphenicol. Chronocoulometry was performed after incubation in reagent solution containing 10 mM formate for a period of (a) 10 min and (b) 15 min.



The addition of 10 mM NaHCO₃ to the buffer containing 50 mM ferricyanide and 10 mM succinate yielded a decreased reduction signal of 87% when compared to control measurements. HCO₃⁻ ions react with water, and this concentration is likely to increase the pH of the assay mixture. However, this reaction showed no effect on observed metabolic changes induced by the presence of 5.01 mM chloramphenicol. Remaining activities of 55 % were found after 10 min exposure to chloramphenicol (Figure 3.18).

Figure 3.18: Chronocoulometric traces obtained for *E. coli* JM105 (OD₆₀₀ 2.9) with 10 mM NaHCO₃ present in the absence (a) and presence of (b) 5.01 mM chloramphenicol. Control signals are obtained in the absence of *E. coli* (c).



Lysozyme is an enzyme that destroys bacterial cell walls by hydrolysing the β (1-4) glycosidic linkages from N-acetylmuramic acid (NAM) to N-acetylglucosamine (NAG) in the alternating NAM-NAG polysaccharide component of cell wall peptidoglycans.¹⁰ Lysozyme occurs widely in the cells and secretions of vertebrates, where it may function as a bacteriocidal agent. However, the observation that few pathogenic bacteria are susceptible to lysozyme alone has prompted the suggestion that this enzyme mainly helps dispose of bacteria that have been killed by other means.⁵⁰ Cell lysis of *E. coli* by lysozyme eliminates the membrane potential and also releases

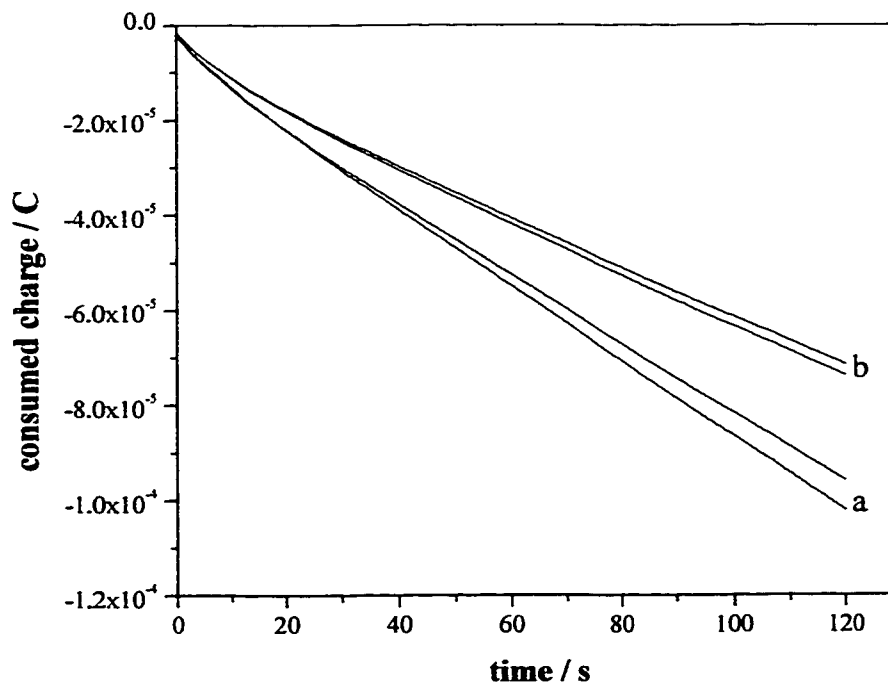
intracellular respiratory substrates into the assay medium. Figure 3.19 shows chronocoulometric traces obtained from a cell sample containing lysozyme (1.5 g/L) after a 15 minute incubation period, which took place prior to obtaining chronocoulometric measurements. An aliquot of bacterial cell suspension (20 μ L) was combined with 10 μ L of lysozyme (1.5 g/L) and incubated for 15 min on ice. At this point, 270 μ L of the reagent solution (50 mM FCN and 10 mM succinate) was added and incubated for 10 min at 37°C. Table 3.20 shows obtained consumed charges obtained with this method. The lower obtained signals (to 81%) in the presence of lysozyme indicate cell lysis had occurred, but again, precision is poor. A more lengthy incubation with lysozyme, at higher temperature, may be expected to improve the signal change.

Table 3.20: Chronocoulometric signals obtained for *E. coli* JM105 (OD₆₀₀ 3.06) after 15 min exposure to 1.5 g/L lysozyme on ice.

Name		Consumed charges*	
		μ C/min	remaining activity
	Control (n=6)	42.6 \pm 3.9	100%
1.5 g/L	Lysozyme (n=2)	34.4 \pm 5.1	81%

* Values are background subtracted

Figure 3.19: Chronocoulometric traces obtained for *E. coli* JM105 (OD₆₀₀ 3.06) after a 15 min preincubation period in (a) buffer or (b) 1.5 g/L lysozyme at 0°C.



EDTA, a well known chelating agent for various cations, binds to Ca²⁺ and Mg²⁺. These cations interact with the outer membrane components (lipopolysaccharide layer) of *E. coli* thus contributing to cell wall rigidity. These positive ions interact with the negatively charged polysaccharide layer. The removal of these ions by complexation with EDTA is a standard method for increasing membrane permeability.⁵¹ It is believed that in the absence of positively charged ions, the lipid-polysaccharide layer collapses, which in turn opens sites to porin proteins. The wider access to porins accelerates the transfer rate for low molecular weight species, such as ferricyanide, into the periplasmic space. Figure 3.20 shows chronocoulometric traces obtained for *E. coli* JM105 (OD₆₀₀ 3.47) in the absence (a) and presence (b) of 4.99 mM EDTA in the buffered reagent solution (50 mM

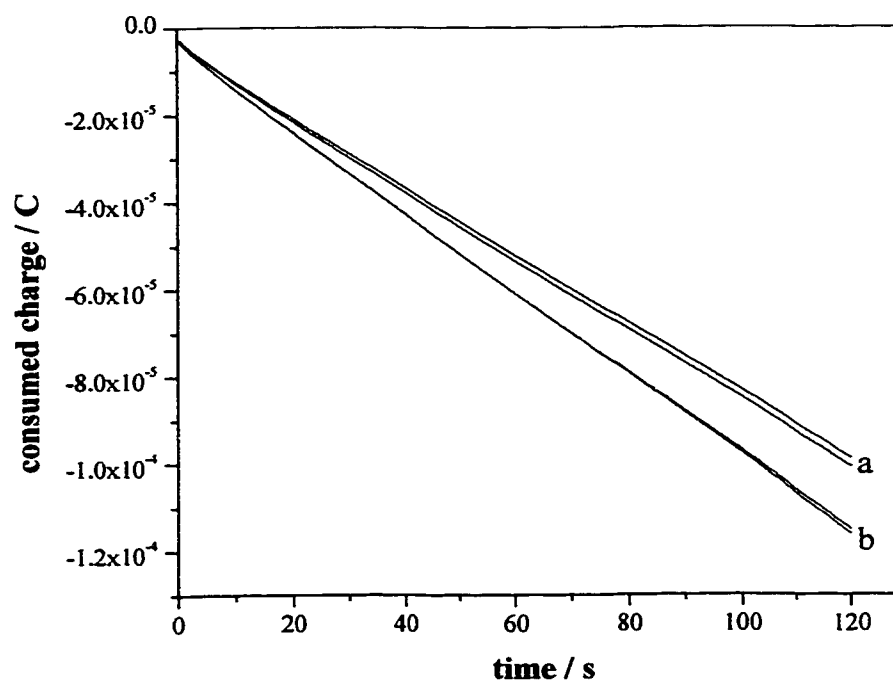
ferricyanide and 10 mM succinate). In relation to controls, small increases in chronocoulometric signals (to 124%) were obtained after a 10 min incubation period of cells in 4.99 mM EDTA as shown in Table 3.21.

Table 3.20: Chronocoulometric signals after 10 min incubation of *E. coli* JM105 (OD₆₀₀ 3.47) in reagent solution in the absence and presence of EDTA.

Name	Consumed charges*	
	$\mu\text{C}/\text{min}$	remaining activity
Control (n=6)	36.7 ± 3.9	100%
4.99 mM EDTA (n=4)	45.5 ± 1.6	124%
0.50 mM EDTA (n=2)	35.9 ± 0.5	98%

* Values are background subtracted

Figure 3.22: Chronocoulometric traces obtained at 37°C for *E. coli* JM105 following 10 min incubation in the absence (a) and presence (b) of 4.99 mM EDTA



The water-soluble redox-cycling agent menadione bisulfite, a structural analog of ubiquinone, is able to penetrate cell membranes and collect intracellular reducing equivalents. The mechanism of menadione reduction involves preferential interaction with NADPH, and less effective interaction with NADH cofactors.^{53,54} Menadione rapidly shuttles two electrons at a time out of the cell into the ferricyanide buffer environment. Hence, two molecules of ferricyanide are reduced by one molecule of menadione, as illustrated in the scheme below.

Figure 3.21: Schematic representation of proposed mechanism of menadione in the chronocoulometric assay.

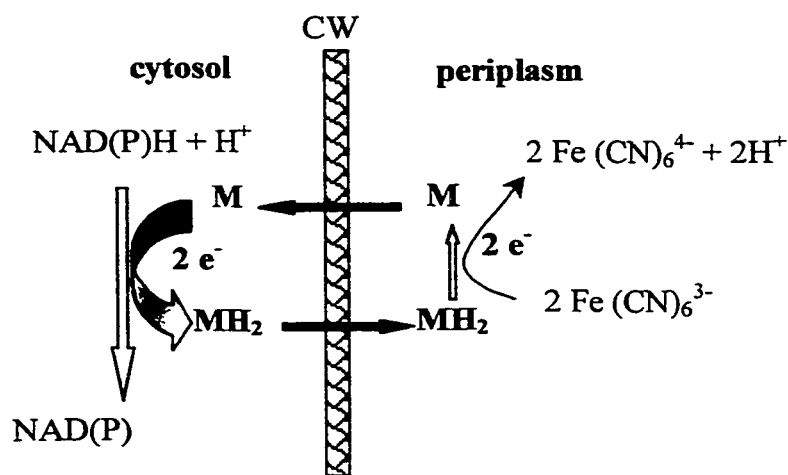


Figure 3.22 shows chronocoulometric traces of a series of samples containing different menadione concentrations, after an incubation period of 10 min. In the presence of 50 μM of menadione, cell samples yielded ferricyanide reduction rates that were 184% higher than those rates obtained using control samples (lacking menadione). Kinetic-constants calculations in respect to menadione were not attempted since the internal menadione concentration (in cytoplasm) was unknown.

Figure 3.22: Consumed charges obtained for chronocoulometry after 10 min incubation of *E. coli* cells (OD_{600} 2.75) in buffer containing 50 mM ferricyanide, 10 mM succinate, and various concentrations of menadione (5 to 500 μM)

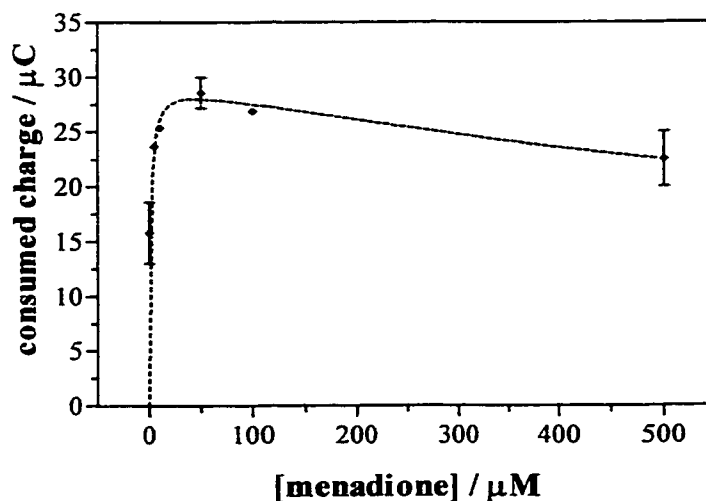
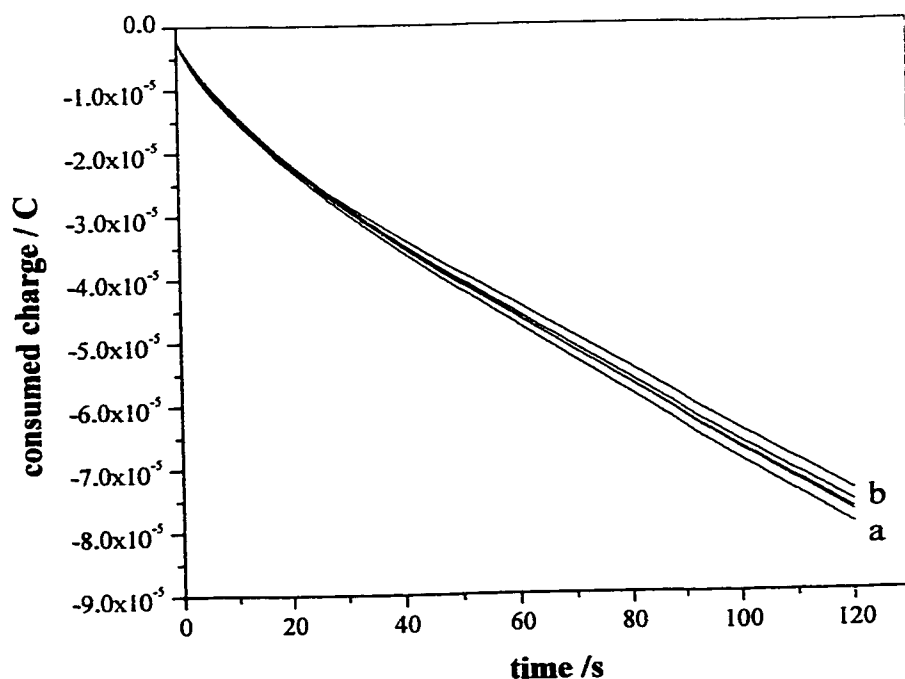


Figure 3.23 shows chronocoulometric traces obtained using *E. coli* (OD_{600} 2.3) after a 10 min incubation period in the reagent solution containing 11.6 μM menadione in the absence (a) and presence (b) of 5.51 mM chloramphenicol. The addition of 11.6 μM menadione to the antimicrobial susceptibility assay buffer was found to significantly increase chronocoulometric signals (to 148%). However, the addition of menadione also decreased differences observed in the absence and presence of chloramphenicol (to 94%).

Consequently, the effects of menadione on the application of the antibiotic susceptibility assay were not investigated further.

Figure 3.23: Chronocoulometric traces obtained at 37°C for *E. coli* JM105 (OD₆₀₀ 2.3) following 10 min incubation in reagent solution containing 11.6 μM menadione in the absence (a) and presence (b) of 5.51 mM chloramphenicol.



To determine the detection limit (in cfu's) of the chronocoulometric assay, bacterial samples were harvested during exponential growth and diluted either in buffer or in growth medium to yield a series of cell culture dilutions that were ultimately stored on ice. An aliquot of each dilution series (20 μL) was combined with 280 μL reagent solution containing 50 mM ferricyanide and 10 mM succinate and incubated for a period of 10 min prior measurement using the chronocoulometric method. Results obtained in this manner are shown in Table 3.22.

Table 3.22: Consumed charges obtained after 10 min incubation in reagent at 37°C for two series of *E. coli* JM105 dilutions in buffer or growth medium.

Diluted samples cfu / sample (20 μ L)	Consumed charges, * μ C/min obtained after dilution in	
	buffer	medium
0.59 x 10 ⁶	-	2.4 \pm 0.9
0.82 x 10 ⁶	0.04 \pm 0.04	1.9 \pm 0.2
0.85 x 10 ⁶	1.3 \pm 0.8	2.0 \pm 0.6
1.22 x 10 ⁶	1.6 \pm 0.1	3.3 \pm 0.2
1.64 x 10 ⁶	2.9 \pm 0.7	4.4 \pm 0.8
1.70 x 10 ⁶	3.4 \pm 0.4	5.3 \pm 0.3
2.43 x 10 ⁶	4.2 \pm 0.2	8.1 \pm 0.4
4.10 x 10 ⁶	8.8 \pm 0.2	11.3 \pm 0.4
4.25 x 10 ⁶	9.7 \pm 0.4	12.9 \pm 0.2
6.10 x 10 ⁶	15.5 \pm 0.2	18.8 \pm 0.3
8.49 x 10 ⁶	-	23.2 \pm 0.1
12.17 x 10 ⁶	-	32.9 \pm 0.1

* Average of two replicate of background subtracted values

Colony forming units (cfu/mL) in the diluted samples are calculated from OD₆₀₀ values as described in Chapter 2, Section 2.3. The detection limit was calculated using the assumption that the standard deviation (σ) of signals obtained at the lowest *E. coli* concentration is roughly equal to the standard deviation of the blank (Eq. 3.4).

$$\sigma_{\text{lowest concentration}} \approx \sigma_{\text{blank}} \quad 3.4$$

For signals that are two standard deviations different from the blank signal, the *E. coli* concentration (cfu/20 μ L) must equal two standard deviations of the blank (2 σ_{blank}) divided by the slope of the calibration curve (m) as seen in Equation 3.5

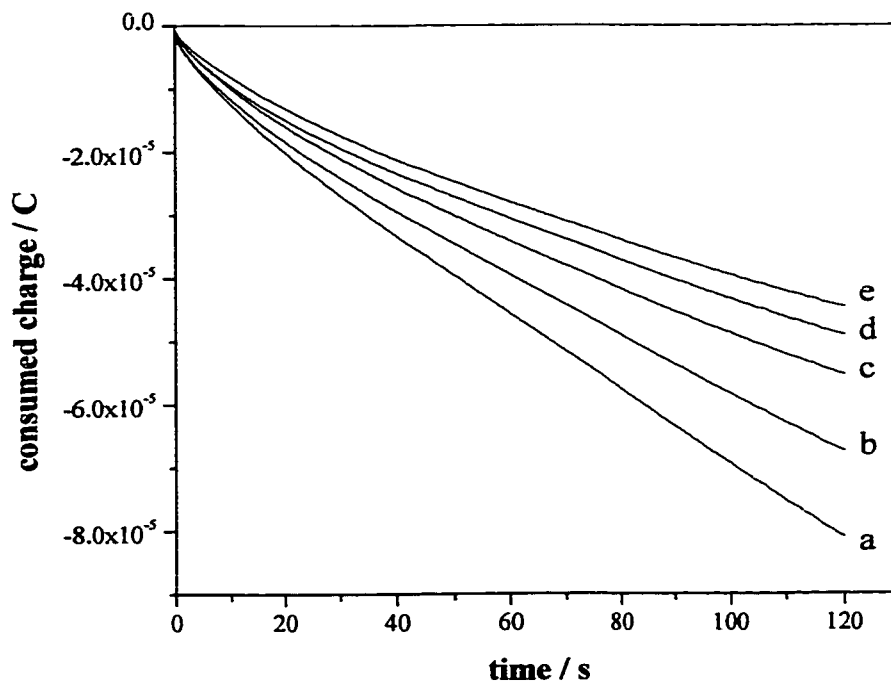
$$X = \frac{2\sigma_{\text{blank}}}{m} \quad 3.5$$

The values of the slope (m) and the standard deviation were taken from the linear regression analysis for samples diluted in either buffer or growth medium (Table 3.23).

Table 3.23: Linear regression analysis from values in Table 3.22 or Figure 3.24.

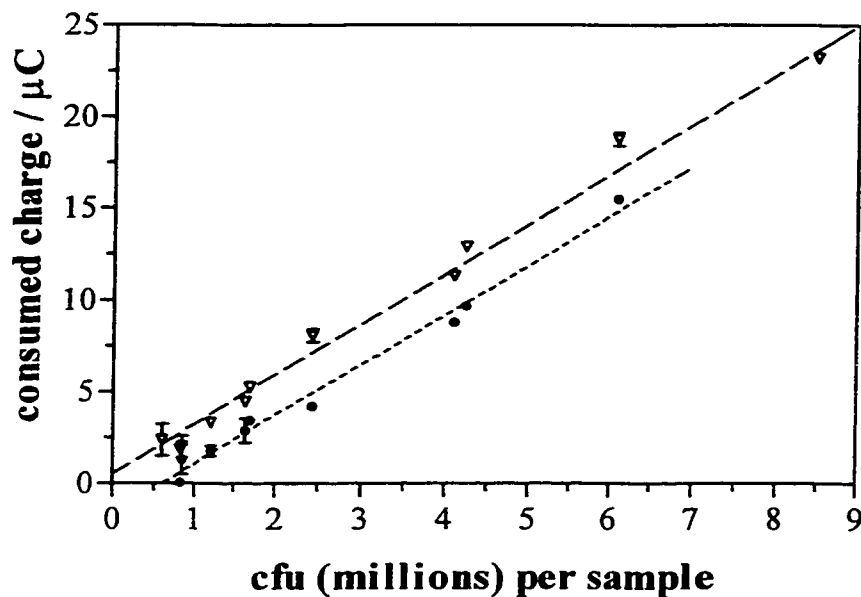
Variables	Medium	Buffer
Slope	$2.72 \pm 0.06 \times 10^{-6}$	$2.70 \pm 0.12 \times 10^{-6}$
Y-intercept	$0.53 \pm 0.32 \mu\text{C}$	$-1.62 \pm 0.32 \mu\text{C}$
X-intercept	$-0.19 \times 10^6 \text{ cfu's / sample}$	$0.60 \times 10^6 \text{ cfu's / sample}$
Linear fit, r^2	0.992	0.978

Figure 3.24: Chronocoulometric traces obtained for *E. coli* JM105 (OD₆₀₀ 2.5) dilutions after 10 min incubation in reagent solution, with (a) undiluted, (b) 1:2 diluted, (c) 1:5 diluted (d) 1:10 diluted cell suspensions, (e) background.



Detection limits obtained for cell dilution in medium and buffer are 2.3×10^5 and 2.4×10^5 cfu / sample ($20 \mu\text{L}$), respectively. These values correspond to a detection limit of 0.074 OD₆₀₀ units. Data and regression curves for both dilution series (buffer and media) are shown in Figure 3.25. The apparent negative Y-intercept obtained for dilutions in buffer may be caused by slight upward curvature in this plot.

Figure 3.25: Consumed charge obtained with chronocoulometry for bacterial dilutions in (a) buffer and (b) growth medium after 10 min incubation in reagent solution containing 50 mM ferricyanide and 10 mM succinate at 37°C.



To further improve the chronocoulometric assay we simplified the electrochemical set-up by implementing a two-electrode system using one silver wire as combined auxiliary and reference electrode. To function as a reference electrode, an initial layer of AgCl was deposited on the pure silver surface prior to experimentation. This was performed by oxidation in a buffer (containing NH_4Cl and CaCl_2) as an electrolyte solution. Bacterial ferricyanide reduction was measured in the absence and presence of formate and succinate using the chronocoulometric assay in the two-electrode set-up. An aliquot of *E. coli* cell suspension ($20\ \mu\text{L}$) was combined with $280\ \mu\text{L}$ reagent solution and incubated for 10 min. At this point, the potential of the Pt working electrode was stepped to $+0.5\ \text{V}$ vs Ag/AgCl and resulting currents were measured and integrated over a period of 2 min. Data obtained in this manner is listed in Table 3.24. The consumed charge obtained in the presence of 10 mM succinate is identical to that obtained using the 3 electrode set-up (Table 3.21). This clearly illustrates the usefulness of a two-electrode system when performing small volume electrochemistry.

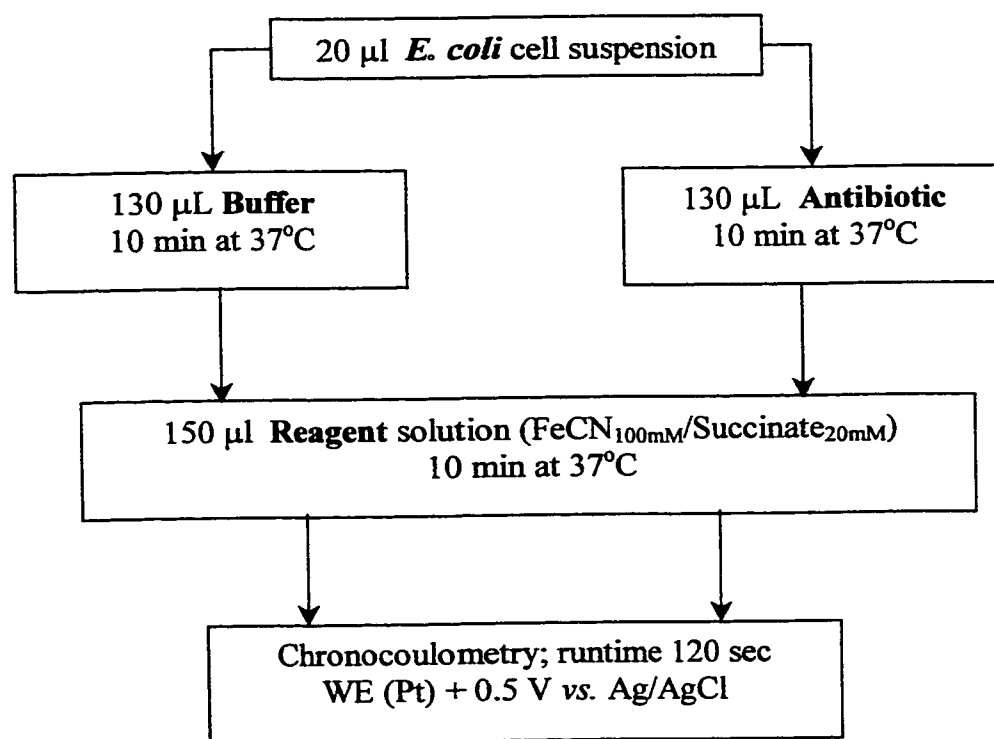
Table 3.24: Consumed charges obtained for *E. coli* (OD_{600} 3.5) with two-electrode chronocoulometry after 10 min incubation in 50 mM ferricyanide in the absence and presence of 10 mM succinate and formate.

50 mM ferricyanide in the presence of		Consumed charge, $\mu\text{C}/\text{min}$		
10 mM	Succinate	n = 4	49.1 ± 1.0	100%
10 mM	Formate	n = 4	50.2 ± 2.3	102%
10 mM	Succinate/formate	n = 3	53.3 ± 3.0	109%

3.3.2.2 Antibiotic Susceptibility Assay

The miniaturised and optimized respiratory cycle activity-based chronocoulometric assay was applied to the determination of antibiotic susceptibility in *E. coli*. Chronocoulometry, as previously described, was used with an integration time of 2 minutes. Figure 3.26 shows a schematic representation of the assay procedure, where the untreated bacterial suspension (20 μL) was added to the assay buffer (130 μL) prepared in the absence or presence of antibiotic and was thus incubated for a period of 10 min. At this point, 150 μL of 100 mM ferricyanide was added for a second 10 min incubation, followed by the chronocoulometric run.

Figure 3.26: Schematic representation of the antibiotic susceptibility assay procedure as described in detail in the experimental section.



In five separate experiments, the metabolic activities expressed in consumed charges of *E. coli* were measured in the absence and presence of high concentrations of antibiotic compounds. Chronocoulometric results were calculated as the difference in integrated current between 1.00 and 2.00 min after application of + 0.5 V (Ag/AgCl) to the Pt working electrode. Results are given in Table 3.25.

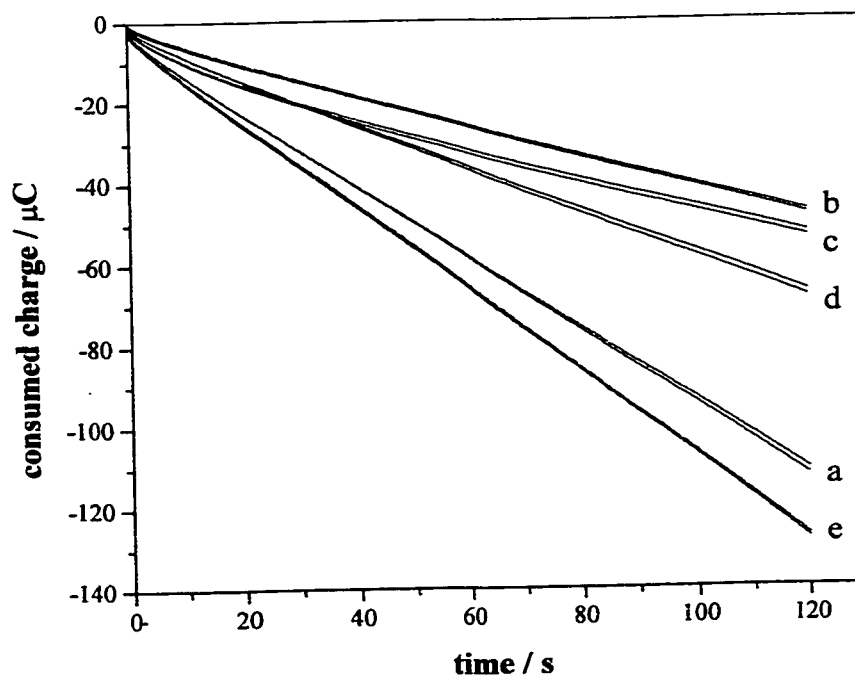
Table 3.25: Chronocoulometric signals obtained in the absence and presence of varying antibiotics for exponential phase *E. coli* JM105.

Antibiotic (conc., mM)	OD ₆₀₀	Charge* consumed ($\mu\text{C}/\text{min}$) for		Percent %
		Control (n = 4 [†] or 5 [‡])	Antibiotic (n = 2)	
Cephalosporin C (0.87)	2.7	33.3 \pm 1.8 [‡]	26.3 \pm 0.3	79
Penicillin G (4.96)	2.7	33.3 \pm 1.8 [‡]	13.4 \pm 0.1	40
Erythromycin (2.03)	2.7	33.3 \pm 1.8 [‡]	33.9 \pm 1.2	102
Rifampicin (0.34)	3.7	51.4 \pm 3.3 [†]	42.6 \pm 0.2	83
Nystatin (0.28)	3.7	51.4 \pm 3.3 [†]	49.4 \pm 1.0	96
Chloramphenicol (5.01)	3.8	51.4 \pm 3.3 [†]	18.0 \pm 0.3	35
Nalidixic Acid (0.87)	3.1	43.3 \pm 2.7 [‡]	26.4 \pm 1.0	61
Bacitracin (5.02)	3.1	43.3 \pm 2.7 [‡]	52.3 \pm 0.1	121
Streptomycin (9.30)	3.1	43.3 \pm 2.7 [‡]	39.0 \pm 1.5	90
Tetracycline (5.20)	3.3	42.0 \pm 1.5 [†]	26.1 \pm 0.2	62
D-Cycloserine (6.95)	3.3	42.0 \pm 1.5 [†]	27.9 \pm 1.6	66
Trimethoprim (3.30)	3.8	62.6 \pm 1.4 [†]	47.8 \pm 2.5	76
Vancomycin (5.15)	3.8	62.6 \pm 1.4 [†]	46.7 \pm 0.8	75

* Values are background subtracted

Figure 3.27 shows chronocoulometric traces obtained for *E. coli* samples exposed to various antibiotics. The shapes of all curves are linear over the 2 minute measurement period, and significant decreases can be seen between control traces and those obtained for effective antibiotics such as chloramphenicol, penicillin G, and tetracycline.

Figure 3.27: Chronocoulometric traces obtained at 37°C in quiet suspensions of *E. coli* JM105 following 10 min incubation in the absence (a) or presence of (b) chloramphenicol, (c) penicillin G, (d) tetracycline and (e) bacitracin, and 10 min incubation after equivolume addition of 100 mM ferricyanide.



The miniaturised chronocoulometric assay for antimicrobial susceptibility shows significant (> 10%) decreases in measured signals for all antibiotics known to also inhibit growth in the overnight disk susceptibility test (Table 3.26). Furthermore, three out of four of the antibiotics to which *E. coli* JM105 is resistant (erythromycin, streptomycin and nystatin) cause no significant change in the chronocoulometric signals, while one (bacitracin) causes increased signals (Figure 3.29e), as it did in the chronoamperometric assay (Table 3.8).

Table 3.26: Chronocoulometric antimicrobial susceptibility assay for exponential-phase *E. coli* JM105 and agar disk diffusion results.

Antibiotic	Concentration, mM	Percent activity* (blank = 100)	Disk diffusion results
Penicillin G	4.96	40	Sensitive
D-Cycloserine	6.95	66	Sensitive
Vancomycin**	5.15	75	Sensitive
Bacitracin	5.06	121	Resistant
Cephalosporin C	0.87	79	Sensitive
Tetracycline	5.20	62	Sensitive
Erythromycin	2.03	102	Resistant
Chloramphenicol	5.01	35	Sensitive
Streptomycin	9.30	90	Resistant
Nalidixic Acid	0.86	61	Sensitive
Rifampicin	0.34	83	Sensitive
Trimethoprim**	3.30	76	Sensitive
Nystatin	0.28	96	Resistant

* Values represent the average of two measurements. Replicate blank measurements (n = 4 or 5) made with various cultivations always yielded RSD values below 7%.

** 20 min incubation was used for these antibiotics prior to ferricyanide addition

Performance characteristics of the new chronocoulometric antibiotic susceptibility assay were evaluated by implementing the following guidelines, adapted from the Microbiology Guidelines published by the Journal of AOAC International in 1999.⁶⁰ The terms of efficiency, sensitivity, and specificity are defined with respect to with the associated true or false (positive and negative) results obtained in Table 3.26. Meanwhile, Table 3.27 demonstrates the procedure used to evaluate these results. A true positive result is defined as susceptibility if both the agar disk-diffusion test (referenced methodology) and the chronocoulometric assay show susceptibility.⁶⁰ In other words, an electrochemically positive test shows decreased respiratory cycle activity and growth inhibition by disk diffusion constitute a true positive result for that antibiotic (N_{11}). Consequently, test positives (decreased activity) that were not confirmed to be true positives (disk diffusion assay) were considered as false positive (N_{21}). Similarly, negative chronocoulometric test results found to be positive by the reference method were false negative (N_{12}), whereas confirmed negative results were true negatives (N_{22}).

Table 3.27: Categorization of obtained results used to define false negative, false positive, specificity and sensitivity of the chronocoulometric assay

Agar disk diffusion Reference method	Chronocoulometric test results		Total
	Positive (N_1)	Negative (N_2)	
Positive (N_1)	9	0	9
Negative (N_2)	0	4	4
Total	9	4	13

* N_{11} = number of results in row 1 and column 1 and N_{12} results in row 1 and column 2.

Sensitivity for defined test conditions represents the proportion of test samples that contained an effective antibiotic (reference method) and responded positively to the chronocoulometric test as shown in Equation 3.6.

$$\text{Sensitivity} = \frac{\text{true positive } (N_{11})}{\text{positive agar plates}} \quad 3.6$$

Referring to Table 3.27, 9 true positive results were obtained with a total of 9 positives in the agar disk-diffusion test. Thus, the chronocoulometric assay yielded 100% sensitivity.

Specificity is the proportion of the test samples that did not contain an effective antibiotic (resistance or growth on agar plate) and thus responded negatively to the chronocoulometric test as shown in Equation 3.7.

$$\text{Specificity} = \frac{\text{true negative } (N_{22})}{\text{negative agar plates}} \quad 3.7$$

From Table 3.27 it is apparent the chronocoulometric assay exhibited 100% specificity. Efficiency is the proportion of true tests (true positive and true negative) in regard to the total number of tests as shown in Equation 3.8.

$$\text{Efficiency} = \frac{\text{true positive } (N_{11}) + \text{true negative } (N_{22})}{\text{total number of all tests}} \quad 3.8$$

Referring to Table 3.28 the chronocoulometric antibiotic susceptibility assay was found to exhibit 100% efficiency.

Chloramphenicol and penicillin G were selected for investigations of quantitative antimicrobial susceptibility testing. The goal of these tests was to identify the concentration at which the chronocoulometric signal is reduced to 50% of its limiting value (IC_{50}). Control experiments were conducted in shake-flask cultures with antibiotic present at known concentrations. Hence, solutions of medium solutions containing a

series of chloramphenicol and penicillin G dilutions were prepared and inoculated with *E. coli* JM105. After a 10 h cultivation period at 37°C, OD₆₀₀ values were measured and expressed as percent growth (Table 3.28).

Table 3.28: Optical density measurements at 600 nm obtained after 10-hour cultivation of *E. coli* JM105 in the absence and presence of antibiotic dilutions.

Concentration μM	Optical density at 600 nm*		% -growth	
	Chloramphenicol	Penicillin G	Chloramphenicol	Penicillin G
0.0	2.95	4.41	100%	100%
1.0	2.45	4.32	83%	98%
2.5	2.09	4.33	71%	98%
5.0	0.59	4.30	20%	98%
10.0	0.06	3.85	2%	93%
50.0	0.00	2.73	0%	62%
100.0	0.00	0.31	0%	7%
500.0	0.00	0.04	0%	0%
1000.0	0.00	0.09	0%	2%

* Average of 4 replicate measurements

Table 3.29 shows the results of these experiments, where exponential-phase *E. coli* JM105 was used for chronocoulometric experiments conducted in an identical manner to those reported for the single step assay (Table 3.17). A single 10 min incubation step involving both antibiotic and ferricyanide was used instead of the two separate steps. The control experiments, based on microorganism growth in the absence and presence of chloramphenicol and penicillin G, yielded sharp decreases in growth as antibiotic concentrations were increased, as seen in Figure 3.30.

Table 3.29: Chronocoulometric measurements obtained for *E. coli* JM105 after 10 min incubation in reagent containing various antibiotic concentrations.

Concentration mM	Consumed charge, * $\mu\text{C}/\text{min}$		% -remaining activity	
	Chloramphenicol	Penicillin G	Chloramphenicol	Penicillin G
0.00	35.8 \pm 1.2	37.8 \pm 1.0	100%	100%
0.05	34.4 \pm 0.8	36.9 \pm 0.1	96%	100%
0.10	32.8 \pm 0.3	38.2 \pm 0.5	92%	100%
0.25	31.0 \pm 2.4	37.4 \pm 0.2	87%	100%
0.50	27.7 \pm 0.5	36.7 \pm 0.3	77%	97%
0.80	22.6 \pm 1.4	35.9 \pm 0.7	63%	95%
1.00	20.2 \pm 1.0	30.2 \pm 0.3	57%	80%
2.50	18.6 \pm 2.1	28.7 \pm 0.6	52%	76%
5.00	12.4 \pm 3.4	13.6 \pm 1.3	35%	36%
10.00	11.5 \pm 0.6	12.5 \pm 5.0	32%	33%

* Average of 4 replicate measurements

Figure 3.28 shows the typical sigmoid shaped curves for increasing concentrations of chloramphenicol and penicillin G calculated with the Hill equation.⁵⁰ This equation can be rearranged to the following:

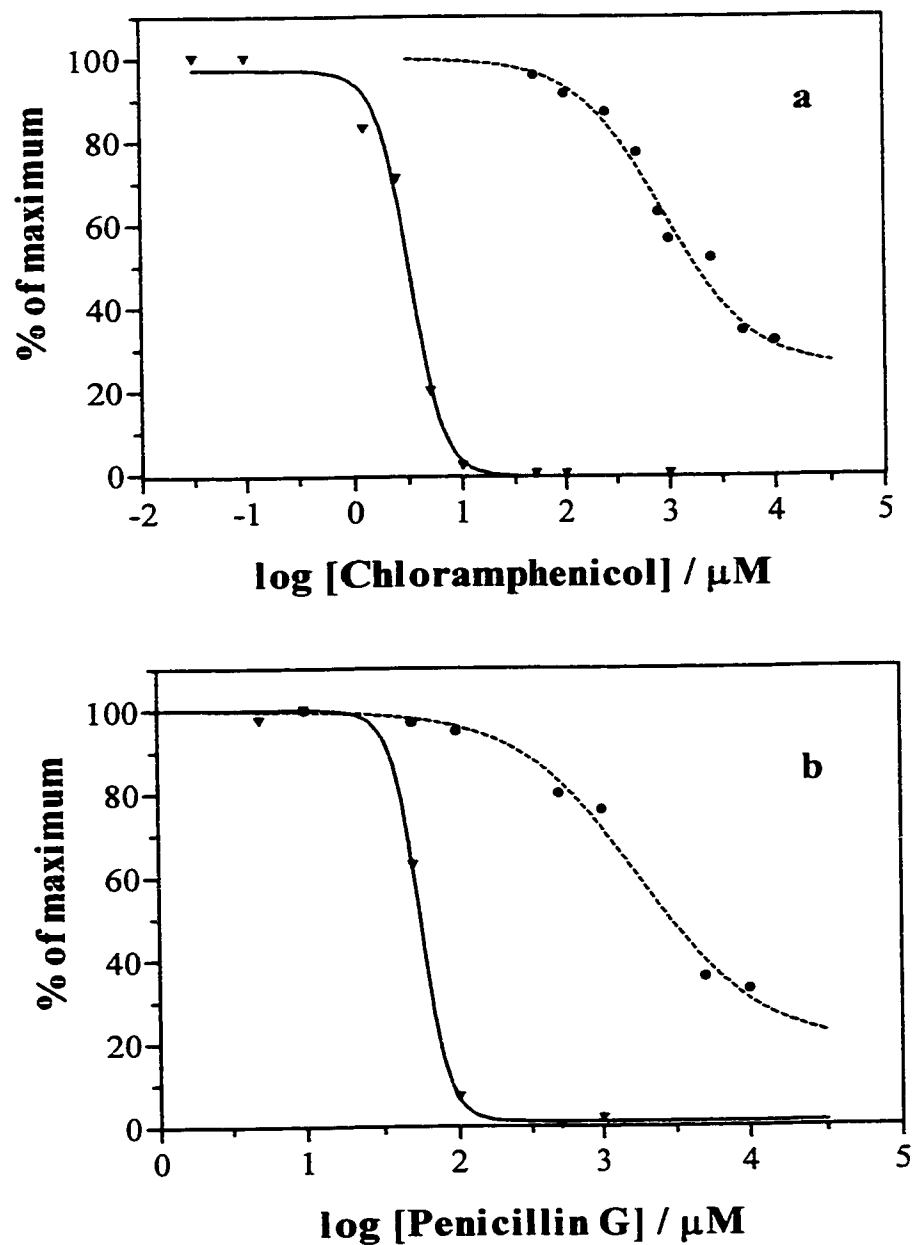
$$Y = \text{Bottom} + \frac{(\text{Top} - \text{Bottom})}{(1 + 10^{((\log \text{IC}_{50} - X) \cdot \text{Hill slope}))}} \quad 3.9$$

where:

Y	percent remaining activity
Bottom	minimum activity, %
Top	maximum activity, %
X	log of concentration, μM

IC_{50} values for growth of $3.2 \mu\text{M}$ and $56 \mu\text{M}$ were obtained by this method (values from Figure 3.28a and Eq. 3.9) for chloramphenicol and penicillin G, respectively. The chronocoulometric assay, on the other hand, yielded relatively slow decreases in signals as antibiotic concentration were increased, which led to much higher apparent values of IC_{50} . From the data shown in Figure 3.28b and Eq. 3.9 we found IC_{50} values for respiratory cycle activity of 0.91 and 1.7 mM obtained for chloramphenicol and penicillin G, respectively. The obvious differences in the IC_{50} values obtained by the two methods, about two orders of magnitude, were likely related to the very different time scales of the experiment. When compared to the growth-based assay (10 h), the incubation period employed in the chronocoulometric assay (10 min prior to measurement) was much shorter and thus not sufficient to allow equilibrium (or steady-state) distributions of the antibiotics to be attained. Therefore, the full effect of these compounds on ferricyanide reduction rates may not be evident until much longer times have elapsed. Although correlation between chronocoulometric and growth-based IC_{50} determinations were not obvious at this point, such a correlation may exist and should be subject of further investigation.⁶²

Figure 3.28: IC₅₀ determination for *E. coli* JM105 with (a) chloramphenicol and (b) penicillin G, by traditional turbidity (OD₆₀₀, solid lines) and chronocoulometric measurements (dashed lines). Turbidity measurements were made following 10 h cultivation in the presence of the indicated concentration of antibiotic. Chronocoulometric results were obtained following 10 min incubation in reagent solution prior 2 min measurement.



3.3.2.3 Chronocoulometry with *Clostridium sporogenes* ATCC8075

All experiments reported thus far were conducted using one microorganism, *E. coli* JM105. To determine whether antimicrobial susceptibility testing may be conducted using other organisms, *Clostridium sporogenes* was chosen as a model. All microorganisms possess respiratory pathways that ultimately reduce their surrounding medium, through oxygen reduction to water in the case of aerobes, or by the anaerobic reduction of species such as nitrate or sulfate. *Clostridium sporogenes* ATCC8075 is Gram-positive, lacking the permeable outer membrane of *E. coli* JM105, and is also an obligate anaerobe, requiring oxygen-free conditions for growth.⁶¹ Due to the impermeability of the outer membrane of *C. sporogenes*, it is necessary to use a low concentration of a hydrophobic electron-transfer mediator (5 μ M DCIP, 2,6-dichlorophenolindophenol) in the chronocoulometric assay buffer to allow ferricyanide reduction. Initial experiments were conducted using anaerobically grown *C. sporogenes* to prove the concept of anaerobic ferricyanide reduction in the presence of 5 μ M 2,6-dichlorophenolindophenol. Results obtained after a 20 min incubation of 20 μ L bacterial suspension in 280 μ L reagent buffer (50 mM ferricyanide, 10 mM succinate and 5 μ M DCIP) at 37°C showed a relative standard deviation of < 6% (n = 8) as listed in Table 3.30.

Table 3.30: Consumed charges obtained for *C. sporogenes* ATCC8075 after 20 min and 10 min incubation in reagent followed by a 2 min chronocoulometric run.

Incubation in reagent at 37°C for	20 min, (n = 8)	10 min, (n = 2)
<i>C. sporogenes</i>	25.0 \pm 1.4 μ C/min	6.5 \pm 1.4 μ C/min

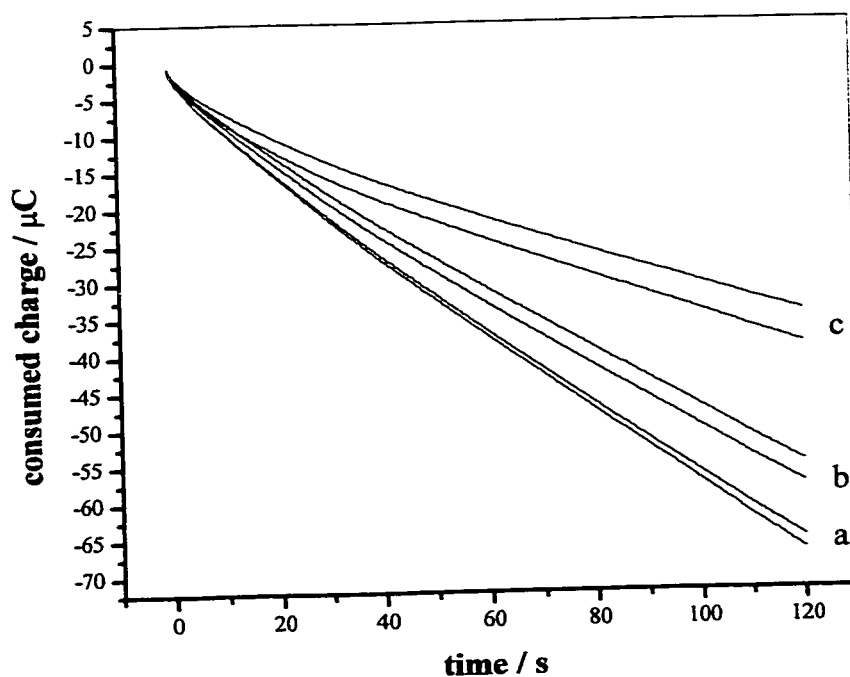
The reduction rate of 6.5 $\mu\text{C}/\text{min}$ obtained after 10 min indicates that antibiotic susceptibility testing on *C. sporogenes* requires longer incubation periods in the reagent solution. Figure 3.29 shows chronocoulometric traces obtained for *C. sporogenes* ATCC8075 (20 μL) incubated for 20 min at 37°C in the absence and presence of 9.96 mM chloramphenicol and 1.14 mg/mL lysozyme (130 μL). This was followed the addition of 150 μL of 100 mM ferricyanide solution containing 10 μM DCIP and 10 mM succinate and by a 20 min incubation period. In the presence of chloramphenicol and lysozyme, samples showed only 24% and 80% remaining activity, respectively (Table 3.31). Attempts at growing *C. sporogenes* ATCC8075 demonstrated this organism cannot be cultivated using the same chloramphenicol concentration originally employed for the electrochemical assay. This clearly demonstrates the chronocoulometric assay is suitable for antimicrobial susceptibility testing on Gram-positive or -negative as well as aerobic or anaerobic organisms.

Table 3.31: Consumed charges obtained for *C. sporogenes* ATCC8075 after 20 min incubation at 37°C in buffer containing chloramphenicol or lysozyme, followed by an additional 20 min incubation in reagent solution (100 mM ferricyanide, 10 mM succinate and 10 μM DCIP) prior to the 2 min chronocoulometric run.

Concentration	name	Consumed charges, *	%-remaining activity
		μC	
	Control (n=6)	18.5 ± 1.4	100%
9.96 mM	Chloramphenicol (n=2)	4.5 ± 1.1	24%
1.14 mg/mL	Lysozyme (n=2)	14.9 ± 0.3	80%

* Averaged values are background subtracted

Figure 3.29: Chronocoulometric traces obtained for *Clostridium sporogenes* at 37°C following 20 min incubation in assay buffer prepared in the (a) absence and presence of (b) 1.14 mg/mL lysozyme and (c) 9.96 mM chloramphenicol. Additional incubation of 20 min with 100 mM ferricyanide containing 10 μ M DCIP and 20 mM succinate preceded chronocoulometric measurement.



3.4 CONCLUSIONS

The ability of microorganisms to reduce non-native redox-active compounds such as ferricyanide was exploited to rapidly determine early toxic effects of antibiotics. Initial experiments performed with chronoamperometry showed a difference between ferrocyanide oxidation signals obtained following incubation in the presence and absence of antibiotic compounds. Cyclic voltammetry showed that platinum is the preferred electrode material in order to avoid electrode fouling by the antibiotics. A range of antibiotics was examined including a 15 min preincubation step with antibiotics that was followed by the addition of reagent solution. The effects of 14 antibiotics on exponential and stationary phase *E. coli* JM105 were studied with the CA method. Reduced respiratory cycle activity was found only for antibiotic compounds that also caused *E. coli* sensitivity by agar disk-diffusion testing.

In order to achieve a more practical application, chronoamperometry was substituted by chronocoulometry, a method that possesses superior sensitivity and speed. Through a series of down-scaling steps, the total assay volume was reduced from an initial 41 mL to 300 μ L, thus making the sample amenable to microtiter plate technology. By omitting sample pretreatment (centrifugation), a 5-fold increase of ferricyanide reduction signals was observed. Further optimization showed that the addition of the respiratory substrates formate and the lipid-soluble redox-mediator, menadione, yielded an increase in observed reduction rates, but only in the presence of succinate was antibiotic susceptibility testing possible. Internal succinate oxidation coupled to ferricyanide reduction by terminal oxidases is particularly sensitive to antibiotic action. We propose that formate facilitates the electron transport to cytochrome oxidases while menadione accepts reducing

equivalents from components of the respiratory chain that are not significantly affected by the antibiotics, since in both cases obtained signals overlap the induced effects of antibiotics.

Three non-antibiotic compounds (lysozyme, EDTA, NaHCO₃) were examined for their effects on measured ferricyanide reduction rates in order to expand the range of the chronocoulometric assay. EDTA showed increased signals by enhancing the mass-transport of ferricyanide, while lysozyme was found to decrease signals.

In summary, a rapid new chronocoulometric assay for antibiotic susceptibility was developed. This method shows complete agreement with traditional susceptibility tests when using *E. coli* JM105 and *C. sporogenes*. The new assay, based on the inhibition of respiratory chain components, provides results in less than 25 min, while traditional methods require hours to days for adequate microorganism growth to be observed. After a brief incubation with effective antibiotics, respiratory inhibition is observed for Gram-negative aerobically cultivated *E. coli* as well as for the Gram-positive obligate anaerobe *C. sporogenes*.

3.5 REFERENCES

1. Desnottes, J. F. *Trends Biotechnol.* 1996, 14, 134.
2. Galperin, M. Y.; Koonin, E. V. *Curr. Opin. Biotechnol.* 1999, 10, 57.
3. Lee, E. H.; Collatz, E.; Padglajen, I.; Guttman, L. *Antimicrob. Agents Chemother.* 1996, 40, 2029.
4. Dougherty, T. J.; Pucci, M. J. *Antimicrob. Agents Chemother.* 1994, 38, 205.
5. Ellard, G. A. *J. Antimicrob. Chemother.* 1991, 28, 347.

6. Petrini, B.; Hoffner, S. *Int. J. Antimicrob. Agents* 1999, 13, 93.
7. Endtz, H. P.; van den Braak, N.; Verburgh, H. A.; van Belkum, A. *Eur. J. Clin. Microbiol. Infect. Dis.* 1999, 18, 683.
8. Gin, A. S.; Zhanel, G. G. *Ann. Pharmacother.* 1996, 30, 615.
9. Saier, M. H.; Paulsen, I. T.; Sliwinski, M. K.; Pao, S. S.; Skurray, R. A.; Nikaido, H. *FASEB J.* 1998, 12, 265.
10. Atlas, R. M. *Principles of Microbiology*, 2nd Ed., Wm. C. Brown, Dubque IA, 1997.
11. Piddock, L. J. V. *J. Appl. Bacteriol.* 1990, 68, 307.
12. Baker, C. N.; Stocker, S. A.; Culver, D. H.; Thornsberry, C. *J. Clin. Microbiol.* 1991, 29, 533.
13. Kelly, L. M.; Jacobs, M. R.; Appelbaum, P. *J. Clin. Microbiol.* 1999, 37, 10, 3296.
14. Sanders, C. C.; Peyret, M.; Moland, D. S.; Shubert, C.; Thomson, K. S.; Boeufgras, J. M.; Sansers, W. E. *J. Clin. Microbiol.* 2000, 38, 570.
15. Huang, A. H.; Wu, J. J.; Weng, Y. M.; Ding H. C.; Chang, T. C. *J. Clin. Microbiol.* 1998, 36, 2882.
16. Phillips, I.; King, A. *J. Chemother.* 1997, 9 (Suppl. 1), 13.
17. Barenfanger, J.; Drake, C.; Kacich, G. *J. Clin. Microbiol.* 1999, 37, 1415.
18. Duncan, S.; Glover, L. A.; Killham, K.; Prosser, J. I. *Appl. Environ. Microbiol.* 1994, 60, 1308.
19. (a) Jepras, R. I.; Carter, J.; Pearson, S. C.; Paul, F. E.; Wilkinson, M. J. *Appl. Environ. Microbiol.* 1995, 61, 2696.

- b) Duncan, S.; Glover, L. A.; Killham, K.; Prossier, J. I. *Appl. Environ. Microbiol.* 1994, 60, 1308.
20. Mason, D. J.; Lopez-Amoros, R.; Allaman, R.; Stark, J. M.; Lloyd, D. *J. Appl. Bacteriol.* 1995, 78, 309.
21. Bascomb, S. *Methods Microbiol.* 1987, 19, 105.
22. Nyren, P.; Edwin, V. *Anal. Biochem.* 1994, 220, 39.
23. (a) Manafi, M.; Kneifel, W.; Bascomb, S. *Microbiol. Ref.* 1994, 55, 335.
 (b) Breeuwer, P.; Drocourt, J.-L.; Rombouts, F. M.; Abee, T. *Appl. Environ. Microbiol.* 1994, 60, 1467.
24. Kogure, K.; Simidu, U.; Taga, N. *Can. J. Microbiol.* 1979, 25, 415.
25. Baxter, G. T.; Bousse, L. J.; Dawes, T. D.; Libby, J. M.; Modlin, D. N.; Owicki, J. C.; Parce, J. W. *Clin. Chem.* 1994, 40, 9, 1800.
26. Pyle, B.; Broadway, S. C.; McFeters, G. A. *Appl. Environ. Microbiol.* 1995, 61, 2614.
27. Jahn, B.; Martin, E.; Stueben, A.; Bhakdi, S. *J. Clin. Microbiol.* 1995, 33, 661.
28. Baker, C. N.; Banerjee, S. N.; Tenover, F. C. *J. Clin. Microbiol.* 1995, 32, 1261.
29. Ertl, P.; Unerladstaetter, B.; Bayer, K.; Mikkelsen, S. R. *Anal. Chem.* 2000, 72, 4949.
30. Dong, H.; Nilsson, L.; Kurland, C. G. *J. Bacteriol.* 1995, 177, 1497.
31. Hadjipetrou, L. P.; Gray-Yound, T.; Lilly, M. D. *J. Gen. Microbiol.* 1966, 45, 479.
32. Ramsay, G.; Truner, A. P. F. *Anal. Chim. Acta* 1988, 215, 61.
33. Ding, G.; Schmid, R. D. *Anal. Chim. Acta* 1990, 234, 247.
34. Richardson, N. J.; Gardner, S.; Rawson, D. M. *J. Appl. Bacteriol.* 1991, 70, 422.

35. Kulys, J.; Wang, L.; Razumas, V. *Electroanalysis* 1992, 4, 527.
36. Gaisford, W. C.; Richardson, N. J.; Haggett, B. G. D.; Rawson, D. M. *Biochem. Soc. Trans.* 1991, 19, 15.
37. Takayama, K.; Kurosaki, T.; Ikeda, T.; Nagasawa, T. *J. Electroanal. Chem.* 1995, 381, 47.
38. Ignatov, O. V.; Rogatcheva, S. M.; Kozulin, S. V.; Khorkina, N. A. *Biosens. Bioelectron.* 1997, 12, 105.
39. Russel, A. D.; Chopra, I. *Understanding Antibacterial Action and Resistance*, Ellis Horwood, New York, 1990.
40. Russel, A. D.; Hugo, W. B. *Pharmaceutical Microbiology*, 3rd Eds., Balckwell Scientific, Oxford, 1983, Chapter 4.
41. Han, F. E., Ed. *Mechansism of Action of Antibacterial Agents*, in *Antibiotics*, vol. V, part 1, Springer Verlag, New York, 1979
42. Kavanagh, F. *Analytical Microbiology*, Academic Press, New York, Vol. I, 1963 and vol. II, 1972.
43. Carniero de Melo, A. M. S.; Cook, G. C.; Miles, R. J.; Poole, R. K. *Appl. Environ. Microbiol.* 1996, 62, 1831.
44. Harel, Y. M.; Bailone, A.; Bibi, E. *J. Bacteriol.* 1999, 181, 6176.
45. Shen, L. L.; Baranowski, J.; Pernet, A. G. *Biochemistry* 1989, 28, 3879.
46. Piddock, L. J. V.; Walters, R. N.; Diver, J. M. *Antimicrob. Agents Chemother.* 1990, 34, 2331.
47. Stone, S. R.; Morrison, J. F. *Biochim. Biophys. Acta* 1996, 869, 275.
48. Kissinger, P. T.; Heineman, W. R. *Laboratory Techniques in Electroanalytical Chemistry*, 2nd Eds., Marcel Dekker, Inc., 1996.

49. Adams; R. N. *Electrochemistry at Solid Electrodes*, Chapter 3, Marcel Dekker, Inc., 1969.
50. Voet D.; Voet, J. G. *Biochemistry*, 2nd Ed., John Wiley & Sons, Inc, New York, 1995.
51. Hamilton-Miller, J. M. *Biochem. J.* 1966, 100, 675.
52. Rabinowitz; J. D.; Cacchin, J. F.; Beeson; C.; McConnell, H. M. *J. Am. Chem. Soc.* 1998, 120, 2460.
53. McManus, D. C.; Josephy, P. D. *Arch. Biochem. Biophys.* 1993, 304, 367.
54. Blondelle, S. E.; Takahashi, E.; Dinh, K. T.; Houghten, R. A. *J. Appl. Bacteriol.* 1995, 78, 39.
55. Poupard, J. A.; Walsh, L. R.; Kleger, B. *Antimicrobial Susceptibility Testing: Critical Issues for the 90s*, Plenum Press, New York, 1994, 1.
56. Collins, L. A.; Franzblau, S. G. *Antimicrob. Agents Chemother.* 1997, 41, 1004.
57. Tenover, F. C.; Swenson, J. M.; O'Hara, C. M.; Stocker, S. A. *J. Clin. Microbiol.* 1995, 33, 1524.
58. Zabransky, R. J.; DiNuzzo, A. R.; Woods, G. L. *J. Clin. Microbiol.* 1995, 33, 791.
59. Nakamura, N.; Shigematsu, A.; Matsunaga, T. *Biosens. Bioelectron.* 1991, 6, 575.
60. Hitchins, A. D.; Mishra-Szymanski, A. *Microbiology Guidelines: Journal of AOAC International*, 1999, vol. 82, pp. 403.
61. Sneath, P. H.; Mair, N. S.; Sharp, M. E.; Holt, J. G. *Bergey's Manual of Systematic Bacteriology*, William & Wilkins, Baltimore, MD, 1984.
62. Ertl, P.; Robello, E.; Battaglini, F.; Mikkelsen, S. R. *Anal. Chem.* 2000, 72, 4957.

Chapter 4

Lectin Immobilization: Creating a Biosensing Layer

4.1 INTRODUCTION

4.1.1 Objective

In the development of biosensors, biochemically selective recognition agents must be associated intimately with a transducer in order to create a biosensing response. In this chapter immobilization methods are studied to link bioselective agents, lectins, to membranes affixed to electrode surface.

Since direct modification of electrode surfaces ultimately limits electron transport processes, thin porous membranes are layered over the electrodes. In this chapter, methods of immobilization are established, including adsorption, crosslinking, avidin-biotin reaction and covalent bonding of the recognition elements onto the membranes. Further, it is shown that lectins can serve as selective recognition agents for cell surfaces. Lectins interact with oligosaccharide components found on the bacterial cell wall and thus are able to selectively bind these cells. The applications of lectins immobilized on various types of membranes are investigated for the selective binding of *E. coli* cells.

Since all lectins feature the same general types of side chain and functional group reactivities, one immobilization technique was sought applicable for all lectins used in this study. However, each type of bioselective agent has its own unique characteristics and optimum individual immobilizations would require separate optimization procedures. We chose to perform all optimizations using one model lectin, Concanavalin A.

4.1.2 Introduction

Over the years, a wide variety of immobilization strategies have been developed for creating the selective reaction layers characteristic of bioanalytical sensors. Technologies for developing selective reaction layers have evolved from hand-built prototypes to sophisticated methods designed for mass-produced devices. Progress is attributable largely to advances in assorted new materials for energy transducers and immobilization matrices, techniques for applying thin films to surfaces, and technologies for producing micromachined devices.¹

Bioselective agents used to achieve a high degree of sensor selectivity include proteins (primarily enzymes and antibodies); smaller molecules such as metal complexes, enzymatic cofactors, mediators and some antigens; oligonucleotides and nucleic acids; and intact cells and tissues.² Additionally, lectins have also been employed as bioselective agents in FIA and FET biosensors.³ Further, immobilized lectins have been incorporated into affinity surfaces that have been used to isolate broad classes of bacterial samples for MALDI mass spectrometric analysis.⁴

Lectins are proteins or glycoproteins with specific carbohydrate binding activities and are discussed in detail in Chapter 5. Lectins are oligomeric proteins consisting of various subunits, with typically one sugar-binding site per subunit. Lectins are structurally diverse, and are found to be specific for different classes of sugar residues.²⁴ Lectin binding constants are known to be K_{ass} of $10^6 - 10^7$ and they can be isolated from a wide variety of biological sources and were used to label cell surface components for tissue typing. Furthermore, lectins have also been used for the separation of thermocytes and lymphocytes; wheat germ agglutinin was the first lectin shown to bind more strongly

to tumour cells than normal cells.^{5,6} Some lectins have also been shown to bind to a number of bacterial cell wall components such as teichoic acids, lipopolysaccharides, peptidoglycans and other bacterial polysaccharides; certain lectins have even been used to distinguish between bacterial species.⁷ Lectins are known to be selective to bacterial surface components⁶ because they are generally specific for a particular carbohydrate structural motif. Consequently, one single lectin may bind to a variety of bacterial species, while a single bacterial strain may also bind to a variety of lectins with different carbohydrate specificities. This characteristic has been used to differentiate species of *Bacillus anthracis* and *Bacillus thurengiensis*.⁴

While each lectin may require unique immobilization conditions for optimal response, there are general approaches for each category of reagent. Since all proteins have the same types of side-chains and functional groups, many of the protein immobilization techniques are generally applicable to both enzymes and lectins. However, each protein has its own characteristics and requirements for immobilization with optimal bioactivity. Thus, an immobilization protocol for achieving accessibility to an enzyme's active site requires variations within a single technique.²

Common methods used to immobilize proteins include adsorption, intermolecular crosslinking, avidin-biotin anchors or covalent binding *via* amide bonds using side chains as well as entrapment and microencapsulation. All these techniques have been used extensively and it would be difficult, if not impossible, to report all existing experimental protocols that have been reported for creating reaction layers of selective agents.

The effects of immobilization on reactivity is also a well-known problem that has been addressed by many researchers.² Exposing the protein to different types of environment and confining it to a microenvironment can have significant effects on the

enzymatic activity and/or binding affinity. The change of orientation of the molecules may lead to shielding the active sites or may even involve a degree of denaturation during immobilization. The microenvironment can shift reaction conditions away from the optimum. For this reason, it is eminent to always consider parameters such as apparent pH, accessibility, ionic strength, polarity of the medium and the presence of confined space.² For example, if the immobilization matrix has an ionic atmosphere different from that surrounding the solution, partitioning of protons and hydroxide ions at the membrane surface will affect the local pH and may shift reaction kinetics considerably.

Adsorption is the simplest form of protein immobilization, where the protein solution is incubated along with an adsorbent (membrane) for several hours. The adsorbent is then removed and rinsed with buffer and ready to use. The adsorption of lectins onto surface carriers is reversible in principle, but careful selection of the material and immobilization conditions can make desorption insignificant. Protein adsorption is a function of the type of surface, the isoelectric point (pI) of the protein, the size of the protein and the solution conditions under which adsorption occurs.² Functional groups found on proteins include amino (-NH₂), carboxyl (-COOH), thiol (-SH) and aromatic amino acids; it is these groups that largely determine adsorption characteristics. Exactly which groups are exposed at the surface of the protein, and their ionization state are both dependent on pH, ionic strength and polarity of the solvent in which immobilization occurs. Primarily van der Waals forces are involved in the adsorption process, but also present may be ionic, polar and hydrogen bonding as well as hydrophobic and aromatic stacking interactions. In summary, all of the above interactions are non-covalent and hence reversible, thus leading to difficulties in reproducibility.

In order to increase reproducibility and to prevent desorption from the immobilization matrix, adsorption has often been followed by crosslinking to form a three-dimensional network. Crosslinking refers to the use of bifunctional agents to create intermolecular links between adsorbed proteins for the purpose of stabilizing the biosensing layers and preventing leaching from the reactive layer. Reactive linking sites on proteins include amino, carboxyl and thiol groups as well as aromatic amino acids in the protein sequence.² A study to compare the sensitivities of enzyme monolayers (glucose oxidase) and crosslinked layers (glutaraldehyde) showed that crosslinked layer provided an overall higher response. The conclusion drawn was that crosslinked layers contained more enzyme molecules, since the enzymatic efficiency was found to be greater in the monolayer.⁹ Losses in enzymatic activity occurred because of the polymeric network of the crosslinked enzymes obscuring the active sites or distorting the tertiary structure. A variety of crosslinking agents have been studied over decades and are commercially available.¹⁰⁻¹⁶

In a separate study, a crosslinking factor has been defined as the ratio of % glutaraldehyde and total protein. This factor has been used to find optimum crosslinking conditions. It was found that the sensitivity of the creatinine sensor decreases with increasing glutaraldehyde concentration. A total drop of 30-fold in sensor sensitivity indicates the degree of influence.³¹ However, crosslinking immobilization is popular because of its speed, while in this study we have investigated a variety of crosslinking agents for optimum effectiveness.

Covalent immobilization methods rely on functional groups on both the protein and the support material, for the formation of stable covalent bonds. For this reason, the choice of a proper support was crucial in order to form stable enzyme-carrier bonds. Acid

cleavage of nylon prior to enzyme coupling has been reported.¹⁷ Amino acid residues constituting the polypeptide component of proteins provide sites at which covalent attachment to the support material may occur. The application of rigid preactivated polystyrene membranes for covalent coupling has also been reported.⁶

The use of the biotin-avidin layer for anchoring biotin labelled species has been shown to increase enzymatic efficiency. Biotin (vitamin H) is a water-soluble organic compound of MW = 244 found in tissue and blood, and it can easily conjugate with proteins without altering their physical characteristics or biological activity. Biotin binds with high affinity to avidin, a protein (MW ~ 70,000) found in egg whites. The avidin-biotin bond involves one of the strongest known ligand-receptor interactions in biochemistry. The bond formation between biotin and avidin is very rapid and, once formed, it is unaffected by extremes of pH, organic solvents and other denaturing agents.¹⁸ Avidin (a glycoprotein) or streptavidin (a protein) each has four binding sites for biotin with an association constant of $\sim 10^{15}$. The streptavidin-biotin bond was also found to have a bond energy of $\sim 35 kT$ (k is Boltzmann constant and T the absolute temperature).¹⁹ The ligand avidin may be immobilized to the carrier surface *via* adsorption or covalent coupling. A comparative study showed that adsorptive and covalent binding of protein G resulted in equal sensitivities, while the avidin-mediated binding to protein G yielded higher responses.²⁰ The avidin-biotin anchor was applied in many sensor devices, such as immunassays, immunosensors and other amperometric biosensors.²¹⁻²³

We now report the optimization techniques implemented to immobilize lectins on various membrane surfaces. The above mentioned immobilization methods will be used to find conditions under which stable and reproducible lectin layers can be created.

Optimizations of the immobilization method are performed using the model lectin, Concanavalin A. Con A is one of the most widely used and thus is the best-characterised lectin. Con A primarily binds to commonly occurring sugar structures such as α -mannose, α -glucose and their derivatives (for more details see Chapter 5). Con A is composed of four identical carbohydrate-binding subunits and the tetrameric form only exists at pH 7. Con A is a metalloprotein, where each subunit contains one Ca^{2+} and one Mn^{2+} at a saccharide binding site. Removal of these cations by acidification abolishes carbohydrate binding activity.²⁷

In this study, only adsorption, intermolecular crosslinking, avidin-biotin anchors and covalent coupling were applied to screen for possible immobilization techniques on carrier surfaces. It is well-known that cellulose triacetate and polyurethanes have been found to be effective for enzyme immobilization.⁸ Consequently, further investigation of the application of different membrane materials, such as nylon or cellulose, as possible immobilization matrices was performed. These thin porous membranes were used as immobilization matrices for lectins, since direct modification of the electrode surface may have resulted in slower electron transport processes. The idea was to mount individually modified membranes on top of the electrochemical transducer, where they could be easily removed and exchanged.

The attempt to immobilize the recognition element (lectin) on membranes that were attached to the electrode surface allowed the omission of the extensive cleaning procedure, or other pretreatments of the transducer surface. In general, before immobilization procedures can be used successfully, the transducer surface must be cleaned carefully and pre-treated for the coupling chemistries of immobilization.

Cleaning solid metal surfaces is frequently accomplished by repeated polishing using alumina slurries or by using a piranha solution. The piranha solution consists of hydrogen peroxide and sulphuric acid ($\text{H}_2\text{O}_2/\text{H}_2\text{SO}_4$), thus making it highly oxidising and requiring caution when using, storing and disposing of the material.² We avoided possible negative effects on electron transport processes by not directly modifying the transducer surface.

Adsorption is one possible lectin immobilization method used to obtain preliminary results. The great advantage of adsorption is that reagents were usually not required. Adsorption is also generally less disruptive to proteins than chemical methods of attachment.²⁵ This is important since only a high ratio of active binding sites of the immobilized lectins would yield the necessary sensitivity as the recognition element. The adsorption of proteins onto the surface of carriers is in principle reversible since no covalent bond formation between the lectin and the membrane is involved.

In addition, two soft preactivated membranes were investigated for their lectin immobilization capabilities. Both membranes mainly react with primary amines found on all lectins. These allow the use of mild coupling conditions in order to avoid the chemical modification of amino acid residues near the active site, as well as any change in tertiary structure.

4.2 EXPERIMENTAL SECTION

4.2.1 Materials and Instrumentation

Sigma supplied all lectins and proteins including *Artocarpus integrifolia* (lyophilized powder ~ 70% protein), *Arachis hypogaea* (lyophilized powder), Concanavalin A (lyophilized powder ~ 15% protein), *Galanthus nivalis* (lyophilized powder), *Phytolacca americana* (lyophilized powder), *Lens culinaris* (lyophilized powder, ~ 80% protein), *Helix pomatia* (lyophilized powder), *Persea americana* (lyophilized powder), *Triticum vulgare* (lyophilized powder), *Codium fragile* (lyophilized powder) and biotinylated Concanavalin A (lyophilized powder, 97% of lectin biotinylated). Bovine Albumin (lyophilized powder, 99%), streptavidin (lyophilized, 14 units/mg protein) avidin (lyophilized, 12.9 units/mg protein), peroxidase biotinamido-caproyl labeled (lyophilized powder, ~ 90% protein with ~ 240 units/mg) as well as ABTS (2',2'-azino-bis(3ethylbenzthiozoline-6sulfuric acid)), sodiumcyanoborohydride (NaCNBH₃), HEPES (N-[2-hydroxyethyl]piperazine-N'-[2-ethanesulfonic acid]) buffer, EDC (1-ethyl-3-(3-dimethylaminopropyl)carbodiimide), menadione (2-methyl-1,4-naphthoquinone sodium bisulfite, ~95%), glutaraldehyde (25% aqueous solution), acetic acid and Coomassie blue R250. Hydrogen peroxide (30% solution) was supplied by BDH and stored at 4°C. Pierce supplied the crosslinking agents Sulfo-MBS (aleimidobenzyl-N-hydroxysuccinimide ester), DMA (dimethyl adipimidate-2 HCl), BS³ (bis(sulfosuccinimidyl)suberate). Gibco BRL supplied the nitrocellulose, supported nitrocellulose, neutral nylon (BiodyneA[®]) and the positively charged nylon (BiodyneB[®]) membranes. Pall Specialty Materials supplied the preactivated membranes ImmunodyneABC[®] and UltraBind[®]. Both membranes are specified with a pore size of 0.45 μm diameter. Bioanalytical Systems Inc., supplied the

platinum electrodes (1.8 mm dia.) as well as Ag/AgCl reference electrodes. The silver wire (1.0 mm dia., 99.99%) was purchased from Aldrich.

4.2.1.1 Buffer Solution

The buffer contained the following components: KH_2PO_4 (2.88 g/L), $\text{K}_2\text{HPO}_4 \cdot 3\text{H}_2\text{O}$ (5.76 g/L), trisodium citrate dihydrate (1.2 g/L), $\text{MgSO}_4 \cdot 7\text{H}_2\text{O}$ (0.48 g/L), $\text{CaCl}_2 \cdot 2\text{H}_2\text{O}$ (0.048 g/L), $(\text{NH}_4)_2\text{SO}_4$ (1.63 g/L) and NH_4Cl (1.34 g/L).

4.2.1.2 Biotinylated Peroxidase Solution

A peroxidase stock solution containing approximately 20 $\mu\text{g}/\text{mL}$ of the biotinylated peroxidase solution was prepared at pH 7.5 in the presence of 10 mM HEPES, 0.15 M NaCl, 0.02 mM MnSO_4 and 0.3 mM CaCl_2 , as recommended by Sigma for optimal enzyme activity.

4.2.1.3 ABTS Reagent Solution

As recommended by the supplier (Sigma) one tablet of ABTS (10 mg) was dissolved in 100 mL of 0.05 M phosphate-citrate buffer at pH 5.0. The buffer was prepared by combining 25.7 mL of a 0.2 M dibasic sodium phosphate solution with 24.3 mL of a 0.1 M citric acid solution adding 50 mL distilled water. This solution contained 0.18 mM ABTS.

4.2.2 Methods

4.2.2.1 Cultivation of *E. coli* JM105

As described in Chapter 2, *E. coli* JM105 was cultivated at 37°C and 250 rpm in a buffered growth medium containing 2.4 g/L tryptone, 1.2 g/L yeast extract, 13.2 g/L glucose and trace element stock solution 240 μL per liter of medium.

4.2.2.2 Agglutination Tests

An aliquot (50 μL) of the centrifuged and resuspended bacterial cell sample was combined with 150 μL of the buffered lectin stock solution containing roughly 200 μg protein/mL buffer. Microtiter-wells were used to compare rows containing lectin-bacterial suspension samples to controls, where buffer was combined with the cell suspension. All lectins were investigated for their ability to form visible agglutinin after 6 h incubation at room temperature. The visible formation of a three dimensional network of lectin and cells was used to classify binding affinities.

4.2.2.3 Coomassie Blue Staining

Concanavalin A adsorption on various membrane materials was visualized using Coomassie blue staining. An aliquot of the buffered lectin solution containing 0.24 mg/mL of Con A was applied to the different membrane materials and adsorption was allowed to occur for one hour at room temperature. Subsequently, the membranes were rinsed repeatedly with buffer and submerged into the staining solution for 30 s. The stained membranes were then rinsed with distilled water, transferred into the destain solution and incubated for several hours at room temperature until differences in color intensity were observed for different membranes. The staining solution contained 0.5 mg/mL Coomassie blue R dissolved in a 30% methanol, 10% acetic acid and 60% distilled water solution. The destain solution lacked only Coomassie blue R, but had the same solvent composition.

4.2.2.4 Crosslinking of Lectins

Crosslinking agents were diluted in a 50 mM HEPES solution at pH ~ 8.5 containing 5 mM MgSO₄ to reach a final concentration of 5 mM for MBS and BS³ or 10 mM for DMA and EDC. Membrane disks with adsorbed lectins were submerged in the crosslinking solution and allowed to react overnight at 4°C.

4.2.2.5 Chronocoulometry on Lectin Modified Membranes

Initial chronocoulometric measurements were conducted using membrane disks that had been incubated in buffered, resuspended *E. coli* JM105. These disks were rinsed and immersed in the assay reagent solution (~ 300 μL) at 37°C. The reagent solution contained 50 mM ferricyanide and 10 mM succinate in buffer solution (see Section 4.2.1.1)

For example, avidin (100 μg/mL) was allowed to adsorb onto the positively charged nylon (BiodyneB[®]) and crosslinked with glutaraldehyde (25%) for 30 min at room temperature in the presence of 10 mM NaCNBH₃. The membrane was then transferred into a solution containing 100 μg/mL biotinylated Concanavalin A; avidin-biotin binding was allowed to take place for 1 hour at room temperature. The modified membrane was incubated in the buffered bacterial cell suspension for 1 h at room temperature. At this point, the rinsed membrane was transferred into the reagent solution and incubated for 15 min at 37°C prior measurement. A chronocoulometric runtime of 90 s was used to determine whether selective cell binding on the modified membrane had occurred and was detectable *via* ferricyanide reduction.

4.2.2.6 ABTS – Assay

The enzymatic assay was performed under the following conditions, unless otherwise noted: Membrane disks were immersed in 300 μL of ~ 100 $\mu\text{g/ml}$ buffered avidin or streptavidin solution (pH ~ 7) and protein adsorption was allowed to occur overnight at 4°C. The rinsed avidin/streptavidin modified disks were then transferred to the crosslinking agent (e.g. in 300 μL of 25% glutaraldehyde solution for 30 min at room temperature plus an additional 15 min in the presence of a mild reducing agent NaCNBH_3 , 10 mM). The modified membranes were transferred into a biotinylated-peroxidase stock-solution and incubated for 1 h at room temperature. The excess of unbound peroxidase was washed away with buffer and the modified membrane was transferred into the ABTS reagent solution. The enzymatic reaction was started by adding 3 μL of 30% H_2O_2 to the assay solution. The accumulation of oxidized dye over time (2 to 6 min) was measured spectrophotometrically at 412 nm using buffer as a blank. The calculation of ABTS conversion ($\mu\text{M}/\text{min}$) was performed using Beer's law ($A = \epsilon * b * C$) with an extinction coefficient (ϵ) of $32400 \text{ M}^{-1} \text{ cm}^{-1}$.²⁹

4.2.2.7 Preactivated Membranes

Membranes that feature activated surfaces were used in the chemical method to covalently immobilize proteins. Protein immobilization was carried out on membrane disks (area, 0.28 cm^2) that were immersed in the lectin, avidin or streptavidin solution and allowed to react for 1 h at room temperature prior to storage on ice.

4.3 RESULTS AND DISCUSSION

4.3.1 Agglutination Test

Initial experiments were conducted on a variety of lectins in order to determine their binding affinities to sugar moieties found on the surfaces of bacterial cells. Lectins were investigated for their ability to specifically bind and to agglutinate bacteria.³ Lectins that exhibited a wide variety of binding specificities were used in this study and results obtained from agglutination tests are listed in Table 4.1. These results were determined by visual inspection of the size of the white, insoluble agglutinin deposit formed during the reaction: " +++ " represents the largest deposit, while " - " indicates the absence of visible agglutination. These preliminary results suggest that the main sugar moiety found on the *E. coli* JM105 cell surface is α -mannose. Only lectins exhibiting selectivity towards mannose residues were found to strongly agglutinate *E. coli*, while Concanavalin A displayed the strongest agglutination ability. Con A, the lectin from the jack bean, binds to α -mannose and α -glucose and derivatives, and is composed of four identical carbohydrate binding subunits.²⁷ Con A was used in most subsequent membrane studies due to its ability to agglutinate *E. coli* JM105.

Table 4.1: Results of agglutination studies obtained for 50 μ L exponential phase *E. coli* JM105 samples that were combined with 150 μ L of lectin solution (\sim 200 μ g/mL) and an incubated for 6 h at room temperature.

Lectin	MW $\times 10^3$	Subunits	Specificity	Agglutination ability
Concanavalin A	102	4	α -man, α -glc	+++
<i>Perseu americana</i>	-	-	-	++
<i>Lens culinaris</i>	49	2	α -man	++
<i>Pisum sativum</i>	49	4	α -man	++
<i>Helix pomatia</i>	79	6	galNAc	+
<i>Artocarpus integrifolia</i>	42	4	α -gal	+
<i>Phytolacca americana</i>	32	-	(glcNAc) ₃	-
<i>Arachis hypogaea</i>	120	4	β -gal(1-3)galNAc	-
<i>Codium fragile</i>	60	4	galNAc	-
<i>Solanum tuberosum</i>	100	2	(glcNAc) ₃	-
<i>Ptilota plumosa</i>	65	-	α -gal	-

4.3.2 Lectin Modified Membranes

We investigated possible immobilization methods to find the necessary conditions for highest binding activity for each lectin. The results of lectin adsorption onto nitrocellulose are shown in Table 4.2, where aliquots of buffered lectin stock solution were spotted onto the nitrocellulose surface and allowed to adsorb for 1 hour at room temperature, followed by extensive rinsing steps. Immobilized lectins were then visualised by using Coomassie blue, which is a widely used dye for protein quantitation.²⁶ Results in Table 4.2 were determined visually, and are indicated by "+++" for the highest and "+" for the lowest colour intensity on the modified membranes.

Table 4.2: Coomassie blue staining of lectins that were spotted onto the surface of nitrocellulose and allowed to adsorb for 1 h at room temperature.

Lectin	Concentration $\mu\text{g/mL}$	Adsorption
Concanavalin A	110	+
<i>Solanum tuberosum</i>	105	+++
<i>Phytolacca americana</i>	112	++
<i>Codium fragile</i>	102	+
<i>Artocarpus integrifolia</i>	100	+
<i>Helix pomatia</i>	120	+
<i>Lens culinaris</i>	123	+++

These results show that the different lectins prefer different adsorption matrices. For this reason, four different membrane materials, nitrocellulose, supported nitrocellulose, neutral nylon (BiodyneA[®]) and positively charged nylon (BiodyneB[®]) were investigated using electrochemical detection.

In an attempt to prove the concept of selective cell binding, lectin-modified nitrocellulose membrane disks ($A = 0.28 \text{ cm}^2$) were incubated along with exponential-phase *E. coli* JM105, and then washed and transferred into the electrochemical cell. All experimental conditions, including adsorption time and temperature, *E. coli* exposure time, ferricyanide/succinate reagent volume and incubation time were varied. Every time, the individual lectin was allowed to adsorb onto the membrane surface, followed by a rinse and incubation step in the bacterial solution. At this point, the membrane was rinsed with distilled water, transferred into the reagent solution and incubated for a defined period of time. Results associated with this series of experiments are shown in Table 4.3. Lectin absorption ($200 \mu\text{g/mL}$, 1h at 22°C) and *E. coli* capture (1 h at 37°C) preceded electrochemical measurements conducted after incubating the membranes at 37°C in 700

μL of buffered 50 mM ferricyanide and 10 mM succinate reagent. After the indicated time (30 or 60 min at 22°C), chronocoulometry was performed for 4 min, and the charge consumed between 1.0 and 4.0 min was recorded.

Table 4.3: Chronocoulometric detection of *E. coli* JM105 bound to lectin-modified nitrocellulose (see text for conditions)

Lectin	n	Incubation time, min	Charge consumed, μC
Concanavalin A	6	30	9.9 ± 4.3
Concanavalin A	2	60	12.6 ± 1.4
<i>Solanum tuberosum</i>	4	30	20 ± 8.4
Control	2	30	0.0

Long ferricyanide reagent incubation periods were required to obtain measurable signals that were different from control experiments, in which unmodified membranes were used. Table 4.3 shows that significant ferricyanide reduction occurs at both lectin-modified membranes following exposure to *E. coli*, but the precision of the results is poor. Nevertheless, these preliminary results reveal the promise of lectin-modified membranes as recognition agents in a biosensor array.

Furthermore, the removal of the modified disks from the reagent solution after each measurement resulted in steadily increasing signals. Chronocoulometry revealed higher signals for ferrocyanide oxidation, indicating viable bacteria desorb into the solution (data not shown) after an additional incubation period of 30 min. Lectins that were immobilized onto nitrocellulose by means of simple adsorption, therefore, did not retain *E. coli* cells on the membrane surface.

Consequently, the adsorbed lectin layer was strengthened by forming a three-dimensional network by means of various crosslinking agents.⁹ Figure 4.1 shows the reaction scheme of the homobifunctional imidoester DMA. Figure 4.2 shows the NHS-ester reaction scheme of the homobifunctional crosslinking agent BS³. Figure 4.3 shows the reaction scheme of the double agent heterobifunctional cross linker Sulfo-MBS. The first reaction targets primary amines *via* the NHS-esters while the second reaction involves the maledimide group, which selectively binds to sulfhydryl groups of proteins. Figure 4.4 shows the reaction scheme of the crosslinker 1-ethyl-3-(3-dimethyl aminopropyl) carbodiimide. EDC reacts with carboxylic acid groups of the lectin, allowing amide bond formation with the amino group of a second lectin.

Lectin adsorption was allowed to occur onto membrane surfaces for 1h at room temperature; the modified disks were then removed and transferred to the crosslinking solution and incubated overnight at 4°C. The reinforced procedure was tested using exponential phase *E. coli* on positively charged nylon (BiodyneB[®]), neutral nylon (BiodyneA[®]), nitrocellulose (NC) and supported nitrocellulose (sNC).

Figure 4.1: Schematic of dimethyl adipimidate-HCl DMA (MW 245; 8.6Å) reactions with amino-groups of proteins.

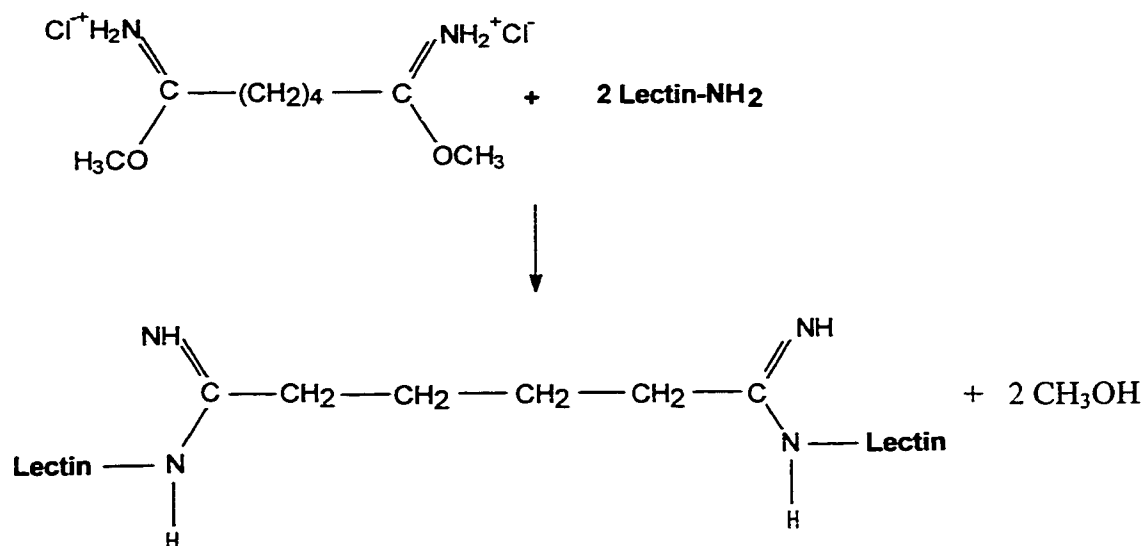


Figure 4.2: Schematic of bis(sulfosuccinimidyl) suberate BS^3 (MW 572.2; 11.4 Å) reactions with amino-groups of proteins.

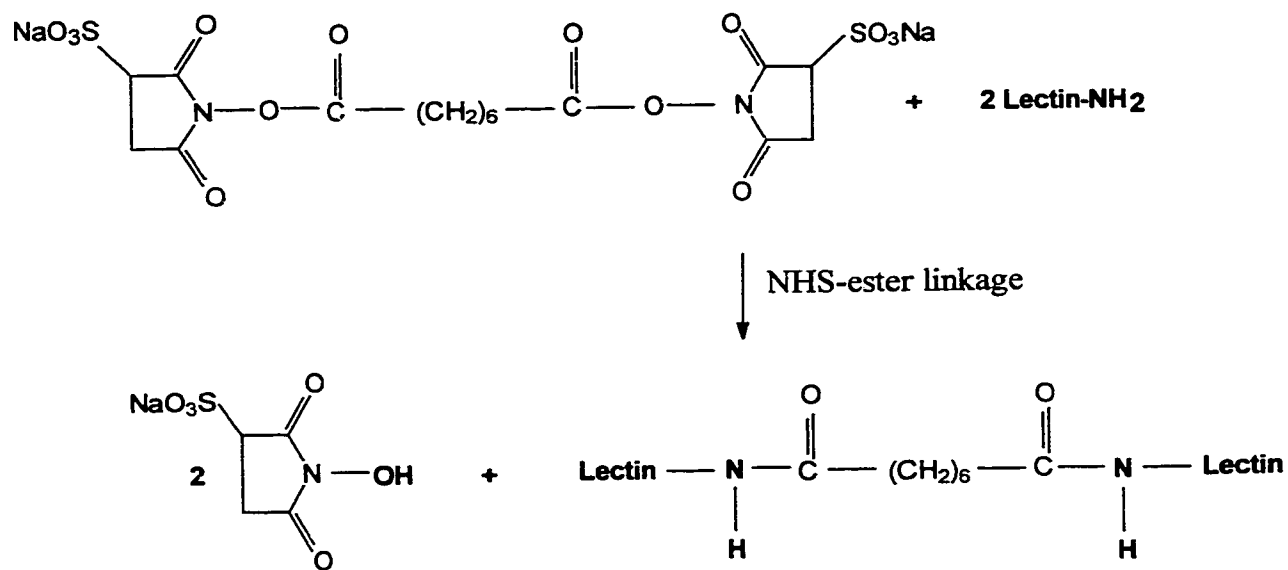


Figure 4.3: Schematic of m-maleimidobenzoyl-N-hydroxysuccinimide ester Sulfo-MBS (MW 314,2; 9.9 Å) reactions with amino-groups of proteins.

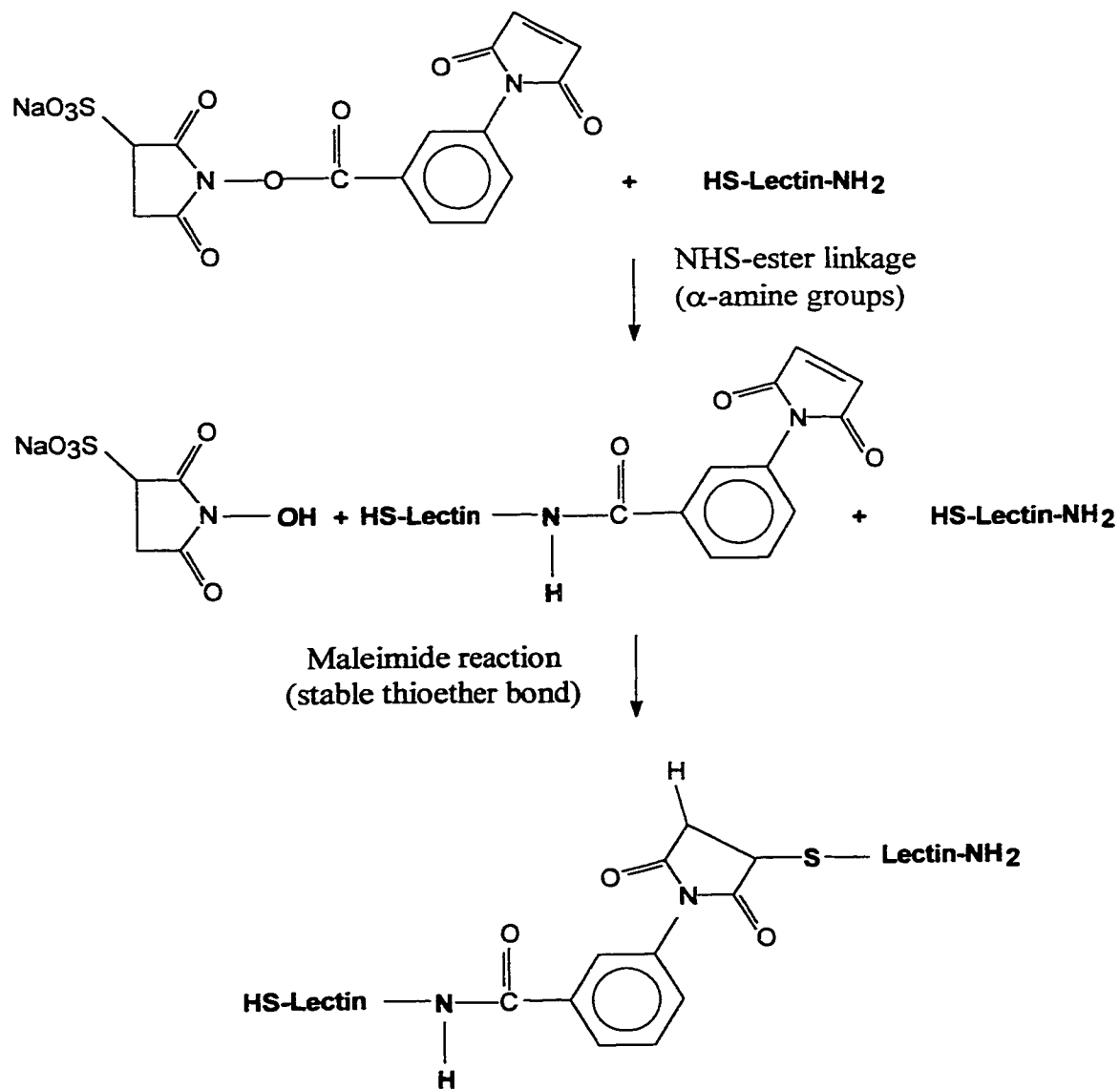
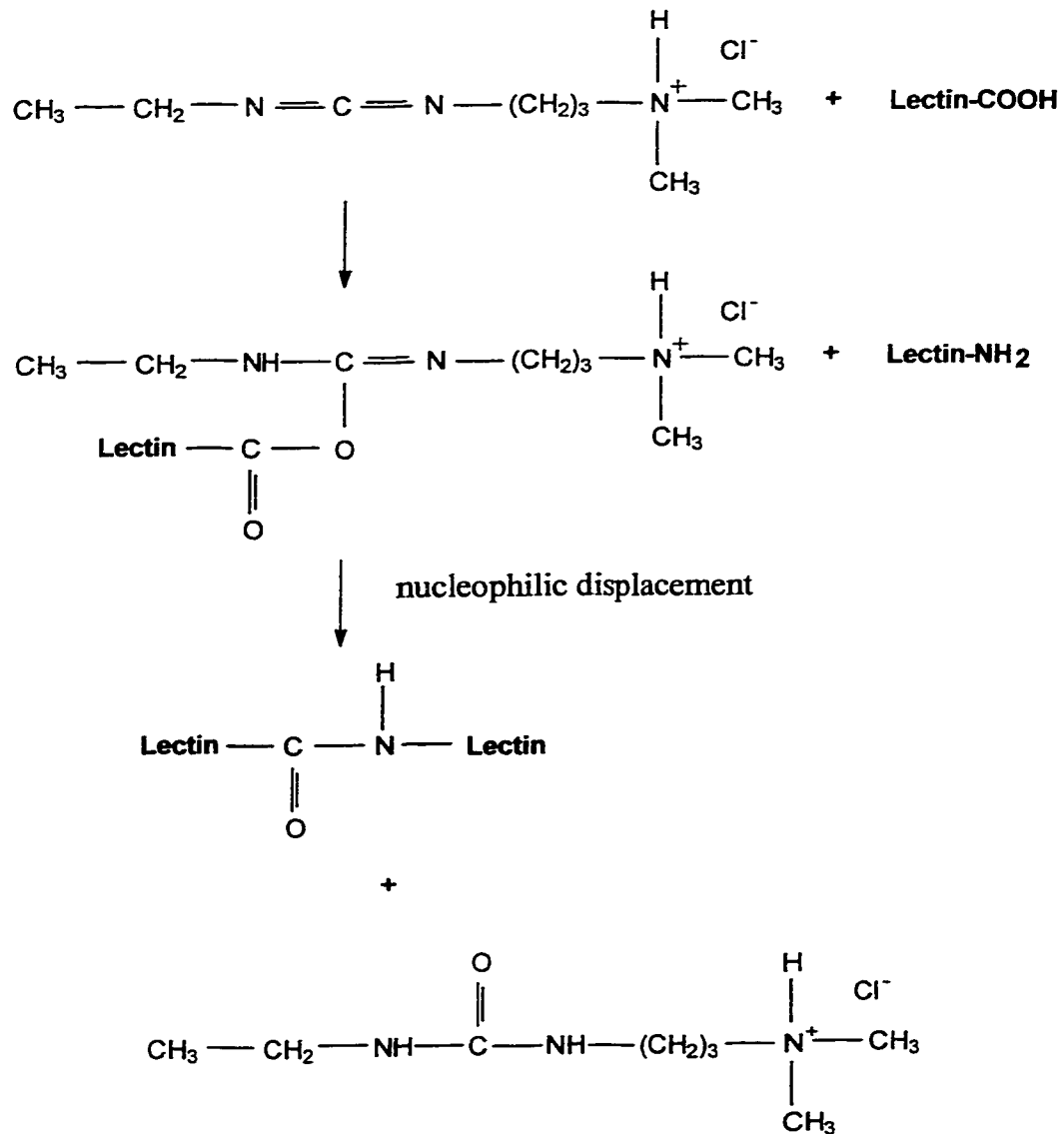


Figure 4.4: Structure of 1-ethyl-3-(3-dimethylaminopropyl) carbodiimide-HCl EDC (MW 191.7) as well as reaction scheme with proteins.



Nonspecific adsorption of bacterial cells onto the different surfaces was studied by incubating *E. coli* for 1 h at 22°C in the presence of unmodified membranes. These membranes were rinsed and transferred into the reagent solution, where ferricyanide reduction was allowed to occur for 1 h at 37°C. In the absence of lectins or crosslinking reagents, we found consumed charges of 12.5 $\mu\text{C}/\text{min}$, 3.2 $\mu\text{C}/\text{min}$, 5.4 $\mu\text{C}/\text{min}$ and 4.9 $\mu\text{C}/\text{min}$ for the BiodyneB[®], BiodyneA[®], nitrocellulose and the supported nitrocellulose membranes, respectively. This suggests that *E. coli*, which exhibits a negative net charge on its outer membrane adheres most strongly to positively charged surfaces.

Concanavalin A, the lectin exhibiting the strongest binding affinity in *E. coli* agglutination tests, (Table 4.1) was chosen to compare the different crosslinking agents with different membrane materials. Preliminary experiments conducted in this manner are shown in Table 4.4, where results were obtained by means of chronocoulometry for Con A modified membranes in the presence of different crosslinking agents. Here, the total amount of ferrocyanide was measured in the bulk solution (total volume of 400 μL) after a 50-min incubation period at 37°C in the reagent solution containing 50 mM ferricyanide and 10 mM succinate. Results shown in Table 4.4 showed that three membrane types (BiodyneA[®], BiodyneB[®] and nitrocellulose) yielded high signals after Con A modification, if Con A is crosslinked with MBS, a heterobifunctional crosslinking agent. The control membranes (lacking Con A) exhibited lower nonspecific *E. coli* adhesion to the BiodyneA[®] and nitrocellulose membranes. These results suggest that a high degree of selective Con A - *E. coli* binding can be achieved using both, BiodyneA[®] (neutral nylon) and nitrocellulose membranes. Therefore these membranes were chosen for subsequent immobilization experiments.

Table 4.4: Consumed charges obtained after 50 min incubation in reagent solution using chronocoulometry for exponential-phase grown *E. coli* bound to Concanavalin A on modified membrane surfaces.

Membrane	Crosslinking agents	Consumed charge, μC obtained for a 2 min reduction period*	
		Con A	Control [†]
BiodyneB [®]	---	9.3 ± 3.3	11.7 ± 5.8
	EDC	5.3 ± 1.9	6.2 ± 3.2
	BS ³	3.4 ± 0.2	8.8 ± 0.1
	MBS	16.7 ± 0.8	7.1 ± 1.7
	DMA	13.0 ± 3.0	12.2 ± 6.8
BiodyneA [®]	---	4.8 ± 3.7	4.6 ± 0.8
	EDC	1.2 ± 0.4	2.6 ± 0.5
	BS ³	2.2 ± 0.1	3.1 ± 0.8
	MBS	17.4 ± 2.4	2.6 ± 0.2
	DMA	7.8 ± 2.0	2.2 ± 0.5
Nitrocellulose	EDC	4.3 ± 0.8	7.0 ± 0.4
	BS ³	2.4 ± 0.1	2.3 ± 0.4
	MBS	17.7 ± 0.4	2.4 ± 1.2
	DMA	17.3 ± 1.5	17.6 ± 2.7
Supported	BS ³	0.7 ± 0.2	2.0 ± 0.3
Nitrocellulose	MBS	2.4 ± 0.1	4.0 ± 1.1
	DMA	3.2 ± 1.0	7.6 ± 2.1

* Average of two replicate measurements

† Control membranes with no lectin were treated identically to Con A modified crosslinked membranes

In an attempt to improve the magnitude and precision of the signals, lectin concentration studies were performed using Concanavalin A. BiodyneA[®] membranes were soaked in a series of Con A dilutions ranging from 0 to 1000 $\mu\text{g}/\text{mL}$ and adsorption proceeded for 5 h at room temperature. Following lectin adsorption, the membranes were rinsed and transferred into the crosslinking agent (MBS 5 mM) solution and allowed to react overnight at 4°C. Table 4.5 shows the results obtained for exponential phase *E. coli* cells that were stored on ice for 20 min prior to experimentation. To ensure the exposure of lectin-modified membranes to high cell densities, 1 mL aliquots of the cell suspension were centrifuged for 1 min (14000 rpm) and resuspended in 0.5 mL buffer. At this point the Con A modified membranes were combined with the buffered cell suspensions for 1 h either at room temperature or at 37°C. Next, membranes were rinsed, combined with reagent and incubated for an additional 50 min at 37°C. At this point, electrochemical determination of ferrocyanide in the bulk solution took place by chronocoulometry.

The results, shown in Table 4.5, indicate that selective cell-adhesion to the lectin layer at room temperature in general yielded higher signals. This means greater cell binding took place at room temperature than at 37°C. It is possible that increased *E. coli* cell mobility at this temperature competes with membrane binding (keeping cells at the membrane surface), leading to leaching into the suspension. Although values obtained for room temperature captured cells are higher, both curves exhibit a distinct signal maximum at a Con A concentration of 500 $\mu\text{g}/\text{mL}$.

Table 4.5: Consumed charges obtained with chronocoulometry after three min measurement time, where *E. coli* were trapped on BiodyneA[®] by Con A immobilization that was crosslinked by 5 mM MBS (pH 9.3).

Concanavalin A concentration $\mu\text{g/mL}$	Incubation in reagent at 37°C	Consumed charge,* $\mu\text{C}/\text{min}$ after 1 h cell binding to Con A at	
		22°C	37°C
1000	50 min	6.7 ± 0.2	2.9 ± 1.5
500	50 min	11.5 ± 3.5	7.4 ± 2.0
100	50 min	4.5 ± 2.2	4.8 ± 0.8
50	50 min	4.8 ± 2.1	-
0	50 min	4.6 ± 0.1	3.5 ± 3.1

* Average of three replicate measurements

Using an identical procedure, nitrocellulose membranes were used to investigate the effects of temperature as well as the effects of lectin concentration on observed signals. These values can be seen in Table 4.6.

Table 4.6: Consumed charges obtained with chronocoulometry after three min measurement time, where *E. coli* were trapped on BiodyneA[®] by Con A immobilization that was crosslinked by 5 mM MBS (pH 9.1).

Concanavalin A concentration $\mu\text{g/mL}$	Incubation in reagent at 37°C	Consumed charge,* $\mu\text{C}/\text{min}$ after 1 h cell binding to Con A at	
		22°C	37°C
1000	50 min	16.2 ± 9.9	10.3 ± 6.2
500	50 min	7.5 ± 3.8	5.9 ± 3.3
100	50 min	11.2 ± 7.1	8.3 ± 4.6
50	50 min	9.3 ± 7.5	3.8 ± 2.1
0	50 min	12.8 ± 5.0	19.9 ± 5.7

* Average of three replicate measurements

Results in Table 4.6 suggest no clear lectin concentration optimum. Additionally, high signals were observed in the absence of the recognition element, thus suggesting that nonspecific adsorption was the predominant cause for cell binding. Given these findings, immobilization through adsorption in the presence of the heterobifunctional crosslinking agent MBS was not deemed suitable for a sensor array application requiring high sensitivity, selectivity and precision.

4.3.3 Avidin-Biotin Immobilization

4.3.3.1 Detection Using ABTS Assay

To avoid loss of binding activity the avidin-biotin reaction was tested for the immobilization of biotinylated peroxidase. This enzyme was used as a detectable model for biotinylated lectins, thus allowing optimization of the avidin immobilization step. Instead of the initial lectin layer, avidin or streptavidin was adsorbed onto the membrane surface and stabilized by means of crosslinking agents, and incubated along with biotinylated peroxidase for the biotin moiety to bind to the adsorbed avidin or streptavidin. The peroxidase indicator reaction was used to optically measure the accumulation of visible dye, which in turn indicated if enzymes were sufficiently immobilized. Peroxidase catalyzes the oxidation of ABTS to an intensely-coloured green product (Equation 4.1) that is readily measured spectrophotometrically.^{28,29,30}

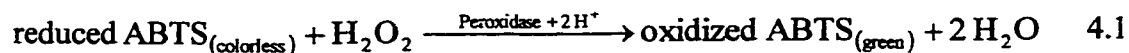
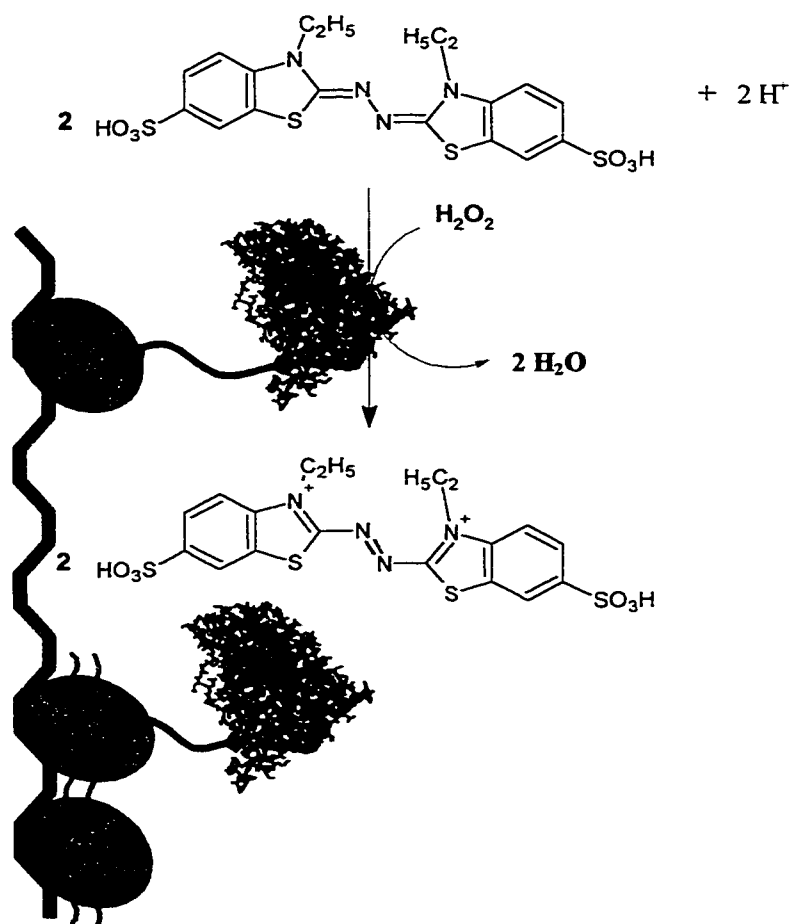


Figure 4.5 displays a schematic representation of the proposed avidin-biotinylated peroxidase complex as well as the structure of ABTS and its reaction cycle. From this figure it is evident that two molecules of dye are oxidized by peroxidase in the presence of one molecule of hydrogen peroxide, thus making this assay very sensitive and rapid.

Figure 4.5: Schematic representation of the sandwich immobilization method, where the avidin-biotinylated peroxidase complex allows measurement of ABTS conversion optically at 412 nm.



Initial experiments were conducted using the glycoprotein avidin adsorbed onto the four different membrane materials and crosslinked with one of the five reagents: glutaraldehyde, EDC, MBS, DMA or BS³. Glutaraldehyde is a homobifunctional amine-selective crosslinking reagent and has been used to chemically immobilize enzymes on sensor surfaces for solution and FIA applications.^{15,16} Unfortunately, when glutaraldehyde is used for intermolecular crosslinking, there also exists the possibility of crosslinking between protein subunits, which ultimately leads to losses of enzymatic activity.²

Glutaraldehyde is used to form imine bonds with primary amine groups on proteins. Cyanoborohydride (10 mM NaCNBH₃) was added to the crosslinking solution to yield more stable secondary amine bonds as seen in the reaction below (Eq. 4.2).

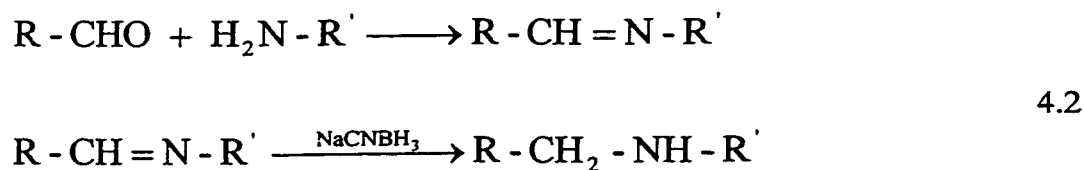


Table 4.7 shows the results obtained using the ABTS assay after avidin was adsorbed onto the four membrane materials and crosslinked with one of five crosslinking agents. Crosslinking was conducted overnight at 4°C, where the avidin-modified membrane disks were soaked in different stock solutions (10 mM EDC, DMA, BS³ and MBS or 25% glutaraldehyde). At this point, biotinylated peroxidase was allowed to bind to the avidin layer (1 h, 22°C) and the membrane was transferred into the ABTS solution. Control measurements were performed to determine the degree of nonspecific peroxidase adsorption.

Table 4.7: ABTS conversion rates measured at 412 nm obtained for avidin-biotinylated peroxidase system, that have been immobilized on various membranes in the presence of different crosslinking agents.

Crosslinking Agent	ABTS conversion rates* in $\mu\text{M}/\text{min}$ obtained at 412 nm			
	BiodyneA [®]	BiodyneB [®]	Nitrocellulose	Supported NC
Control**	17.2	17.0	13.7	14.8
Control/BSA***	9.5	8.8	8.7	12.9
Glutaraldehyde	7.6	10.7	3.7	4.6
EDC	7.3	3.2	8.8	5.6
MBS	2.8	1.2	6.8	1.7
DMA	8.2	6.4	8.4	6.7
BS ³	9.8	9.1	0.0	0.0

* Average of three replicate measurements with an RSD < 10%.

** Control measurements indicate nonspecific adsorption at unmodified membranes.

*** BSA was used instead of avidin to indicate nonspecific peroxidase adsorption.

These results indicate that avidin adsorbed onto the BiodyneB[®] membrane and crosslinked with glutaraldehyde, yields highest ABTS conversion rates. Both nylon membranes exhibited higher signals than the nitrocellulose or supported nitrocellulose membranes, indicating higher adsorption rates of avidin for nylon. Control experiments displaying highest signals were those that lacked avidin and crosslinking agents, and where only peroxidase was allowed to adsorb onto the membrane prior to measuring. However, control measurements that included BSA showed reduced conversion rates (factor of 2 for nylon membranes). Data obtained for BiodyneB[®] with all crosslinking agents indicated that the avidin layer formed in the presence of glutaraldehyde resulted in highest signals (10.7 $\mu\text{M}/\text{min}$). Further experiments were therefore conducted using the crosslinking agent glutaraldehyde with positively charged BiodyneB[®] membranes.

A later comparative study investigated streptavidin and the avidin-biotin anchor as well as their effects on ABTS conversion when employing various membrane materials. Streptavidin and avidin, its glycoprotein counterpart, exhibit similar binding affinities to biotin. However, these proteins may exhibit different adsorption characteristics because of their different surface structures. ATBS conversion rates were measured for avidin and streptavidin layers, which were crosslinked with glutaraldehyde on different membrane surfaces prior to incubation with biotinylated peroxidase. Control measurements were also conducted in the presence and absence of BSA and were consequently compared to signals obtained for specific binding of biotinylated peroxidase to the crosslinked avidin/streptavidin layers. Results obtained in this manner are shown in Table 4.8 and 4.9.

Table 4.8: ABTS conversion rates by peroxidase (25 $\mu\text{g}/\text{mL}$ in incubation solution) measured at 412 nm obtained for avidin crosslinked with glutaraldehyde on various membranes.

Crosslinker	ABTS conversion rates* in $\mu\text{M}/\text{min}$ obtained at 412 nm			
	BiodyneA [®]	BiodyneB [®]	Nitrocellulose	Supported NC
Glutaraldehyde/BSA [‡]	7.6	12.9	3.9	7.3
Glutaraldehyde	9.4	11.6	3.1	7.3
Control/BSA	4.9	7.2	9.7	22.0
Control	7.6	21.9	17.4	25.6

* Average of three replicate measurements with an RSD < 8%

‡ A solution containing 100 $\mu\text{g}/\text{mL}$ of avidin and BSA was used for immobilization prior the addition of glutaraldehyde.

Table 4.9: ABTS conversion rates by peroxidase (50 $\mu\text{g}/\text{mL}$ in incubation solution) measured at 412 nm obtained for streptavidin crosslinked with glutaraldehyde on various membranes.

Crosslinker	ABTS conversion rates* in $\mu\text{M}/\text{min}$ obtained at 412 nm			
	BiodyneA [®]	BiodyneB [®]	Nitrocellulose	Supported NC
Glutaraldehyde/BSA [‡]	34.6	38.3	5.9	5.9
Glutaraldehyde	58.3	64.2	12.2	5.9
Control/BSA	38.2	52.8	10.3	41.8
Control	55.5	72.1	48.2	54.0

* Average of three replicate measurements with an RSD < 15%

‡ A solution containing 100 $\mu\text{g}/\text{mL}$ of avidin and BSA was used for immobilization prior the addition of glutaraldehyde.

These findings suggest the avidin-biotin anchor immobilized onto positively charged nylon surface (BiodyneB[®]) yielded the best results. In addition, we found that the nonspecific adsorption of peroxidase onto BiodyneB[®], can be efficiently blocked using a BSA co-adsorption step. The two-fold increase of peroxidase concentration in the stock solution (50 $\mu\text{g}/\text{mL}$) used for streptavidin-modified membranes yielded generally higher conversion rates, indicating that further signal improvement could be achieved by finding the optimum biotinylated peroxidase concentration. However, the results obtained for avidin or streptavidin in the presence of BSA on BiodyneB[®] show that only avidin yielded higher ABTS signals (12.9 $\mu\text{M}/\text{min}$) compared to control measurements (7.2 $\mu\text{M}/\text{min}$; in the presence of BSA).

In an attempt to find the optimum avidin concentration for further signal improvements, a series of experiments using varying avidin concentrations were conducted. Measurements were performed after avidin adsorption on BiodyneB[®]

membrane surfaces followed by glutaraldehyde crosslinking for 1 h at 22°C, and incubation for 30 min after addition of 10 mM NaCNBH₃. To further inhibit nonspecific peroxidase adsorption, the avidin-modified membrane was incubated in a BSA solution (100 µg/mL) for 1 h. Table 4.10 shows the effect of varying avidin concentrations on measured ABTS conversion rates. Results indicate that 100 µg/mL of avidin in the adsorption stock solution cause the highest ABTS oxidation signals. Avidin concentrations exceeding 100 µg/mL may have resulted in steric hindrance and thus yielded lower ABTS conversion rates.

Table 4.10: ABTS conversion rates by peroxidase (25 µg/mL) measured at 412 nm obtained for varying avidin concentrations. Avidin adsorption was conducted on positively charge nylon membranes (BiodyneB[®]) and crosslinked with glutaraldehyde prior to biotinylated peroxidase binding.

Avidin concentration	ABTS conversion *
50 µg/mL	9.6 ± 0.4 µM/min
100 µg/mL	13.3 ± 3.2 µM/min
250 µg/mL	12.3 ± 1.1 µM/min
500 µg/mL	10.8 ± 0.5 µM/min
Control(BiodyneB [®] /BSA/peroxidase)	14.8 ± 1.2 µM/min
Control (BiodyneB [®] /peroxidase)	25.6 ± 2.1 µM/min

* Average of two replicate measurements

In summary, results indicate that avidin adsorption onto BiodyneB[®] is favoured over streptavidin, and that a maximum conversion rate was achieved when 100 µg/mL avidin was used during the adsorption step. Higher signals were also obtained when avidin was crosslinked with glutaraldehyde in the presence of sodium cyanoborohydride.

4.3.3.2 Detection of *E. coli* by Chronocoulometry

The above mentioned immobilization procedure was used to create a biosensing layer that was composed of a crosslinked avidin anchor in combination with a biotinylated lectin (Con A). After incubating in a bacterial cell suspension, the membrane was attached onto electrodes by means of nylon netting and a rubber o-ring. This was followed by a brief incubation period in the ferricyanide reagent solution, where the captured *E. coli* reduced ferricyanide in close proximity to the electrode, prior to chronocoulometric measurement. The measurements of ferrocyanide concentrations in a localised fashion (near the electrode surface) was expected to yield significantly higher signals than those found with membranes immersed in the bulk solution and thus should ultimately increase sensor sensitivity.

Initial calibration measurements were conducted using cells trapped on the electrode surface in order to investigate bacterial detection limits and correlate signals with cfu's. A series of chronocoulometric experiments were performed with a runtime of 90 s, where listed values indicate the difference in total charge consumed between 30 and 90 s. Aliquots (5 μ L) of exponential phase *E. coli* JM105 culture ($OD_{600} = 3.51$), centrifuged and resuspended in varying volumes of buffer to create a dilution series, were added onto an unmodified membrane disk and mounted on the Pt working electrode. A dialysis membrane (MW cut-off 6 – 8000) was used to fix the membrane and retain *E. coli* cells on the electrode surface. Nevertheless, ferricyanide could still diffuse freely through the porous membrane. An incubation period of 10 min at 37°C in reagent solution yielded measurable accumulation of ferrocyanide, which was then measured electrochemically.

Figure 4.6 shows the obtained signals plotted against colony forming units (cfu), where values obtained for cfu were determined as described in Chapter 2 Section 2.2.2.5.

Figure 4.6: Consumed charges obtained for a series of cell dilutions, where an aliquot ($5\ \mu\text{L}$) of cell suspension were spotted onto a membrane surface, that was fixed at the Pt working electrode surface with a dialysis membrane (MW cut-off 6 – 8000). Each point is the average of two background-subtracted replicate measurements.

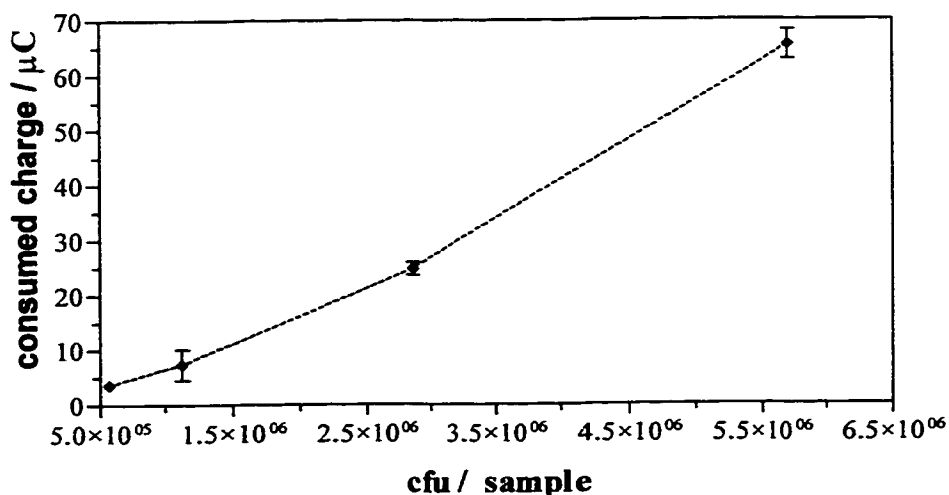
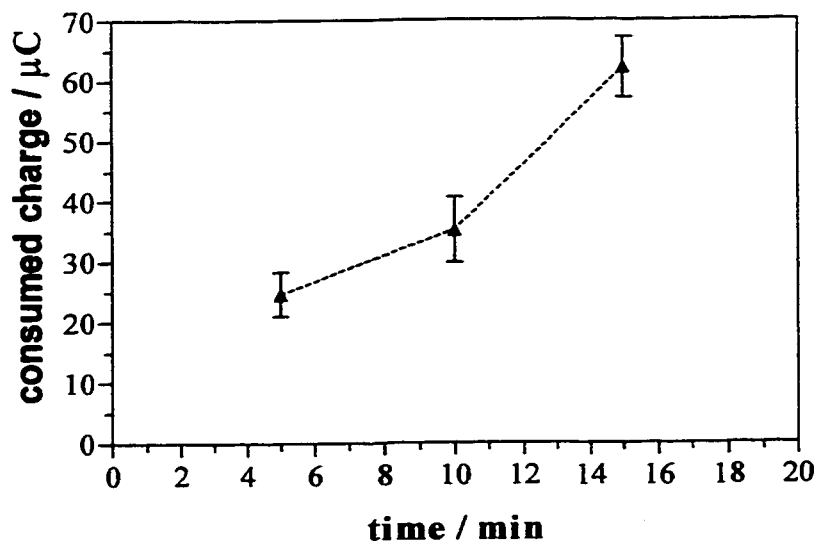


Figure 4.6 indicates a nonlinear response in variation with cell number. The curvature may be related to different local environments (pH, metabolite/product concentrations) that would exist in the cell's microenvironment due to the metabolic activity of the bacteria. Minimum detectable signals in the experiment occurred at around 0.5×10^6 cells.

The effect of ferricyanide incubation time on signals obtained with bacterial cells trapped at the electrode surface was studied using an experimental set-up similar to the one described above. An aliquot ($10\ \mu\text{L}$ or 8.2×10^6 cells) of exponential phase *E. coli* ($\text{OD}_{600} = 2.52$) were spotted on BiodyneB[®] membrane and mounted on the electrode surface. A dialysis membrane was used to retain cells and consumed charges were measured after incubating for 5, 10 and 15 min. Incubation took place in a reagent solution containing 50 mM ferricyanide and 10 mM succinate. The observed curvature in Figure 4.7 is most likely attributed to signal variances observed for the small sample volumes ($10\ \mu\text{L}$) used in this experiment.

Figure 4.7: Signals obtained for 8.2×10^6 exponential phase *E. coli* cells by chronocoulometry at 37°C after entrapment on the electrode surface with varying incubation times in the reagent solution. Each point is the average of three background-subtracted replicate measurements, and error bars represent one standard deviation.



Results displayed in Figure 4.7 show an upward curvature clearly indicating that ferricyanide reduction by surface-entrapped *E. coli* over a 15 min period is stable and reproducible.

Nonspecific cell adhesion was then determined for the four membrane materials used in previous experiments. This was achieved by comparing obtained cfu numbers to rates observed for nonspecific cell adsorption. Membrane disks ($A = 0.28 \text{ cm}^2$) were immersed in bacterial cell suspension and incubated for 1 h at room temperature. The washed membrane was then mounted on the electrode surface using a nylon net, and incubated for 10 min in reagent solution. Table 4.11 shows the results obtained in this manner, where the signal of 10 μL of trapped *E. coli* suspensions were compared to nonspecific adsorption occurring on various membrane materials.

Table 4.11: Consumed charges and colony forming units obtained for *E. coli* cells that are either trapped at the electrode surface with a dialysis membrane or allowed to adhere for 1 h at room temperature prior chronocoulometric run

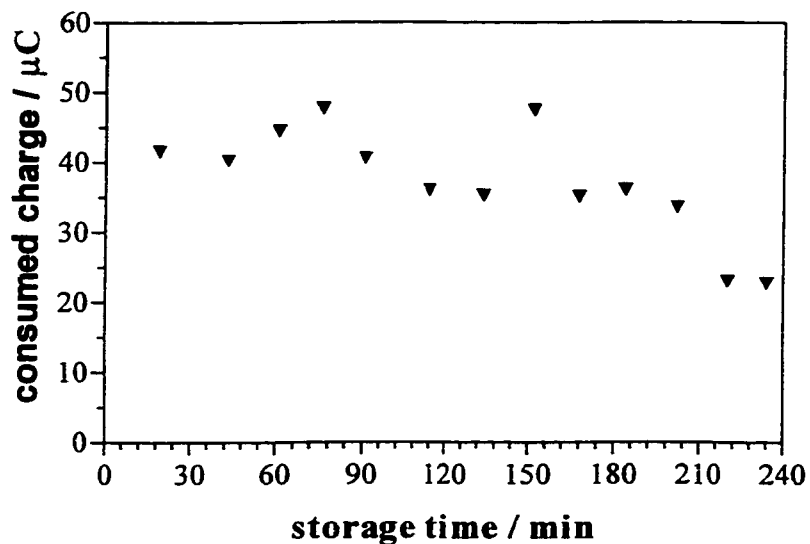
Membrane	Charge*	Nonspecific adsorption*
BiodyneA [®]	$61.6 \pm 0.3 \mu\text{C}/\text{min}$	$4.2 \pm 1.1 \mu\text{C}/\text{min}$
BiodyneB [®]	$86.3 \pm 1.8 \mu\text{C}/\text{min}$	$9.5 \pm 2.6 \mu\text{C}/\text{min}$
BiodyneB [®]	$60.9 \pm 1.1 \mu\text{C}/\text{min}$	$10.1 \pm 1.9 \mu\text{C}/\text{min}$
NC	$86.2 \pm 2.8 \mu\text{C}/\text{min}$	$3.5 \pm 0.2 \mu\text{C}/\text{min}$

*Average of two replicate measurements

The BiodyneB[®] membrane exhibited highest rates of nonspecific adsorption as seen in Table 4.11.

A maximum bacterial storage period had to be determined since the cell suspension was stored on ice prior to chronocoulometric measurements. Figure 4.8 shows the signal as a function of storage time for bacteria that had been stored on ice over 4 h. It is evident that bacterial ferricyanide reduction rates experienced a significant decrease after cells were stored for about 200 min. Therefore, all subsequent measurements were performed using cells that had been stored on ice for less than 3.5 h.

Figure 4.8: Chronocoulometric signal obtained after 10 min incubation in reagent solution for *E. coli* JM105 cells stored on ice. Aliquots (5 μL) of the chilled cell suspension were trapped at the electrode surface using a dialysis membrane (MW cut-off 6 – 8 kDa)



Following these preliminary experiments, avidin-modified, glutaraldehyde crosslinked BiodyneB[®] membranes were transferred into a solution containing biotinylated Con A and avidin-biotin binding was allowed to occur. The modified membranes were then incubated in bacterial cell suspension for a minimum of 1 hour at room temperature. After several washing steps, the membranes were mounted onto the electrode surface, held in place with a nylon net and o-ring, and then transferred into the reagent solution. Results obtained in this manner for varying concentrations ($\mu\text{g/mL}$) of avidin and biotinylated Con A are shown in Table 4.12.

Table 4.12: Chronocoulometric signals obtained for exponential phase *E. coli*, captured at the avidin-biotinylated Con A modified BiodyneB[®] membranes. A 15 min incubation with reagent (50 mM ferricyanide and 10 mM succinate) was used prior to measurement.

Membrane Modification	Avidin ($\mu\text{g/mL}$)	Con A ($\mu\text{g/mL}$)	Consumed Charge,* $\mu\text{C/min}$
Modified with avidin, no Con A (control)	100	-	3.1
Modified with BSA (control)	-	-	0.2
Modified with avidin	100	25	0.0
	100	25	2.5
	500	50	3.6
	100	100	3.0
	500	100	2.7
	500	25	1.4

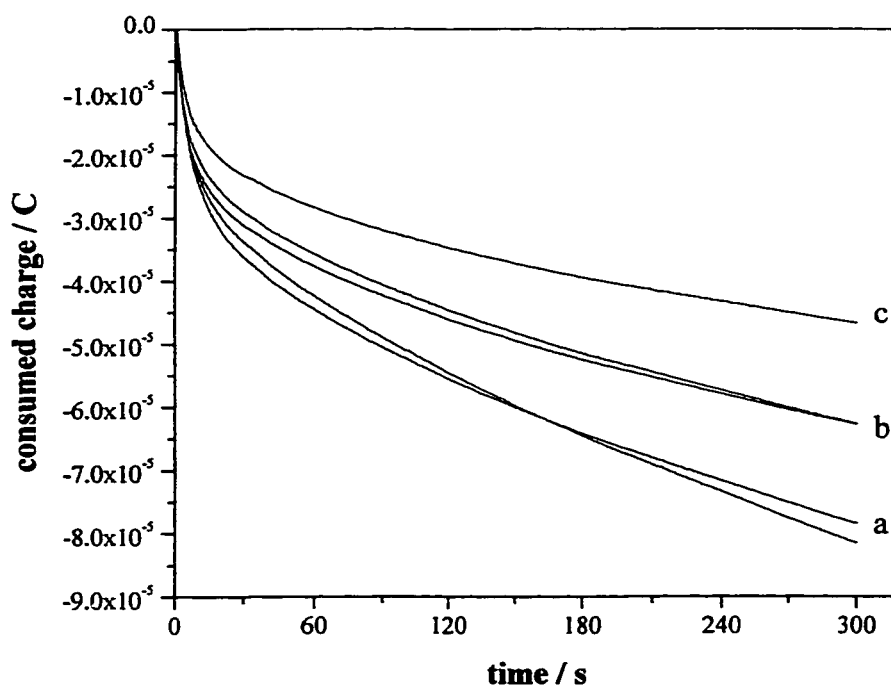
* Average of two replicate measurements

These results show that the ratio of avidin to biotinylated Concanavalin A concentration clearly influences measured charge, and that the higher Con A concentrations yielded

higher signals. The largest signals for Concanavalin A were obtained using concentrations of 50 or 100 $\mu\text{g/mL}$. Variation in the avidin concentration, on the other hand, had little effect on signals.

In a final attempt to increase signals, the electrochemical measurement time was extended from 90 s to 300 s. Figure 4.9 shows chronocoulometric traces obtained for *E. coli* cells captured on the biotinylated Concanavalin A–avidin modified (BiodyneB[®]) nylon membrane after a 10 minute incubation period in ferricyanide.

Figure 4.9: Chronocoulometric traces obtained for *E. coli* JM105 captured on (a) biotinylated Con A modified and (b) unmodified BiodyneB[®] membrane after 10 min incubation period in reagent solution ($V_{\text{total}} = 200 \mu\text{L}$). Chronocoulometry was also performed in the absence of *E. coli* cells (c).



Here, a 100 $\mu\text{g}/\text{mL}$ avidin solution was allowed to interact with the membrane overnight at 4°C. This was followed by a 40 min crosslinking step in a 25% glutaraldehyde solution prior to the addition of NaCNBH₃ (10 mM). After 30 min the crosslinked avidin layer was washed and transferred into a BSA (blocking) solution to allow protein adsorption (1 h; 22°C). Finally, the avidin layer was allowed to bind to biotinylated Concanavalin A (50 $\mu\text{g}/\text{mL}$) for 1 h at room temperature, followed by a 1 h incubation step in bacterial suspension. At this point the washed membrane was mounted onto the electrode surface and immersed in the reagent solution. After an incubation period of 10 min at 37°C, accumulated ferrocyanide was detected by chronocoulometry. Table 4.13 shows the results calculated from the traces shown in Figure 4.9, where chronocoulometry (two electrode system) was performed in a total volume of 200 μL for 5 min.

Table 4.13: Consumed charges obtained for *E. coli* captured cells after 10 min incubation in reagent solution of the modified membrane. Values represent calculated differences of charges obtained for $t_1 = 300$ s and $t_2 = 240$ s.

Name	Consumed charge, * μC
Nonspecific cell binding (no biot. Con A)	1.8 ± 0.3
Specific cell binding	4.4 ± 0.6

* Average of 3 replicate measurements; background subtracted values

The results shown in Table 4.13 and Figure 4.9 indicate the successful application of a lectin-modified membrane to selectively bind and detect *E. coli* cells. Although the chronocoulometric assay was able to measure viable *E. coli* cells selectively bound to a lectin-modified electrode, a complex and lengthy immobilization procedure was needed. As described for Figure 4.9 and Table 4.13, the immobilization method involved a multi-step procedure requiring a total of 48 h to modify a single membrane surface. Alternative

immobilization procedures to enable simplification of the previously reported technique were therefore investigated.

4.3.4 Lectin Immobilization on Preactivated Membranes

The application of preactivated membranes that offer covalent protein binding at their surface was investigated for lectin immobilization. ImmunodyneABC[®] is a nylon 6,6 affinity membrane that features a chemically activated surface and offers a high density of covalent binding sites. According to manufacturing specification, ImmunodyneABC[®] (pore size of 0.45 μm) forms covalent linkages with nucleophilic groups found on proteins. The company also specifies that its primary reactivity is with amine groups at neutral pH. UltraBind[®], another nylon membrane, possesses aldehyde functional groups on its inner and outer surfaces thus providing effective covalent bonding to amine groups on proteins.

The previously described immobilization procedure used for the avidin–biotin adsorption system was applied to the ImmunodyneABC[®] membrane in order to investigate the signals achievable with this membrane. Table 4.14 shows results obtained for *E. coli* cells that had been bound to the avidin-biotinylated Con A surface. Control measurements were performed using BSA modified membranes that had been incubated in cell suspension prior to electrochemical measurement. BSA was allowed to react with the activated surface to prevent nonspecific *E. coli* adhesion on the membrane. Background measurements were conducted with modified electrodes (ImmunodyneABC[®] /avidin-biotinylated Con A) in the absence of bacterial cells.

Table 4.14: Chronocoulometric signals obtained by chronocoulometry (runtime 5 min) after a 10 min incubation period in reagent at 37°C. ImmunodyneABC[®] was modified using avidin (crosslinked) – biotinylated Con A.

ImmunodyneABC [®] modified with	Incubation in reagent	Consumed charge, * μC
BSA - <i>E. coli</i>	10 min	85.9 \pm 0.5 (n = 2)
Concanavalin A - <i>E. coli</i>	10 min	40.6 \pm 5.9 (n = 3)
Background 1 (Imm. ABC / BSA)	10 min	11.9
Background 2 (Imm. ABC/avidin-biot. ConA)	10 min	44.5
Background 3 (Imm. ABC/avidin-biot. ConA)	15 min	82.0
Background 4 (Imm. ABC/avidin-biot. ConA)	20 min	118.4

Results in Table 4.15 show that background measurements using electrodes modified with avidin–biotinylated Con A membranes exhibited increased signals compared to background measurements using BSA. We further found a linear increase in background signals with time, suggesting that components of the ImmunodyneABC[®] avidin-biotinylated Con A layer react with ferricyanide. For this reason, signals obtained for *E. coli* experiments remain inconclusive.

We thus omitted the crosslinking step using glutaraldehyde and NaCNBH₃ to eliminate potential interference as well as to simplify the immobilization procedure. The revised immobilization step allowed the ImmunodyneABC[®] membrane to react with either avidin or streptavidin, followed by an incubation step in a biotinylated Con A solution. The modified membranes were immersed into the *E. coli* cell suspension for 1 h prior to incubation in ferricyanide. Table 4.15 shows the results of this comparative study.

Table 4.15: Chronocoulometric signals obtained for *E. coli* that had been captured onto avidin or streptavidin–biotinylated Con A ImmunodyneABC[®] membrane. No crosslinking agents were implemented.

ImmunodyneABC [®] modified electrode	Consumed charge, μC
Background	13.3 ± 0.5 (n = 2)
BSA - <i>E. coli</i>	13.9 ± 1.8 (n = 3)
Biotin. Con A / avidin– <i>E. coli</i>	17.4 ± 2.6 (n = 3)
Biotin. Con A / streptavidin– <i>E. coli</i>	16.7 ± 1.6 (n = 3)

Stable background signals were observed in the absence of the crosslinking solution (glutaraldehyde and NaCNBH_3), suggesting that residual reducing agent remained on or in the membranes used in the previous experiment in which ferricyanide reduction appeared to occur in the absence of *E. coli*. Signals using avidin modified membranes showed best results on average, although statistically, avidin and streptavidin are equally effective.

Next, Concanavalin A was directly bound to the ImmunodyneABC[®] surface, thus creating a lectin layer while minimizing the time and steps required. The ABC membrane disks were immersed in a solution of $100 \mu\text{g/mL}$ Con A and allowed to react for 1 h at room temperature prior to storage at 4°C . Table 4.16 shows the consumed charges obtained for *E. coli* that had been captured on the Con A modified electrode surface. It is evident that BSA is an efficient blocking agent, preventing nonspecific adhesion of *E. coli* onto the ImmunodyneABC[®] membrane. Direct covalent linkage of Concanavalin A onto the ImmunodyneABC[®] surface yielded distinctly higher and more precise signals. We were therefore able to simplify the immobilization method from a multi-step to a

single step procedure and hence shortened the time needed to modify the membrane from 48 hours to 1h.

Table 4.16: Consumed charges obtained for *E. coli* JM105 after 10 min incubation in reagent solution at 37°C. Con A was covalently attached to the ImmunodyneABC[®] surface and used as selective cell recognition agent.

ImmunodyneABC [®] modified electrode	Consumed charge, * μC
ImmunodyneABC [®] - <i>E. coli</i>	8.5
BSA - <i>E. coli</i>	0.3 ± 0.1 (n = 2)
Concanavalin A- <i>E. coli</i>	2.5 ± 0.3 (n = 3)

* All values are background subtracted

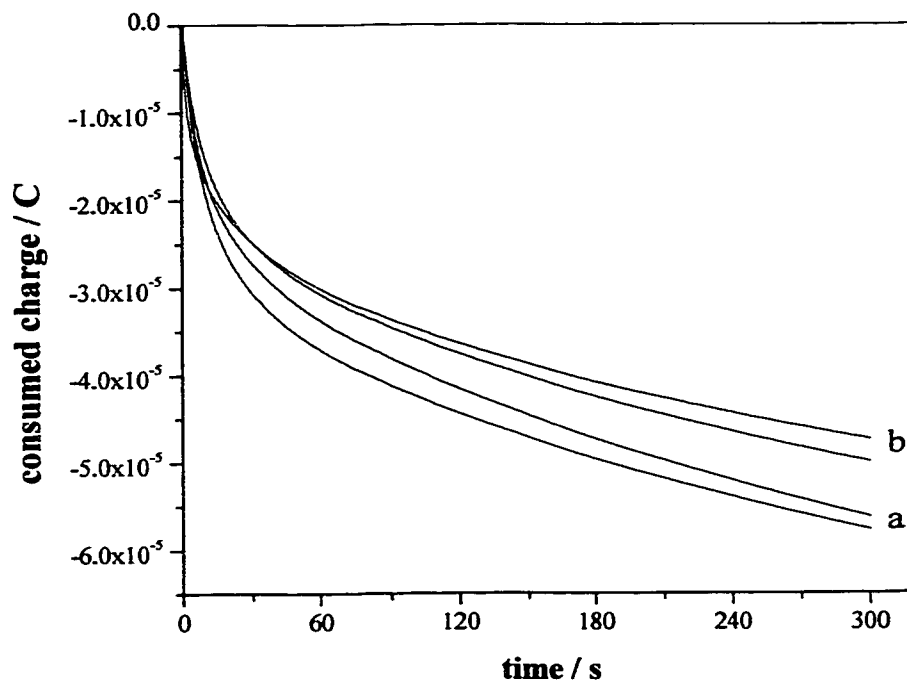
A second preactivated membrane featuring an aldehyde surface was investigated for its possible application as an immobilization matrix. The activated polyethersulfone membrane UltraBind[®] was used for this study. Figure 4.10 shows chronocoulometric traces obtained for *E. coli* adhesion to Con A and BSA modified surfaces. The simple one step (1 h) immobilization procedure, followed by *E. coli* and reagent incubation, were used to electrochemically determine the degree of selective *E. coli* binding to Con A modified membranes. Signals calculated from these chronocoulometric traces are listed in Table 4.17, where control measurements were performed on BSA modified membrane surfaces. The obvious differences within the chronocoulometric traces obtained for selective Con A binding and nonspecific *E. coli* adhesion indicate the practical utility of preactivated membranes.

Table 4.17: Chronocoulometric signals obtained for *E. coli* JM105 after 10 min incubation in reagent solution at 37°C. Con A or BSA were covalently attached to UltraBind® and used as recognition agent.

UltraBind® modified electrode	Consumed charge,* μC
BSA - <i>E. coli</i>	1.7 ± 0.7 (n = 2)
Concanavalin A- <i>E. coli</i>	4.2 ± 0.8 (n = 3)

* All values are background subtracted

Figure 4.10: Chronocoulometric traces obtained with Con A (a) and BSA (b) modified UltraBind® surfaces. Captured *E. coli* JM105 cells were incubated for 10 min in reagent solution.



We then investigated the application of the avidin–biotin system as potential immobilization procedure for lectins on Ultrabind[®] membranes. In a comparative study, the glycoprotein avidin and the protein streptavidin were covalently linked to the active sites of the membrane, followed by a reaction step in biotinylated Concanavalin A solution. Table 4.18 shows the results obtained after *E. coli* capture and 10 min incubation in ferricyanide/succinate solution.

Table 4.18: Consumed charges obtained for *E. coli* that have been captured onto avidin or streptavidin – biotinylated Con A UltraBind[®]. No crosslinking agents were employed.

Ultrabind [®] modified electrode with	Consumed charge,* μC
BSA - <i>E. coli</i>	1.5 - 3.7 (n = 2)
biotin. Con A / avidin– <i>E. coli</i>	1.8 - 4.8 (n = 3)
biotin. Con A / streptavidin– <i>E. coli</i>	3.7 - 4.5 (n = 3)

* Averaged values are background subtracted

As in previous experiments using avidin-biotin immobilizations, poor precision resulted, and the three values shown in Table 4.18 are not statistically different.

In a final comparison, the performance of ImmunodyneABC[®] and UltraBind[®] were evaluated directly. A simple and direct Concanavalin A immobilization procedure was used for both ImmunodyneABC[®] and UltraBind[®]. Observed results were background subtracted and the amount of nonspecific adsorption was determined using BSA modified membranes. Table 4.19 lists obtained charges after the modified electrodes were immersed and incubated for 10 min in reagent solution. The chronocoulometric runtime

was set for 5 min and consumed charges were calculated as the charge difference between $t = 300$ s and $t = 240$ s.

Table 4.19: Consumed charges obtained for exponential phase *E. coli* JM105 after 10 min incubation in reagent solution at 37°C. Con A and BSA were covalently attached to UltraBind® or ImmunodyneABC® and used as recognition agent.

<i>E. coli</i> captured on	Consumed charge,* μC
UltraBind® - BSA	1.6 ± 0.3 (n = 2)
UltraBind® - Con A	2.1 ± 0.5 (n = 3)
ImmunodyneABC® - BSA	1.4 ± 0.2 (n = 2)
ImmunodyneABC® - Con A	4.4 ± 0.9 (n = 3)

* Averaged values are background subtracted

Results in Table 4.19 clearly illustrate that under the same conditions, ImmunodyneABC® yields higher signals than UltraBind®. From these results it is evident that the direct covalent bonding method, where lectins are directly linked to the preactivated surface, results in a fast and easy immobilization procedure that forms a lectin layer with a high degree of binding selectivity.

4.4 CONCLUSIONS

In preliminary agglutination tests, lectins were investigated for their abilities to bind to *E. coli*. Direct immobilization of lectins onto the electrode surface was avoided by investigating the use of thin porous membranes that could be layered above the electrode. These immobilization carriers (membranes) allow easy modification in large quantities to produce selective membranes that could be stored for long periods of time and discarded after single use.

Consequently, lectin-adsorption abilities were investigated using four membrane materials, as a simple physical immobilization method. After lengthy incubation periods, the membrane-lectin-cell complexes in the reagent solution generated small reduction signals. Different crosslinking agents were studied in order to prevent leaching from the membrane surface and improve signals. Consequently, we made use of an enzymatic assay to substitute the slower cell-binding kinetics found in the electrochemical assay, and to perform a multitude of experiments in short periods of time. To avoid losses in activity, the avidin-biotin immobilization system was used, where avidin and streptavidin were adsorbed onto the membrane surface and stabilised by crosslinking agents instead of using direct lectin immobilization.

Summarised results obtained from the ABTS sandwich assay used to improve the immobilization procedure showed that avidin is favoured over streptavidin adsorption on BiodyneB[®] (positive nylon). We further found that glutaraldehyde used as a crosslinking agent in the presence of the mild reducing agent cyanoborohydride, yielded the highest signals.

The optimized immobilization procedure was then used in an electrochemical set-up, where biotinylated Con A was immobilized on the avidin layer on a BiodyneB[®] membrane. An assay time increase up to 300 s was used to achieve higher chronocoulometric signals and results were obtained after only 10 min incubation in reagent.

Preactivated membranes were then investigated in order to simplify the immobilization procedure, because up to this point, a long and tedious immobilization procedure was required to obtain results. ImmunodyneABC[®] and UltraBind[®] were chosen because both membranes feature a chemically modified surfaces that form covalent linkages with amine groups of peptides.

In a comparative study, both membranes were investigated for their performance under various conditions such as the absence and presence of the avidin-biotin anchor. We found that ImmunodyneABC[®] membranes, after direct linkage with Con A yielded highest signals compared to the UltraBind[®] membrane.

In summary, the application of membranes that feature an activated surface capable of covalent linkage to lectins significantly reduced the time required to efficiently create a lectin layer on the membrane surface. By mounting the membrane with the recognition element onto the electrode surface, we were able to detect localised ferrocyanide concentrations that, could in turn, be correlated to cell numbers. Furthermore, the fast direct linkage of lectins onto removable membrane disks allowed multiple measurements within short periods of time. As a result, we incorporated the ImmunodyneABC[®] membrane into a fast and direct immobilization procedure for the final application in the lectin-based biosensor array.

4.5 REFERENCES

1. Kovacs, G. T. A.; Petersen, K.; Albin, M. *Anal. Chem.* 1996, 68, 407.
2. Cunningham, A. J. *Introduction to Bioanalytical Sensors*, John Wiley & Sons, Inc. 1996.
3. Keneke, R.; Menzel, C.; Ulber, R.; Schuegerl, K.; Scheper, T. *Biosens. Bioelectron.* 1996, 11, 12.
4. Bundy, J.; Fenselau, C. *Anal. Chem.* 1999, 71, 1460.
5. Wright, C. S.; Kellogg, G. *Prot. Sci.* 1996, 5, 1466.
6. Payne, M. J.; Campbell, S.; Patchett, R. A.; Kroll, R. G. *J. Appl. Bacteriol.* 1992, 73, 41.
7. Patchett, R. A.; Kelly, A. F.; Kroll, R. G. *J. Appl. Bacteriol.* 1991, 71, 277.
8. Yim, H.-S.; Kibbey, L. E.; Ma, S.-L.; Kilza, D. M.; Liu, D.; Park, S.-B, Torre, C. E.; Meyerhoff, M. E. *Biosens. Bioelectron.* 1993, 8, 1.
9. Tatsuma, T.; Watanabe, T. *Anal. Chem.* 1992, 64, 625.
10. Staros, J.; Wright, W; Swingle, D. *Anal. Biochem.* 1986, 156, 220.
11. Braun, B.; Klein, E.; Lopez, J. L. *Biotechol. Bioeng.* 1996, 51, 327.
12. Oswald, P. R.; Evans, R. A.; Henderson, W.; Daniel, R. M.; Fee, C. J. *Enz. Microb. Tech.* 1998, 23, 14.
13. Cochrane, F. C.; Petach, H. H.; Henderson, W. *Enz. Microb. Tech.* 1996, 18, 373.
14. Yoshitake, S.; Imagawa, M.; Ishikava, E. *Anal. Lett.* 1982, 15, 147.
15. Saurina, J.; Hernandez-Cassou, S.; Fabregas, E.; Alegret, S. *Anal. Chim. Acta* 1998, 371, 49.

16. Moody, J.; Sanghera, G. S.; Thomas, J. D. R. *Analyst* 1986, 111, 605.
17. Alkorta, I.; Garbisu, C.; Llama, M. J.; Serra, J. L. *Enz. Microb. Tech.* 1995, 18, 141.
18. Green, N. M. Avidin. *Advanced Protein Chemistry*, Academic Press, New York, 1975.
19. Wong, J. Y.; Kuhl, T. L.; Israelachvili, J. W.; Mullah, N.; Zalipsky, S. *Science* 1997, 275, 820.
20. Polzius, R.; Schneider, T.; Bier, F. F.; Bilitewski, U. *Biosens. Bioelectron.* 1999, 14, 503.
21. Cosnier, S.; Stoytcheva, M.; Seniliou, A.; Perrot, H.; Furriel, R. P. M.; Leone, F. A. *Anal. Chem.* 1999, 71, 3692.
22. Rehak, M.; Snejdarkova, M.; Otto, M. Tiefenauer, L. X.; Kossek, S.; Padeste, C.; Thiebaud, P. *Biosens. Bioelectron.* 1997, 12, 213.
23. Oda, Y.; Kinoshita, M.; Kakehi, K. *Anal. Chem.* 1997, 254, 41.
24. Sharon, N.; Lis, H. *Lectins*, Chapman and Hall, New York, 1984.
25. Turner, A. P. F.; Karube, I.; Wilson, G. *Biosensors: Fundamentals and Application*, Oxford University Press, New York, 1987.
26. Voet, D.; Voet, J. G. *Biochemistry* 2nd Ed. John Wiley & Sons, Inc. New York, 1995, chapter 5.
27. Liener, I. E.; Sharon, N.; Goldstein, I. J. *The Lectins: Functions and Application in Biology and Medicine*, Academic Press, Inc. 1978.
28. Childs, R. E.; Bardsley, W. G. *Biochem. J.* 1975, 145, 93.
29. Makinen, K. K.; Tenovuo, J. *Anal. Biochem.* 1982, 126, 100.
30. Shindler, J. S.; Childs, R. E.; Bardsley, W. G. *Eur. J. Biochem.* 1976, 64, 325.

31. Mádâras, M. B.; Buck, R. P. *Anal. Chem.* 1996, 68, 3832.
32. Halina, L.; Sharon, N. *Chem. Rev.* 1998, 98, 637.

Chapter 5

Microbial Identification *via* Pattern Recognition

5.1 INTRODUCTION

5.1.1 Objective

The last stage in the development of a biosensor is concerned with the characterization of the sensor itself. In this chapter, chronocoulometric data obtained using different microbial strains are assessed. The application of factor analysis is examined as a possible tool to distinguish between six different microbial strains. Lectin-binding kinetics are examined by means of chronocoulometry. This method measures bacterial ferricyanide reduction rates after selective cell-binding to lectin-modified membranes, and it provides information about oligosaccharide moieties found on microbial cell walls.

Atomic force microscopy is implemented to further study the immobilization carrier used in this assay. AFM images are used to gain information about the orientation of chemisorbed lectins on the membrane surface and about the completeness of the layer. A biosensor array, consisting of 10 differently modified electrodes, is shown to yield signal patterns that are characteristic of microbial strains. Results obtained from the biosensor array are subjected to factor analysis to allow pattern recognition of six different microbial strains.

5.1.2 Introduction

Detection, identification and quantitation of microorganisms play a vital role in fermentation technology, medical practice and environmental monitoring. Bacteria, viruses and other microorganisms are found throughout nature and hence bacterial pathogens are distributed in soil, marine waters, water contaminated with fecal matter or the intestinal tract of animals. An average person carries more than 150 kinds of bacteria inside and outside the body.¹ However, certain potentially harmful microorganisms can have profound effects on humans and can also be the cause of different infectious diseases. Table 5.1 gives an overview of microbial pathogens, the disease they cause or the toxins they release.

Worldwide, infectious diseases account for nearly 40% of the total 50 million annual estimated deaths. Microbial diseases constitute the major cause of death in many developing countries of the world. A growing number of bacterial pathogens have been identified as important food- and waterborne pathogens and incidences of human diseases caused by food-borne pathogens have not yet decreased.² Estimates of food-borne illness vary widely from several million cases to 81 million cases in the USA, with bacterial food-borne outbreaks accounting for 91% of the total outbreaks.³

The term 'rapid' is widely used to describe any method that significantly shortens the analysis time compared to conventional detection procedures. It is more specifically applied to methods that require less than 24 h to obtain results; usually a colony containing 10^6 organisms takes 18 – 24 hours to develop. A rapid, sensitive and reliable screening method for bacterial contamination in drinking water, food and dairy products,

industrial waste and clinical samples would be very important for the prevention of infections and epidemics.

Table 5.1: Some pathogenic bacteria* and their diseases, toxins and infection sources.⁵

Bacteria	Disease	Toxin	Infection sources
<i>Bacillus anthracis</i>	Anthrax	Edema factor	Milk or meat
<i>Brucella melitensis</i>	Brucellosis		Milk or meat
<i>Campylobacter jejuni</i>	Diarrhea dysentery		Dairy, meat
<i>Clostridium botulinum</i>	Botulism	Neurotoxin	Food
<i>Escherichia coli</i>	Gastroenteritis	Enterotoxin	Meats, fish, milk
<i>Corynebacterium diphtheriae</i>	Diphtheria	Diph. Toxin	Water
<i>Salmonella paratyphi</i>	Pratyphoid		Eggs, milk, meat
<i>Shigella dysenteriae</i>	Bacillary dysentery	Neurotoxin	Fecal contamination
<i>Staphylococcus aureus</i>	Pneumonia	Enterotoxin	Human carrier
<i>Treponema pallidum</i>	Syphilis		Blood
<i>Vibrio cholerae</i>	Cholera	Enterotoxin	Fecal contamination

* Many more bacterial strains are known to be highly infectious and some of them were also abused as biological warfare agents (BWF). These include strains that can cause high mortality rates such as *Coxiella burnetti* (Pneumonia), *Francisella tularensis* (Tularmia), *Mycobacterium tuberculosis* (Tuberculosis), *Rickettsia rickettsi* (Rocky Mountain-spotted fever), *Salmonella typhi* (Typhoid fever) and *Yersinia pestis* (Bubonic plague).

Generally, no single test provides a definitive identification of an unknown bacterium. Traditional bacterial detection methods involve a pre-enrichment step, and a selective enrichment step, followed by biochemical screening and serological confirmations. This complex series of tests is inherently time-consuming and can last up to 72 h.⁴ Almost all of the available analytical instrumentation has been employed for microbial detection. Common instrumental methods used for identifying bacteria include

surface plasmon resonance, fiber optics and flow cytometry. Other methods include piezoelectric crystals, impedimetry, calorimetry and by detecting cellular compounds such ATP, DNA, protein and lipid derivatives as well as monitoring redox processes.⁵⁻⁷ Furthermore, infrared spectroscopy and gas chromatographic mass spectrometric detection of fatty acids has also been used for the detection of and identification of microorganisms.²

In recent years, intensive research has been undertaken to develop portable, rapid and sensitive biosensors capable of detecting microbes with high specificity and sensitivity. Bacterial detection by biosensors generally require a biological recognition component such as receptors, nucleic acids or antibodies, in intimate contact with an appropriate transducer.⁵ In a previous study, antibodies immobilized on magnetic beads were used to capture and retain microbial cells in a magnetic field. The magnetic beads were then resuspended and transferred onto selective agar plates. This method was used to detect strains of *Salmonella*, *E. coli* O157 and *Listeria*.⁴ Other transduction methods such as surface plasmon resonance and evanescent wave have shown promise in providing direct measurement of antigen-antibody interactions occurring at the surface-solution interface.^{4,8}

In this study lectins have been employed as selective recognition elements in a sensor array set-up using electrochemical signals to identify bacterial strains. Atomic force microscopy (AFM) has been used to study the orientation and completeness of immobilized selective lectin layers. Among the scanning probe microscopy techniques, atomic force microscopy is the most predominant, capable of imaging insulating or conducting surfaces at atomic resolution.⁹ One major advantage of AFM is its ability to image surfaces under liquids, thus making it a novel tool to image biological specimens

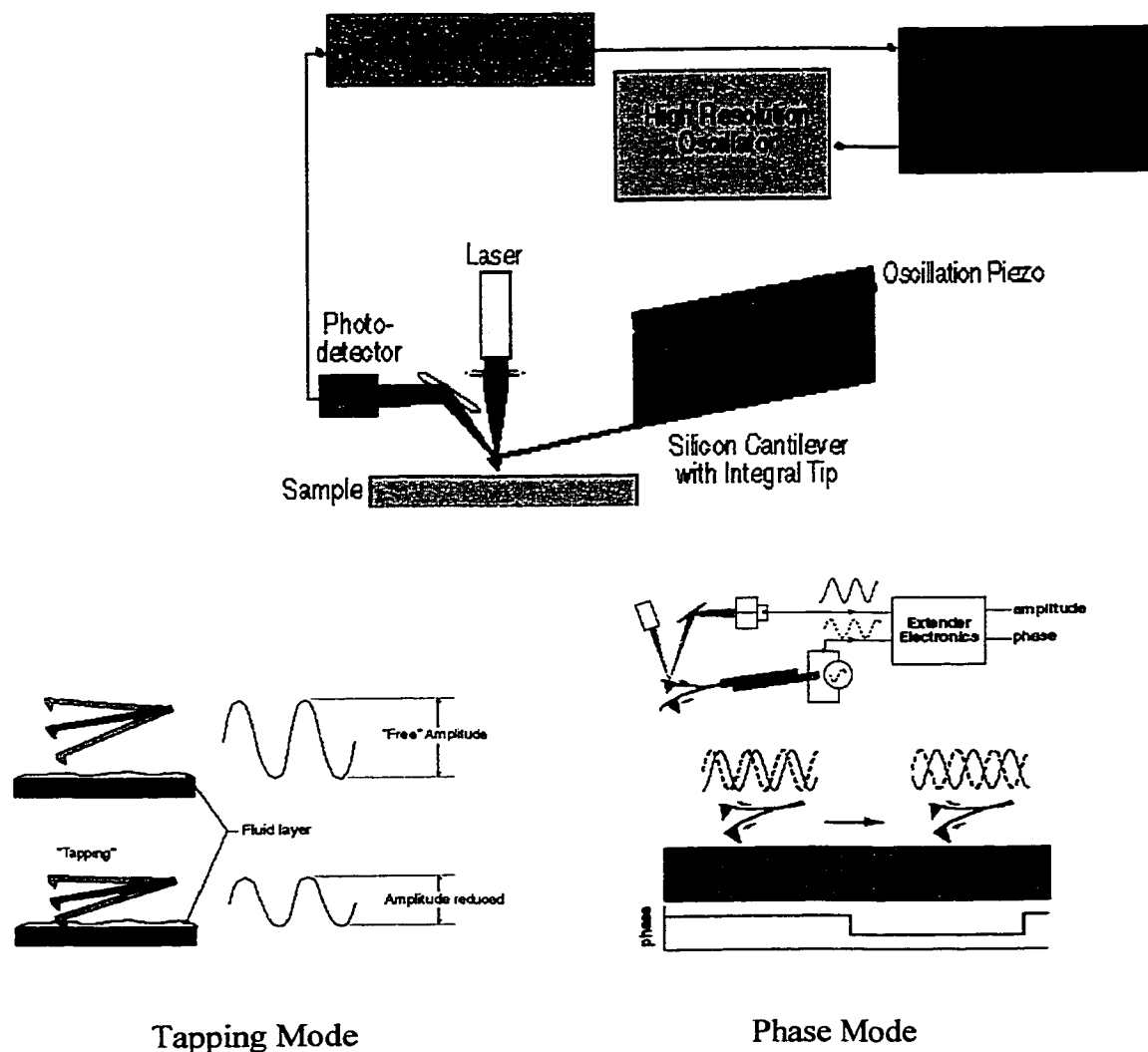
under near-native conditions of pH and ionic strength. Consequently, high resolution of biological samples such as membranes, membrane-bound proteins and DNA molecules, can be achieved.⁹⁻¹¹

Figure 5.1 displays a picture of the AFM, a schematic diagram of this instrument and the two modes of operation that were implemented in this study. A flexible cantilever with an attached stylus (tip) of approximate atomic-sharpness was held in a fixed position directly above the sample. The piezoelectric drive (i.e.: the x, y, z scanner) displaces the sample directly underneath the tip to keep the cantilever deflection, or z-distance, constant. There are four major modes of imaging in AFM: contact, error signal, tapping and phase mode. In this work, only tapping and phase modes were used to investigate the recognition layer under native conditions. When the tip was not in contact with the surface, the amplitude of the oscillating cantilever was measured, which decreased rapidly when the tip was moved toward the surface until it began to lightly touch or “tap” the surface. This reduction in oscillation amplitude was used to identify and measure surface features. During scanning, when the tip passed over a bump in the surface, the cantilever had less room to oscillate and the amplitude thus decreased. On the contrary, when the tip passed over a depression, the cantilever had more room to oscillate and the amplitude increased. Operating the AFM in this tapping mode prevented the tip from continuous contact with the surface that causes damage (and artifacts) during scanning.¹²⁻¹⁴

Phase mode is a sub-division of tapping mode AFM because the mechanical action of the cantilever is identical. The only difference between the two modes of imaging is the measured signal. Tapping mode records the z-amplitude (its position and force) whereas the phase mode measures changes in the phase of the oscillating

cantilever. The phase of oscillation varies with the viscosity of the surface under investigation, therefore the phase signal represents a sensitive contrast of the sample materials.^{15,16} The application of AFM to the lectin modified surfaces would be expected to reveal surface irregularities and help to understand immobilization phenomena. Hence it will facilitate the design of the sensing element leading to an improved recognition layer.

Figure 5.1: Schematic diagram of an atomic force microscope and scanning modes used in this study.



The recognition element should exhibit a high degree of specificity towards sugar moieties found on bacterial cell wall surfaces. Enzymes, antibodies and lectins are the predominant proteins that interact with carbohydrates non-covalently. Lectins are found in most organisms, ranging from viruses and bacteria to plants and animals, and they bind to mono- and oligosaccharides reversibly with high specificity, but they do not exhibit catalytic activity nor are they products of the immune response.¹⁷ Lectins have been shown to be invaluable tools for the structural and functional investigation of complex carbohydrates, especially glycoproteins. They have been also used in the differentiation of cancer cells as well as the application of recognition determinants in the intracellular traffic of glycoproteins, adhesion of infectious agents to host cells and cell-cell interactions.^{17,18}

On the basis of their specificity, lectins can be classified into five groups according to the monosaccharide for which they exhibit highest affinity (mannose, galactose/N-acetylgalactosamine, N-acetylglucosamine, fucose, and N-acetylneuraminic acid). The affinity of the lectins for monosaccharides is usually weak, with dissociation constants of 10^6 to 10^7 , yet it is often highly selective.¹⁹ For example, lectins specific for galactose do not react with glucose or mannose, and those specific for mannose do not bind to galactose. However, the selectivity of lectins for monosaccharides is not always so high because many lectins tolerate variations (e.g. C-2) in the structure of the pyranose ring. The presence of aromatic glycosides can also affect lectin selectivity; those glycosides that bind more strongly to lectins containing aliphatic groups close the carbohydrate-binding site.^{20,21}

Nevertheless, lectins often exhibit higher specificity for di-, tri-, and tetrasaccharides, with association constants that are up to 1000-fold higher than the

monosaccharide. Certain lectins were found to interact only with oligosaccharides. Moreover, lectins of the same specificity group may differ markedly in their affinities for different oligosaccharides. From a functional point of view, the higher binding affinities to oligosaccharides is of special significance because they are the most likely natural ligands of lectins.²⁰

Lectins have been further classified according to structural differences categorised as simple, mosaic or multidomain and macromolecular assemblies. Simple lectins consist of a small number of subunits with a molecular weight usually below 40 kD. This class comprises practically all known plant lectins where the most thoroughly studied family is that of legumes. Concanavalin A, isolated from jack bean, was first isolated in 1919 and was found to be selective towards mannose and glucose. Typically, legume lectins consist of two or four identical subunits, each with a small carbohydrate-binding site. They also contain a tightly bound Ca^{2+} and Mn^{2+} ions (one per subunit) necessary for sugar binding. These metal ions are situated in close proximity to the carbohydrate-binding site, where they help to position the amino acids that form contacts with the carbohydrate. Mosaic lectins include a diverse group of proteins from different sources, such as viral hemagglutinins and animal lectins. They are all composite molecules with a wide range of molecular weights and several protein domains, but only one of which possesses a carbohydrate-binding site. Macromolecular lectins are commonly found in bacteria, usually in the form of fimbriae. These are filamentous, heteropolymeric organelles present on the surface of bacteria.^{20, 22}

The binding sites of lectins exist in the form of shallow depressions on the surface of the protein. Lectins bind carbohydrates by means of a network of hydrogen bonds and hydrophobic interactions, although coordination with metal ions may also play a

important role. The hydrogen bonds are formed between carbohydrate hydroxyl groups and amino, hydroxyl, and other oxygen functional groups on the protein. Nevertheless, van der Waals forces and hydrophobic interactions may make a significant contribution to binding. Since most saccharides are uncharged, ionic (charge-charge) interactions do not commonly participate in sugar association, but water bridges sometimes mediate contacts between protein and its ligands. Water molecules act as both hydrogen donors and hydrogen acceptors, and can be thought of as structural extensions of the protein.²⁰

Bacteria have chemically well-defined surface carbohydrate structures, and other microorganisms, such as yeasts, contain carbohydrate structures that can also be used in lectin-mediated agglutination studies.²² Consequently, lectins have been employed for bacterial identification purposes due to their ability to bind cell wall oligosaccharides. In addition, lectins also found their way into analytical chemistry because they can be used as selective cell recognition elements capable of retaining microbial cells at transducer surfaces.²³ Furthermore, immobilized lectins have been used to selectively capture bacteria or were incorporated into affinity surfaces that were used to isolate broad classes of bacterial samples for MALDI mass spectrometric analysis.^{24,25}

Applications of chemometrics in chemical analysis are growing from pattern recognition and multivariate analysis to neural networks. Chemometrics are used to relate instrumental measurements to chemical information. Generally, chemometric processes measure signals to transform chemical data into information by means of statistical and mathematical techniques.²⁶ Modern computational systems and software packages allow the user to move beyond simple classical least-square analysis to factor-based techniques using principal component analysis (PCA). We chose to use factor-based techniques for the qualitative analysis of the chronocoulometric signals obtained for the different

microbial strains. Principal component analysis (PCA) is one of the so-called continuum regression methods, more commonly known as factor based methods, where a large number of instrumental measurements are combined to extract chemical information. More importantly, the factor based (PCA) method can be used to classify data obtained from individual samples into population groupings through pattern recognition. Consequently, the data matrix is transformed into abstract scores used to differentiate sub-populations.²⁶

Principal component analysis (PCA) aims to use mathematics to reduce the total variance to a number that adequately represents the real or chemical variance within a data set. Random noise in the signals can be minimized and finally PCA can reveal the combinations of variables; these combinations determine the patterns present in the original data set.²⁷ The program generates principle components which are defined as orthogonal weighted and linear combinations of the experimental data, and are simply a new set of axes upon which to plot the original data. This is important, since these abstract principal components can rapidly produce accurate and precise information about the analytical signal compared with traditional techniques. The first principle component (PC1) contains a maximum of variance present in the data matrix. Further principal components are generated from the remaining variance and are not related to PC1.²⁷ Therefore, the first principal component can be described as the linear combination that contains the largest variance while the second principal component contains the next largest variance. Both the first and second PCs usually account for approximately 99.9% of the total variances found in a data matrix.²⁸

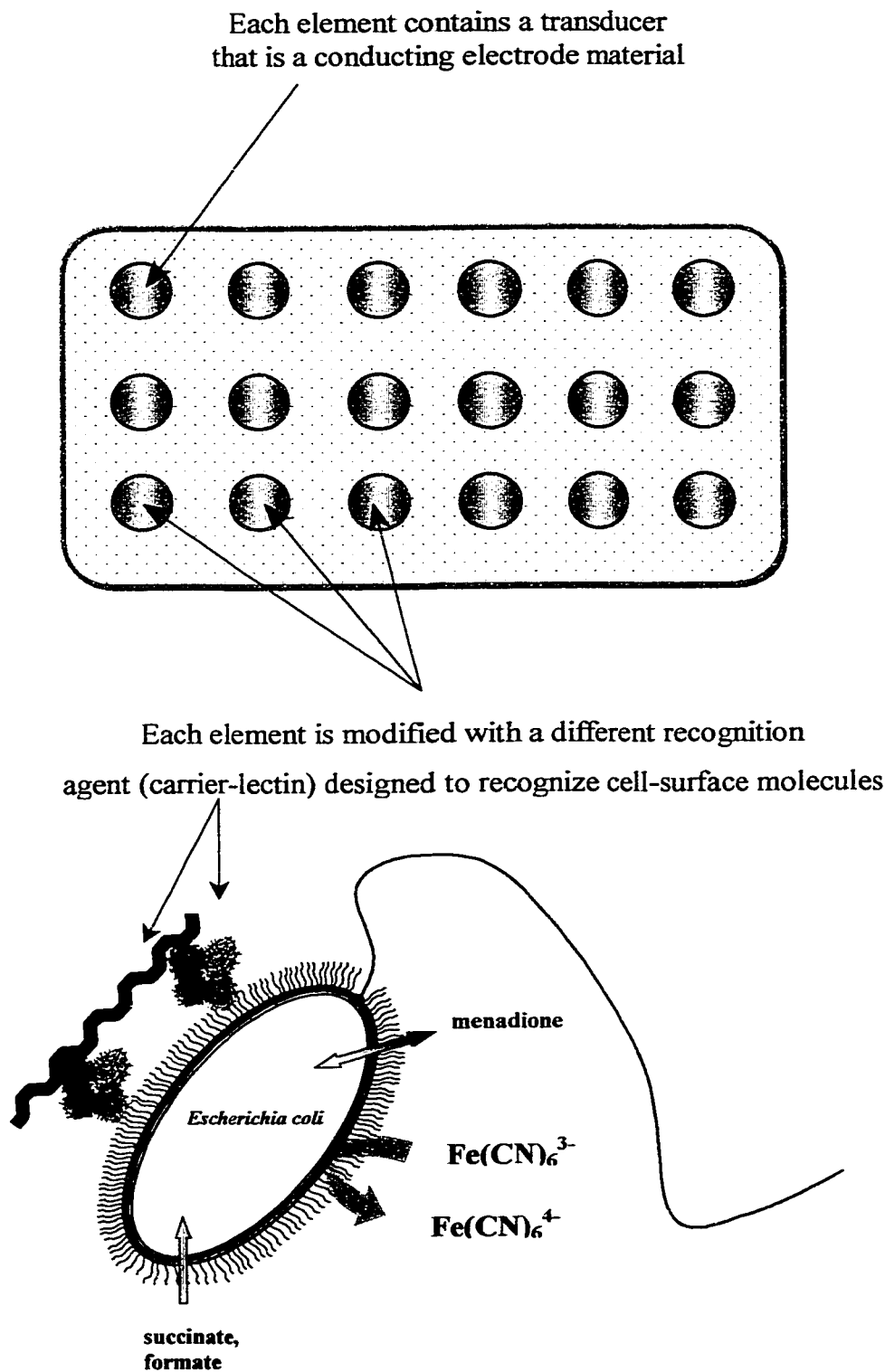
Chemometric techniques have been used in food analysis, odor analysis and for various quality control applications.²⁹ Principal component analysis (PCA) was also used

to generate pattern recognition plots from data obtained from chemical sensors. A gas sensor array operating five semiconductors were used to determine vintage years of wine.³⁰ Pattern recognition was also successfully implemented in the detection of pesticides in water mixtures using data obtained from uv-vis spectrophotometry.³¹

In this work, ferricyanide reduction rates measured after selective cell capture on the transducer surface are used to differentiate between microbial strains. Figure 5.2 shows a schematic diagram of the biosensor array. The final sensor array will consist of numerous electrodes with membranes layered on top of each transducer. These carriers were subject to immobilization, where a variety of lectins were covalently linked to the membrane surface in order to form a homogenous and selective cell-recognition layer. The modified electrode surfaces were then exposed to a single microbial strain and selective cell binding was allowed to occur. The bacterial suspension was then removed and transducer surfaces were rinsed prior to adding the reagent solution. Chronocoulometric signals obtained for all electrodes yielded a pattern of signals that can be used to identify or differentiate between bacterial strains. Lectins that exhibited stronger binding affinities to one strain retained more cells than other lectins. Multivariate data analysis was used to examine the observed signals at different transducers. The goal was to obtain a pattern recognition plot capable of grouping microbial strains with similar signal patterns.

In this chapter, the useful application of atomic force microscopy for the investigation of lectin-based recognition layers under native conditions is also demonstrated. Furthermore, an array of 10 lectins was used to distinguish between 6 different microbial strains, by chemometric data analysis for pattern recognition.

Figure 5.2: Graphical display of the biosensor array set-up used to distinguish between microbial strains.



A brief taxonomic description of the individual strains used in this study is given below. *Escherichia coli* grows in small rods, 1.1-1.5 μm diameter and 2.0-6.0 μm length and is mobile by peritrichous flagella. *E. coli* is a Gram-negative, facultative anaerobe and it exhibits both a respiratory and a fermentative type of metabolism. Glucose and other carbohydrates are fermented with the production of pyruvate, which is further converted into lactic acid, acetic acid and formic acid. The lipopolysaccharide layer of the outer membrane can be described as smooth (S) or rough (R), where smooth usually indicates the development of polysaccharide side chains. Some strains of *E. coli* produce enterotoxins, from which two toxins have been well studied. Both toxins, thermolabile (TL), which is closely related to cholera, and thermostable (TS) can be present alone or together in enterotoxigenic *E. coli*. However, *E. coli* can be looked upon primarily as an opportunistic pathogen, although indications show that they also play an important role in intestinal and extraintestinal diseases.³⁵

Enterobacter aerogenes ATCC 13048e grows in small rods, 0.6-1.0 μm diameter and 1.2 – 3.0 μm length, conforming to the general definition used for the family *Enterobacteriaceae*. *E. aerogenes* is a Gram-negative, facultative anaerobe and exhibits mobility by means of peritrichous flagella (generally 4-6). It grows readily on ordinary media and is able to ferment glucose with the production of acid and gas. Its optimum growth temperature is 30°C, but most clinical strains grow at 37°C. *E. aerogenes* is widely distributed in nature and is also commonly found in man and other animals. In particular, *E. aerogenes* can be isolated from human and animal faeces, but is not known to be an enteric pathogen. It is rather an opportunistic pathogen that was found to inhabit the respiratory tract, genitourinary tract and in pus. *E. aerogenes* can occasionally be isolated from blood and spinal fluids as well.³⁵

Proteus vulgaris ATCC6380 grows in straight rods of 0.4 to 0.8 μm in diameter and 1.0 to 3.0 μm in length. *P. vulgaris* is a Gram-negative organism and is mobile by means of peritrichous flagella. The organisms in this genus conform to the definitions outlined for the family *Enterobacteriaceae*. *P. vulagris* may cause primary and secondary infections in man (urinary tract infections). Although its role in the intestine is not well understood, it is estimated that approximately one quarter of the world population are intestinal carries of *Proteus*. This strain is widely spread in nature and is thought to have an important function in the decomposition of organic materials in manure, soil and polluted waters.³⁵

Bacillus cereus is a rod-shaped cell with straight features and forms endospores. *B. cereus* is a Gram-positive organism that carries peritichous flagella and is considered to be an aerobe or a facultatively anaerobe. The strain is widely distributed in nature and many strains are considered to be a pathogen although *B. cereus* plays a minor role in food-transmitted gastroenteritis. *B. cereus*' cell wall peptidoglycan is composed of murein and is directly cross-linked with meso-diaminopimelic acid. The bacillus also forms paracrystalline cell surface layers (S-layer) consisting of glycoproteins with structural regularities that completely cover the cell surface. *B. cereus* is undoubtedly the causative organism of a variety of somewhat severe infections in both man and other animals. Two types of food poisoning, an emetic type and a diarrheal type, are best known. Strains of *B. cereus* are most commonly found in soil and in plant litter, where they play an important role in the biological cycling of carbon and nitrogen.³⁵

Staphylococcus aureus ATCC6538P grows to spherical cells that are 0.5 to 1.5 μm in diameter and are found in single cells or in pairs. *S. aureus* is a Gram-positive, non-mobile, facultative anaerobe, with both a respiratory as well as a fermentative metabolism

with optimum growth between the temperatures of 18 and 45°C. Acid is produced aerobically and anaerobically from glucose. Natural populations are mainly found in skin, skin-glands and mucous membranes of warm-blooded animals. Some species are opportunistic pathogens affecting humans and other animals. Some strains also produce an epidermolytic toxin known as skin syndrome. Many strains produce enterotoxins that may produce symptoms of food poisoning if ingested (*via* contaminated food). *S. aureus* is a potential pathogen causing a wide range of infections. Some of the major infections include furuncles, toxic epidermal necrolysis, meningitis, mastitis, food poisoning and enterocolitis.³⁵

Saccharomyces cerevisiae ATCC 9896 is a fungus that belongs to the yeast genus (family Saccharomycetaceae). Cells grow in spherical, ellipsoidal or cylindrical shapes and are also diploid or haploid and do not form hyphae. Strains of *S. cerevisiae* can form ascospores. Under certain circumstances, yeast may cause infections in man and other animals (mostly opportunistic invasion). Although *S. cerevisiae* is not normally seen as a pathogen, some strains can cause diseases ranging from superficial infections of the cutaneous and mucosal sites to serious systemic diseases involving circulatory fluids. Some strains can cause food spoilage in particular where bacterial growth is hindered by pH values under 5. Species of *Saccharomyces* can ferment one or more sugars such as glucose (all), galactose, sucrose and maltose, and may also conduct a respiratory metabolism at the same time, given the right conditions. *S. cerevisiae* is important in the manufacturing of alcoholic beverages and fermented foods such as bread, beer, wine, sake and much more.^{36,37}

5.2 EXPERIMENTAL SECTION

5.2.1 Materials and Instrumentation

Sigma supplied all lectins and proteins including *Artocarpus integrifolia* (lyophilized powder ~ 70% protein), *Arachis hypogaea* (lyophilized powder), Concanavalin A (lyophilized powder ~ 15% protein), *Galanthus nivalis* (lyophilized powder), *Phytolacca americana* (lyophilized powder), *Lens culinaris* (lyophilized), *Lens culinaris* (lyophilized powder, ~ 80% protein), *Helix pomatia* (lyophilized powder), *Triticum vulgare* (lyophilized powder), *Codium fragile* (lyophilized powder). Bovine Albumin (99%). Platinum working electrodes as well as a silver wire 1.0 mm in diameter, were also supplied by Sigma. The pure silver wire (99.99%) was used as a reference electrode after depositing a Ag/AgCl layer.

Pall Specialty Materials supplied the preactivated nylon 6,6 membrane (Immodyne® ABC, pore size 0.45 μm). Fisher Scientific supplied the bi-directional rotator and a 4.5 cubic foot incubator. All electrochemical measurements were performed on the potentiostat/galvanostat Model 263 A supplied by EG&G Princeton Applied Research. Optical measurements were carried out on a Cary 1 uv-vis spectrophotometer (Varian). A Beckman centrifuge model J2-20 was used for cell samples over 10 mL. Digital Instruments supplied the Multimode atomic force microscope with the NanoScope® IIIa controller used in this study.

The strains *Saccharomyces cerevisiae* ATCC9896, *Bacillus cereus*, *Staphylococcus aureus* ATCC6538P, *Enterobacter aerogenes* ATCC13048e and *Proteus vulgaris* ATCC6380 were obtained from Karin Pike, Department of Biology, University

of Waterloo. The strain *Escherichia coli* JM105 was obtained from Prof. G. Guillemette, Department of Chemistry, University of Waterloo.

5.2.1.1 Buffer solution

The buffer contained the following components: KH_2PO_4 (2.88 g/L), $\text{K}_2\text{HPO}_4 \cdot 3\text{H}_2\text{O}$ (5.76 g/L), trisodium citrate dihydrate (1.2 g/L), $\text{MgSO}_4 \cdot 7\text{H}_2\text{O}$ (0.48 g/L), $\text{CaCl}_2 \cdot 2\text{H}_2\text{O}$ (0.048 g/L), $(\text{NH}_4)_2\text{SO}_4$ (1.63 g/L), NH_4Cl (1.34 g/L). The buffer had a pH of 6.9.

5.2.1.2 Reagent solution

The reagent solution consisted of the previously mentioned buffer solution, in addition to 50 mM ferricyanide, 10 mM succinate, 10 mM formate and 0.1 M menadione. The reagent solution was prepared on a daily basis.

5.2.2 Methods

5.2.2.1 Detection Limit

An aliquot (5 μL) of various bacterial cell dilutions were added onto an unmodified membrane disk and mounted on the Pt working electrode. A dialysis membrane (MW cut off 6 – 8000) was used to hold the disk membrane in place and to also retain *E. coli* cells at the electrode surface. The detection limit was calculated from the chronocoulometric signals as described in Chapter 3 (Figure 3.26 and Eq. 3.5).

5.2.2.2 Lectin Immobilization

Fresh buffered lectin solutions (~200 $\mu\text{g}/\text{mL}$) were prepared prior immersion of the preactivated membranes. The membrane disks were allowed to react with the surface components of the ImmunodyABC[®] membrane for 20 min at room temperature, and stored at 4°C until usage.

5.2.2.3 Optimization

After 4 to 5 h of *E. coli* cultivation, the lectin-modified membrane disks ($A = 0.28 \text{ cm}^2$) were added to the growth medium. The cells were allowed to bind to the lectin layer for a 1 h incubation period. At this point, the membrane disks were removed and transferred into a buffered *E. coli* cell suspension and stored on ice for a minimum of 1 additional h. The membranes were then removed, washed with buffer and mounted on the Pt working electrode and immersed in the electrochemical cell. The Pt working and Ag/AgCl reference electrodes were connected and the consumed charge was measured over a 800 second period. Control measurements were also performed using glycine modified ImmunodyABC[®] membranes.

5.2.2.4 Lectin Binding Kinetics

The centrifuged (5,000 rpm) and in-buffer (containing 10 mM succinate) resuspended *E. coli* samples were stored on ice and gently rotated by an orbital shaker. At this point the lectin-modified membrane disk was added to the cell suspension and incubated on ice. Specific cell binding was allowed to take place for various periods of time. The rinsed membrane was then affixed on the working electrode surface and transferred into the reagent solution. Chronocoulometry was conducted at 37°C for 800 s.

5.2.2.5 Chronocoulometry with Modified Electrodes

Exponential phase bacteria were harvested, centrifuged at 5,000 rpm (3000 x g), resuspended in buffer containing 10 mM succinate and stored on ice. The lectin-modified membranes were added to the bacterial suspension and incubated for 100 min on ice (unless otherwise indicated). At this point, the washed membrane was affixed onto the electrode surface and immersed into the electrochemical cell containing 200 μL of the

reagent solution. Chronocoulometry was then performed using a two-electrode setting at 37°C, with a runtime of 800 s unless otherwise stated.

5.2.2.6 Agglutination Tests

Agglutination tests for all 6 microbial strains were performed in the same manner as described in Chapter 4, Section 4.2.2.2. The visible formation of a three-dimensional network of lectin and cells were used to classify binding affinities.

5.2.2.7 Atomic Force Microscopy (AFM)

A commercial AFM equipped with a 120 μm scanner (j-scanner) was located at either a liquid or dry cell setting. The laser was aligned to generate highest deflection signals, and the photodiodes were positioned to yield a centered laser signal. The probe was then affixed onto the sample holder using a double-sided adhesive, and the height of the cantilever was subsequently lowered to the probe surface. An oxide sharpened silicon nitride tip (stylus) was adjusted for its scan frequency before engaging the AFM. High-resolution imaging using the tapping mode AFM required frequencies close to 8.7 ± 0.5 kHz. Before engaging, microscope scan size and offset were set to zero to minimize sample deformation and contamination of the stylus. To engage the AFM stylus, the piezoelectric drive amplitude was set to 100 mV, resulting in a ~ 0.5 V amplitude (corresponding to ~ 16 nm with ~ 4 nm/125 mV) of the cantilever. Imaging at a low magnification of about 1 μm was performed in a liquid cell. Both the noise of the topograph and the amplitude signals were minimized by adjusting gains and scan speed. The raw data constitute the height and phase images recorded in the tapping mode. These images were converted into a graphical file (tif format) and displayed in the Windows based PhotoEditor.

5.2.2.8 Microbial Growth Conditions

All strains were cultivated under the same conditions using the same growth medium containing the following components: KH_2PO_4 (2.88 g/L), $\text{K}_2\text{HPO}_4 \cdot 3\text{H}_2\text{O}$ (5.76 g/L), tryptone (2.4 g/L), yeast extract (1.2 g/L), trisodium citrate dihydrate (1.2 g/L), $\text{MgSO}_4 \cdot 7\text{H}_2\text{O}$ (0.48 g/L), $\text{CaCl}_2 \cdot 2\text{H}_2\text{O}$ (0.048 g/L), $(\text{NH}_4)_2\text{SO}_4$ (1.63 g/L), NH_4Cl (1.34 g/L), glucose (13.2 g/L) and 240 μL of the trace element stock solution per liter of medium. The trace element stock solution was prepared in 5 N HCl (Merck) and contained the following compounds: $\text{FeSO}_4 \cdot 7\text{H}_2\text{O}$ (40 g/L), $\text{MnSO}_4 \cdot \text{H}_2\text{O}$ (10 g/L), $\text{AlCl}_3 \cdot 6\text{H}_2\text{O}$ (10 g/L), $\text{CoCl}_2 \cdot 6\text{H}_2\text{O}$ (4 g/L), $\text{ZnSO}_4 \cdot 7\text{H}_2\text{O}$ (2 g/L), $\text{Na}_2\text{MoO}_4 \cdot 2\text{H}_2\text{O}$ (10 g/L), $\text{CuCl}_2 \cdot 2\text{H}_2\text{O}$ (1 g/L) and H_3BO_3 (0.5 g/L). Glucose was prepared as a concentrated aqueous solution, sterilized separately, and added to the growth medium prior to inoculation. Cultivations were performed by adding 1 mL of 1:1 glycerol cell culture mixture (previously stored at -80°C) to 50 mL of growth medium in a shake flask. Growth proceeded for a maximum of 10 h in an incubator shaker (200 rpm, at 37°C).

5.2.2.9 Viability assay

Growth curves obtained by means of optical density at 600 nm were compared to ferricyanide reduction rates obtained by means of chronocoulometry. The strains *E. coli*, *Proteus vulgaris* and *Enterobacter aerogenes* were investigated on the basis of their ability to reduce 50 mM ferricyanide in the presence of 10 mM formate, 10 mM succinate and 0.1 mM menadione at maximum rates. Cell culture samples were chilled on ice for a minimum of 15 min prior to chronocoulometric measurements. An aliquot (20 μL) of the untreated cell sample was then injected into the electrochemical cell containing 280 μL of the reagent solution. After an incubation period of 10 min at 37°C , the accumulation of

ferrocyanide was detected by means of chronocoulometry. The potential of the Pt working electrode was stepped to + 0.5 V vs Ag/AgCl (2-electrode system) and the resulted current was then integrated over the 2 min measurement time yielding a plot of total charge vs time. The difference in total charges was measured between $t = 200$ s and $t = 800$ s, unless otherwise indicated.

5.2.2.10 Chemometric Data Analysis

Normalised chronocoulometric data obtained for each lectin-modified electrode were converted into spreadsheet format using Microsoft Excel. The data consisted of triplicate measurements on each of 6 different microorganisms was then converted into a Lotus file for incorporation into MATLAB programs. Factor analysis (PCA and mean-centring) was performed using the Chemometrics Toolbox of MATLAB (Version 2.3, The MathWorks, Natick, MA, 1998). Factor analysis in PCA involved generation of the reduced eigenvectors to determine the optimal number of factors. By starting from the highest rank (x axes) and working towards lower ranks, we chose to use 4 factors for further analysis since these contained ~ 91% of the total variance (see Table 5.15). Having decided on the optimal number of factors to use, we then generated a residual plot. The plot of residuals should only show random noise; this could only be accomplished if the number of factors was chosen correctly. Finally, PCA was performed using the optimal number of factors in order to generate score plots. These are two- or three-factor plots of the resulting PCA analysis and were used to classify sub-populations of data sets to find qualitative information in the form of groupings. The scores for factor one (PC 1) and factor two (PC 2) were exported to GraphPad Prism version 3.0 for Windows in order to plot the results.

5.3 RESULTS AND DISCUSSION

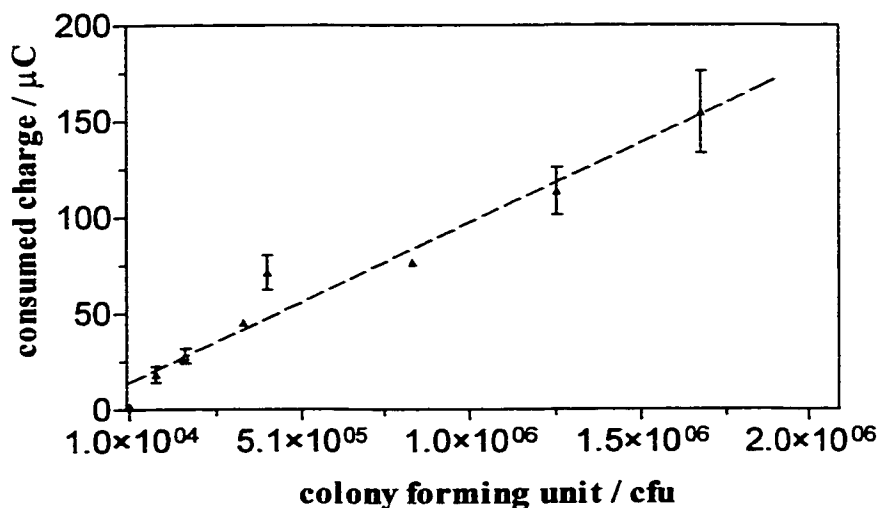
5.3.1 Optimization

Results for Chapter 4 showed that covalent coupling of the lectin Con A to the preactivated membrane ImmunodyneABC[®] yielded best results (see Table 4.19). Consequently, this immobilization method using ImmunodyneABC[®] was used for all available lectins. In Chapter 3 it was shown the addition of formate and menadione significantly increased electrochemical signals. Intracellular oxidation of formate increased the flux of electrons to the terminal oxidases of *E. coli*, while the lipid-soluble menadione increased the electron uptake rate by the ferricyanide mediator. As a result, these compounds were added to further enhance the signals for microbial ferricyanide reduction.

In a comparative study, the detection limit for the new reagent solution was investigated. An aliquot (5 μL) of various bacterial cell dilutions were added onto an unmodified membrane disk and mounted onto the Pt working electrode. A dialysis membrane (MW cut off 6 – 8000) was used to fix the membrane and retain *E. coli* cells at the electrode surface. Electrochemical signals were compared to optical density readings and converted into colony forming units using the method described in Chapter 2, Section 2.2.2.5 and Eq.2.2.

Figure 5.3 shows chronocoulometric signals plotted against colony forming units (cfu). The calculated linear regression yielded a fit (r^2) of 0.924 with a slope of $0.83 \pm 0.06 \times 10^{-4} \mu\text{C}/\text{cfu}$ and showed a Y-intercept of $13.6 \pm 5.0 \mu\text{C}$.

Figure 5.3: Consumed charges plotted against colony forming units. Chronocoulometry was performed at 37°C in a total volume of 200 μL and a runtime of 800 s.



Data obtained by means of chronocoulometry were also used to calculate the detection limit for bacterial cell numbers. Equation 3.5 described in Chapter 3 was used to estimate the minimum colony forming units needed to generate a signal in the current chronoamperometric set-up. The detection limit obtained for the new reagent solution (presence of ferricyanide, succinate, formate and menadione) yielded roughly a 30-fold decrease compared to the values obtained under similar conditions in the absence of formate and menadione (0.5×10^6 in Chapter 4).

Preliminary experiments were conducted to find the optimum lectin concentration for the immobilization procedure. Here, the model lectin Concanavalin A was allowed to form covalent bonds with the preactivated membranes for 20 min room temperature and the membranes were stored over night at 4°C. After a 1 h incubation period in a buffered *E. coli* JM105 suspension, the rinsed membrane was affixed to the electrode surface and

introduced into the electrochemical cell containing 200 μL of reagent solution. After a chronocoulometric measurement period of 10 min, the charge differences occurring during the last minute ($t_{600 \text{ sec}} - t_{540 \text{ sec}}$) were calculated. Table 5.2 shows the chronocoulometric results obtained for varying Concanavalin A concentrations.

Table 5.2: Consumed charges obtained for exponential phase grown *E. coli* JM105 after capture on Con A modified BiodyneA[®] ($A = 0.28 \text{ cm}^2$). Chronocoulometry was performed in 200 μL for 10 min at 37°C with a runtime of 600 s.

Con A concentration, $\mu\text{g/mL}$	Consumed charges, * $\mu\text{C/min}$
500	2.6 ± 0.4
300	3.8 ± 0.1
100	3.5 ± 0.1
50	0.7 ± 0.1

* Average of two background subtracted values

Results obtained in this experiment showed highest obtained signals when 300 $\mu\text{g/mL}$ Concanavalin A was used for immobilization. For this reason the concentration for all lectins was kept at about this same level.

In an attempt to further increase chronocoulometric signals a pre-capture step was introduced during the cultivation period. Until this point, *E. coli* were harvested, centrifuged and resuspended in buffer, and stored on ice prior to exposure to the modified membrane. Bacterial cells were also captured on the lectin layer during cultivation for 1 h, followed by a 1 h exposure period to a cell sample containing the membranes on ice. In this study seven different lectins were examined and results obtained for individual experiments are listed in Table 5.3.

Table 5.3: Signals obtained for *E. coli* JM105 after cell captured on lectin modified membranes during cell cultivation and storage on ice. Chronocoulometry was performed in 200 μ L at 37°C.

Name	Concentration [‡]	Consumed charge,* μ C	OD ₆₀₀ at sampling
Concanavalin A	300 μ g/mL	10.3 \pm 3.6	3.0
<i>Solanum tuberosum</i>	430 μ g/mL	6.7 \pm 1.8	
Glycine	0.1 M	4.5 \pm 2.7	
<i>Helix pomatia</i>	280 μ g/mL	4.7 \pm 0.6	2.6
<i>Perseu americana</i>	340 μ g/mL	-	
Glycine	0.1 M	3.4 \pm 0.7	
<i>Codium fragile</i>	325 μ g/ml	1.4 \pm 0.6	2.8
Glycine	0.1 M	1.5 \pm 2.0	
<i>Phytolacca americana</i>	400 μ g/mL	0.8 \pm 0.1	2.6
<i>Artocarpus integrifolia</i>	200 μ g/mL	2.8 \pm 0.2	
Glycine	0.1 M	20.3 \pm 5.9	
Conacanvalin A	350 μ g/mL	2.2 \pm 0.7	2.4
<i>Solanum tuberosum</i>	450 μ g/mL	1.9 \pm 1.4	
Glycine	0.1 M	53.5 \pm 38.3	

*Average of three replicate measurements

‡conc. During lectin immobilization step

It is well known that lectins preferentially bind to oligosaccharides, but they will also bind to monosaccharides,²⁰ both of which may be present in bacterial cultures. We observed different signals for various lectins, suggesting that selective cell binding took place. This makes the application of lectins as recognition agent a feasible tool in a sensor array setting. However, the poor reproducibility of these findings led us to omit the initial

cell-capture step in the culture medium for all further experiments; it is possible that free monosaccharides (e.g. glucose) interfere with cell-lectin binding.

In this study we also investigated the application of glycine modified membranes, which were tested as a potential control measurement. Glycine, a non-polar amino acid, can not be utilized by bacterial cells as a food source and should prevent nonspecific adhesion of *E. coli* cells. The latter experiments listed in Table 5.4 showed that glycine modified membranes yielded unusually high values with a high degree of imprecision. Consequently, glycine modified membranes were not used for control measurements in further experiments.

5.3.2 Lectin Binding Kinetics

The number of lectin molecules that selectively capture bacteria must be related to the time allowed for cell capture. In a comparative study, the effects of capture time on *E. coli* binding were investigated. Here, 11 lectins and BSA were immobilized onto ImmunodyABC[®] membrane disks and incubated with buffered *E. coli* cell suspension for extended periods of time. Results obtained for all 12 individual experiments are shown below, where lectin concentrations, optical densities, capture times and consumed charges are listed.

Chronocoulometric signals obtained after increasing cell capture time are shown in Tables 5.4 to 5.7.

Table 5.4: Chronocoulometric signals vs cell capture time of *A. hypogaea* (300 $\mu\text{g/mL}$), *C. fragile* (200 $\mu\text{g/ml}$) and Con A (400 $\mu\text{g/mL}$) modified ImmunodyABC[®] membranes and exp. phase *E. coli* JM105 (OD₆₀₀ = 2.0).

Capture time min	Consumed charges,* μC		
	Con A	<i>Arachis hypogaea</i>	<i>Codium fragile</i>
60	18.2		
80		4.0	
100			65.0
120	58.8		
140		39.6	
160			267.2
180	165.3		
200		44.7	
220			53.4

* Values are background subtracted

Table 5.5: Chronocoulometric signals vs cell capture time of *A. integrifolia* (200 $\mu\text{g/mL}$), *S. tuberosum* (350 $\mu\text{g/ml}$) and *L. culinaris* (250 $\mu\text{g/mL}$) modified ImmunodyABC[®] membranes and exp. phase *E. coli* JM105 (OD₆₀₀ = 2.7).

Capture time min	Consumed charges,* μC		
	<i>Artocarpus integrifolia</i>	<i>Solanum tuberosum</i>	<i>Lens culinaris</i>
60	116.2		
80		35.8	
100			61.8
120	71.3		
140		67.6	
160			97.7
180	62.8		
200		106.9	
220			153.1

* Values are background subtracted

Table 5.6: Chronocoulometric signals vs cell capture time of *T. vulgaris* (200 $\mu\text{g/mL}$), *H. pomatia* (230 $\mu\text{g/mL}$) and *G. nivalis* (400 $\mu\text{g/mL}$) modified ImmunodyABC[®] membranes and exp. phase *E. coli* JM105 (OD₆₀₀ = 1.6).

Capture time min	Consumed charges,* μC		
	<i>Triticum vulgaris</i>	<i>Helix pomatia</i>	<i>Galanthus nivalis</i>
60	23.4		
80		37.4	4.3
100	76.4		
120		167.4	3.6
140	59.6		
160		81.7	27.4
180	92.6		
200		65.6	

* Values are background subtracted

Table 5.7: Chronocoulometric signals vs cell capture time of *P. americana* (250 $\mu\text{g/mL}$) and BSA (200 $\mu\text{g/mL}$) modified ImmunodyABC[®] membranes and exp. phase *E. coli* JM105 (OD₆₀₀ = 2.5).

Capture time min	Consumed charges,* μC		
	Buffer	BSA	<i>Phytolacca americana</i>
60	43.1	29.1	10.7
80			
100	38.7		0.0
120		77.8	
140	42.6		22.3
160			
180	20.9		
200			
220		126.0	

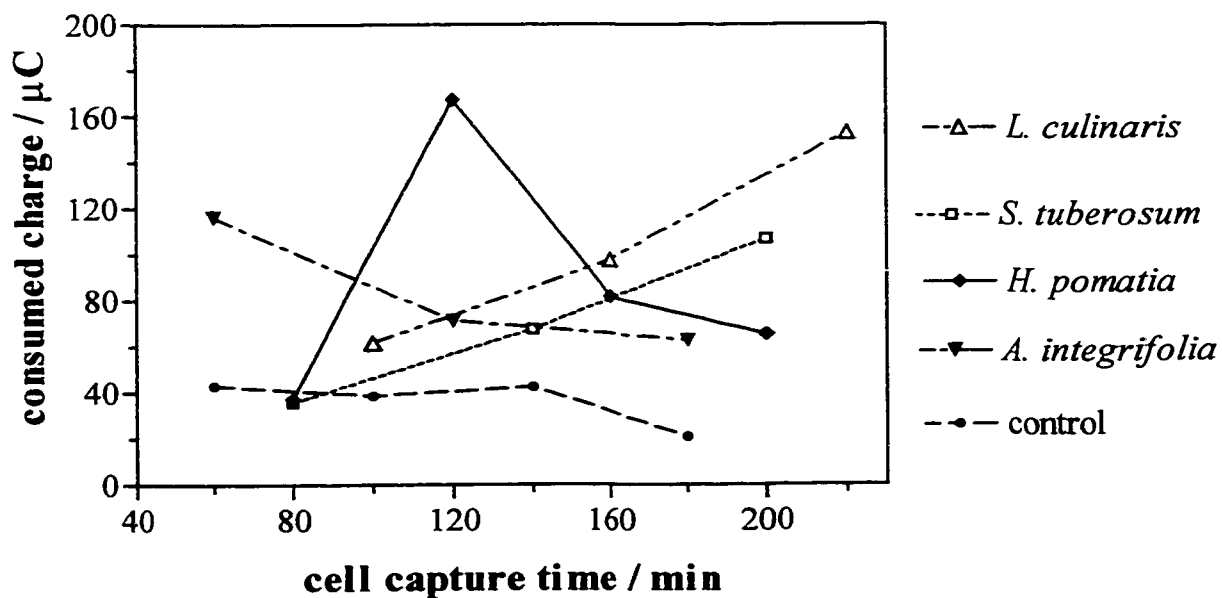
* Values are background subtracted

Results of these experiments show clearly that different capture times yield different chronocoulometric signals. Sixty minutes represents the minimum capture time needed to obtain signals over $10 \mu\text{C}$. The long capture times may be attributed to the low temperature (0°C) used during cell capture, which may have influenced binding dynamics. The applied temperature of 0°C was used to keep changes to the cooled and growth-arrested cell suspension to a minimum, thus allowing a variety of measurements to be conducted under similar sample conditions.

Results in Tables 5.4-5.7 show that each lectin exhibited its own time-dependent binding kinetics. Furthermore, we found five trends in lectin-cell binding, although no trend was seen in control experiments (lacking modification). Linear increasing binding dynamics were seen when using the lectins Concanavalin A, *Solanum tuberosum*, *Lens culinaris* as well as BSA. Meanwhile the lectins *Arachis hypogaea*, *Galanthus nivalis* and *Phytolacca americana* exhibited a non-linear increase over time. Three lectins (*Helix pomatia*, *Triticum vulgare* and *Codium fragile*) showed distinct peaks in their time traces, whereas *Artocarpus integrifolia* yielded a constant decline over time.

Figure 5.4 shows plots of chronocoulometric measurements performed using five modified working electrodes. These five curves are representative of all the lectins tested, and show varying binding dynamics. Although no correlation between lectin selectivity and their capture times were found, the shapes of these curves clearly illustrate the time dependence of cell binding to lectins. Furthermore, chronocoulometric results suggest that measurements performed after cell binding at 0°C should be conducted after a minimum incubation time of 60 min.

Figure 5.4: Chronocoulometric signals as a function of cell capture time obtained for *E. coli* JM105 that were captured over extended time periods on lectin modified ImmunodyABC[®] membrane disks at 0°C. Chronocoulometry was performed at 37°C and a runtime of 800 s.



Agglutination test results were compared to the electrochemical results to determine whether known lectin sugar-specificities correlate with chronocoulometric signals found for *E. coli* captured by these same lectins. Lectin specificities to bacterial cells were obtained through agglutination tests and are expressed either as high (+++), medium (++), low (+) or no (-) cell agglutination, in Table 5.8.

A numerical approach was used in an attempt to normalize data obtained by chronocoulometry using different cell capture times, examples of which are shown in Figure 5.4. The areas under these curves were determined for each lectin, and these values ($\mu\text{C}\cdot\text{min}$) were divided by the range of cell capture times studied (min). This calculation takes the differing curve shapes into account. These values were further normalized for BDM because cultures with differing OD_{600} values were used as show in Equation 5.2.

$$\text{Chronocoulometric signal} = \frac{\text{area}}{\text{width}} \div \text{BDM} \quad 2.1$$

where:

area	integrated vaules over time, ($\mu\text{C}\cdot\text{min}$)
width	cell capture time over integration occurred (min)
BDM	biological dry matter, g/L

Table 5.8 shows the results of this comparative study, where sugar specificity, *E. coli* specificity and agglutination tests are listed. This table shows that with the exception of BSA, calculated CC signals that exhibit numeric values above 20 correspond to lectins that were found to agglutinate *E. coli* cells. The qualitatively similarity of the results obtained by the two methods suggests that a numerical representation of cell selectivity is possible, since all CC signals lower than ~ 10 occurred with lectins that caused no visible cell agglutination in control experiments.

Table 5.8: Comparison of lectin-*E. coli* binding from data that were obtained through cell agglutination tests and chronocoulometry after cell capture.

Name	Sugar Specificity	BDM g/L	Area / width	CC Signal ($\mu\text{C}\cdot\text{L}/\text{g}$)	Cell agglutinin
Buffer	-	3.24	34.6	10.7	-
BSA	-	3.24	96.2	29.7	-
Con A	α -man, α -glc	2.58	75.3	29.2	++
<i>A. hypogaea</i>	β -gal(1-3), galNAc	2.58	31.9	12.4	-
<i>C. fragile</i>	(galNAc)	2.58	163.2	63.3	+
<i>A. integrifolia</i>	α -gal	3.45	80.4	23.3	+
<i>S. tuberosum</i>	(glcNAc) ₃	3.45	69.5	20.1	+
<i>L. culinaris</i>	α -man	3.45	102.6	29.7	+
<i>P. americana</i>	(glcNAc) ₃	2.09	5.5	2.6	-
<i>G. nivalis</i>	non-red. α -man	2.09	9.7	4.6	-
<i>T. vulgaris</i>	(glcNAc) ₂ , NeuNAc	2.01	64.7	32.2	++
<i>H. pomatia</i>	galNAc	2.01	100.2	49.9	+

The known lectin-sugar specificities were then compared with CC signals and agglutination test results. Only lectins that exhibited binding affinities to α -mannose, α -glucose and (glcNAc)₃/NeuNAc were able to agglutinate *E. coli* cells. These results correspond very well to CC signals that have a numerical value over 20. The correlation is not perfect, however since unusually high numbers were found for *Codium fragile* and *Helix pomatia*. Both lectins are specific to galNAc and exhibited only low cell agglutination after 5 h. The high CC signal values are a result of the mathematical approach, since both lectins showed a distinct peak in their time-dependent binding kinetics, and thus yielded a high area value. Reasons for this behavior are unknown and need further investigation.

Although a relationship between agglutination tests results, sugar specificities and the obtained CC signals exist, it does not appear to be a quantitative correlation. Covalent linkage of proteins may introduce changes to the ternary or quaternary structure capable of producing different binding constants; immobilization may also limit accessibility of active sites. This approach to the determination of binding affinities and immobilization-induced changes may still be feasible but it will have to be a subject for further investigation.

5.3.3 Atomic Force Microscopy (AFM)

AFM was used to investigate the ImmunodyneABC[®] membrane surface before and after covalent modification with Con A. Figure 5.5 shows the image of an air-dried ImmunodyneABC[®] membrane obtained using a tapping mode operated AFM. The image, with a scan size of $5 \times 5 \mu\text{m}$, reveals the complexity of this membrane. Multiple features with differences in height of about $5 \mu\text{m}$ were found, suggesting a high degree of roughness on the surface; pores were also identified. Figure 5.6 shows a smaller area ($1 \times 1 \mu\text{m}$) of the ImmunodyneABC[®] membrane that was obtained using a liquid cell after the membrane was spotted with buffer in order to simulate solution conditions. Although AFM is capable of near atomic scale resolution (on flat surfaces only), we found that clear images of the ImmunodyneABC[®] membrane could only be attained for scan areas of $1 \mu\text{m}^2$. The extreme degree of surface roughness on this membrane made it impossible to obtain clear images for scan sizes less than $1 \mu\text{m}^2$.

Figures 5.7 and 5.8 show the phase images of an ImmunodyneABC[®] membranes in the presence and absence of Con A.

Figure 5.5: AFM image of ImmunodyneABC[®] membrane obtained with tapping mode in a dry cell. A drive frequency of 8,74 kHz was used to scan an area of 5 x 5 μm with scan rate of 2.1 Hz and data scale of 5 μm .

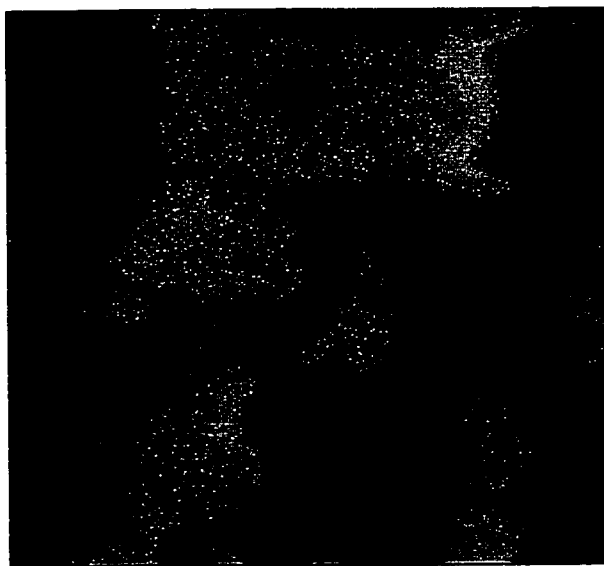


Figure 5.6: AFM image of ImmunodyneABC[®] membrane obtained with tapping mode in a liquid cell setting. A drive frequency of 8,74 kHz was used to scan an area of 1 x 1 μm with scan rate of 1.0 Hz and data scale of 1 μm .

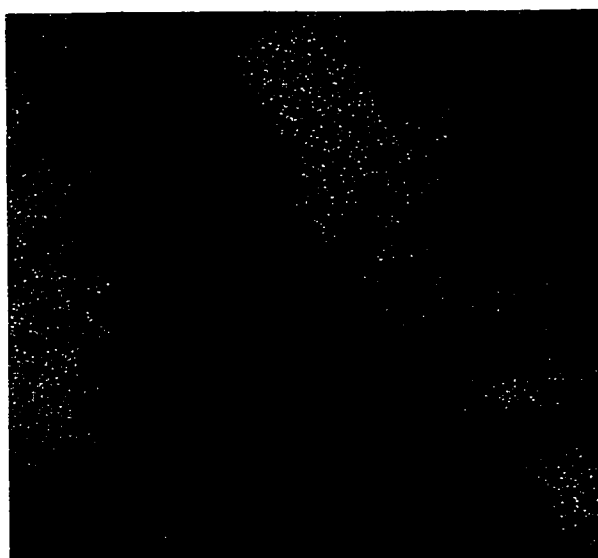


Figure 5.7: Phase image of ImmunodyneABC[®] membrane obtained using tapping mode and a liquid cell setting. A drive frequency of 8,74 kHz was used to scan an area of 1 x 1 μm with scan rate of 1.0 Hz and data scale of 30 degrees.

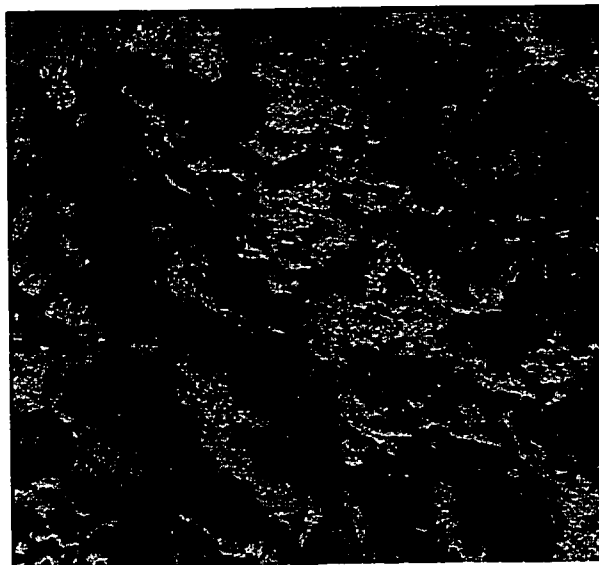
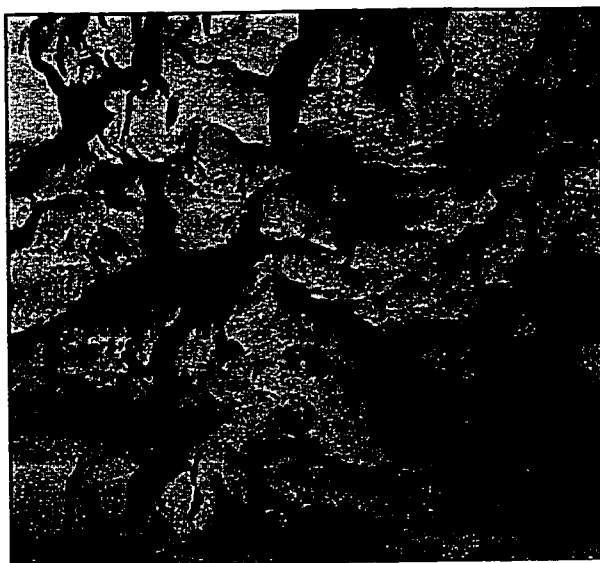


Figure 5.8: Phase image of Con A modified ImmunodyneABC[®] membrane obtained using tapping mode and a liquid cell. A drive frequency of 8,74 kHz was used to scan an area of 1 x 1 μm with scan rate of 1.0 Hz and data scale of 30 degrees.



ImmunodyneABC[®] surfaces were investigated before and after lectin immobilization, to obtain information about the extent of lectin modification. Phase mode images were obtained before and after Con A immobilization. Figure 5.7 shows the phase image of an unmodified ImmunodyneABC[®] membrane obtained using the tapping mode in a liquid cell. Once again, the image displays high surface roughness with features similar to those seen in the height image in Figure 5.6. Figure 5.8 displays the phase image of the lectin-modified ImmunodyneABC[®] membrane that was obtained under the same conditions. No clustering or other features could be distinguished; the homogeneity that was observed in this image suggests the presence of a uniform lectin layer. Nevertheless, with the relatively large scan size of 1 μm^2 we were unable to determine the molecular-level properties of lectin proteins at the surface.

5.3.4 Chronocoulometry with the Biosensor Array

Five bacterial strains and yeast, grown under identical conditions, were now subjected to an electrochemical investigation after cell binding to the membrane-immobilized recognition agent had taken place. The accumulation of ferrocyanide at the sensing layer was detected by means of chronocoulometry with a measurement time of 800 s.

Chronocoulometric results were obtained throughout growth of *E. coli* in order to find conditions with highest reduction activity. Figure 5.9 shows the growth curve of *E. coli* obtained in relation to the ability to reduce ferricyanide.

Figure 5.9: Growth curve for *E. coli* JM105 obtained by (a) optical density at 600 nm, and (b) chronocoulometric assay (n = 2) after 10 min incubation in 50 mM ferricyanide, 10 mM succinate, 10 mM formate and 0.1 mM menadione.

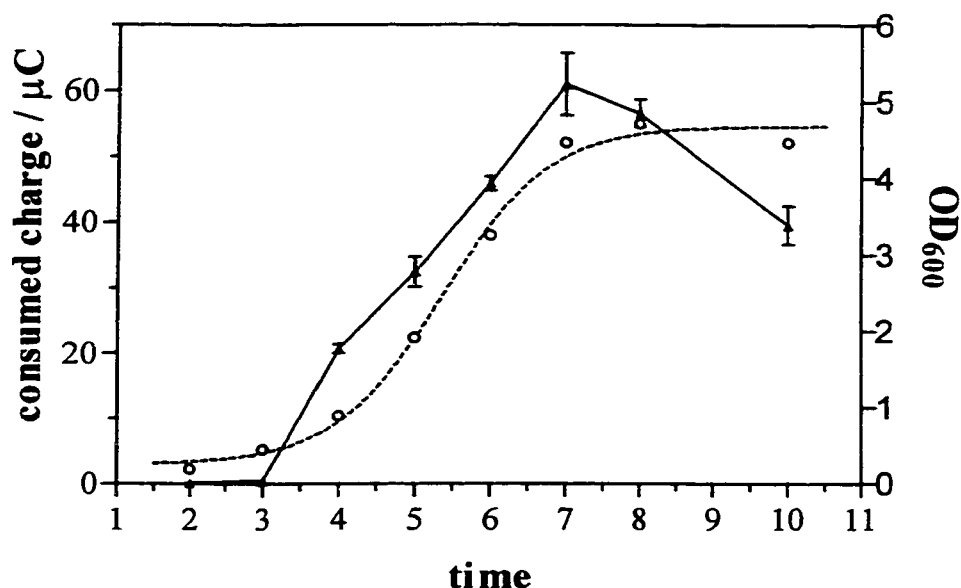


Figure 5.9 shows that maximal chronocoulometric signals for *E. coli* JM105 occurred when cell cultures exhibit an OD₆₀₀ ranging from 4.0 to 5.0 or after periods of incubation ranging between 6-7 hours. Under these conditions, harvested cells were centrifuged (5000 rpm for 5 min), resuspended in buffer (containing succinate) and stored on ice. Lectin modified membranes were then added and cells were allowed to bind to the membrane surface for a total period of 100 min prior to taking chronocoulometric measurements. Results obtained for individual experiments are compared to agglutination results and to known binding specificities in Table 5.9. Again, chronocoulometric results correlate with agglutination test results. Lectins specific for α -man, α -glc, glcNAc yielded highest chronocoulometric traces and showed a good ability to agglutinate *E. coli*.

In addition, *E. coli* binding to BSA modified ImmunodyneABC[®] membrane resulted in highest chronocoulometric signals.

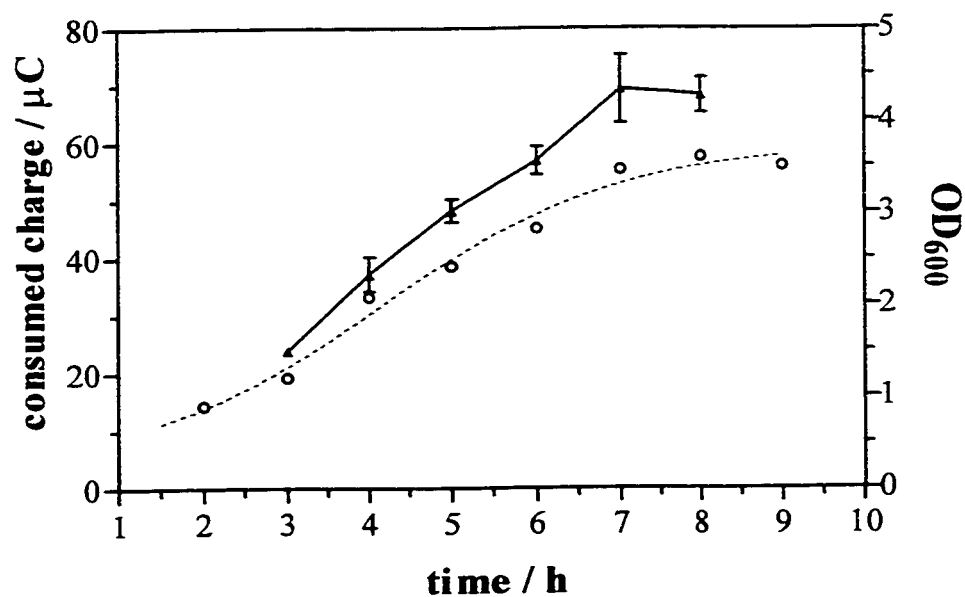
Table 5.9: Chronocoulometric and agglutination results obtained for *E. coli* JM105 in the presence of different lectins. Agglutination was allowed to take place over 6 h at room temperature; these are the results of the experiment shown in also in Table 5.8

Name	Conc. $\mu\text{g/mL}$	Consumed charges, *			Sugar Specificity	Agglut.
		μC				
Con A	300	33	30	31	α -man, α -glc	++
<i>S. tuberosum</i>	240	16	13	15	(glcNAc) ₃	+
<i>L. culinaris</i>	166	29	46	25	α -man	+
<i>A. integrifolia</i>	175	32	13	8	α -gal	+
<i>H. pomatia</i>	100	25	13	19	galNAc	+
<i>T. vulgaris</i>	350	52	32	42	(glcNAc) ₃ , NeuNAc	++
<i>A. hypogaea</i>	275	19	12	15	β -gal, galNAc	-
<i>C. fragile</i>	200	27	14	20	galNAc	+
<i>P. americana</i>	100	32	26	26	(glcNAc) ₃	-
<i>G. nivalis</i>	220	15	19	11	non-red. α -man	-
Control	-	77	8	74	-	-
BSA	300	138	271	18	-	-

*Chronocoulometric values are background subtracted

In an initial experiment, the bacterial growth curve and the reduction behaviour of *Enterobacter aerogenes* was determined in order to find optimum harvest conditions. Figure 5.10 shows results obtained by chronocoulometry and optical density readings at 600 nm.

Figure 5.10: Growth curve for *Enterobacter aerogenes* ATCC 13048e obtained by (a) optical density at 600 nm, and (b) chronocoulometric assay (n = 2) after 10 min incubation in 50 mM ferricyanide with 10 mM succinate, 10 mM formate and 0.1 mM menadione.



Further chronocoulometric measurements using *Enterobacter aerogenes* ATCC13048e were performed after cell cultures were harvested in their exponential phase with an OD₆₀₀ ranging from 3.0 to 4.0 or after the cells were cultivated for a period of 6-7 h. The centrifuged and resuspended cells were stored on ice. Lectin modified membranes were added and cells were allowed to bind to the membrane surface for a total period of 100 min prior to taking chronocoulometric measurements. Results obtained for individual experiments were compared to agglutination results and to known binding specificities. Results are listed in Table 5.10.

Table 5.10: Chronocoulometric and agglutination results obtained for *Enterobacter aerogenes* ATCC13048e in the presence of different lectins. Agglutination was allowed to take place over 6 h at room temperature.

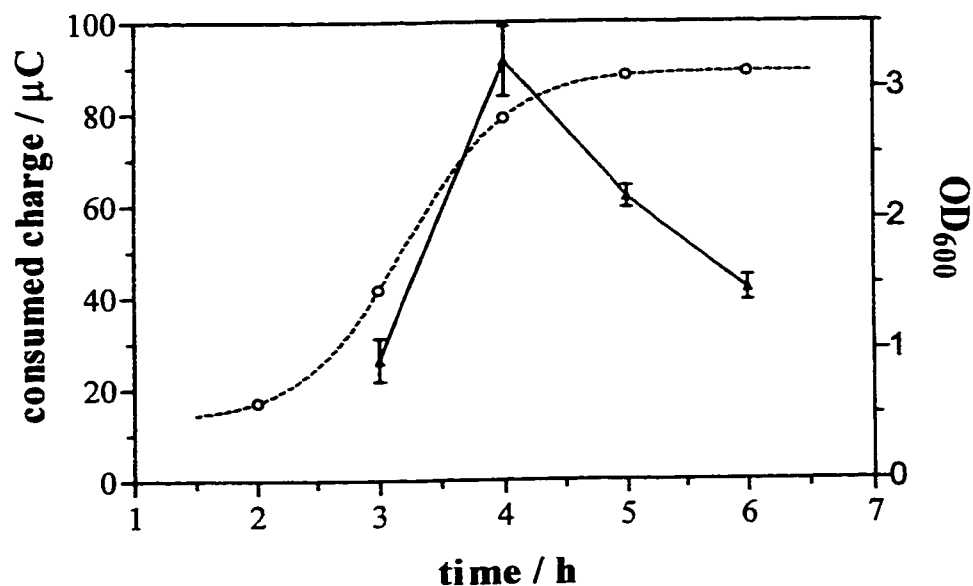
Name	Conc. $\mu\text{g/mL}$	Consumed charges, *			Sugar Specificity	Agglut.
		μC	μC	μC		
Con A	300	188	109	101	$\alpha\text{-man,}\alpha\text{-glc}$	-
<i>S. tuberosum</i>	200	34	37	36	(glcNAc) ₃	+++
<i>L. culinaris</i>	300	139	151	106	$\alpha\text{-man}$	+++
<i>A. integrifolia</i>	300	116	144	223	$\alpha\text{-gal}$	++
<i>H. pomatia</i>	200	139	176	159	galNAc	++
<i>T. vulgaris</i>	230	116	230	173	(glcNAc) ₃ , NeuNAc	+
<i>A. hypogaea</i>	330	160	113	104	$\beta\text{-gal, galNAc}$	+++
<i>C. fragile</i>	230	77	61	110	galNAc	+++
<i>P. americana</i>	160	92	157	125	(glcNAc) ₃	+++
<i>G. nivalis</i>	230	44	159	83	non-red. $\alpha\text{-man}$	+++
Control	-	116	133	143	-	-
BSA	230	35	35	35	-	-

*Chronocoulometric values are background subtracted

Highest chronocoulometric signals were found for modified membranes carrying lectins specific for galNAc, $\beta\text{-gal/galNAc}$, (glcNAc)₃ and $\alpha\text{-man}$. Additionally, agglutination tests showed that lectins specific for galNAc, $\beta\text{-gal/galNAc}$, (glcNAc)₃ and non-red. $\alpha\text{-man}$ have the ability to agglutinate *E. aerogenes*.

In initial experiments, the bacterial growth curve and the reduction behaviour of *Proteus vulgaris* was determined in order in order to find optimum harvest conditions. Figure 5.11 shows these results for *Proteus vulgaris* performed by means of chronocoulometry and by means of optical density readings at 600 nm.

Figure 5.11: Growth curve for *Proteus vulgaris* ATCC6380 obtained by (a) optical density at 600 nm, and (b) chronocoulometric assay (n = 2) after 10 min incubation in 50 mM ferricyanide with 10 mM succinate, 10 mM formate and 0.1 mM menadione.



Highest reduction rates ($\sim 90 \mu\text{C}$) were found after a 4 h cultivation period and thus all following chronocoulometric measurements were performed with cell cultures with an OD₆₀₀ of 2.0 to 3.0. Results obtained for individual experiments are then compared to agglutination results and to known binding specificities in Table 5.11.

We found highest chronocoulometric signals were found with membranes modified with lectins specific for (glcNAc)₃/NeuNAc, galNAc, α -gal and (glcNAc)₃. Furthermore, agglutination results showed that lectins specific for α -gal, galNAc and (glcNAc)₃/NeuNAc have the highest ability to agglutinate *P. vulgaris*.

Table 5.11: Chronocoulometric and agglutination results obtained for *Proteus vulgaris* ATCC6380 in the presence of different lectins. Agglutination was allowed to take place over 6 h at room temperature.

Name	Conc. $\mu\text{g/mL}$	Consumed charges, *			Sugar Specificity	Agglut.
		μC				
Con A	267	203	124	148	α -man, α -glc	++
<i>S. tuberosum</i>	200	213	95	204	(glcNAc) ₃	-
<i>L. culinaris</i>	200	182	253	163	α -man	++
<i>A. integrifolia</i>	300	210	257	102	α -gal	+++
<i>H. pomatia</i>	260	132	49	65	galNAc	+++
<i>T. vulgaris</i>	200	68	46	57	(glcNAc) ₃ , NeuNAc	-
<i>A. hypogaea</i>	200	209	118	310	β -gal, galNAc	++
<i>C. fragile</i>	260	268	389	253	galNAc	-
<i>P. americana</i>	200	177	196	105	(glcNAc) ₃	++
<i>G. nivalis</i>	166	128	237	197	non-red. α -man	+
Control	-	172	113	110	-	-
BSA	320	243	66	122	-	-

*Chronocoulometric values are background subtracted

B. cereus cultivated in shake flasks yielded an optical density (at 600 nm) of ~ 3.5 after incubating for 5 h. At this point, a cell sample was harvested, centrifuged and resuspended in buffer containing 10 mM succinate and was subsequently stored on ice. Lectin modified membranes were added and cells were allowed to bind to the membrane surface for a total period of 100 min prior to taking chronocoulometric measurements. Results obtained for individual experiments were compared to agglutination results and known binding specificities in Table 5.12.

Table 5.12: Chronocoulometric and agglutination results obtained for *Bacillus cereus* in the presence of different lectins. Agglutination was allowed to take place over 6 h at room temperature.

Name	Conc. $\mu\text{g/mL}$	Consumed charges, *			Sugar Specificity	Agglut.
		μC				
Con A	230	0	0	0	α -man, α -glc	-
<i>S. tuberosum</i>	270	0	0	0	(glcNAc) ₃	-
<i>L. culinaris</i>	200	16	23	18	α -man	-
<i>A. integrifolia</i>	1160	40	73	23	α -gal	+
<i>H. pomatia</i>	130	17	0	20	galNAc	+
<i>T. vulgaris</i>	160	6	1	2	(glcNAc) ₃ , NeuNAc	-
<i>A. hypogaea</i>	230	23	52	38	β -gal, galNAc	+
<i>C. fragile</i>	200	16	37	20	galNAc	+
<i>P. americana</i>	160	0	1	0	(glcNAc) ₃	-
<i>G. nivalis</i>	200	11	8	3	non-red. α -man	-
Control	-	16	16	10	-	-
BSA	200	8	18	15	-	-

*Chronocoulometric values are background subtracted

Results observed by means of chronocoulometry show that highest signals were obtained when using lectin modified membranes specific for α -gal, β -gal/galNAc and galNAc. Similar results were observed for agglutination tests. Low agglutination results were observed for lectins specific for α -gal, galNAc and β -gal/galNAc.

Cell cultures of *Staphylococcus aureus* harvested after a 5 h incubation period showed an optical density measured at 600 nm of ~ 2.0 . Chronocoulometric and agglutination results obtained for all lectins are shown in Table 5.13.

Table 5.13: Chronocoulometric and agglutination results obtained for *Staphylococcus aureus* ATCC6538P in the presence of different lectins. Agglutination was allowed to take place over 6 h at room temperature.

Name	Conc. $\mu\text{g/mL}$	Consumed charges, *			Sugar Specificity	Agglut.
		μC				
Con A	200	139	248	193	α -man, α -glc	++
<i>S. tuberosum</i>	260	151	69	177	(glcNAc) ₃	+
<i>L. culinaris</i>	200	72	98	102	α -man	+
<i>A. integrifolia</i>	160	35	97	86	α -gal	+
<i>H. pomatia</i>	430	128	130	143	galNAc	++
<i>T. vulgaris</i>	360	100	113	120	(glcNAc) ₃ , NeuNAc	+
<i>A. hypogaea</i>	230	193	169	140	β -gal, galNAc	+++
<i>C. fragile</i>	200	58	198	130	galNAc	++
<i>P. americana</i>	200	187	239	213	(glcNAc) ₃	+++
<i>G. nivalis</i>	260	144	114	140	non-red. α -man	++
Control	-	144	131	105	-	-
BSA	260	118	100	135	-	+

*Chronocoulometric values are background subtracted

Results obtained by chronocoulometric means were highest when membranes modified with lectins specific for α -man/ α -glc, (glcNAc)₃, galNAc/ β -gal, galNAc and α -man were used. Agglutination tests showed highest levels of agglutination when using lectins specific for galNAc/ β -gal, (glcNAc)₃, galNAc and α -man/ α -glc.

Overnight cell cultures of *Saccharomyces cerevisiae* ATCC9896 yielded an optical density at 600 nm of ~ 3.5. Chronocoulometric and agglutination results obtained using all lectins are shown in Table 5.14.

Table 5.14: Chronocoulometric and agglutination results obtained for *Saccharomyces cerevisiae* ATCC9896 in the presence of different lectins. Agglutination was allowed to take place over 6 h at room temperature.

Name	Conc. $\mu\text{g/mL}$	Consumed charges, *			Sugar Specificity	Agglut.
		μC	μC	μC		
Con A	300	6	3	0	α -man, α -glc	-
<i>S. tuberosum</i>	200	5	4	0	(glcNAc) ₃	+
<i>L. culinaris</i>	300	0	0	0	α -man	-
<i>A. integrifolia</i>	200	3	0	0	α -gal	-
<i>H. pomatia</i>	200	19	9	7	galNAc	+
<i>T. vulgaris</i>	230	27	4	0	(glcNAc) ₃ , NeuNAc	+
<i>A. hypogaea</i>	330	0	2	1	β -gal, galNAc	-
<i>C. fragile</i>	230	3	0	6	galNAc	+
<i>P. americana</i>	160	44	0	0	(glcNAc) ₃	+
<i>G. nivalis</i>	230	58	16	11	non-red. α -man	+
Control		0	0	0	-	-
BSA	230	0	3	2	-	+

*Chronocoulometric values are background subtracted

Better chronocoulometry results were found when membranes were modified with lectins specific for non-reducing α -man, (glcNAc)₃, (glcNAc)₃/NeuNAc and galNAc. A similar behaviour was observed in agglutination tests performed using lectins specific for (glcNAc)₃, (glcNAc)₃/NeuNAc and galNAc.

Overall, with these six organisms, general agreement was observed between chronocoulometric and agglutination test results. Larger chronocoulometric signals were observed for lectins that also cause agglutination in cell suspensions. Occasional non-correspondence of results from the two methods may be attributed to changes that may occur upon covalent immobilization of the lectins onto the ImmunodyneABC[®] membranes.

5.3.5 Microbial Identification *via* Pattern Recognition

Differences in binding affinities and resulting chronocoulometric signals from previous experiments were now used to distinguish and identify these microbial strains. These binding affinities yielded a signal pattern characteristic for each strain. Chemometric pattern recognition analysis was used to scientifically assess the sum of all experimental data obtained.

The goal of pattern recognition is to identify samples by analyzing the amount of variation present. After generating the principal components in PCA, a qualitative analysis of the samples was possible by creating pattern recognition plots. The multidimensional data matrix was presented as a two-dimensional or three-dimensional plot, with the axes corresponding to the three factors containing the majority of the variance, PC 1, PC 2 and PC 3. In pattern recognition, scores were computed from factor analysis for the principal components and then plotted against each other. Numerical similarities between samples across a single row, relates by definition, to the samples' chemical similarities. The closer the points are to each other, the more chemical similarities there are. The distance between points is commonly measured as the Euclidean distance, which is defined as the distance between two points in three-dimensional space. There is no actual physical or chemical meaning to the distance, except as a measure of similarity, as defined by the human observer. The similar points are then assigned class membership; a class is defined as a collection of similar points.²⁵

Six types of microbial strains were examined using lectin modified electrodes that generated 36 chronocoulometric results (triplicates) for each strain. Therefore, the data matrix consisted of 12 x 18 vectors or 216 values. By using MATLAB for factor analysis,

we generated the Eigenvectors thus producing Eigenvalues, which were further reduced to determine the optimum number of factors as outlined in the experimental section. Table 5.15 lists the computed reduced Eigenvalues and their associated variances.

Table 5.15: Reduced Eigenvalues, their rank and content of variance found in the data matrix.

Number of factors (rank)	Reduced Eigenvalues	%-variance
1	1.05×10^4	76.3
2	7.67×10^2	5.6
3	7.53×10^2	5.5
4	5.10×10^2	3.7
5	3.11×10^2	2.3
6	3.10×10^2	2.3
7	1.92×10^2	1.4
8	1.23×10^2	0.9
9	1.32×10^2	0.9
10	8.99×10^1	0.7
11	3.09×10^1	0.2
12	2.92×10^1	0.2

Table 5.16 shows that the factor number one contains 76% of the found variances within the data matrix, whereas factor two and three account for only ~ 6% of the total variances. In other words almost 90% of all information about the pattern can be found in the first 3 factors.

This is important because in a qualitative pattern recognition plot only two or sometimes three factors, which account for the majority of variances, are actually plotted. A pattern recognition plot for the six strains was generated from the results obtained from

all triplicate measurements (Results are shown in Figure 5.12). In the scores plot each point represents 12 chronocoulometric experiments (10 different lectins, BSA and control) made for each strain; groupings of individual strains were identified and circled.

From these results it is evident that all six microbial strains form sub-populations that can be distinguished from one another. Variances between microbial strains appear to be high enough for them to be distinguished, while at the same time individual strains are similar enough to cluster together. Mean centering of raw data is one method of pretreatment that is often used prior to principal component analysis. This data set adjustment centers the origin of the coordinate system. From a statistical point of view, centering prevents data points located far away from the point of origin to undermine data points elsewhere on the center. Unfortunately, centering data ultimately leads to the loss of information about the origin of the factor space, which may incorporate information about the relative magnitudes of the Eigenvalues and the relative errors.²⁶ Nevertheless, principal component analysis was performed for a mean-centered data matrix. Figure 5.13 shows the generated score plots for the mean-centered data matrix. Results are very similar to those shown in Figure 5.12 and indicated that mean centering is capable of displaying groupings and thus capable of distinguish between strains.

Variances listed in Table 5.16 showed that factors two and three revealed similar information. For that reason we generated a pattern recognition plot that plotted the first three principle components against each other. Here we investigated the influence of the third principle component on the generated pattern.

Figure 5.12: Pattern recognition plot obtained from the data matrix containing the results of all chronocoulometric experiments.

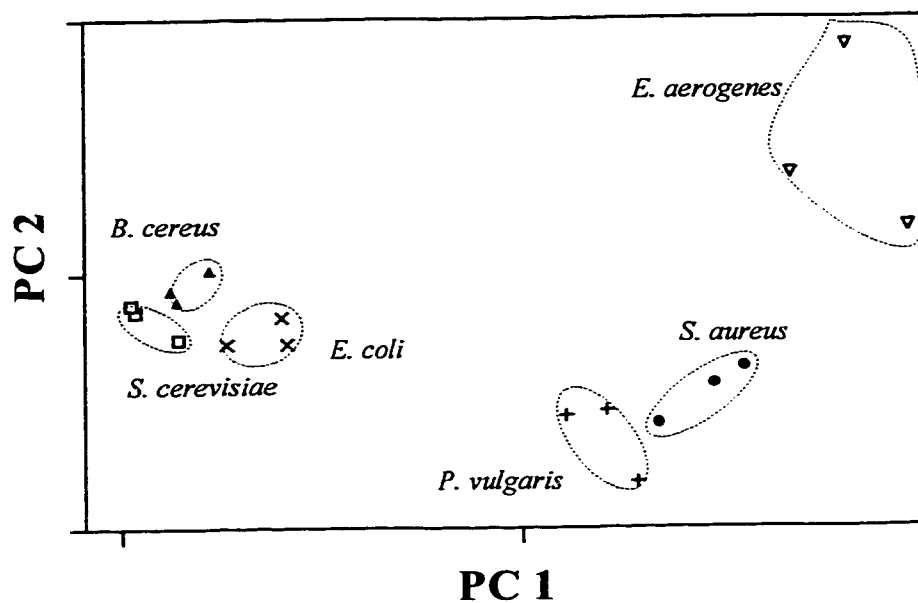


Figure 5.13: Pattern recognition plot obtained from the mean centered data matrix containing the results of all chronocoulometric experiments.

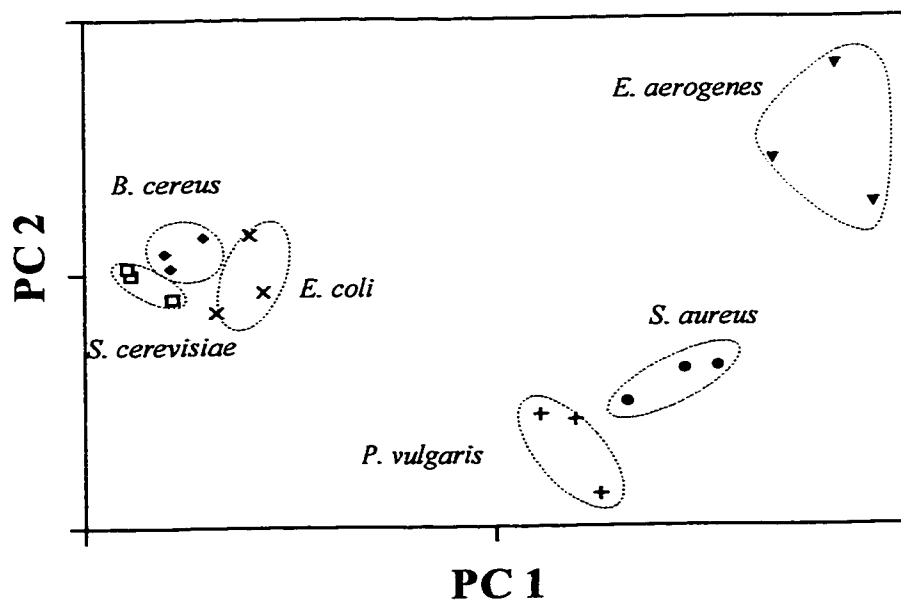
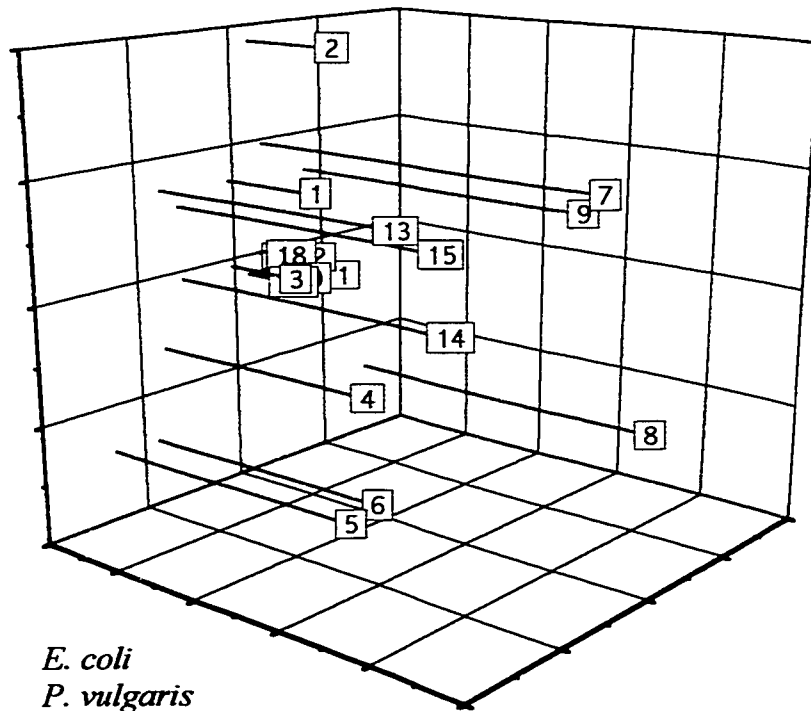


Figure 5.14 shows a three-dimensional plot using three principal components to identify additional groupings of the different strains. It is evident that *Staphylococcus aureus*, *Enterobacter aerogenes* and *Proteus vulgaris* not only formed a single group but also exhibited a similar magnitude in their trajectories onto PC 3. *E. coli* can be identified on its own trajectory because all three measurements showed the same magnitude in their PC 3 values. *S. cerevisiae* and *B. cereus* were located behind *E. coli* and were overlapping according to the angle of view.

Figure 5.14: Three-dimensional pattern recognition plot obtained from the data matrix containing the results of all chronocoulometric experiments.



- | | |
|------------|----------------------|
| 1, 2, 3 | <i>E. coli</i> |
| 4, 5, 6 | <i>P. vulgaris</i> |
| 7, 8, 9 | <i>E. aerogenes</i> |
| 10, 11, 12 | <i>B. cereus</i> |
| 13, 14, 15 | <i>S. aureus</i> |
| 16, 17, 18 | <i>S. cerevisiae</i> |

In summary, chemometric data analysis was successfully implemented for the assessment of a complex data matrix in order to identify and distinguish microbial strains. Results obtained from the pattern recognition plot using two principle components made it possible to identify groupings that were easily distinguishable from other strains. It was also possible to distinguish and identify strains after the data matrix was mean-centered prior to analysis. This indicates that mean-centering did not cause the loss of structural information and that unintended biases were not introduced by the process. Both principal component analysis methods can be used to identify the six strains. A plot of three principle components (Figure 5.14) showed similar magnitudes of trajectories for the individual strains, suggesting that the third principle component can be used to distinguish between close or overlapping points.

5.4 CONCLUSIONS

Chapters 2 and 3 showed that the addition of respiratory substrates or redox-mediators to the cocktail used for respiratory cycle activity measurements increases obtained ferricyanide reduction signals. Consequently, work reported in this chapter used a final reagent composition of 50 mM ferricyanide, 0.1 mM menadione, 10 mM succinate and 10 mM formate. Other experiments allowed further optimization of the immobilization procedure established in Chapter 4. Chronocoulometric signals obtained for covalently immobilized Con A on preactivated ImmunodyneABC[®] membranes were largest when Con A was immobilized from a stock solution containing 300 $\mu\text{g/mL}$ Con A.

Preliminary results with *E. coli* obtained at seven lectin-modified electrodes showed differences in signal intensities. These findings indicated that selective lectin binding to cell wall components of *E. coli* had taken place. It also became evident that lectin binding constants to sugars moieties were strong enough to retain bacterial cells, even after extensive rinsing of the membrane surfaces.

Further, the relationship between cell capture times and chronocoulometric signals was assessed, and we found a number of different response patterns for different lectins. Whereas bacterial adhesion to unmodified membranes yielded constant signals over time, increasing signals, either linear or curved, were observed for some lectin-modified membranes, while some curves exhibited a distinct peak over time or simply decreased over a 3 h capture period.

Atomic force microscopy was used to investigate the surfaces of modified and unmodified membranes. Initial tapping mode results obtained for the unmodified ImmunodyneABC[®] membrane revealed a high degree of surface roughness, which restricted imaging of surface areas to about 1 μm^2 . Generally, phase mode operated AFM provides image contrasts caused by differences in surface adhesion and viscoelasticity. Phase images of both unmodified and modified ImmunodyneABC[®] membranes showed significant differences between their contrasts and thus indicated the presence of a uniform Con A layer.

Furthermore, ferricyanide reduction rates were measured using a sensor array in which membranes were selectively modified with ten different lectins and BSA. Observed signals were compared to agglutination results and known sugar specificities of the various lectins and general agreement between these methods was found.

Although only ten lectins were used in this study, their potential for selective cell-surface recognition became apparent nonetheless. The varying degrees of binding to sugar moieties located on microbial cell walls made it possible to clearly identify each of the 6 microbial strains. This involved the statistical identification of specific microbial strains according to their binding pattern to individual lectins. Pattern recognition plots obtained for the normal and mean-centered data matrices (216 measurements) distinguished and identified the microbial strains.

The concept of using lectins to identify or characterize microbial strains is not new. However, the application of lectins as recognition agents in an electrochemical biosensor array has never been reported. Although existing methods for bacterial detection have led to well-established technologies capable of identifying microbial strains, none of them utilize lectins as recognition elements. Furthermore, if lectins are used as recognition agents, they are readily available and inexpensive and thus are well suited for the implementation in a sensor design that is targeted towards mass production.

5.5 REFERENCES

1. Atlas, R. M. *Principles of Microbiology*, 2nd Ed., Wm. C. Braun Publishers, 1997.
2. Swaminathan, B.; Feng, P. *Ann. Rev. Microbiol.* 1994, 48, 401.
3. Doyle, M. P.; Beuchat, L. R.; Montville, T. J. *Food Microbiology: Fundamentals and Frontiers*, 1997 (Ed), ASM Press, Washington, DC.
4. Hobsen, N. S.; Tothill, I. E. ; Turner, A. F. P. *Biosens. Bioelectron.* 1996, 11, 455.

5. Ivnitski, D.; Abdel-Hamid, I.; Atanasov, P.; Wilkins, E. *Biosens. Bioelectron.* 1999, 14, 599.
6. Wood, K. V.; Gruber, M. G. *Biosens. Bioelectron.* 1996, 11, 207.
7. Mouritsen, C. L.; Hillyard, D. R. *Anal. Chem.* 1999, 71, 366R.
8. Zhou, C.; Pivarnik, P.; Rand, G.; Letcher, S. V. *Biosens. Bioelectron.* 1998, 13, 495.
9. Bining, G.; Quate, C. F. *Phys. Rev. Lett.*, 1986, 56(9), 930.
10. Bustante, C.; Rivetti, C.; Keller, D. J. *Curr. Opin. Struct. Biol.* 1997, 7, 709.
11. Pang, D.; Vidic, B.; Rodgers, J.; Berman, B.S.; Dritschilo, A. *Radiat. Oncol. Investig.* 1997, 5, 163.
12. Moeller, C.; Allen, M.; Elings, V.; Engel, A.; Mueller, D. *Biophys. J.* 1999, 77, 1150.
13. Schabert, F. A.; Engel, A. *Biophys. J.* 1994, 67, 2394.
14. Mueller, D. J.; Engel, A. *J. Mol. Biol.* 1999, 285, 1347.
15. Engel, A.; Gaub, H. E.; Muller, D. J. *Curr. Biol.* 1999, 9, R133.
16. Fritzsche, W.; Takac, L.; Hansma, H.G.; Pietrasanta, L. *Curr. Biol. Struct. Biol.* 1998, 2, 572.
17. Liener, I. E.; Sharon, N.; Goldstein, I. J. *The Lectins: Properties, Functions and Applications in Biology and Medicine*, Academic Press, 1986.
18. Dwek, R. A. *Chem. Rev.* 1996, 96, 683.
19. Sharon, N.; Lis, H. *Lectins* Chapman and Hall, London, 1989.
20. Lis, H.; Sharon, N. *Chem. Rev.* 1998, 98, 637.
21. Oldenberg, K. R.; Loganathan, D.; Goldstein, I. J.; Schultz, P. G.; Gallop, M. A. *Proc. Natl. Acad. Sci.* 1992, 89, 5393.

22. Mirelman, D.; Ofek, I. *Microbial Lectins and Agglutinins, Properties and Biological Activity*, John Wiley & Sons, Inc., New York, 1986.
23. Keneke, R.; Menzel, C.; Schuegerl, K.; Scheper, T. *Biosens. Bioelectron.* 1996, 11, 12.
24. Patchett, R. A.; Kelly, A. F.; Kroll, R. G. *J. Appl. Bacteriol.* 1991, 71, 277.
25. Bundy, J.; Fenselau, C. *Anal. Chem.* 1999, 71, 1460.
26. Bebe, K. R.; Pell, R. J.; Seasholtz, M. B.; *Chemometrics: A Practical Guide*, Wiley-Interscience Pub., New York, 1998.
27. Kramer, R. *Chemometric Techniques for Quantitative Analysis*, Marcel-Dekker Inc., New York, 1998.
28. Malinowski, E. R. *Factor Analysis in Chemistry*, 2nd Ed., Wiley-Interscience, New York, 1991.
29. Schonkopf, S. *Am. Lab.* 1999, 31, 32.
30. Di Natale, C.; Davide, F. A. M.; D'Amico, A.; Sberveglieri, G.; Nelli, P.; Faglia, G.; Perego, C. *Sens. Actuators B*, 1995, 24-25, 801.
31. Diaz, T. G.; Guiberteau, A.; Burguillos, J. M. D.; Salinal, F. *Analyst*, 1997, 122, 513.
32. Harris, D. C. *Quantitative Chemical Analysis* 5th Ed., W. H. Freeman and Company, 1999, Chapter 5.
33. Kellner, R.; Mermet, J. M.; Otto, M.; Widmer, H. M. *Analytical Chemistry* Wiley-VCH, GmbH, 1998, Chapter 7.
34. Duschl, C.; Hall, E. A. H.; *J. Coll. Int. Sci.* 1991, 114, 368.
35. Krieg, N. R.; Holt, J. G. *Bergey's Manual of Systematic Bacteriology*, Williams & Wilkins, London, 1984.

36. Laskin, A. I.; Lechevalier, H. A. *Handbook of Microbiology* 2nd Ed., vol 2, CRC Press, Florida, 1997.
37. Singleton, P.; Sainsbury, D. *Dictionary of Microbiology and Molecular Biology*, 2nd Ed., Wiley & Sons, New York, 1996.

Chapter 6

Summary and Suggestions for Further Research

Chapter 1 provided information about the terminology of biosensors as well as their historic development in the sixties where enzymes were used for the first time to improve sensor selectivity. The scientific contributions in the seventies and eighties led to the launch of many commercially available devices for an ever-increasing market. Further descriptions of existing bacterial identification methods and an introduction to microbial respiration were given.

In Chapter 2 the respiratory cycle activity of *E. coli* was studied electrochemically by FIA and CA using ferricyanide and other electron-transfer mediators. In the presence of the respiratory substrate succinate, the complex multi-enzyme ferricyanide reduction process could be modelled by simple Michaelis-Menten kinetics. Further investigation of the respiratory cycle activity in exponential phase *E. coli* JM105 showed that ferricyanide is mainly reduced by cytochrome *o* oxidase.

The assessment of respiratory cycle activity also allowed rapid and reliable screening for antibiotic susceptibility in microorganisms. Chronoamperometry and chronocoulometry of aerobically cultivated *E. coli* yielded signals that were much smaller after *E. coli* was briefly incubated with effective antibiotic compounds. A range of antibiotic compounds representing different mechanisms of action were examined by chronocoulometry and compared to standard agar-disk diffusion testing. The miniaturized chronocoulometric assay provided results in less than 25 min and thus bacterial ferricyanide reduction was measured in the absence of significant cell growth. Following

a 10-20 min incubation with antibiotic in assay buffer (300 μ L) containing 50 mM ferricyanide and 10 mM succinate a 2 min measurement (at + 0.5 V vs Ag/AgCl at a Pt working electrode) was needed to obtain differences in signals when compared to controls. Quantitative determination of IC₅₀ values of the antibiotic compounds penicillin G and chloramphenicol yielded values that were 100-fold higher than those obtained by standard turbidity methods (10 h). Furthermore, the addition of 5 μ M DCIP, a hydrophobic electron-transfer mediator, to the assay mixture allowed susceptibility testing of a Gram-positive obligate anaerobe, *Clostridium sporogenes*. The rapid, new low volume assay will facilitate clinical susceptibility testing, allowing appropriate treatment as soon as a clinical isolate can be obtained.

The next step in the development of the microbial biosensor array dealt with the creation of a bioselective layer, in which the recognition agent was associated intimately with a transducer. Therefore, Chapter 4 was mainly concerned with the optimization of lectin immobilization procedures. Membranes that feature different surfaces were examined as potential immobilization matrices for lectins, where immobilized lectins were used to recognize and bind to cell-surface lipopolysaccharides. Optimizations performed using the model lectin Con A showed that preactivated membranes, especially ImmunodyneABC[®], significantly shorten the time required to create a functional lectin layer on the membrane surface. Completeness and homogeneity of the applied lectin layer were confirmed by atomic force microscopy.

A variety of lectins were then examined to assess the utility of this class of biomolecule for recognition in a sensor array. Chronocoulometric measurements of cells captured on the lectin modified membranes were performed in an assay buffer (200 μ L) containing 50 mM ferricyanide, 0.1 mM menadione, 10 mM succinate and 10 mM

formate. Ten different 10 lectins were used in this study, along with six microbial strains (*E. coli*, *P. vulgaris*, *B. cereus*, *E. aerogenes*, *S. aureus* and *S. cerevisiae*). The implementation of a chemometric factor analysis method allowed the identification of variations within the data matrix. Pattern recognition plots obtained for the raw and mean-centered data matrices revealed that it is possible to discriminate between the different microbial strains. Identification was made possible because repetitive measurements made using one strain exhibited a distinct grouping or clustering within scores plots.

The two most important original contributions in this thesis are therefore the rapid electrochemical antibiotic susceptibility assay, presented in Chapter 3, and the electrochemical biosensor array for the identification of microorganisms, presented in Chapter 5. Further studies should be done in both of these areas, to allow development and commercialization.

In the first area, I suggest that the antibiotic assay be further developed to examine clinical relevant organisms. In the same manner, antibiotics critical to health care, should be included in this study. In particular those antibiotics that are routinely used in standard antibiotic susceptibility testing should be examined using the new assay. In both cases, it is important to see if the performance of the chronocoulometric susceptibility test will yield 100% specificity, sensitivity and efficiency when a wider range of organisms and antibiotics is examined. The presence of an effective antimicrobial compound will be confirmed when lower respiratory cycle activity is measured. The presence of resistant strains will be indicated when no changes in activity are observed. In addition, it is essential to systematically determine assay performance in comparison to existing rapid technologies. A large number of antibiotics and a variety of bacterial strains should be studied using both the new chronocoulometric assay and the Vitek[®] system. This

commercially available assay/instrument system has become the standard in clinical diagnostics, and monitors antibiotic susceptibility through the accumulation of coloured dye (as an indication of bacterial growth) within 4 h.

The miniaturization of the assay should be another subject of future research. The two-electrode system used in this thesis has the potential to become a hand-held, portable device by implementing screen-printing technology. The implementation of this technology will allow the fabrication of a large number of sensors at competitive prices. This is particularly important since antibiotic susceptibility testing should be routinely done in high-risk areas, such as hospitals. The ideal environment for the development of antibiotic resistant pathogens is an area where a large number of potential hosts such as the elderly and immunocompromised patients are kept in close proximity and where the extensive and heavy use of antibiotics facilitates the development of resistant bacteria.

Furthermore, the determination of MIC values for new and existing antibiotics is also important. Although the assay will give reliable information about positive or negative results, it does not yet provide useful quantitative information about the MIC values of effective antibiotics. Further research should be conducted to establish a correlation between IC_{50} values obtained using our assay and the internationally established MIC values. Moreover, the possible assessment of the degree of effectiveness should be studied further. A great deal of pharmaceutical research involves the development of new, more effective antibiotic compounds. New technologies allow the syntheses of many variations of the same antibiotic compound. A rapid screening method for the most effective antimicrobial compounds would facilitate these efforts.

The microbial identification method developed in this work successfully implemented lectins to discriminate between six microbial strains. This is only the

beginning in the development of a biosensor array for rapid identification and quantitation of microorganisms. It will be important to simplify the existing sample pretreatment by omitting the centrifugation step, shortening the incubation period to less than 30 min and implementing a room temperature incubation. I further suggest the replacement of glucose with succinate as a carbon source during microorganism growth. This will allow direct cell capture, since remaining succinate in the growth medium does not interfere with lectin binding. Furthermore, it is known that bacterial growth on glucose suppresses the expression levels of succinate dehydrogenases, an important contributor to the measured respiratory cycle activity. Hence the substitution of glucose with succinate will further enhance obtained chronocoulometric signals, which will ultimately reduce measurement times. The implementation of screen-printing technology to fabricate disposable sensor arrays will further facilitate the measuring procedure by eliminating cleaning steps.

Ultimately it will be necessary to discriminate between bacterial subspecies within one strain. For example, it is expected that varying species of *Escherichia coli* exhibit similar cell-surfaces, which may pose problems for the existing method. In order to increase sensor specificity, a greater spectrum of lectins should be used. I further suggest the incorporation of antibodies into the sensor array. The immobilization of highly specific antibodies may provide enough variance within data sets to be detected by multivariate factor analysis (pattern recognition) and thus allow identification of subspecies. Here, mean centering may be investigated as a tool for preprocessing data prior to principle component analysis. In addition, the native abilities of microorganisms to adhere to various surfaces (containing sugar moieties such as glucose or mannose) may be exploited as well.

In summary, such a biosensor array has the potential to identify subpopulations within a single bacterial strain while only assessing viable cells. Furthermore, lectins used as recognition agents are readily available and inexpensive, thus making this array a promising tool for medical diagnostics and to supplement existing bacterial identification kits (selective-growth agars). Although many obstacles will have to be overcome in order to develop this technology, the combination of the bacterial identification method *via* lectins (\pm antibodies), along with the assessment of antibiotic susceptibility, will yield a useful and complete tool for medical analysis.